

Drivers of plant nutrient acquisition and allocation strategies and their influence
on plant responses to environmental change

by

Evan A. Perkowski, B.S.

A Dissertation

In

Biological Sciences

Submitted to the Graduate Faculty
of Texas Tech University in
Partial Fulfillment of
the Requirements for
the Degree of

Doctor of Philosophy

Approved

Nicholas G. Smith, Ph.D.
Chair of Committee

Aimée T. Classen, Ph.D.

Natasja van Gestel, Ph.D.

Lindsey C. Slaughter, Ph.D.

Dylan W. Schwilk, Ph.D.

Mark Sheridan, Ph.D.
Dean of the Graduate School

May 2023

Copyright 2023, Evan A. Perkowski

Acknowledgements

This dissertation was made possible by the mentorship, collaboration, and friendship of many people. I am so thankful to be surrounded by such supportive and helpful mentors, peers, and friends that have made navigating through graduate school and finishing this dissertation an enjoyable experience. Specifically, I am thankful for the incredible mentorship of my advisor and committee chair, Dr. Nick Smith, who provided invaluable insight and tools that have helped shape me into the plant ecophysiological I claim to be today. I am also indebted to my committee members, Drs. Aimée Classen, Natasja van Gestel, Dylan Schwilk, and Lindsey Slaughter, for useful feedback, invaluable support, and encouragement as I planned and implemented experiments.

I am also thankful for past and present members of the EcoHealth lab for encouragement, support, and extracurricular activities that made time inside and outside the lab enjoyable and memorable. Particular thanks go to Dr. Lizz Waring, Dr. Xiulin Gao, Helen Scott, and Risa McNellis, Billi Jean Petermann, and the late Dr. Kris Petterson, all of whom were invaluable to helping me navigate my first year. I am especially thankful for the mentorship and friendship of Dr. Lizz Waring, as our weekly coffee chats were instrumental for helping me feel welcome in Lubbock and acclimate to life as a graduate student. I am also grateful for the friendship of Billi Jean Petermann and the late Dr. Kris Petterson for their encouragement and willingness to discuss microbial symbioses over coffee on random Saturday mornings.

Additional thanks go out to Isa Beltran, Snehanjana Chatterjee, Jeff Chi-

eppa, Peter Eludini, Zinny Ezekannagha, Hannah German, Eve Gray, Monika Kelley, Azaj Mahmud, Jorge Ochoa, Brad Posch, Avery Schoenherr, and Jose Villeda for help with experiments or for lending an ear over puzzling results. I am also thankful for collaborators Dr. Christy Goodale and Dave Frey, who provided invaluable insight for the second experimental chapter.

I would like to thank my undergraduate advisor, Dr. Janice Krumm, for continued mentorship and friendship and for insightful advice about navigating graduate school, but most of all for helping me realize my career aspirations and pushing me to pursue this endeavor. Additional thanks go out to my family, particularly my parents, partner, and dog for continued support and distractions outside the lab. The experiments included here would not have been possible without their emotional and monetary support.

This work was made possible from funding by the NSF, USDA, Braun and Gresham, PLLC., and was a contribution to the LEMONTREE (Land Ecosystem Models based On New Theory, obseRvations and ExperimEnts) project. The LEMONTREE project is funded through the generosity of Eric and Wendy Schmidt by recommendation of the Schmidt Futures programme and the Imperial College initiative on Grand Challenges in Ecosystems and the Environment. This work was also funded by graduate student research awards from Texas Tech University and the Botanical Society of America.

I have inevitably missed mentioning folks that were instrumental to the completion of these experiments and contributed to my development as a plant physiological ecologist. Please know that I am grateful and appreciative of our interactions.

Table of Contents

Acknowledgements	ii
Abstract	ix
List of Tables	xi
List of Figures	xv
1. Introduction	1
2. Structural carbon costs to acquire nitrogen are determined by nitrogen and light availability in two species with different nitrogen acquisition strategies	7
2.1 Introduction	7
2.2 Methods	11
2.2.1 <i>Experiment setup</i>	11
2.2.2 <i>Plant measurements and calculations</i>	12
2.2.3 <i>Statistical analyses</i>	13
2.3 Results	15
2.3.1 <i>Carbon costs to acquire nitrogen</i>	15
2.3.2 <i>Whole plant nitrogen biomass</i>	18
2.3.3 <i>Root carbon biomass</i>	20
2.3.4 <i>Root nodule biomass</i>	22
2.4 Discussion	26
2.4.1 <i>Carbon costs to acquire nitrogen increase with light availability and decrease with fertilization</i>	26
2.4.2 <i>Modeling implications</i>	28
2.4.3 <i>Study limitations</i>	30
2.4.4 <i>Conclusions</i>	32
3. Soil nitrogen availability modifies leaf nitrogen economies in mature temperate deciduous forests: a direct test of photosynthetic least-cost theory	34
3.1 Introduction	34

3.2	Methods	38
3.2.1	<i>Study site description</i>	38
3.2.2	<i>Experimental design</i>	39
3.2.3	<i>Leaf gas exchange and trait measurements</i>	39
3.2.4	A_{net}/C_i curve-fitting and parameter estimation	42
3.2.5	<i>Proportion of leaf nitrogen allocated to photosynthesis and structure</i>	44
3.2.6	<i>Tradeoffs between nitrogen and water use</i>	45
3.2.7	<i>Soil nitrogen availability and pH</i>	46
3.2.8	<i>Statistical analyses</i>	48
3.3	Results	50
3.3.1	<i>Leaf nitrogen content</i>	50
3.3.2	<i>Net photosynthesis and leaf biochemistry</i>	53
3.3.3	<i>Leaf nitrogen allocation</i>	56
3.3.4	<i>Tradeoffs between nitrogen and water use</i>	59
3.4	Discussion	62
3.4.1	<i>Soil nitrogen availability modifies tradeoffs between nitrogen and water use</i>	63
3.4.2	<i>Soil pH did not modify tradeoffs between nitrogen and water usage</i>	65
3.4.3	<i>Species identity explains a large amount of variation in leaf and whole plant traits</i>	66
3.4.4	<i>Implications for photosynthetic least-cost theory model development</i>	67
3.4.5	<i>Conclusions</i>	69
4.	The relative cost of resource use for photosynthesis drives variance in leaf nitrogen content across a climate and soil resource availability gradient	70
4.1	Introduction	70
4.2	Methods	76
4.2.1	<i>Site descriptions and sampling methodology</i>	76

4.2.2	<i>Leaf trait measurements</i>	77
4.2.3	<i>Site climate data</i>	82
4.2.4	<i>Site edaphic characteristics</i>	82
4.2.5	<i>Plant functional group assignments</i>	84
4.2.6	<i>Data analysis</i>	85
4.3	Results	88
4.3.1	<i>Cost to acquire nitrogen relative to water</i>	88
4.3.2	<i>Leaf $C_i:C_a$</i>	91
4.3.3	<i>Leaf nitrogen content</i>	94
4.3.4	<i>Structural equation model</i>	98
4.4	Discussion	101
4.4.1	<i>Negative effects of leaf $C_i:C_a$ on N_{area} are driven by reductions in M_{area}, not N_{mass}</i>	101
4.4.2	<i>Soil nitrogen availability increases N_{area} through changes in the cost to acquire nitrogen</i>	103
4.4.3	<i>Soil moisture increases N_{area} by facilitating increases in soil nitrogen availability</i>	104
4.4.4	<i>Indirect effects of climate on N_{area} are mediated through changes in leaf $C_i:C_a$ and β</i>	105
4.4.5	<i>Species identity traits modify effects of the environment on β, leaf $C_i:C_a$, and N_{area}</i>	105
4.4.6	<i>Next steps for optimality model development</i>	107
4.4.7	<i>Conclusions</i>	108
5.	Optimal resource investment to photosynthetic capacity maximizes nutrient allocation to whole plant growth under elevated CO₂	109
5.1	Introduction	109
5.2	Methods	114
5.2.1	<i>Seed treatments and experimental design</i>	114
5.2.2	<i>Growth chamber conditions</i>	115
5.2.3	<i>Leaf gas exchange measurements</i>	117

5.2.4 <i>Leaf trait measurements</i>	118
5.2.5 <i>A/C_i curve fitting and parameter estimation</i>	120
5.2.6 Stomatal limitation	120
5.2.7 <i>Proportion of leaf nitrogen allocated to photosynthesis and structure</i>	121
5.2.8 <i>Whole plant traits</i>	123
5.2.9 <i>Statistical analyses</i>	125
5.3 Results	127
5.3.1 <i>Leaf nitrogen and chlorophyll content</i>	127
5.3.2 <i>Leaf biochemistry and stomatal conductance</i>	131
5.3.3 <i>Leaf nitrogen allocation</i>	135
5.3.4 <i>Whole plant traits</i>	139
5.3.5 <i>Nitrogen fixation</i>	143
5.4 Discussion	147
5.4.1 <i>Soil nitrogen fertilization has divergent effects on leaf and whole plant acclimation responses to CO₂</i>	148
5.4.2 <i>Implications for future model development</i>	152
5.4.3 <i>Study limitations and future directions</i>	153
5.4.4 <i>Conclusions</i>	155
6. Conclusions	157
References	168
Appendix A: Supplemental material for "Structural carbon costs to acquire nitrogen are determined by nitrogen and light availability in two species with different nitrogen acquisition strategies"	205
Appendix B: Supplemental material for "Soil nitrogen availability modifies leaf nitrogen economies in mature temperate deciduous forests: a direct test of photosynthetic least-cost theory"	209

Appendix C: Supplemental material for "The relative cost of resource use for photosynthesis drives variance in leaf nitrogen content across a climate and soil resource availability gradient"	214
Appendix D: Supplemental material for "Optimal resource investment to photosynthetic capacity maximizes nutrient allocation to whole plant growth under elevated CO₂" . . .	221

Abstract

Photosynthesis is the largest carbon flux between the atmosphere and is constrained by ecosystem carbon and nutrient cycle dynamics, which causes terrestrial biosphere models to be sensitive to the formulation of photosynthetic processes. Terrestrial biosphere models exhibit high divergence in simulated carbon and nitrogen fluxes under future environmental conditions, which may be due to uncertainty in the acclimation response of photosynthetic processes to environmental change. Photosynthetic least-cost theory provides a promising framework for understanding effects of climatic and edaphic factors on photosynthetic acclimation responses to changing environments. Yet, empirical tests of the theory are rare, limiting our ability to assess whether the theory is suitable for implementation in next-generation terrestrial biosphere models.

Here, I present four experiments designed to test assumptions of photosynthetic least-cost theory using a combination of greenhouse, growth chamber, field manipulation, and field gradient experiments. Experiment chapters are flanked by a general introduction chapter and conclusions chapter. The first experimental chapter quantifies structural carbon costs to acquire nitrogen in *Glycine max* and *Gossypium hirsutum* grown under four nitrogen fertilization levels and four light availability levels in a full factorial greenhouse experiment. I find that carbon costs to acquire nitrogen in both species increase with increasing light availability and decrease with increasing fertilization, though responses to fertilization in *G. max* were markedly less than *G. hirsutum*. The second experimental chapter quantifies leaf nitrogen and photosynthetic traits in upper canopy leaves of deciduous trees

growing in a 9-year nitrogen-by-sulfur field manipulation experiment. I find strong evidence for nitrogen-water use tradeoffs with increasing soil nitrogen availability, evidenced through a strong negative relationship between leaf nitrogen content and leaf $C_i:C_a$ and stronger increase in leaf nitrogen content with increasing soil nitrogen availability than leaf $C_i:C_a$. The third experiment investigates variance in leaf nitrogen content across a climate and soil resource availability gradient in Texan grasslands, showing that effects of soil resource availability and climate on leaf nitrogen content are driven by changes in leaf $C_i:C_a$. Finally, the fourth experiment quantifies leaf and whole plant acclimation responses in *G. max* grown under two atmospheric CO₂ levels, with and without inoculation with *Bradyrhizobium japonicum*, and across nine nitrogen fertilization treatments in a full factorial growth chamber experiment. I find that leaf acclimation responses to CO₂ were independent of soil nitrogen fertilization or inoculation treatment, though stimulations in whole plant growth under elevated CO₂ were enhanced with increasing soil nitrogen fertilization and in inoculated pots under low nitrogen fertilization.

Experiments included in this dissertation provide consistent support for patterns expected from photosynthetic least-cost theory. The use of multiple experimental approaches allowed me to examine mechanisms driving patterns expected from the theory and investigate whether these patterns occur naturally across environmental gradients. Findings from these chapters challenge common paradigms in plant ecophysiology, providing evidence that including photosynthetic least-cost frameworks in next-generation terrestrial biosphere models may improve the observed divergence in simulated outcomes across terrestrial biosphere model products.

List of Tables

2.1 Analysis of variance results exploring species-specific effects of light availability, nitrogen fertilization, and their interactions on carbon costs to acquire nitrogen, whole-plant nitrogen biomass, and root carbon biomass	16
2.2 Analysis of variance results exploring effects of light availability, nitrogen fertilization, and their interactions on <i>G. max</i> root nodule biomass (g) and the ratio of root nodule biomass to root biomass (g g^{-1})	23
2.3 Slopes of the regression line describing the relationship between each dependent variable and nitrogen fertilization at each light level	24
3.1 Effects of soil nitrogen availability, soil pH, and species on leaf nitrogen content per unit leaf area, leaf nitrogen content per unit leaf mass, and leaf mass per unit leaf area	51
3.2 Effects of soil nitrogen availability, soil pH, species, and N_{area} on net photosynthesis, the maximum rate of Rubisco carboxylation, the maximum rate of RuBP regeneration, and the ratio of the maximum rate of RuBP regeneration to the maximum rate of Rubisco carboxylation	54
3.3 Effects of soil nitrogen availability, soil pH, and species on the proportion of leaf nitrogen content allocated to photosynthesis, Rubisco, bioenergetics, and structure	57

3.4 Effects of soil nitrogen availability, soil pH, species, and N_{area} on χ , photosynthetic nitrogen use efficiency, leaf nitrogen content per unit χ , and maximum Rubisco carboxylation rate per unit χ	60
4.1 Site locality information, sampling year, 2006-2020 mean annual precipitation, mean annual temperature, and water holding capacity	80
4.2 Effects of soil moisture, soil nitrogen availability, and plant functional group on β	89
4.3 Effects of soil moisture, soil nitrogen availability, and plant functional group on leaf $C_i:C_a$	92
4.4 Effects of soil moisture, soil nitrogen availability, plant functional group, and leaf $C_i:C_a$ on leaf nitrogen content per unit leaf area, leaf nitrogen content per unit leaf biomass, and leaf biomass per unit leaf area	96
4.5 Structural equation model results investigating direct effects of climatic and soil resource availability on leaf nitrogen content	99
5.1 Effects of soil nitrogen fertilization, inoculation, and CO_2 treatments on N_{area} , N_{mass} , M_{area} , and Chl_{area}	129
5.2 Effects of soil nitrogen fertilization, inoculation, and CO_2 on leaf biochemistry	133
5.3 Effects of soil N availability, soil pH, species, and N_{area} on leaf nitrogen allocation	137

5.4	Effects of soil N availability, soil pH, species, and N_{area} on total leaf area, whole plant biomass, and carbon costs to acquire nitrogen	141
5.5	Effects of soil N availability, soil pH, species, and N_{area} on root nodule biomass and plant investments in symbiotic nitrogen fixation	145
A1	Summary table containing volumes of compounds used to create modified Hoagland's solutions for each soil nitrogen fertilization treatment. All volumes are expressed as milliliters per liter (mL/L)	205
A2	Analysis of variance results exploring species-specific effects of light availability, nitrogen fertilization, and their interactions on the ratio of whole plant biomass to pot volume	206
A3	Slopes of the regression line describing the relationship between each dependent variable and nitrogen fertilization at each light level*	207
B1	Sample sizes of each species, abbreviated by their USDA NRCS PLANTS database code, within each plot at each site	209
B2	Analysis of variance results exploring the linear effect of leaf temperature on net photosynthesis rate and stomatal conductance measured at 400 $\mu\text{mol mol}^{-1}$ CO_2	210
B3	Second order log-polynomial regression coefficients that described the effect of leaf temperature on net photosynthesis and stomatal conductance measured at 400 $\mu\text{mol mol}^{-1}$ CO_2	211
B4	Mean, standard error, and 95% confidence interval ranges of soil nitrogen availability estimates across all measured plots. All units are expressed as $\mu\text{g N g}^{-1}$ resin d^{-1}	212

C1	List of sampled species and their plant functional group assignment	216
C2	List of sampled species and their plant functional group assignment (cont.)	217
C3	List of sampled species and their plant functional group assignment (cont.)	218
C4	Model selection results for soil moisture, air temperature, and vapor pressure deficit. Soil moisture was used in a bivariate regression against β , while vapor pressure deficit was used in bivariate regressions against leaf $C_i:C_a^*$	219
D1	Summary table containing volumes of compounds used to create modified Hoagland's solutions for each soil nitrogen fertilization treatment. All volumes are expressed as milliliters per liter (mL/L)	221
D2	Summary of the daily growth chamber growing condition program	222

List of Figures

2.1 Relationships between soil nitrogen fertilization and light availability on carbon costs to acquire nitrogen in <i>G. hirsutum</i> and <i>G. max</i>	17
2.2 Relationships between soil nitrogen fertilization and light availability on whole-plant nitrogen biomass in <i>G. hirsutum</i> and <i>G. max</i>	19
2.3 Relationships between soil nitrogen fertilization and light availability on root carbon biomass in <i>G. hirsutum</i> and <i>G. max</i>	21
2.4 Effects of shade cover and nitrogen fertilization on root nodule biomass and the ratio of root nodule biomass to root biomass in <i>G. max</i>	25
3.1 Effects of soil nitrogen availability and species on leaf nitrogen content per unit leaf area, leaf nitrogen content per unit leaf biomass, and leaf mass per leaf area	52
3.2 Effects of soil nitrogen availability, species, and leaf nitrogen content on net photosynthesis, maximum Rubisco carboxylation rate, and maximum RuBP regeneration rate	55
3.3 Effects of soil nitrogen availability, species, and leaf nitrogen content on the fraction of leaf nitrogen allocated to photosynthesis and structure	58
3.4 Effects of soil N availability, species, and leaf N content on tradeoffs between nitrogen and water use	61

4.1	Site locations along 2006-2020 mean annual precipitation and mean annual temperature gradients in Texas, USA.	81
4.2	Effects of soil nitrogen availability and soil moisture on the cost of acquiring and using nitrogen	90
4.3	Effects of 4-day mean vapor pressure deficit, 2-day soil moisture (per water holding capacity), and soil nitrogen availability on leaf $C_i:C_a$	93
4.4	Effects of leaf $C_i:C_a$, soil nitrogen availability, and soil moisture on leaf nitrogen content per unit leaf area, leaf nitrogen content per unit leaf biomass, and leaf mass per area.	97
4.5	Structural equation model results exploring drivers of N_{area}	100
5.1	Effects of CO_2 , fertilization, and inoculation on leaf nitrogen per unit leaf area, leaf nitrogen content, leaf mass per unit leaf area, and chlorophyll content per unit leaf area.	130
5.2	Effects of CO_2 , fertilization, and inoculation on maximum rate of Rubisco carboxylation, the maximum rate of RuBP regeneration, and the ratio of the maximum rate of RuBP regeneration to the maximum rate of Rubisco carboxylation leaf mass per unit leaf area, dark respiration, stomatal conductance, and stomatal limitation. .	134
5.3	Effects of CO_2 , fertilization, and inoculation on the relative fraction of leaf nitrogen allocated to photosynthesis and the fraction of leaf nitrogen allocated to structure.	138

5.4	Effects of CO ₂ , fertilization, and inoculation on total leaf area, total biomass, and structural carbon costs to acquire nitrogen.	142
5.5	Effects of CO ₂ , fertilization, and inoculation on nodule biomass, nodule: root biomass, and percent nitrogen fixed from the atmosphere.	146
A1	Effects of shade cover and nitrogen fertilization on the ratio of plant biomass to rooting volume in <i>G. hirsutum</i> and <i>G. max</i>	208
B1	Effects of leaf temperature on net photosynthesis rate and stomatal conductance values when measured at 400 μmol mol ⁻¹ CO ₂ . . .	213
C1	Model selection results exploring relevant timescales for soil moisture and vapor pressure deficit	220
D1	Relationships between area-based leaf nitrogen content, mass-based leaf nitrogen content, and leaf mass per unit leaf area measured on the focal leaf used to generate A_{net}/C_i curves and leaf nitrogen content measured on the leaf used for chlorophyll extractions . . .	223
D2	Effects of CO ₂ , fertilization, and inoculation on the ratio of whole plant biomass to pot volume	224

1 Chapter 1

2 Introduction

3 Photosynthesis represents the largest carbon flux between the atmosphere
4 and biosphere, and is regulated by complex ecosystem carbon and nutrient cy-
5 cles (Hungate et al. 2003; IPCC 2021). As a result, the inclusion of robust,
6 empirically tested representations of photosynthetic processes is critical in order
7 for terrestrial biosphere models to accurately and reliably simulate carbon and
8 nutrient fluxes between the atmosphere and terrestrial biosphere (Oreskes et al.
9 1994; Smith and Dukes 2013; Prentice et al. 2015; Wieder et al. 2015). Despite
10 evidence that the inclusion of coupled carbon and nutrient cycles can improve
11 model uncertainty, widespread divergence in predicted carbon and nutrient fluxes
12 is still apparent across model products (Friedlingstein et al. 2014; Arora et al.
13 2020; Davies-Barnard et al. 2020). Divergence in predicted carbon and nutrient
14 fluxes across terrestrial biosphere models may be due to an incomplete under-
15 standing of how plants acclimate to changing environments (Smith and Dukes
16 2013; Davies-Barnard et al. 2020), as terrestrial biosphere models are sensitive to
17 the formulation of photosynthetic processes (Bonan et al. 2011; Ziehn et al. 2011;
18 Booth et al. 2012; Smith et al. 2016; Smith et al. 2017; Rogers et al. 2017).

Many terrestrial biosphere models predict leaf-level photosynthesis through linear relationships between area-based leaf nitrogen content and the maximum rate of Ribulose-1,5-bisphosphate carboxylase/oxygenase ("Rubisco"), following the idea that large fractions of leaf nitrogen content are allocated to the construction and maintenance of Rubisco and other photosynthetic enzymes (Evans

24 1989). The inclusion of coupled carbon and nutrient cycles in terrestrial bio-
25 sphere models (Shi et al. 2016; Braghieri et al. 2022) allows for the prediction
26 of leaf nitrogen content through soil nitrogen availability, which causes models to
27 indirectly predict photosynthetic processes through shifts in soil nitrogen avail-
28 ability (Smith et al. 2014; Lawrence et al. 2019). While these patterns are
29 commonly observed in ecosystems globally (Brix 1971; Evans 1989; Firn et al.
30 2019; Liang et al. 2020), this formulation does not allow for the prediction of
31 leaf and whole plant acclimation responses to changing environments (Smith and
32 Dukes 2013; Rogers et al. 2017; Harrison et al. 2021), and suggests that constant
33 leaf nitrogen-photosynthesis relationships are ubiquitous across ecosystems.

34 Photosynthetic least-cost theory (Prentice et al. 2014; Wang et al. 2017;
35 Smith et al. 2019; Scott and Smith 2022; Harrison et al. 2021) provides a con-
36 temporary framework for predicting leaf and whole plant acclimation responses
37 to environmental change. The theory, which unifies photosynthetic optimal coor-
38 dination (Chen et al. 1993; Maire et al. 2012) and least-cost (Wright et al. 2003)
39 theories, posits that plants optimize photosynthetic processes by minimizing the
40 summed cost of nutrient and water use (referred to here and in the rest of this
41 dissertation as β). The summed cost of nutrient and water use is predicted to
42 be positively correlated with the ratio of intercellular CO₂ to atmospheric CO₂
43 (referred to here and in the rest of this dissertation as leaf $C_i:C_a$). Leaf $C_i:C_a$ is
44 determined by factors that influence leaf nutrient demand, such as CO₂, temper-
45 ature, vapor pressure deficit, and light availability (Prentice et al. 2014; Wang
46 et al. 2017; Smith et al. 2019; Stocker et al. 2020), and may change in response to
47 changing edaphic characteristics through changes in β . Photosynthetic processes

48 are optimized such that nutrients are allocated to photosynthetic enzymes to allow
49 net photosynthesis rates to be equally co-limited by the maximum rate of Rubisco
50 carboxylation and the maximum rate of Ribulose-1,5-bisphosphate (RuBP) regen-
51 eration (Chen et al. 1993; Maire et al. 2012). The theory indicates that costs
52 of nutrient and water use are substitutable such that, in a given environment,
53 optimal photosynthesis rates can be achieved by sacrificing inefficient use of a
54 relatively more abundant (and less costly to acquire) resource for more efficient
55 use of a relatively less abundant (and more costly to acquire) resource.

56 Optimality models leveraging patterns expected from photosynthetic least-
57 cost theory have been developed for both C₃ (Wang et al. 2017; Smith et al. 2019;
58 Stocker et al. 2020) and more recently for C₄ species (Scott and Smith 2022). Such
59 models show broad agreement with patterns observed across environmental gradi-
60 ents (Smith et al. 2019; Paillassa et al. 2020; Querejeta et al. 2022; Westerband
61 et al. 2023), and are capable of reconciling dynamic leaf nitrogen-photosynthesis
62 relationships and acclimation responses to elevated CO₂, temperature, light avail-
63 ability, and vapor pressure deficit (Dong et al. 2017; Dong et al. 2020; Smith
64 and Keenan 2020; Luo et al. 2021; Peng et al. 2021; Dong et al. 2022; Dong
65 et al. 2022; Querejeta et al. 2022; Westerband et al. 2023). Current versions of
66 optimality models that invoke patterns expected from photosynthetic least-cost
67 theory hold β constant across growing environments. As growing evidence sug-
68 gests that costs of nutrient use change across resource availability and climatic
69 gradients in species with different nutrient acquisition strategies (Fisher et al.
70 2010; Brzostek et al. 2014; Terrer et al. 2018; Allen et al. 2020), one might
71 expect that β should dynamically change across environments and in species with

72 different nutrient acquisition strategies.

73 Despite recent recognition that patterns expected from photosynthetic
74 least-cost theory occur across broad environmental gradients, no study has investi-
75 gated how β varies across edaphic and climatic gradients aside from a single study
76 investigating variance in β due to soil water stress (Lavergne et al. 2020). Further-
77 more, no previous study has investigated whether β varies in species with different
78 nutrient acquisition strategies, or if changes in β due to changes in edaphic char-
79 acteristics scale to influence leaf or whole plant acclimation responses to changing
80 environments. The lack of these studies provided motivation for the experimental
81 chapters included in this dissertation.

82 In this dissertation, I use a combination of greenhouse, field manipulation,
83 environmental gradient, and growth chamber experiments to quantify leaf and
84 whole plant acclimation responses across various climatic and edaphic conditions
85 and different nutrient acquisition strategies. Together, these experiments eval-
86 uate patterns expected from photosynthetic least-cost theory and test mechanisms
87 predicted to drive responses expected from theory. The empirical data collected
88 in these experiments will also provide important information needed to refine ex-
89 isting optimality models that include photosynthetic least-cost frameworks, and
90 could help determine whether such models are suitable for implementing in next-
91 generation terrestrial biosphere models. While theory suggests that plants accli-
92 mate across environments by minimizing the summed cost of nutrients relative
93 to water, I choose to isolate effects of soil nitrogen availability on costs of nitro-
94 gen acquisition relative to water for the sake of brevity. Though, I acknowledge
95 that patterns expected from theory may be modified by other nutrients (e.g.,

96 phosphorus) or edaphic characteristics, and, though not included here, should be
97 investigated.

98 In the first experimental chapter, I re-analyze data from a greenhouse ex-
99 periment that grew *Glycine max* and *Gossypium hirsutum* seedlings under full-
100 factorial combinations of four light treatments and four fertilization treatments
101 to examine effects of nitrogen and light availability on structural carbon costs to
102 acquire nitrogen. In the second experimental chapter, I measure leaf physiological
103 traits in the upper canopy of mature trees growing in a 9-year nitrogen-by-pH
104 field manipulation experiment to assess whether changes in soil nitrogen availabil-
105 ity or soil pH modify nitrogen-water use trade-offs expected from photosynthetic
106 least-cost theory. The third experimental chapter leverages a broad precipitation
107 and soil nutrient availability gradient in Texan grasslands to investigate primary
108 drivers of leaf nitrogen content. In the fourth experimental chapter, I use growth
109 chambers to quantify leaf and whole plant acclimation responses to CO₂ across
110 a soil nitrogen fertilization gradient, while also manipulating nutrient acquisition
111 strategy by controlling whether seedlings were able to form associations with sym-
112 biotic nitrogen-fixing bacteria.

113 Across experiments, I find strong and consistent support for patterns ex-
114 pected from photosynthetic least-cost theory, showing that shifts in edaphic char-
115 acteristics predictably alter β , and that shifts in β facilitate changes in leaf
116 nitrogen-water use tradeoffs and leaf nitrogen-photosynthesis relationships. I also
117 show that costs of nitrogen acquisition vary in species with different nitrogen
118 acquisition strategies. Finally, I show strong evidence suggesting that leaf accli-
119 mation responses to elevated CO₂ are decoupled from soil nitrogen availability and

120 inoculation with symbiotic nitrogen-fixing bacteria. It is my hope that these ex-
121 periments will encourage future iterations of optimality models that adopt photo-
122 synthetic least-cost frameworks to consider frameworks for implementing dynamic
123 β values across soil resource availability gradients and in species with different nu-
124 trient acquisition strategies.

125 Finally, the four experimental chapters presented in this dissertation are
126 presented either as previously published journal articles (copyright clearance avail-
127 able upon request) or as manuscript drafts currently in preparation for journal
128 submission. Specifically, the first experimental chapter was published in *Journal*
129 *of Experimental Botany* in 2021 and the second chapter is currently in review,
130 while the third and fourth chapters are each in preparation for journal submis-
131 sion. This dissertation concludes with a sixth chapter that summarizes experiment
132 findings and briefly synthesizes common themes observed across experiments.

133

Chapter 2

134

Structural carbon costs to acquire nitrogen are determined by
135 nitrogen and light availability in two species with different nitrogen
136 acquisition strategies

137 2.1 Introduction

138 Carbon and nitrogen cycles are tightly coupled in terrestrial ecosystems. This
139 tight coupling influences photosynthesis (Walker et al. 2014; Rogers et al. 2017),
140 net primary productivity (LeBauer and Treseder 2008; Thomas et al. 2013), de-
141 composition (Cornwell et al. 2008; Bonan et al. 2013; Sulman et al. 2019), and
142 plant resource competition (Gill and Finzi 2016; Xu-Ri and Prentice 2017). Ter-
143 restrial biosphere models are beginning to include connected carbon and nitrogen
144 cycles to improve the realism of their simulations (Fisher et al. 2010; Brzostek
145 et al. 2014; Wieder et al. 2015; Shi et al. 2016; Zhu et al. 2019). Simula-
146 tions from these models indicate that coupling carbon and nitrogen cycles can
147 drastically influence future biosphere-atmosphere feedbacks under global change,
148 such as elevated carbon dioxide or nitrogen deposition (Thornton et al. 2007;
149 Goll et al. 2012; Wieder et al. 2015; Wieder et al. 2019). Nonetheless, there
150 are still limitations in our quantitative understanding of connected carbon and
151 nitrogen dynamics (Thomas et al. 2015; Meyerholt et al. 2016; Rogers et al.
152 2017; Exbrayat et al. 2018; Shi et al. 2019), forcing models to make potentially
153 unreliable assumptions.

154

Plant nitrogen acquisition is a process in terrestrial ecosystems by which
155 carbon and nitrogen are tightly coupled (Vitousek and Howarth 1991; Delaire
156 et al. 2005; Brzostek et al. 2014). Plants must allocate photosynthetically de-

157 rived carbon belowground to produce and maintain root systems or exchange with
158 symbiotic soil microbes in order to acquire nitrogen (Högberg et al. 2008; Hög-
159 berg et al. 2010). Thus, plants have an inherent carbon cost associated with
160 acquiring nitrogen, which can include both direct energetic costs associated with
161 nitrogen acquisition and indirect costs associated with building structures that
162 support nitrogen acquisition (Gutschick 1981; Rastetter et al. 2001; Vitousek
163 et al. 2002; Menge et al. 2008). Model simulations (Fisher et al. 2010; Brzostek
164 et al. 2014; Shi et al. 2016; Allen et al. 2020) and meta-analyses (Terrer et al.
165 2018) suggest that these carbon costs vary between species, particularly those
166 with different nitrogen acquisition strategies. For example, simulations using iter-
167 ations of the Fixation and Uptake of Nitrogen (FUN) model indicate that species
168 that acquire nitrogen from non-symbiotic active uptake pathways (e.g. mass flow)
169 generally have larger carbon costs to acquire nitrogen than species that acquire
170 nitrogen through symbiotic associations with nitrogen-fixing bacteria (Brzostek
171 et al. 2014; Allen et al. 2020).

172 Carbon costs to acquire nitrogen likely vary in response to changes in soil
173 nitrogen availability. For example, if the primary mode of nitrogen acquisition
174 is through non-symbiotic active uptake, then nitrogen availability could decrease
175 carbon costs to acquire nitrogen as a result of increased per-root nitrogen up-
176 take (Franklin et al. 2009; Wang et al. 2018). However, if the primary mode of
177 nitrogen acquisition is through symbiotic active uptake, then nitrogen availabil-
178 ity may incur additional carbon costs to acquire nitrogen if it causes microbial
179 symbionts to shift toward parasitism along the parasitism–mutualism continuum
180 (Johnson et al. 1997; Hoek et al. 2016; Friel and Friesen 2019) or if it reduces

181 the nitrogen acquisition capacity of a microbial symbiont (van Diepen et al. 2007;
182 Soudzilovskaia et al. 2015; Muñoz et al. 2016). Species may respond to shifts in
183 soil nitrogen availability by switching their primary mode of nitrogen acquisition
184 to a strategy with lower carbon costs to acquire nitrogen in order to maximize
185 the magnitude of nitrogen acquired from a belowground carbon investment and
186 outcompete other individuals for soil resources (Rastetter et al. 2001; Menge et al.
187 2008).

188 Environmental conditions that affect demand to acquire nitrogen to sup-
189 port new and existing tissues could also be a source of variance in plant carbon
190 costs to acquire nitrogen. For example, an increase in plant nitrogen demand could
191 increase carbon costs to acquire nitrogen if this increases the carbon that must be
192 allocated belowground to acquire a proportional amount of nitrogen (Kulmatiski
193 et al. 2017; Noyce et al. 2019). This could be driven by a temporary state of
194 diminishing return associated with investing carbon toward building and main-
195 taining structures that are necessary to support enhanced nitrogen uptake, such
196 as fine roots (Matamala and Schlesinger 2000; Norby et al. 2004; Arndal et al.
197 2018), mycorrhizal hyphae (Saleh et al. 2020), or root nodules (Parvin et al.
198 2020). Alternatively, if the environmental factor that increases plant nitrogen de-
199 mand causes nitrogen to become more limiting in the system (e.g. atmospheric
200 CO₂) (Luo et al. 2004; LeBauer and Treseder 2008; Vitousek et al. 2010; Liang
201 et al. 2016), species might switch their primary mode of nitrogen acquisition to
202 a strategy with lower relative carbon costs to acquire nitrogen in order to gain a
203 competitive advantage over species with either different or more limited modes of
204 nitrogen acquisition (Ainsworth and Long 2005; Taylor and Menge 2018).

205 Using a plant economics approach, I examined the influence of plant ni-
206 trogen demand and soil nitrogen availability on plant carbon costs to acquire
207 nitrogen. This was done by growing a species capable of forming associations
208 with nitrogen-fixing bacteria (*Glycine max* L. (Merr)) and a species not capable
209 of forming these associations (*Gossypium hirsutum* L.) under four levels of light
210 availability (plant nitrogen demand proxy) and four levels of soil nitrogen fertil-
211 ization (soil nitrogen availability proxy) in a full-factorial, controlled greenhouse
212 experiment. I used this experimental set-up to test the following hypotheses:

- 213 1. An increase in plant nitrogen demand due to increasing light availability will
214 increase carbon costs to acquire nitrogen through a proportionally larger
215 increase in belowground carbon than whole-plant nitrogen acquisition. This
216 will be the result of an increased investment of carbon toward belowground
217 structures that support enhanced nitrogen uptake, but at a lower nitrogen
218 return.
- 219 2. An increase in soil nitrogen availability will decrease carbon costs to acquire
220 nitrogen as a result of increased per root nitrogen uptake in *G. hirsutum*.
221 However, soil nitrogen availability will not affect carbon costs to acquire
222 nitrogen in *G. max* because of the already high return of nitrogen supplied
223 through nitrogen fixation.

224 2.2 Methods

225 2.2.1 *Experiment setup*

226 *Gossypium hirsutum* and *G. max* were planted in individual 3 liter pots (NS-300; **227** Nursery Supplies, Orange, CA, USA) containing a 3:1 mix of unfertilized potting **228** mix (Sungro Sunshine Mix #2, Agawam, MA, USA) to native soil extracted from **229** an agricultural field most recently planted with *G. max* at the USDA-ARS Lab-**230** oratory in Lubbock, TX, USA (33.59°N, -101.90°W). The field soil was classified **231** as Amarillo fine sandy loam (75% sand, 10% silt, 15% clay). Upon planting, **232** all *G. max* pots were inoculated with *Bradyrhizobium japonicum* (Verdesian N-**233** Dure™ Soybean, Cary, NC, USA) to stimulate root nodulation. Individuals of **234** both species were grown under similar, unshaded, ambient greenhouse conditions **235** for 2 weeks to germinate and begin vegetative growth.

236 Three blocks were set up in the greenhouse, each containing four light **237** treatments created using shade cloth that reduced incoming radiation by either 0 **238** (full sun), 30, 50, or 80%. Two weeks post-germination, individuals were randomly **239** placed in the four light treatments in each block. Individuals received one of four **240** nitrogen fertilization doses as 100ml of a modified Hoagland solution (Hoagland **241** and Arnon 1950) equivalent to either 0, 70, 210, or 630 ppm N twice per week **242** within each light treatment. Nitrogen fertilization doses were received as topical **243** agents to the soil surface. Each Hoagland solution was modified to keep concen-**244** trations of other macro- and micronutrients equivalent (Table A1). Plants were **245** routinely well watered to eliminate water stress.

246 2.2.2 *Plant measurements and calculations*

247 Each individual was harvested after 5 weeks of treatment, and biomass was sepa-
248 rated by organ type (leaves, stems, and roots). Nodules on *G. max* roots were also
249 harvested. Except for the 0% shade cover and 630 ppm N treatment combination,
250 all treatment combinations in both species had lower average dry biomass:pot vol-
251 ume ratios than the 1:1 ratio recommended by Poorter et al. (2012) to minimize
252 the likelihood of pot volume-induced growth limitation (Table A2; Table A3; Fig.
253 A1).

254 All harvested material was dried, weighed, and ground by organ type.
255 Carbon and nitrogen content (g g^{-1}) was determined by subsampling from ground
256 and homogenized biomass of each organ type using an elemental analyzer (Costech
257 4010; Costech, Inc., Valencia, CA, USA). I scaled these values to total leaf, stem,
258 and root carbon and nitrogen biomass (g) by multiplying dry biomass of each
259 organ type by carbon or nitrogen content of each corresponding organ type. Whole
260 plant nitrogen biomass (g) was calculated as the sum of total leaf (g), stem (g),
261 and root (g) nitrogen biomass. Root nodule carbon biomass was not included in
262 the calculation of root carbon biomass; however, relative plant investment toward
263 root or root nodule standing stock was estimated as the ratio of root biomass to
264 root nodule biomass (g g^{-1}), following similar metrics to those adopted by Dovrat
265 et al. (2018) and Dovrat et al. (2020).

266 Carbon costs to acquire nitrogen (N_{cost} ; gC gN^{-1}) were estimated as the
267 ratio of total root carbon biomass (C_{bg} ; gC) to whole-plant nitrogen biomass
268 (N_{wp} ; gN). This calculation quantifies the relationship between carbon spent on
269 nitrogen acquisition and whole plant nitrogen acquisition by using root carbon

270 biomass as a proxy for estimating the magnitude of carbon allocated toward ni-
271 trogen acquisition. This calculation therefore assumes that the magnitude of root
272 carbon standing stock is proportional to carbon transferred to root nodules or my-
273 corrhizae, or lost through root exudation or turnover. The assumption has been
274 supported in species that associate with ectomycorrhizal fungi (Hobbie 2006; Hob-
275 bie and Hobbie 2008), but is less clear in species that acquire nitrogen through
276 non-symbiotic active uptake or symbiotic nitrogen fixation. It is also unclear
277 whether relationships between root carbon standing stock and carbon transfer to
278 root nodules are similar in magnitude to carbon lost through exudation or when
279 allocated toward other active uptake pathways. Thus, because of the way mea-
280 surements were calculated, proximal values of carbon costs to acquire nitrogen are
281 underestimates.

282 2.2.3 *Statistical analyses*

283 I explored the effects of light and nitrogen availability on carbon costs to acquire
284 nitrogen using separate linear mixed-effects models for each species. Models in-
285 cluded shade cover, nitrogen fertilization, and interactions between shade cover
286 and nitrogen fertilization as continuous fixed effects, and also included block as a
287 random intercept term. Three separate models for each species were built with
288 this independent variable structure for three different dependent variables: (i)
289 carbon costs to acquire nitrogen (gC gN^{-1}); (ii) whole plant nitrogen biomass
290 (denominator of carbon cost to acquire nitrogen; gN); and (iii) belowground car-
291 bon biomass (numerator of carbon cost to acquire nitrogen; gC). I constructed two
292 additional models for *G. max* with the same model structure described above to

293 investigate the effects of light availability and nitrogen fertilization on root nodule
294 biomass (g) and the ratio of root nodule biomass to root biomass (unitless).

295 I used Shapiro–Wilk tests of normality to determine whether species spe-
296 cific linear mixed-effects model residuals followed a normal distribution. Zero
297 models satisfied residual normality assumptions when models were fit using un-
298 transformed data (Shapiro–Wilk: $p < 0.05$ in all cases). I attempted to satisfy
299 residual normality assumptions by first fitting models using dependent variables
300 that were natural-log transformed. If residual normality assumptions were still
301 not met (Shapiro–Wilk: $p < 0.05$), then models were fit using dependent variables
302 that were square root transformed. All residual normality assumptions were satis-
303 fied when models were fit with either a natural-log or square root transformation
304 (Shapiro–Wilk: $p > 0.05$ in all cases). Specifically, I natural-log transformed *G.*
305 *hirsutum* carbon costs to acquire nitrogen and *G. hirsutum* whole-plant nitrogen
306 biomass. I also square root transformed *G. max* carbon costs to acquire nitrogen,
307 *G. max* whole-plant nitrogen biomass, root carbon biomass in both species, *G.*
308 *max* root nodule biomass, and the *G. max* ratio of root nodule biomass to root
309 biomass. I used the ‘lmer’ function in the ‘lme4’ R package (Bates et al. 2015) to
310 fit each model and the ‘Anova’ function in the ‘car’ R package (Fox and Weisberg
311 2019) to calculate Wald’s χ^2 to determine the significance ($\alpha = 0.05$) of each fixed
312 effect coefficient. Finally, I used the ‘emmeans’ R package (Lenth 2019) to conduct
313 post-hoc comparisons of our treatment combinations using Tukey’s tests. Degrees
314 of freedom for all Tukey’s tests were approximated using the Kenward–Roger ap-
315 proach (Kenward and Roger 1997). All analyses and plots were conducted in R
316 version 4.0.1 (R Core Team 2021).

317 2.3 Results

318 2.3.1 *Carbon costs to acquire nitrogen*

319 Carbon costs to acquire nitrogen in *G. hirsutum* increased with increasing light
320 availability ($p<0.001$; Table 2.1; Fig. 2.1) and decreased with increasing nitrogen
321 fertilization ($p<0.001$; Table 2.1; Fig. 2.1). There was no interaction between
322 light availability and nitrogen fertilization ($p=0.486$, Table 2.1; Fig. 2.1).

323 Carbon costs to acquire nitrogen in *G. max* also increased with increasing
324 light availability ($p<0.001$, Table 2.1; Fig. 2.1) and decreased with increasing
325 nitrogen fertilization ($p<0.001$; Table 2.1; Fig. 2.1). There was no interaction
326 between light availability and nitrogen fertilization ($p=0.261$, Table 2.1; Fig. 2.1).

Table 2.1. Analysis of variance results exploring species-specific effects of light availability, nitrogen fertilization, and their interactions on carbon costs to acquire nitrogen (N_{cost} ; gC gN $^{-1}$), whole plant nitrogen biomass (N_{wp} ; gN), and root carbon biomass (C_{bg} ; gC)

	N_{cost}			N_{wp}			C_{bg}			
	df	Coefficient	χ^2	p	Coefficient	χ^2	p	Coefficient	χ^2	p
<i>G. hirsutum</i>										
Intercept		1.594	-	-	-3.232	-	-	0.432	-	-
Light (L)	1	-1.09E-02	56.494	<0.001	-6.41E-03	91.275	<0.001	-2.62E-03	169.608	<0.001
Nitrogen (N)	1	-1.34E-03	54.925	<0.001	1.83E-03	118.784	<0.001	1.15E-04	2.901	0.089
L*N	1	3.88E-06	0.485	0.486	-1.34E-05	10.721	0.001	-1.67E-06	3.140	0.076
<i>G. max</i>										
Intercept		1.877	-	-	0.239	-	-	0.438	-	-
Light (L)	1	-7.67E-03	174.156	<0.001	-6.72E-04	39.799	<0.001	-2.55E-03	194.548	<0.001
Nitrogen (N)	1	-2.35E-04	21.948	<0.001	1.55E-04	70.771	<0.001	2.52E-04	19.458	<0.001
L*N	1	-2.89E-06	1.262	0.261	-6.32E-07	1.435	0.231	-3.16E-06	10.803	0.001

16

327 *Significance determined using Wald's χ^2 tests ($p=0.05$). P -values less than 0.05 are in bold and p -values between
 328 0.05 and 0.1 are italicized. Negative coefficients for light treatments indicate a positive effect of increasing light
 329 availability on all response variables, as light availability is treated as percent shade cover in all linear mixed-effects
 330 models.

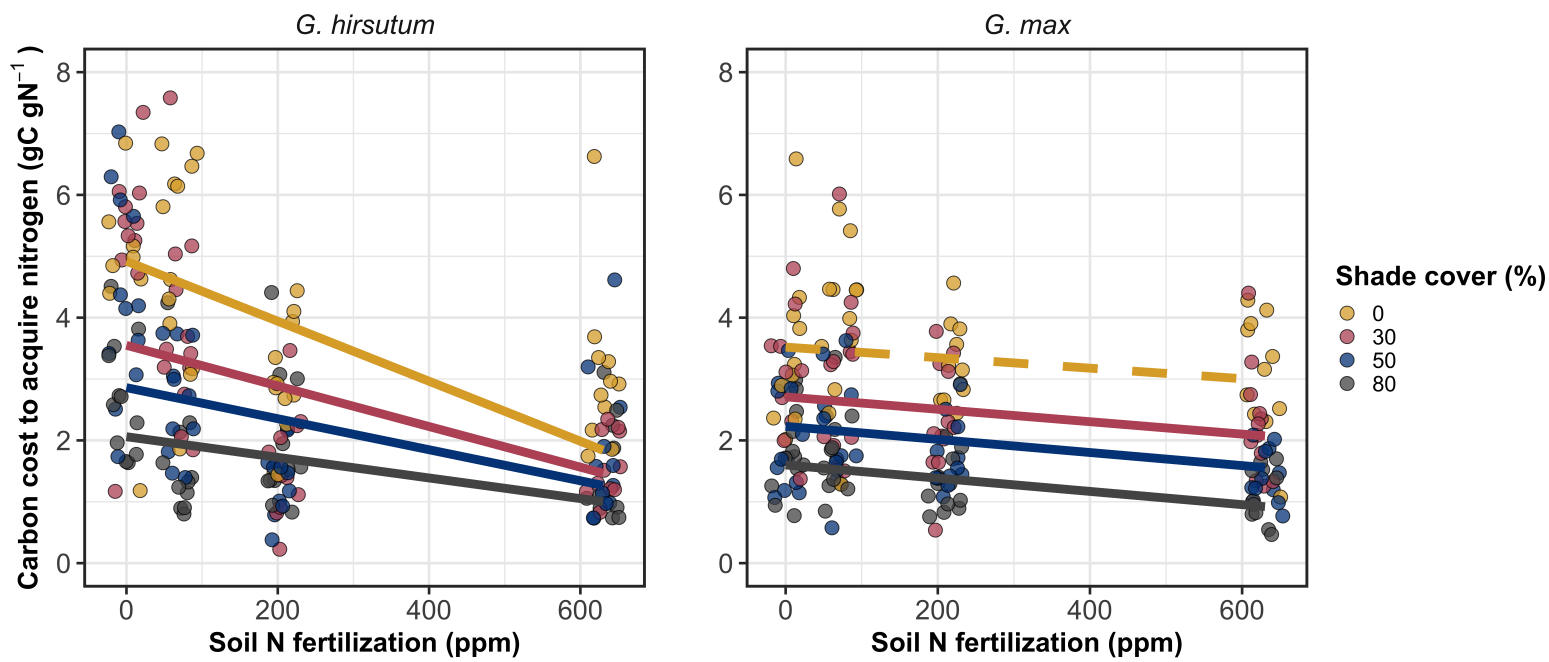


Figure 2.1. Relationships between soil nutrient fertilization and light availability on carbon costs to acquire nitrogen in *G. hirsutum* and *G. max*. Nitrogen fertilization treatments are represented on the x-axis. Shade cover treatments are represented through colored points and trendlines. Trendlines were created by back-transforming marginal mean slopes and intercepts from species-specific linear mixed-effects models. These values were calculated using the ‘emtrends’ and ‘emmeans’ functions in the ‘emmeans’ R package (Lenth, 2019). Yellow points and trendlines represent the 0% shade cover treatment, red points and trendlines represent the 30% shade cover treatment, blue points and trendlines represent the 50% shade cover treatment, and gray points and trendlines represent the 80% shade cover treatment. Solid trendlines indicate slopes that are significantly different from zero (Tukey: $p < 0.05$), while dashed trendlines indicate slopes that are not statistically different from zero.

331 2.3.2 *Whole plant nitrogen biomass*

332 Whole plant nitrogen biomass in *G. hirsutum* was driven by an interaction between
333 light availability and nitrogen fertilization ($p=0.001$; Table 2.1; Fig. 2.2). This
334 interaction indicated a greater stimulation of whole-plant nitrogen biomass by
335 nitrogen fertilization as light levels increased (Table 2.1; Fig. 2.2).

336 Whole plant nitrogen biomass in *G. max* increased with increasing light
337 availability ($p<0.001$) and nitrogen fertilization ($p<0.001$), with no interaction
338 between light availability and nitrogen fertilization ($p=0.231$; Table 2.1; Fig. 2.2).

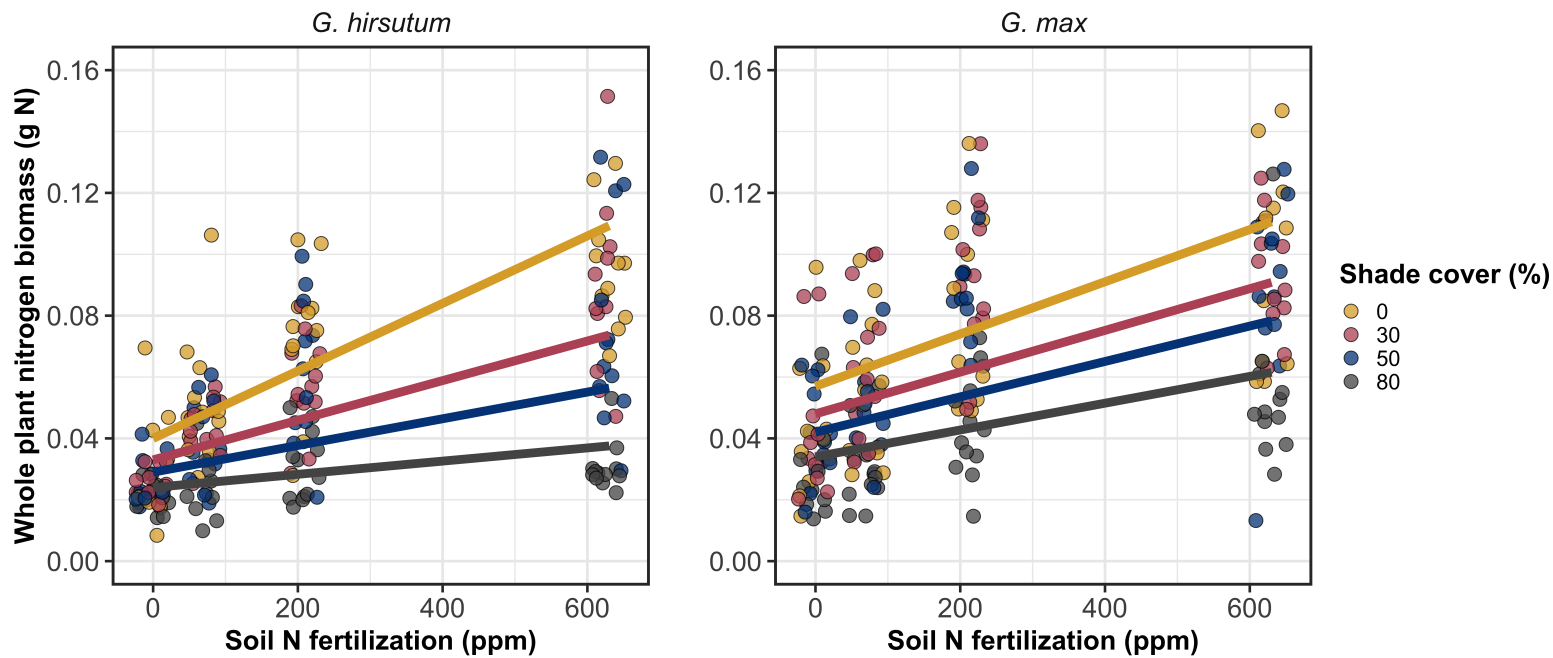


Figure 2.2. Relationships between soil nutrient fertilization and light availability on whole-plant nitrogen biomass in *G. hirsutum* and *G. max*. Whole-plant nitrogen biomass is the denominator of the carbon cost to acquire nitrogen calculation. Nitrogen fertilization treatments are represented on the x-axis. Shade cover treatments are represented through colored points and trendlines. Trendlines were created by back-transforming marginal mean slopes and intercepts from species-specific linear mixed-effects models. These values were calculated using the ‘emtrends’ and ‘emmeans’ functions in the ‘emmeans’ R package (Lenth 2019). Points are jittered for visibility. Colored points and trendlines are as explained in Fig. 2.1. Solid trendlines indicate slopes that are significantly different from zero (Tukey: $p < 0.05$), while dashed trendlines indicate slopes that are not statistically different from zero.

339 2.3.3 *Root carbon biomass*

340 Root carbon biomass in *G. hirsutum* significantly increased with increasing light
341 availability ($p<0.001$; Table 2.1; Fig. 2.3) and marginally increased with nitrogen
342 fertilization ($p=0.089$; Table 2.1; Fig. 2.3). There was also a marginal interaction
343 between light availability and nitrogen fertilization ($p=0.076$; Table 2.1), driven by
344 an increase in the positive response of root carbon biomass to increasing nitrogen
345 fertilization as light availability increased (Table 2.3). This resulted in significantly
346 positive trends between root carbon biomass and nitrogen fertilization in the two
347 highest light treatments (Tukey: $p<0.05$ in both cases; Table 2.3; Fig. 2.3) and no
348 effect of nitrogen fertilization in the two lowest light treatments (Tukey: $p>0.05$
349 in both cases; Table 2.3; Fig. 2.3).

350 There was an interaction between light availability and nitrogen fertiliza-
351 tion on root carbon biomass in *G. max* ($p=0.001$; Table 2.1; Fig. 2.3). Post-hoc
352 analyses indicated that the positive effects of nitrogen fertilization on *G. max*
353 root carbon biomass increased with increasing light availability (Table 2.3; Fig.
354 2.3). There were also positive individual effects of increasing nitrogen fertilization
355 ($p<0.001$) and light availability ($p<0.001$) on *G. max* root carbon biomass (Table
356 2.1; Fig. 2.3).

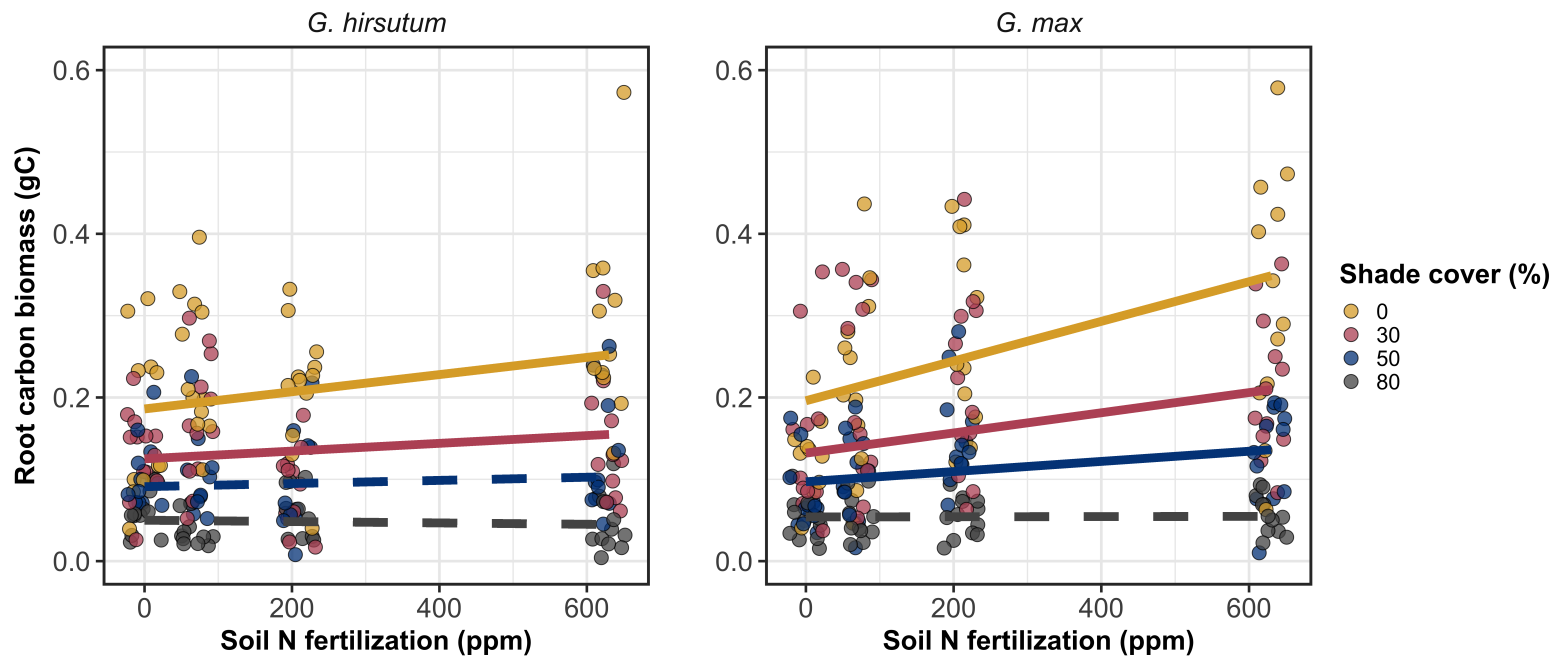


Figure 2.3. Relationships between soil nutrient fertilization and light availability on root carbon biomass in *G. hirsutum* and *G. max*. Root carbon biomass is the numerator of the carbon cost to acquire nitrogen calculation. Nitrogen fertilization treatments are represented on the x-axis. Colored points and trendlines are as explained in Fig. 2.1. Trendlines were created by back-transforming marginal mean slopes and intercepts from species-specific linear mixed-effects models. These values were calculated using the ‘emtrends’ and ‘emmeans’ functions in the ‘emmeans’ R package (Lenth 2019). Points are jittered for visibility. Colored points and trendlines are as explained in Fig. 2.1.

357 2.3.4 *Root nodule biomass*

358 Root nodule biomass in *G. max* increased with increasing light availability ($p<0.001$);
359 Table 2.2; Fig. 2.4a) and decreased with increasing nitrogen fertilization ($p<0.001$;
360 Table 2.2; Fig. 2.4a). There was no interaction between nitrogen fertilization and
361 light availability ($p=0.133$; Table 2.2; Fig. 2.4a). The ratio of root nodule biomass
362 to root biomass did not change in response to light availability ($p=0.481$; Table
363 2.2; Fig. 2.4b) but decreased with increasing nitrogen fertilization ($p<0.001$; Ta-
364 ble 2.2; Fig. 2.4b). There was no interaction between nitrogen fertilization and
365 light availability on the ratio of root nodule biomass to root biomass ($p=0.621$;
366 Table 2.2; Fig. 2.4b).

Table 2.2. Analysis of variance results exploring effects of light availability, nitrogen fertilization, and their interactions on *G. max* root nodule biomass and the ratio of root nodule biomass to root biomass*

	Nodule biomass			Nodule biomass: root biomass			<i>p</i>
	df	Coefficient	χ^2	<i>p</i>	Coefficient	χ^2	
(Intercept)		0.302	-	-	0.448	-	-
Light (L)	1	-1.81E-03	72.964	<0.001	-8.76E-05	0.496	0.481
Nitrogen (N)	1	-2.83E-04	115.377	<0.001	-5.09E-04	156.476	<0.001
L*N	1	1.14E-06	2.226	0.133	-7.30E-07	0.244	0.621

367 *Significance determined using Wald's χ^2 tests ($\alpha=0.05$). *P*-values less than 0.05 are in bold. Negative coefficients for
 368 light treatments indicate a positive effect of increasing light availability on all response variables, as light availability
 369 is treated as percent shade cover in all linear mixed-effects models. Root nodule biomass and nodule biomass: root
 370 biomass models were only constructed for *G. max* because *G. hirsutum* was not inoculated with *B. japonicum* and
 371 is not capable of forming root nodules.

Table 2.3. Slopes of the regression line describing the relationship between each dependent variable and nitrogen fertilization at each light level*

Shade cover	Carbon cost to acquire nitrogen	Whole plant nitrogen biomass	Belowground carbon biomass	Root nodule biomass	Nodule biomass: root biomass
<i>G. hirsutum</i>					
0%	-1.34E-03^a	1.83E-03^a	1.15E-04^b	-	-
30%	-1.22E-03^a	1.43E-03^a	1.17E-04^b	-	-
50%	-1.14E-03^a	1.17E-03^a	3.12E-05 ^b	-	-
80%	-1.02E-03^a	7.66E-04^a	-1.89E-06 ^b	-	-
<i>G. max</i>					
0%	-2.35E-04 ^b	1.55E-05^b	2.51E-04^b	-2.83E-04^b	-5.09E-04^b
30%	-3.22E-04^b	1.35E-05^b	1.57E-04^b	-2.49E-04^b	-5.31E-04^b
50%	-3.80E-04^b	1.23E-05^b	9.37E-05^b	-2.26E-04^b	-5.45E-04^b
80%	-4.66E-04^b	1.04E-05^b	-9.95E-07 ^b	-1.92E-04^b	-5.67E-04^b

24

372 * Slopes represent estimated marginal mean slopes from linear mixed-effects models described in the Methods. Slopes
373 were calculated using the ‘emmeans’ R package (Lenth 2019). Superscripts indicate slopes fit to natural-log (^a) or
374 square root (^b) transformed data. Slopes statistically different from zero (Tukey: $p<0.05$) are indicated in bold.
375 Marginally significant slopes (Tukey: $0.05< p<0.1$) are italicized.

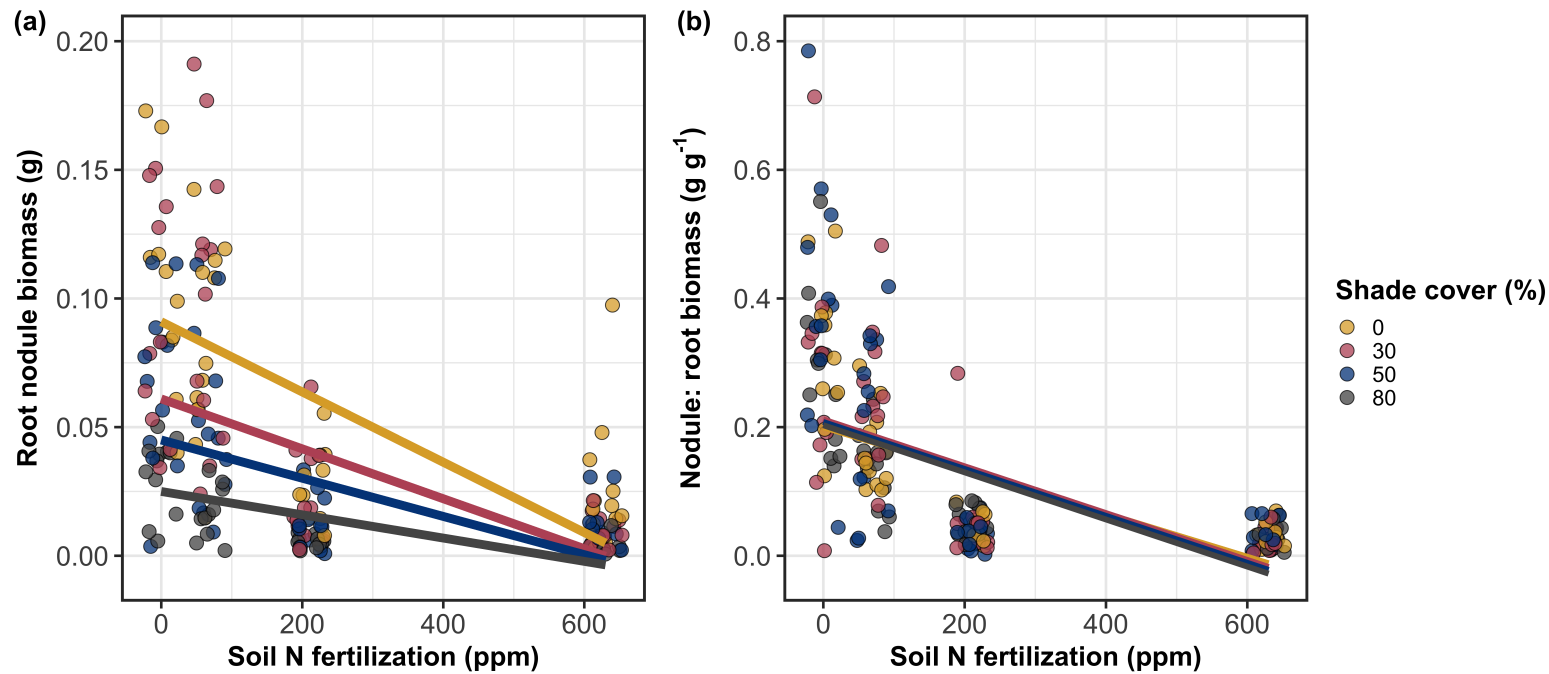


Figure 2.4. Effects of shade cover and nitrogen fertilization on root nodule biomass (a) and the ratio of root nodule biomass to root biomass (b) in *G. max*. Nitrogen fertilization treatments are represented on the x-axis. Shade cover treatments are represented through colored points and trendlines. Trendlines were created by back-transforming marginal mean slopes and intercepts from species-specific linear mixed-effects models. These values were calculated using the ‘emtrends’ and ‘emmmeans’ functions in the ‘emmeans’ R package (Lenth 2019). Points are jittered for visibility. Yellow points and trendlines represent the 0% shade cover treatment, blue points and trendlines represent the 30% shade cover treatment, green points and trendlines represent the 50% shade cover treatment, and purple points and trendlines represent the 80% shade cover treatment. Solid trendlines indicate slopes that are significantly different from zero (Tukey: $p < 0.05$), while dashed trendlines indicate slopes that are not statistically different from zero.

376 2.4 Discussion

377 In this chapter, I determined the effects of light availability and soil nitrogen
378 fertilization on root mass carbon costs to acquire nitrogen in *G. hirsutum* and *G.*
379 *max*. In support of my hypotheses, I found that carbon costs to acquire nitrogen
380 generally increased with increasing light availability and decreased with increasing
381 soil nitrogen fertilization in both species. These findings suggest that carbon costs
382 to acquire nitrogen are determined by factors that influence plant nitrogen demand
383 and soil nitrogen availability. In contrast to my second hypothesis, root nodulation
384 data suggested that *G. max* and *G. hirsutum* achieved similar directional carbon
385 cost responses to nitrogen fertilization despite a likely shift in *G. max* allocation
386 from nodulation to root biomass along the nitrogen fertilization gradient.

387 2.4.1 *Carbon costs to acquire nitrogen increase with light availability and*
388 *decrease with fertilization*

389 Both *G. max* and *G. hirsutum* experienced an increase in carbon costs to ac-
390 quire nitrogen due to increasing light availability. These patterns were driven by
391 a larger increase in root carbon biomass than whole-plant nitrogen biomass. In-
392 creases in root carbon biomass due to factors that increase plant nitrogen demand
393 are a commonly observed pattern, as carbon allocated belowground provides sub-
394 strate needed to produce and maintain structures that satisfy aboveground plant
395 nitrogen demand (Nadelhoffer and Raich 1992; Giardina et al. 2005; Raich et al.
396 2014). Findings suggest that plants allocate relatively more carbon for acquiring
397 nitrogen when demand increases over short temporal scales, which may cause a
398 temporary state of diminishing return due to asynchrony between belowground

399 carbon and whole-plant nitrogen responses to plant nitrogen demand (Kulmatiski
400 et al. 2017; Noyce et al. 2019). These responses might be attributed to a temporal
401 lag associated with producing structures that enhance nitrogen acquisition. For
402 example, fine roots (Matamala and Schlesinger 2000; Norby et al. 2004; Arndal
403 et al. 2018) and root nodules (Parvin et al. 2020) take time to build and first
404 require the construction of coarse roots. Thus, full nitrogen returns from these
405 investments may not occur immediately (Kayler et al. 2010; Kayler et al. 2017),
406 and may vary by species acquisition strategy. I speculate that increases in ni-
407 trogen acquisition from a given carbon investment may occur beyond the 5-week
408 scope of this experiment. A similar study conducted over a longer temporal scale
409 would address this.

410 Increasing soil nitrogen fertilization generally decreased carbon costs to
411 acquire nitrogen in both species. These patterns were driven by a larger increase
412 in whole-plant nitrogen biomass than root carbon biomass. In *G. hirsutum*, re-
413 ductions in carbon costs to acquire nitrogen may have been due to an increase in
414 per-root nitrogen uptake, allowing individuals to maximize the amount of nitro-
415 gen acquired from a belowground carbon investment. Interestingly, increased soil
416 nitrogen fertilization increased whole-plant nitrogen biomass in *G. max* despite
417 reductions in root nodule biomass that likely reduced the nitrogen-fixing capac-
418 ity of *G. max* (Andersen et al. 2005; Muñoz et al. 2016). While reductions in
419 root nodulation due to increased soil nitrogen availability are commonly observed
420 (Gibson and Harper 1985; Fujikake et al. 2003), root nodulation responses were
421 observed in tandem with increased root carbon biomass, implying that *G. max*
422 shifted relative carbon allocation from nitrogen fixation to soil nitrogen acquisition

423 (Markham and Zekveld 2007; Dovrat et al. 2020). This was likely because there
424 was a reduction in the carbon cost advantage of acquiring fixed nitrogen relative
425 to soil nitrogen, and suggests that species capable of associating with symbiotic
426 nitrogen-fixing bacteria shift their relative nitrogen acquisition pathway to opti-
427 mize nitrogen uptake (Rastetter et al. 2001). Future studies should investigate
428 these patterns with a larger quantity of phylogenetically related species, or differ-
429 ent varieties of a single species that differ in their ability to form associations with
430 symbiotic nitrogen-fixing bacteria to more directly test the impact of nitrogen
431 fixation on the patterns observed in this study.

432 2.4.2 *Modeling implications*

433 Carbon costs to acquire nitrogen are subsumed in the general discussion of eco-
434 nomic analogies to plant resource uptake (Bloom et al. 1985; Rastetter et al.
435 2001; Vitousek et al. 2002; Phillips et al. 2013; Terrer et al. 2018; Henneron
436 et al. 2020). Despite this, terrestrial biosphere models rarely include costs of
437 nitrogen acquisition within their framework for predicting plant nitrogen uptake.
438 There is currently one plant resource uptake model, FUN, that quantitatively
439 predicts carbon costs to acquire nitrogen within a framework for predicting plant
440 nitrogen uptake for different nitrogen acquisition strategies (Fisher et al. 2010;
441 Brzostek et al. 2014). Iterations of FUN are currently coupled to two terrestrial
442 biosphere models: the Community Land Model 5.0 and the Joint UK Land En-
443 vironment Simulator (Shi et al. 2016; Lawrence et al. 2019; Clark et al. 2011).
444 Recent work suggests that coupling FUN to CLM 5.0 caused a large overpredic-
445 tion of plant nitrogen uptake associated with nitrogen fixation (Davies-Barnard

446 et al. 2020) compared to other terrestrial biosphere model products. Thus, em-
447 pirical data from manipulative experiments that explicitly quantify carbon costs
448 to acquire nitrogen in species capable of associating with nitrogen-fixing bacteria
449 across different environmental contexts is an important step toward identifying
450 potential biases in models such as FUN.

451 These findings broadly support the FUN formulation of carbon costs to
452 acquire nitrogen in response to soil nitrogen availability. FUN calculates carbon
453 costs to acquire nitrogen based on the sum of carbon costs to acquire nitrogen
454 via nitrogen fixation, mycorrhizal active uptake, non-mycorrhizal active uptake,
455 and retranslocation (Fisher et al. 2010; Brzostek et al. 2014). Carbon costs to
456 acquire nitrogen via mycorrhizal or non-mycorrhizal active uptake pathways are
457 derived as a function of nitrogen availability, root biomass, and two parameterized
458 values based on nitrogen acquisition strategy (Brzostek et al. 2014). Due to this,
459 FUN simulates a net decrease in carbon costs to acquire nitrogen with increasing
460 nitrogen availability for mycorrhizal and non-mycorrhizal active uptake pathways,
461 assuming constant root biomass. This was a pattern I observed in *G. hirsutum* re-
462 gardless of light availability. In contrast, FUN would not simulate a net change in
463 carbon costs to acquire nitrogen via nitrogen fixation due to nitrogen availability.
464 This is because carbon costs to acquire nitrogen via nitrogen fixation are derived
465 from a well established function of soil temperature, which is independent of soil
466 nitrogen availability (Houlton et al. 2008; Fisher et al. 2010). I observed a net
467 reduction in carbon costs to acquire nitrogen in *G. max*, except when individu-
468 als were grown under 0% shade cover. While a net reduction of carbon costs in
469 response to nitrogen fertilization runs counter to nitrogen fixation carbon costs

470 simulated by FUN, these patterns were likely because *G. max* individuals switched
471 their primary mode of nitrogen acquisition from symbiotic nitrogen fixation to a
472 non-symbiotic active uptake pathway.

473 2.4.3 *Study limitations*

474 It should be noted that the metric used in this study to determine carbon costs
475 to acquire nitrogen has several limitations. Most notably, this metric uses root
476 carbon biomass as a proxy for estimating the amount of carbon spent on nitrogen
477 acquisition. While it is true that most carbon allocated belowground has at least
478 an indirect structural role in acquiring soil resources, it remains unclear whether
479 this assumption holds true for species that acquire nitrogen via symbiotic nitro-
480 gen fixation. I also cannot quantify carbon lost through root exudates or root
481 turnover, which may increase due to factors that increase plant nitrogen demand
482 (Tingey et al. 2000; Phillips et al. 2011), and can increase the magnitude of
483 available nitrogen from soil organic matter through priming effects on soil micro-
484 bial communities (Uselman et al. 2000; Bengtson et al. 2012). It is also not
485 clear whether these assumptions hold under all environmental conditions, such
486 as those that shift belowground carbon allocation toward a different mode of ni-
487 trogen acquisition (Taylor and Menge 2018; Friel and Friesen 2019) or between
488 species with different acquisition strategies. In this study, increasing soil nitrogen
489 fertilization increased carbon investment to roots relative to carbon transferred to
490 root nodules. By assuming that carbon allocated to root carbon was proportional
491 to carbon allocated to root nodules across all treatment combinations, these ob-
492 served responses to soil nitrogen fertilization were likely to be overestimated in *G.*

493 *max*. I encourage future research to quantify these carbon fates independently.

494 Researchers conducting pot experiments must carefully choose pot volume
495 to minimize the likelihood of growth limitations induced by pot volume (Poorter
496 et al. 2012). Poorter et al. (2012) indicate that researchers are likely to avoid
497 growth limitations associated with pot volume if measurements are collected when
498 the plant biomass:pot volume ratio is less than 1 g L^{-1} . In this experiment, all
499 treatment combinations in both species had biomass:pot volume ratios less than
500 1 g L^{-1} except for *G. max* and *G. hirsutum* that were grown under 0% shade
501 cover and had received 630 ppm N. Specifically, *G. max* and *G. hirsutum* had
502 average respective biomass:pot volume ratios of $1.24 \pm 0.07 \text{ g L}^{-1}$ and 1.34 ± 0.13
503 g L^{-1} , when grown under 0% shade cover and received 630 ppm N (Table A2;
504 Table A3; Fig. A1). If growth in this treatment combination was limited by pot
505 volume, then individuals may have had larger carbon costs to acquire nitrogen
506 than would be expected if they were grown in larger pots. This pot volume
507 induced growth limitation could cause a reduction in per-root nitrogen uptake
508 associated with more densely packed roots, which could reduce the positive effect
509 of nitrogen fertilization on whole-plant nitrogen biomass relative to root carbon
510 biomass (Poorter et al. 2012).

511 Growth limitation associated with pot volume provides a possible expla-
512 nation for the marginally insignificant effect of increasing nitrogen fertilization on
513 *G. max* carbon costs to acquire nitrogen when grown under 0% shade cover. This
514 is because the regression line describing the relationship between carbon costs to
515 acquire nitrogen and nitrogen fertilization in *G. max* grown under 0% shade cover
516 would have flattened if growth limitation had caused larger than expected carbon

517 costs to acquire nitrogen in the 0% shade cover, 630 ppm N treatment combi-
518 nation. This may have been exacerbated by the fact that *G. max* likely shifted
519 relative carbon allocation from nitrogen fixation to soil nitrogen acquisition, which
520 could have increased the negative effect of more densely packed roots on nitrogen
521 uptake. These patterns could have also occurred in *G. hirsutum* grown under 0%
522 shade cover; however, there was no change in the effect of nitrogen fertilization on
523 *G. hirsutum* carbon costs to acquire nitrogen grown under 0% shade cover relative
524 to other shade cover treatments. Regardless, the possibility of growth limitation
525 due to pot volume suggests that effects of increasing nitrogen fertilization on car-
526 bon costs to acquire nitrogen in both species grown under 0% shade cover could
527 have been underestimated. Follow-up studies using a similar experimental design
528 with a larger pot volume would be necessary in order to determine whether these
529 patterns were impacted by pot volume-induced growth limitation.

530 2.4.4 *Conclusions*

531 In conclusion, this chapter provides empirical evidence that carbon costs to ac-
532 quire nitrogen are influenced by light availability and soil nitrogen fertilization
533 in a species capable of acquiring nitrogen via symbiotic nitrogen fixation and a
534 species not capable of forming such associations. We show that carbon costs to
535 acquire nitrogen generally increase with increasing light availability and decrease
536 with increasing nitrogen fertilization. This chapter provides important empirical
537 data needed to evaluate the formulation of carbon costs to acquire nitrogen in
538 terrestrial biosphere models, particularly carbon costs to acquire nitrogen that
539 are associated with symbiotic nitrogen fixation. My findings broadly support the

540 general formulation of these carbon costs in the FUN biogeochemical model in
541 response to shifts in nitrogen availability. However, there is a need for future
542 studies to explicitly quantify carbon costs to acquire nitrogen under different en-
543 vironmental contexts, over longer temporal scales, and using larger selections of
544 phylogenetically related species. In addition, I suggest that future studies mini-
545 mize the limitations associated with the metric used here by explicitly measuring
546 belowground carbon fates independently.

547

Chapter 3

548 Soil nitrogen availability modifies leaf nitrogen economies in mature
549 temperate deciduous forests: a direct test of photosynthetic least-cost
550 theory

551 3.1 Introduction

552 Photosynthesis represents the largest carbon flux between the atmosphere and
553 land surface (IPCC 2021), and plays a central role in biogeochemical cycling at
554 multiple spatial and temporal scales (Vitousek and Howarth 1991; LeBauer and
555 Treseder 2008; Kaiser et al. 2015; Wieder et al. 2015). Therefore, carbon and
556 energy fluxes simulated by terrestrial biosphere models are sensitive to the formu-
557 lation of photosynthetic processes (Ziehn et al. 2011; Bonan et al. 2011; Booth
558 et al. 2012; Smith et al. 2016; Smith et al. 2017) and must be represented using
559 robust, empirically tested processes (Prentice et al. 2015; Wieder et al. 2019).
560 Current formulations of photosynthesis vary across terrestrial biosphere models
561 (Smith and Dukes 2013; Rogers et al. 2017), which causes variation in modeled
562 ecosystem processes (Knorr 2000; Knorr and Heimann 2001; Bonan et al. 2011;
563 Friedlingstein et al. 2014) and casts uncertainty on the ability of these models to
564 accurately predict terrestrial ecosystem responses and feedbacks to global change
565 (Zaehle et al. 2005; Schaefer et al. 2012; Davies-Barnard et al. 2020).

566 Terrestrial biosphere models commonly represent C₃ photosynthesis th-
567 rough variants of the Farquhar et al. (1980) biochemical model (Smith and Dukes
568 2013; Rogers 2014; Rogers et al. 2017). This well-tested photosynthesis model
569 estimates leaf-level carbon assimilation, or photosynthetic capacity, as a function
570 of the maximum rate of Ribulose-1,5-bisphosphate carboxylase-oxygenase (Ru-

571 bisco) carboxylation (V_{cmax}) and the maximum rate of Ribulose-1,5-bisphosphate
572 (RuBP) regeneration (J_{max}) (Farquhar et al. 1980). Many terrestrial biosphere
573 models predict these model inputs based on plant functional group specific lin-
574 ear relationships between leaf nutrient content and V_{cmax} (Smith and Dukes 2013;
575 Rogers 2014; Rogers et al. 2017) under the tenet that a large fraction of leaf nutri-
576 ents, and nitrogen in particular, are partitioned toward building and maintaining
577 enzymes that support photosynthetic capacity, such as Rubisco (Brix 1971; Gul-
578 mon and Chu 1981; Evans 1989; Kattge et al. 2009; Walker et al. 2014). Terres-
579 trial biosphere models predict leaf nutrient content from soil nutrient availability
580 based on the assumption that increasing soil nutrients generally increases leaf nu-
581 trients (Firn et al. 2019; Li et al. 2020; Liang et al. 2020) which, in the case of
582 nitrogen, generally corresponds with an increase in photosynthetic processes (Li
583 et al. 2020; Liang et al. 2020).

584 Recent work calls the generality of relationships between soil nutrient avail-
585 ability, leaf nutrient content, and photosynthetic capacity into question, suggest-
586 ing instead that leaf nutrients and photosynthetic capacity are better predicted as
587 an integrated product of aboveground climate, leaf traits, and soil nutrient avail-
588 ability, rather than soil nutrient availability alone (Dong et al. 2017; Dong et al.
589 2020; Dong et al. 2022; Firn et al. 2019; Smith et al. 2019; Peng et al. 2021).
590 It has been reasoned that this result is because plants allocate added nutrients to
591 growth and storage rather than alterations in leaf chemistry (Smith et al. 2019),
592 perhaps as a result of nutrient limitation of primary productivity (LeBauer and
593 Treseder 2008; Fay et al. 2015). Additionally, recent work suggests that relation-
594 ships between leaf nutrient content and photosynthesis vary across environments,

595 and that the proportion of leaf nutrient content allocated to photosynthetic tis-
596 sue varies over space and time with plant acclimation and adaptation responses
597 to light availability, vapor pressure deficit, soil pH, soil nutrient availability, and
598 environmental factors that influence leaf mass per area (Pons and Pearcy 1994;
599 Niinemets and Tenhunen 1997; Evans and Poorter 2001; Hikosaka and Shigeno
600 2009; Ghimire et al. 2017; Onoda et al. 2017; Luo et al. 2021). The use of linear
601 relationships between leaf nutrient content and V_{cmax} to predict photosynthetic
602 capacity, as commonly used in terrestrial biosphere models (Rogers 2014), is not
603 capable of detecting such responses.

604 Photosynthetic least-cost theory provides an alternative framework for un-
605 derstanding relationships between soil nutrient availability, leaf nutrient content,
606 and photosynthetic capacity (Harrison et al. 2021). Leveraging a two-input mi-
607 croeconomics approach (Wright et al. 2003), the theory posits that plants accli-
608 mate to a given environment by optimizing leaf photosynthesis rates at the lowest
609 summed cost of using nutrients and water (Prentice et al. 2014; Wang et al. 2017;
610 Smith et al. 2019; Paillassa et al. 2020). Across resource availability gradients,
611 the theory predicts that optimal photosynthetic rates can be achieved by trading
612 less efficient use of a resource that is less costly to acquire (or more abundant)
613 for more efficient use of a resource more costly to acquire (or less abundant). For
614 example, an increase in soil nutrient availability should reduce the cost of acquir-
615 ing and using nutrients (Bae et al. 2015; Eastman et al. 2021; Perkowski et al.
616 2021), which could increase leaf nutrient investments in photosynthetic proteins to
617 allow similar photosynthetic rates to be achieved with higher nutrient use (lower
618 nutrient use efficiency) but lower water use (greater water use efficiency). The

619 theory suggests similar tradeoffs in response to increasing soil pH (Paillassa et al.
620 2020), specifically, that increasing soil pH should reduce the cost of acquiring soil
621 nutrients due to an increase in plant-available nutrient concentration (Paillassa
622 et al. 2020; Dong et al. 2022). The theory is also capable of reconciling dynamic
623 leaf nutrient-photosynthesis relationships at global scales (Luo et al. 2021).

624 Patterns expected from photosynthetic least-cost theory have recently re-
625 ceived empirical support both in global environmental gradient (Smith et al.
626 2019; Paillassa et al. 2020; Luo et al. 2021; Querejeta et al. 2022; Wester-
627 band et al. 2023) and local manipulative invasion (Bialic-Murphy et al. 2021)
628 studies. However, nutrient addition experiments that directly examine nutrient-
629 water use tradeoffs expected from the theory are rare (but see Guerrieri et al.
630 2011), and only global gradient studies testing the theory have considered soil pH
631 in their analyses. As a result, there is a need to use nutrient addition and soil pH
632 manipulation experiments to test mechanisms driving responses predicted by the
633 theory.

634 In this study, I measured leaf responses to soil nitrogen availability in five
635 deciduous tree species growing in the upper canopy of mature closed canopy tem-
636 perate forests in the northeastern United States. Soil nitrogen availability and pH
637 were manipulated through a nitrogen-by-pH field manipulation experiment with
638 treatments applied since 2011, eight years prior to measurement. Two different
639 soil nitrogen treatments were applied to increase nitrogen availability with op-
640 posing effects on soil pH. An additional N-free acidifying treatment was expected
641 to decrease soil pH. I hypothesized that increased soil nitrogen availability would
642 enable plants to increase nutrient uptake and create more photosynthetic enzymes

643 per leaf, allowing similar photosynthetic rates achieved with lower leaf C_i:C_a and
644 increased leaf nitrogen content allocated to photosynthetic leaf tissue. I expected
645 that this response would be driven by a reduction in the cost of acquiring nitrogen,
646 which would cause trees to sacrifice efficient nitrogen use to enable more efficient
647 use of other limiting resources (i.e., water). Finally, I hypothesized similar leaf
648 responses to increasing soil pH.

649 3.2 Methods

650 3.2.1 *Study site description*

651 I conducted this study in summer 2019 at three stands located within a 20-km ra-
652 dius of Ithaca, NY, USA (42.444 °N, 76.502 °W). All stands contain mature,
653 closed-canopy forests dominated by deciduous tree species. Stands contained
654 abundant sugar maple (*Acer saccharum* Marshall), American beech (*Fagus gran-*
655 *difolia* Ehrh.), and white ash (*Fraxinus americana* L.), accounting for 43%, 15%,
656 and 17% of the total aboveground biomass across the three stands, respectively,
657 with less frequent red maple (*Acer rubrum* L.; 9% of total aboveground biomass)
658 and red oak occurrences (*Quercus rubra* L.; 10% of total aboveground biomass).
659 Soils at each site were broadly classified as a channery silt loam Inceptisols using
660 the USDA NRCS Web Soil Survey data product (Soil Survey Staff 2022). Between
661 2006 and 2020, study sites averaged 972 mm of precipitation per year and had an
662 average temperature of 7.9 °C per a weather station located near the Cornell Uni-
663 versity campus (42.449 °N, 76.449 °W) part of the NOAA NCEI Global Historical
664 Climatology Network (Menne et al. 2012).

665 3.2.2 *Experimental design*

666 Four 40 m x 40 m plots were set up at each site in 2009, each with an additional
667 10 m buffer along plot perimeters (60 m x 60 m total). The plots were set up as a
668 nitrogen-by-pH field manipulation experiment, with one each of four treatments
669 at each site. Two nitrogen treatments were applied, both at $50 \text{ kg N ha}^{-1} \text{ yr}^{-1}$, as
670 either sodium nitrate (NaNO_3) to raise soil pH, or ammonium sulfate ($(\text{NH}_4)_2\text{SO}_4$)
671 to acidify; an elemental sulfur treatment was selected to acidify without nitrogen,
672 applied at the same rate of S addition ($57 \text{ kg S ha}^{-1} \text{ yr}^{-1}$); and control plots
673 received no additions. All amendments were added in pelletized form using hand-
674 held fertilizer spreaders to both the main plots and buffers. Amendments were
675 divided into three equal doses distributed across the growing season from 2011-
676 2017 and added as a single dose from 2018 onward. During 2019, plots were
677 fertilized during the week of May 20.

678 3.2.3 *Leaf gas exchange and trait measurements*

679 I sampled one leaf each from 6 to 10 individuals per plot between June 25 and
680 July 12, 2019 for gas exchange measurements (Table B1). Leaves were collected
681 from deciduous broadleaf trees represented across all sites and plots and were
682 replicated in efforts to mimic the species abundance of each plot at each site.
683 We also attempted to collect leaves from the upper canopy to reduce differential
684 shading effects on leaf physiology. Leaves were accessed by pulling down small
685 branches using an arborist's slingshot and weighted beanbag attached to a throw
686 line. Branches were immediately recut under deionized water and remained sub-
687 merged to reduce stomatal closure and avoid xylem embolism, as done in Smith

688 and Dukes (2018), until gas exchange data were collected.

689 Randomly selected leaves with little to no visible external damage were
690 attached to a Li-COR LI-6800 (Li-COR Bioscience, Lincoln, Nebraska, USA)
691 portable photosynthesis machine to measure net photosynthesis (A_{net} ; $\mu\text{mol m}^{-2}$
692 s^{-1}), stomatal conductance (g_{sw} ; $\text{mol m}^{-2} \text{s}^{-1}$), and intercellular CO_2 concentra-
693 tion (C_i ; $\mu\text{mol mol}^{-1}$) at different reference CO_2 concentrations (C_a ; $\mu\text{mol mol}^{-1}$)
694 concentrations (i.e., an A_{net}/C_i curve) under saturating light conditions (2,000
695 $\mu\text{mol m}^{-2} \text{s}^{-1}$). Reference CO_2 concentrations followed the sequence: 400, 300,
696 200, 100, 50, 400, 400, 600, 800, 1000, 1200, 1500, and 2000 $\mu\text{mol mol}^{-1} \text{CO}_2$. Leaf
697 temperatures were not controlled in the cuvette and ranged from 21.8 °C to 31.7
698 °C (mean±SD: 27.2 ± 2.2 °C). A linear and second order log-polynomial nonlinear
699 regression suggested no effect of temperature on stomatal conductance measured
700 at 400 $\mu\text{mol mol}^{-1} \text{CO}_2$ or net photosynthesis measured at 400 $\mu\text{mol mol}^{-1} \text{CO}_2$
701 (Table B2-B3; Fig. B1). All A_{net}/C_i curves were generated within one hour of
702 branch severance.

703 Leaf morphological and chemical traits were collected on the same leaf used
704 to generate each A_{net}/C_i curve. Images of each leaf were taken using a flat-bed
705 scanner to determine fresh leaf area using the ‘LeafArea’ R package (Katabuchi
706 2015), which automates leaf area calculations using ImageJ software (Schneider
707 et al. 2012). Each leaf was dried at 65°C for at least 48 hours, weighed, and
708 ground using a Retsch MM200 ball mill grinder (Verder Scientific, Inc., Newtown,
709 PA, USA) until homogenized. Leaf mass per area (M_{area} , g m^{-2}) was calculated
710 as the ratio of dry leaf biomass to fresh leaf area. Using a subsample of ground
711 and homogenized leaf biomass, leaf nitrogen content (N_{mass} ; gN g^{-1}) and leaf

712 $\delta^{13}\text{C}$ (‰, relative to VPDB) were measured at the Cornell Stable Isotope Lab
713 with an elemental analyzer (NC 2500, CE Instruments, Wigan, UK) interfaced to
714 an isotope ratio mass spectrometer (Delta V Isotope Ratio Mass Spectrometer,
715 ThermoFisher Scientific, Waltham, MA, USA). Leaf nitrogen content per unit leaf
716 area (N_{area} ; gN m⁻²) was calculated by multiplying N_{mass} by M_{area} .

717 I used leaf $\delta^{13}\text{C}$ values to estimate χ (unitless), which is an isotope-derived
718 estimate of the leaf $C_i:C_a$ ratio. While intercellular and atmospheric CO₂ con-
719 centrations were directly measured during each A_{net}/C_i curve, deriving χ from
720 $\delta^{13}\text{C}$ provides a more integrative estimate of the $C_i:C_a$ over an individual leaf's
721 lifespan. We derived χ following the approach of Farquhar et al. (1989) described
722 in Cernusak et al. (2013):

$$\chi = \frac{\Delta^{13}C - a}{b - a} \quad (3.1)$$

723 where $\Delta^{13}\text{C}$ represents the relative difference between leaf $\delta^{13}\text{C}$ (‰) and air $\delta^{13}\text{C}$
724 (‰), and is calculated from the following equation:

$$\Delta^{13}C = \frac{\delta^{13}C_{\text{air}} - \delta^{13}C_{\text{leaf}}}{1 + \delta^{13}C_{\text{leaf}}} \quad (3.2)$$

725 where $\delta^{13}C_{\text{air}}$ is assumed to be -8‰ (Keeling et al. 1979; Farquhar et al. 1989), a
726 represents the fractionation between ¹²C and ¹³C due to diffusion in air, assumed
727 to be 4.4‰, and b represents the fractionation caused by Rubisco carboxylation,
728 assumed to be 27‰ (Farquhar et al. 1989).

729 3.2.4 A_{net}/C_i curve-fitting and parameter estimation

730 I fit A_{net}/C_i curves of each individual using the ‘fitaci’ function in the ‘plante-
731 cophys’ R package (Duursma 2015). This function estimates the maximum rate
732 of Rubisco carboxylation (V_{cmax} ; $\mu\text{mol m}^{-2} \text{s}^{-1}$) and maximum rate of electron
733 transport for RuBP regeneration (J_{max} ; $\mu\text{mol m}^{-2} \text{s}^{-1}$) based on the Farquhar,
734 von Caemmerer, and Berry biochemical model of C₃ photosynthesis (Farquhar
735 et al. 1980). For each curve fit, I included triose phosphate utilization (TPU)
736 limitation to avoid underestimating J_{max} (Gregory et al. 2021). Curves were
737 visually examined to confirm the likely presence of TPU limitation.

738 I determined Michaelis-Menten coefficients for Rubisco affinity to CO₂ (K_c ;
739 $\mu\text{mol mol}^{-1}$) and O₂ (K_o ; $\mu\text{mol mol}^{-1}$), and the CO₂ compensation point (Γ^* ;
740 $\mu\text{mol mol}^{-1}$) using leaf temperature and equations described in Medlyn et al.
741 (2002) and derived in Bernacchi et al. (2001). Specifically, K_c and K_o were
742 calculated as:

$$K_c = 404.9 * \exp^{\frac{79430(T_k - 298)}{298RT_k}} \quad (3.3)$$

743 and

$$K_o = 278.4 * \exp^{\frac{36380(T_k - 298)}{298RT_k}} \quad (3.4)$$

744 while Γ^* was calculated as:

$$\Gamma^* = 42.75 * \exp^{\frac{37830(T_k - 298)}{298RT_k}} \quad (3.5)$$

745 In all three equations, T_k is the leaf temperature (in Kelvin) during each A_{net}/C_i

746 curve and R is the universal gas constant ($8.314 \text{ J mol}^{-1} \text{ K}^{-1}$).

747 I standardized V_{cmax} and J_{max} estimates to 25°C using a modified Arrhe-

748 nius equation (Kattge and Knorr 2007):

$$k_{25} = \frac{k_{\text{obs}}}{e^{\frac{H_a(T_{\text{obs}} - T_{\text{ref}})}{T_{\text{ref}}RT_{\text{obs}}}} * \frac{1+e^{\frac{T_{\text{ref}}\Delta S - H_d}{T_{\text{obs}}}}}{1+e^{\frac{T_{\text{obs}}\Delta S - H_d}{T_{\text{obs}}}}}} \quad (3.6)$$

749 k_{25} represents the standardized V_{cmax} or J_{max} rate at 25°C , k_{obs} represents the

750 V_{cmax} or J_{max} estimate at the average leaf temperature measured inside the cuvette

751 during the A_{net}/C_i curve. H_a is the activation energy of V_{cmax} ($71,513 \text{ J mol}^{-1}$)

752 Kattge and Knorr (2007) or J_{max} ($49,884 \text{ J mol}^{-1}$) (Kattge and Knorr 2007). H_d

753 represents the deactivation energy of both V_{cmax} and J_{max} ($200,000 \text{ J mol}^{-1}$) (Med-

754 lyn et al. 2002), and R represents the universal gas constant ($8.314 \text{ J mol}^{-1} \text{ K}^{-1}$).

755 T_{ref} represents the standardized temperature of 298.15 K (25°C) and T_{obs} rep-

756 resents the mean leaf temperature (in K) during each A_{net}/C_i curve. ΔS is an

757 entropy term that (Kattge and Knorr 2007) derived as a linear relationship with

758 average growing season temperature (T_g ; $^\circ\text{C}$), where:

$$\Delta S_{v_{\text{cmax}}} = -1.07 T_g + 668.39 \quad (3.7)$$

759 and

$$\Delta S_{j_{\text{max}}} = -0.75 T_g + 659.70 \quad (3.8)$$

760 I estimated T_g in Equations 3.7 and 3.8 based on mean daily (24-hour) air tem-
761 perature of the 30 days leading up to the day of each sample collection using the
762 same weather station reported in the site description. I used V_{cmax25} and J_{max25}
763 estimates to calculate the ratio of J_{max25} to V_{cmax25} ($J_{max25}:V_{cmax25}$; unitless).

764 3.2.5 *Proportion of leaf nitrogen allocated to photosynthesis and structure*

765 I used equations from Niinemets and Tenhunen (1997) to estimate the proportion
766 of leaf nitrogen content allocated to Rubisco and bioenergetics. The proportion of
767 leaf nitrogen allocated to Rubisco ($\rho_{rubisco}$; gN gN⁻¹) was calculated as a function
768 of V_{cmax25} and N_{area} :

$$\rho_{rubisco} = \frac{V_{cmax25} N_r}{V_{cr} N_{area}} \quad (3.9)$$

769 where N_r is the amount of nitrogen in Rubisco, set to 0.16 gN (gN in Rubisco)⁻¹
770 and V_{cr} is the maximum rate of RuBP carboxylation per unit Rubisco protein,
771 set to 20.5 μmol CO₂ (g Rubisco)⁻¹. The proportion of leaf nitrogen allocated to
772 bioenergetics (ρ_{bioe} ; gN gN⁻¹) was similarly calculated as a function of J_{max25} and
773 N_{area} :

$$\rho_{bioe} = \frac{J_{max25} N_b}{J_{mc} N_{area}} \quad (3.10)$$

774 where N_b is the amount of nitrogen in cytochrome f, set to 0.12407 gN (μmol
775 cytochrome f)⁻¹ assuming a constant 1: 1: 1.2 cytochrome f: ferredoxin NADP
776 reductase: coupling factor molar ratio (Evans and Seemann 1989; Niinemets and
777 Tenhunen 1997), and J_{mc} is the capacity of electron transport per cytochrome f,

778 set to 156 μmol electron (μmol cytochrome f) $^{-1}\text{s}^{-1}$.

779 I estimated the proportion of leaf nitrogen content allocated to photosynthetic tissue (ρ_{photo} ; gN gN^{-1}) as the sum of ρ_{rubisco} and ρ_{bioe} . This calculation
780 is an underestimate of the proportion of leaf nitrogen allocated to photosynthetic
781 tissue because it does not include nitrogen allocated to light harvesting proteins.
782 This leaf nitrogen pool was not included because I did not perform chlorophyll
783 extractions on focal leaves. However, the proportion of leaf nitrogen content al-
784 located to light harvesting proteins tends to be small relative to ρ_{rubisco} and ρ_{bioe} ,
785 and may scale with changes in ρ_{rubisco} and ρ_{bioe} (Niinemets and Tenhunen 1997).

787 Finally, I estimated the proportion of leaf nitrogen content allocated to
788 structural tissue ($\rho_{\text{structure}}$; gN gN^{-1}) using an empirical equation from Onoda
789 et al. (2017):

$$N_{\text{cw}} = 0.000355 * M_{\text{area}}^{1.39} \quad (3.11)$$

790 where N_{cw} is the leaf nitrogen content allocated to cell walls (gN m^{-2}). $\rho_{\text{structure}}$
791 was estimated by dividing N_{cw} by N_{area} .

792 3.2.6 *Tradeoffs between nitrogen and water use*

793 Photosynthetic nitrogen use efficiency (PNUE; $\mu\text{mol CO}_2 \text{ mol}^{-1} \text{ N s}^{-1}$) was cal-
794 culated by dividing A_{net} by N_{area} , first converting N_{area} to mol N m^{-2} using the
795 molar mass of nitrogen (14 g mol^{-1}). I used χ as an indicator of water use effi-
796 ciency, which exploratory analyses suggest had similar responses to soil nitrogen
797 availability and pH as intrinsic water use efficiency measured from gas exchange

798 ($A_{\text{net}}/g_{\text{sw}}$). Tradeoffs between nitrogen and water use were determined by cal-
799 culating the ratio of N_{area} to χ ($N_{\text{area}}:\chi$; gN m⁻²) and V_{cmax25} to χ ($V_{\text{cmax25}}:\chi$;
800 $\mu\text{mol m}^{-2} \text{s}^{-1}$). This approach is similar to tradeoff calculations in which nitrogen-
801 water use tradeoffs are measured as the ratio of N_{area} or V_{cmax25} to g_{sw} (Paillassa
802 et al. 2020; Bialic-Murphy et al. 2021). In this chapter, I quantify these rela-
803 tionships using χ in lieu of g_{sw} because g_{sw} rapidly changes with environmental
804 conditions and therefore may have been altered by recent tree branch severance
805 and/or placement in the cuvette.

806 3.2.7 *Soil nitrogen availability and pH*

807 To characterize soil nitrogen availability at the time of our leaf gas exchange
808 measurements, I used mixed bed resin bags to quantify mobile ammonium-N and
809 nitrate-N concentrations in each plot. Lycra mesh bags were filled with 5 g of
810 Dowex® Marathon MR-3 hydrogen and hydroxide form resin (MilliporeSigma,
811 Burlington, MA USA) and sealed with a zip tie. Each bag was activated by
812 soaking in 0.5 M HCl for 20 minutes, then in 2 M NaCl until pH of the saline
813 solution stabilized, as described in Allison et al. (2008). Five resin bags were
814 inserted about 10 cm below the soil surface at each plot on June 25, 2019: one
815 near each of the four plot corners and one near the plot center. All resin bags
816 were collected 24 days later on July 19, 2019 and were frozen until extracted.

817 Prior to anion and cation extraction, each resin bag was rinsed with ul-
818 trapure water (MilliQ IQ 7000; Millipore Sigma, Burlington, MA) to remove any
819 surface soil residues. Anions and cations were extracted from surface-cleaned
820 resin bags by individually soaking and shaking each bag in 100 mL of a 0.1 M

821 HCl/2.0 M NaCl matrix for one hour. Using a microplate reader (Biotek Synergy
822 H1; Biotek Instruments, Winooski, VT USA), I quantified nitrate-N concentra-
823 tions spectrophotometrically at 540 nm with the end product of a single reagent
824 vanadium (III) chloride reaction (Doane and Horwáth 2003), and ammonium-N
825 concentrations quantified at 650 nm with the end product of a modified phenol-
826 hypochlorite reaction (Weatherburn 1967; Rhine et al. 1998). Both the single
827 reagent vanadium (III) chloride and modified phenol-hypochlorite methodologies
828 are well established for determining nitrate-N and ammonium-N concentrations
829 in resin bag extracts (Arnone 1997; Allison et al. 2008). I used a series of negative
830 and positive controls throughout each well plate to verify the accuracy and preci-
831 sion of our measurements, assaying each resin bag extract and control in triplicate.
832 Soil N availability was estimated as the sum of the nitrate-N and ammonium-N
833 concentration in each resin bag, normalized per g of resin and duration in the field
834 ($\mu\text{g N g}^{-1} \text{ resin d}^{-1}$), then subsequently averaged across all resin bags in a plot
835 for a plot-level mean.

836 Soil pH was measured on 0-10 cm mineral soil samples collected prior to
837 fertilization in 2019. Near each of the four plot corners, three 5.5 cm diameter soil
838 cores were collected after first removing the forest floor where present. Each set
839 of three cores was placed in a plastic bag, and later composited by hand mixing
840 and sieved to 4mm. Soil pH was determined for a 1:2 soil:water slurry (10 g field-
841 moist soil to 20 mL DI water) of each sample using an Accumet AB15 pH meter
842 with flushable junction probe (Fisher Scientific; Hampton, NH, USA), and was
843 estimated at the plot level as the mean soil pH within each plot.

844 3.2.8 *Statistical analyses*

845 I built two separate series of linear mixed-effects models to explore effects of soil
846 nitrogen availability, soil pH, species, and leaf nitrogen content on leaf physiolog-
847 ical traits. In the first series of linear mixed-effects models, I explored the effect
848 of soil nitrogen availability, soil pH, and species on leaf nitrogen content, leaf
849 photosynthesis, stomatal conductance, and nitrogen-water use tradeoffs. Models
850 included plot-level soil N availability and plot-level soil pH as continuous fixed ef-
851 fects, species as a categorical fixed effect, and site as a categorical random intercept
852 term. Interaction terms between fixed effects were not included due to the small
853 number of experimental plots. I built a series of separate models with this indepen-
854 dent variable structure to quantify individual effects of soil nitrogen availability,
855 soil pH, and species on N_{area} , M_{area} , N_{mass} , A_{net} , V_{cmax25} , J_{max25} , $J_{\text{max25}}:V_{\text{cmax25}}$,
856 ρ_{rubisco} , $\rho_{\text{bioenergetics}}$, ρ_{photo} , $\rho_{\text{structure}}$, χ , PNUE, $N_{\text{area}}:\chi$, and $V_{\text{cmax25}}:\chi$.

857 A second series of linear mixed-effects models were built to investigate
858 relationships between leaf N content and photosynthetic parameters. Statistical
859 models included N_{area} as a single continuous fixed effect with species and site
860 designated as individual random intercept terms. I used this independent variable
861 structure to quantify individual effects of leaf nitrogen content on A_{net} , V_{cmax25} ,
862 J_{max25} , $J_{\text{max25}}:V_{\text{cmax25}}$, and χ .

863 For all linear mixed-effects models, I used Shapiro-Wilk tests of normality
864 to determine whether linear mixed-effects models satisfied residual normality as-
865 sumptions. If residual normality assumptions were not met, then models were fit
866 using dependent variables that were natural log transformed. If residual normal-
867 ity assumptions were still not met (Shapiro-Wilk: $p < 0.05$), then models were fit

868 using dependent variables that were square root transformed. All residual nor-
869 mality assumptions for both sets of models that did not originally satisfy residual
870 normality assumptions were met with either a natural log or square root data
871 transformation (Shapiro-Wilk: $p>0.05$ in all cases).

872 In the first series of models, models for N_{area} , M_{area} , N_{mass} , $V_{\text{cmax}25}$, $J_{\text{max}25}$,
873 χ , $N_{\text{area}}:\chi$, and $V_{\text{cmax}25}:\chi$, ρ_{rubisco} , $\rho_{\text{bioenergetics}}$, ρ_{photo} , $\rho_{\text{structure}}$ satisfied residual
874 normality assumptions without data transformations (Shapiro-Wilk: $p>0.05$ in
875 all cases). The model for $J_{\text{max}25}:V_{\text{cmax}25}$ satisfied residual normality assumptions
876 with a natural log data transformation, while models for A_{net} and PNUE each
877 satisfied residual normality assumptions with square root data transformations.
878 In the second series of models, models for $V_{\text{cmax}25}$, $J_{\text{max}25}$, χ , and $V_{\text{cmax}25}:\chi$ satis-
879 fied residual normality assumptions without data transformations (Shapiro-Wilk:
880 $p>0.05$ in all cases). The model for $J_{\text{max}25}:V_{\text{cmax}25}$ required a natural log data
881 transformation and the model for A_{net} required a square root data transformation
882 (Shapiro-Wilk: $p>0.05$ in both cases).

883 In all models, I used the ‘lmer’ function in the ‘lme4’ R package (Bates
884 et al. 2015) to fit each model and the ‘Anova’ function in the ‘car’ R package
885 (Fox and Weisberg 2019) to calculate Type II Wald’s χ^2 and determine the signif-
886 icance level ($\alpha=0.05$) of each fixed effect coefficient. Finally, I used the ‘emmeans’
887 R package (Lenth, 2019) to conduct post-hoc comparisons using Tukey’s tests,
888 where degrees of freedom were approximated using the Kenward-Roger approach
889 (Kenward and Roger 1997). All analyses and plots were conducted in R version
890 4.1.1 (R Core Team 2021). All figure regression lines and associated 95% confi-
891 dence interval error bars were plotted using predictions generated across the soil

892 nitrogen availability gradient using the ‘emmeans’ R package (Lenth 2019).

893 3.3 Results

894 3.3.1 *Leaf nitrogen content*

895 Increasing soil nitrogen availability generally increased N_{area} (Table 3.1; Fig. 3.1a).

896 This pattern was driven by an increase in N_{mass} (Table 3.1; Fig. 3.1c) and a

897 marginal increase in M_{area} (Table 3.1; Fig. 3.1e) with increasing soil nitrogen

898 availability. There was no effect of soil pH on N_{area} , N_{mass} , or M_{area} (Table 3.1);

899 however, I also observed strong differences in N_{area} (Fig. 3.1b), N_{mass} (Fig. 3.1d),

900 and M_{area} (Fig. 3.1e) between species (Table 3.1).

Table 3.1. Effects of soil nitrogen availability, soil pH, and species on leaf nitrogen content per unit leaf area (N_{area} ; gN m⁻²), leaf nitrogen content per unit leaf mass (N_{mass} ; gN g⁻¹), and leaf mass per unit leaf area (M_{area} ; g m⁻²)*

	N_{area}			N_{mass}			M_{area}			
	df	Coefficient	χ^2	p	Coefficient	χ^2	p	Coefficient	χ^2	p
Intercept	-	9.03E-01	-	-	1.68E+00	-	-	4.60E+01	-	-
Soil N	1	1.68E-02	11.990	0.001	1.25E-02	6.902	0.009	4.87E-01	4.143	0.042
Soil pH	1	9.28E-02	0.836	0.361	8.08E-02	0.663	0.415	4.05E+00	0.653	0.419
Species	4	-	72.128	<0.001	-	35.074	<0.001	-	29.869	<0.001

901 *Significance determined using Type II Wald χ^2 tests ($\alpha=0.05$). P-values<0.05 are in bold.

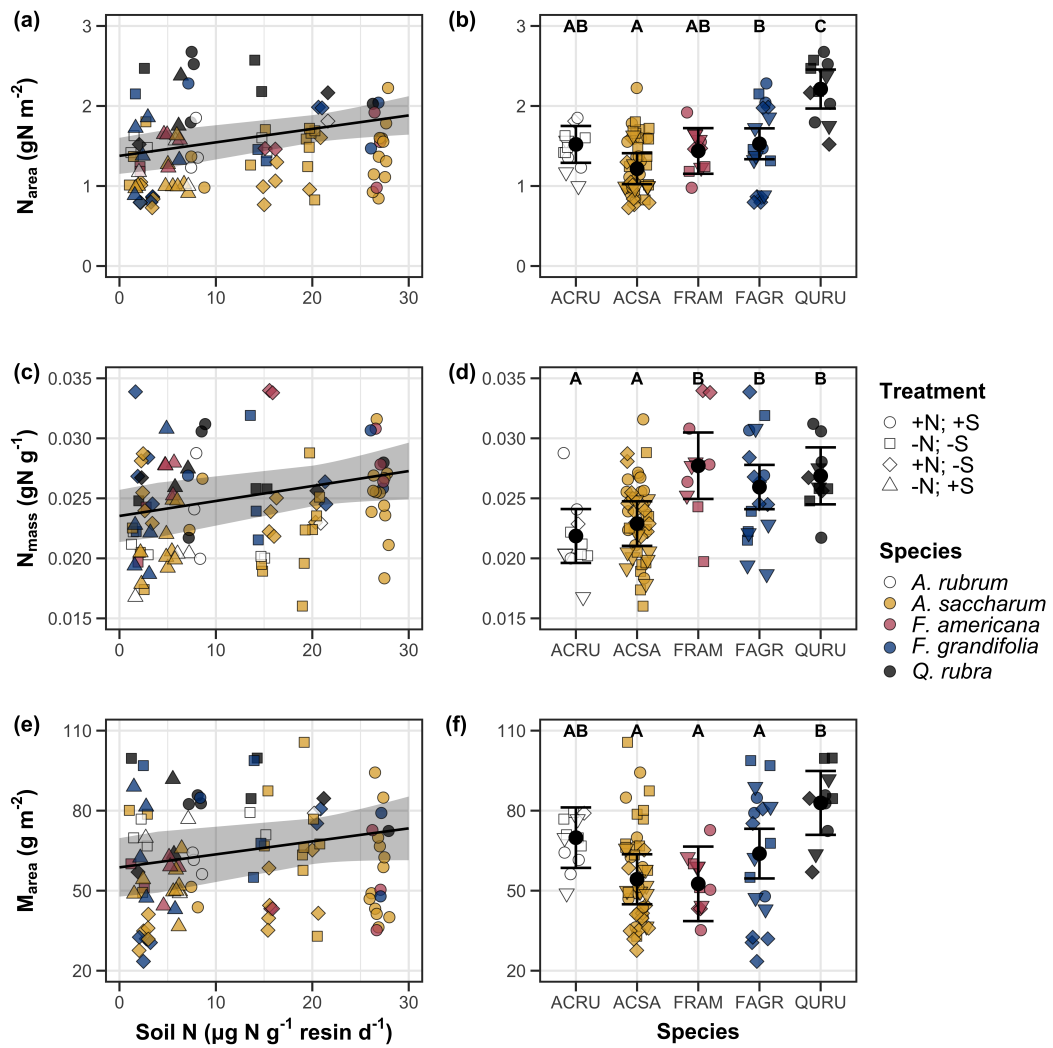


Figure 3.1. Effects of soil N availability and species on leaf nitrogen content per unit leaf area (a-b), leaf nitrogen content per unit leaf biomass (c-d), and leaf mass per unit leaf area (e-f). Soil nitrogen availability is represented on the x-axis in the left column of panels, while species is represented on the x-axis in the right column of panels. Tree species are represented as colored points and treatment plots are represented as shaped points, jittered for visibility. Species are abbreviated in the right column of panels through their assigned NRCS PLANTS Database symbol (USDA NRCS 2022), grouped along the x-axis per common mycorrhizal association, where the first three species commonly associate with arbuscular mycorrhizae (ACRU, ACSA, FAGR) and the second two species with ectomycorrhizae (FAGR, QURU). Trendlines are only included when the regression slope is statistically different from zero ($p < 0.05$).

902 3.3.2 *Net photosynthesis and leaf biochemistry*

903 Increasing soil nitrogen availability generally had no effect on A_{net} , V_{cmax25} , J_{max25} ,
904 or $J_{\text{max25}}:V_{\text{cmax25}}$ (Table 3.2, Figs. 3.2a, 3.2d, 3.2g). I also observed strong species
905 effects on all measured leaf photosynthetic traits (Table 3.2; Figs. 3.2b, 3.2e, 3.2h).
906 Increasing soil pH had a marginal negative effect on A_{net} , but had no effect on
907 V_{cmax25} , J_{max25} , or $J_{\text{max25}}:V_{\text{cmax25}}$ (Table 3.2). There was a weak positive effect of
908 increasing N_{area} on A_{net} (Fig. 3.2c), but quite strong positive effects of increasing
909 N_{area} on V_{cmax25} and J_{max25} (Table 3.2; Fig. 3.2f and 3.2i).

Table 3.2. Effects of soil nitrogen availability, soil pH, species, and N_{area} on net photosynthesis (A_{net} ; $\mu\text{mol m}^{-2} \text{s}^{-1}$), the maximum rate of Rubisco carboxylation (V_{cmax25} ; $\mu\text{mol m}^{-2} \text{s}^{-1}$), the maximum rate of RuBP regeneration (J_{max25} ; $\mu\text{mol m}^{-2} \text{s}^{-1}$), and the ratio of the maximum rate of RuBP regeneration to the maximum rate of Rubisco carboxylation ($J_{\text{max25}}:V_{\text{cmax25}}$; unitless)*

	A_{net}			V_{cmax25}			J_{max25}			
	df	Coefficient	χ^2	p	Coefficient	χ^2	p	Coefficient	χ^2	p
(Intercept)	-	3.29E+00 ^b	-	-	6.38E+01	-	-	1.12E+02	-	-
Soil N	1	-1.23E-03 ^b	1.798	0.180	-3.84E-01	1.745	0.187	-6.70E-01	2.172	0.141
Soil pH	1	-3.09E-01 ^b	3.312	0.069	-4.91E+00	0.655	0.418	-8.18E+00	0.742	0.389
Species	4	-	11.838	0.019	-	31.748	<0.001	-	27.291	<0.001
(N_{area} int.)	-	6.59E-01 ^b	-	-	1.45E-01	-	-	2.86E+01	-	-
N_{area}	4	3.13E-01 ^b	4.790	0.029	2.43E+01	22.616	<0.001	4.04E+01	28.259	<0.001

	$J_{\text{max25}}:V_{\text{cmax25}}$			
	df	Coefficient	χ^2	p
(Intercept)	-	6.59E-01 ^a	-	-
Soil N	1	7.04E-04 ^a	0.088	0.767
Soil pH	1	-7.84E-03 ^a	0.025	0.874
Species	4	-	12.745	0.013
(N_{area} int.)	-	6.69E-01 ^a	-	-
N_{area}	4	-4.69E-02 ^a	1.142	0.285

54

910 *Significance determined using Type II Wald χ^2 tests ($\alpha=0.05$). P-values less than 0.05 are in bold, while p-values
 911 between 0.05 and 0.1 are italicized. Superscript letters indicate model coefficients fit to natural-log (^a) or square-root
 912 (^b) transformed data. Relationships between N_{area} and each response variable were fit using the second series of
 913 bivariate mixed-effects models, so model coefficients and results are independent of model coefficients and results
 914 reported for relationships between soil nitrogen, soil pH, and species for each response variable.

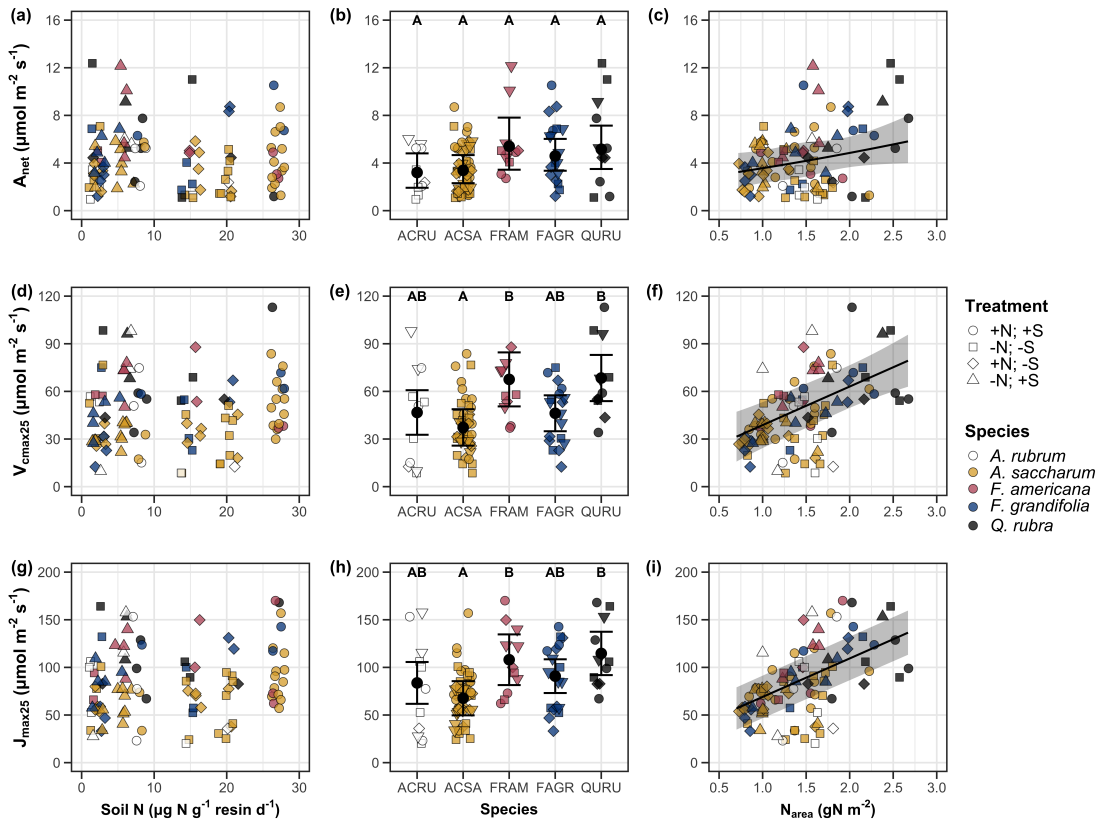


Figure 3.2. Effects of soil nitrogen availability (left column of panels), species (middle column of panels), and leaf nitrogen content per unit leaf area (right column of panels) on net photosynthesis (a-c), maximum Rubisco carboxylation rate (d-f), and maximum RuBP regeneration rate (g-i). Soil nitrogen availability is represented on the x-axis in the left column of panels, species is represented on the x-axis in the middle column of panels, and leaf nitrogen content per unit leaf area is represented continuously on the x-axis in the right column of panels. Species abbreviations and position along the x-axis in the middle column of panels, colored points, shapes, and trendlines are as explained in Figure 3.1.

915 3.3.3 *Leaf nitrogen allocation*

916 Neither soil nitrogen availability nor soil pH affected the proportion of leaf nitro-
917 gen allocated to Rubisco or bioenergetics (Table 3.3; Fig. 3.3a, Fig. 3.3c), nor was
918 there any subsequent effect on the proportion of leaf nitrogen allocated to photo-
919 synthesis (Table 3.3; Fig. 3.3f). I also found no effect of soil nitrogen availability
920 or soil pH on the proportion of leaf nitrogen allocated to structure (Table 3.3;
921 Fig 3.3g). Species varied in the proportion of leaf nitrogen allocated to Rubisco,
922 photosynthesis, and structure (Fig 3.3b, Fig. 3.3d, Fig 3.3h), with no detectable
923 species effect on the proportion of leaf nitrogen allocated to bioenergetics (Table
924 3.3).

Table 3.3. Effects of soil nitrogen availability, soil pH, and species on the proportion of leaf nitrogen content allocated to photosynthesis (ρ_{photo} ; gN gN⁻¹), Rubisco (ρ_{rubisco} ; gN gN⁻¹), bioenergetics (ρ_{bioe} ; gN gN⁻¹), and structure ($\rho_{\text{structure}}$; gN gN⁻¹)*

	ρ_{photo}			ρ_{rubisco}			ρ_{bioe}			
	df	Coefficient	χ^2	p	Coefficient	χ^2	p	Coefficient	χ^2	p
Intercept	-	4.93E-01	-	-	4.17E-01	-	-	7.64E-02	-	-
Soil N	1	-1.23E-03	0.521	0.470	-1.04E-03	0.501	0.479	-1.77E-04	0.557	0.455
Soil pH	1	-4.37E-02	1.581	0.209	-3.70E-02	1.511	0.219	-6.84E-03	1.941	0.164
Species	4	-	13.106	0.011	-	14.152	0.007	-	7.300	0.121

	$\rho_{\text{structure}}$			
	df	Coefficient	χ^2	p
Intercept	-	9.77E-02	-	-
Soil N	1	-2.29E-04	1.165	0.280
Soil pH	1	-1.87E-03	0.179	0.672
Species	4	-	16.428	0.002

925 *Significance determined using Type II Wald χ^2 tests ($\alpha=0.05$). P-values less than 0.05 are in bold.

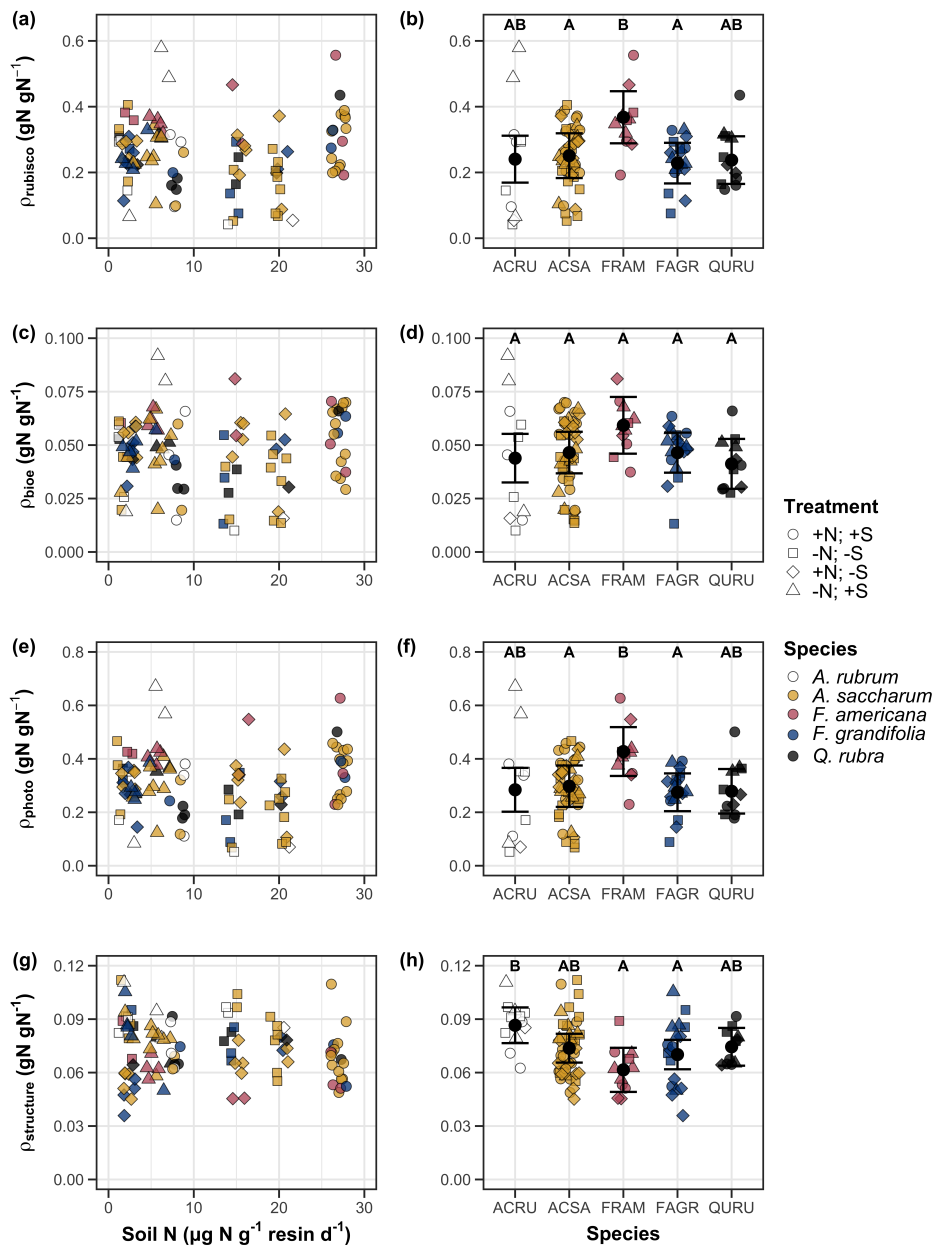


Figure 3.3. Effects of soil nitrogen availability and species on the proportion of leaf nitrogen content allocated to Rubisco (a-b), bioenergetics (c-d), photosynthesis (e-f), and structure (g-h). Soil nitrogen availability is represented on the x-axis in the left column of panels and species are represented on the x-axis in the right column of panels. Species abbreviations and position along the x-axis in the middle column of panels, colored points, shapes, trendlines, error bars, and compact lettering are as explained in Figure 3.1.

926 3.3.4 *Tradeoffs between nitrogen and water use*

927 Although soil nitrogen availability did not affect χ (Table 3.4; Fig. 3.4a), increasing
928 soil nitrogen availability decreased PNUE (Table 3.4; Fig. 3.4d) and increased
929 the ratio of $N_{\text{area}}:\chi$ (Table 3.4; Fig. 3.4f). Specifically, this response yielded a
930 26% reduction in PNUE and 37% stimulation in $N_{\text{area}}:\chi$ across the soil nitrogen
931 availability gradient. There was no apparent effect of soil nitrogen availability on
932 $V_{\text{cmax25}}:\chi$ (Table 3.4; Fig. 3.4h). Increasing soil pH had a weak marginal nega-
933 tive effect on PNUE, but did not influence χ , $N_{\text{area}}:\chi$, or $V_{\text{cmax25}}:\chi$ (Table 3.4). I
934 observed differences in χ (Fig. 3.4b), PNUE (Fig. 3.4e), $N_{\text{area}}:\chi$ (Fig. 3.4g), and
935 $V_{\text{cmax25}}:\chi$ (Fig. 3.4i) between species (Table 3.4). Finally, increasing N_{area} had a
936 strong negative effect on χ (Table 3.4; Fig. 3.4c) and a strong positive effect on
937 $V_{\text{cmax25}}:\chi$ (Table 3.4; Fig. 3.4j).

Table 3.4. Effects of soil nitrogen availability, soil pH, species, and N_{area} on χ (unitless), photosynthetic nitrogen use efficiency (PNUE; $\mu\text{mol CO}_2 \text{ mol}^{-1} \text{ N s}^{-1}$), leaf nitrogen content per unit χ ($N_{\text{area}}:\chi$; gN m^{-2}), and maximum Rubisco carboxylation rate per unit χ ($V_{\text{cmax25}}:\chi$; $\mu\text{mol m}^{-2} \text{ s}^{-1}$)^{*}

	df	χ		PNUE				$N_{\text{area}}:\chi$		
		Coefficient	χ^2	p	Coefficient	χ^2	p	Coefficient	χ^2	p
(Intercept)	-	8.12E-01	-	-	9.57E+00 ^b	-	-	9.19E-01	-	-
Soil N	1	-1.14E-03	1.698	0.193	-6.63E-02 ^b	6.396	0.011	2.60E-02	9.533	0.002
Soil pH	1	-1.91E-02	1.087	0.297	-9.25E-01 ^b	2.843	<i>0.092</i>	2.03E-01	1.321	0.250
Species	4	-	18.843	0.001	-	13.454	0.009	-	52.983	<0.001
(N_{area} int.)	-	8.93E-01	-	-	-	-	-	-	-	-
N_{area}	1	-1.11E-01	80.606	<0.001	-	-	-	-	-	-

	df	$V_{\text{cmax25}}:\chi$		
		Coefficient	χ^2	p
(Intercept)	-	7.20E+01	-	-
Soil N	1	3.99E-01	0.963	0.326
Soil pH	1	-3.12E+00	0.138	0.711
Species	4	-	31.450	<0.001
(N_{area} int.)	-	1.18E+01	-	-
N_{area}	4	3.87E+01	32.797	<0.001

60

938 *Significance determined using Type II Wald χ^2 tests ($\alpha = 0.05$). P -values less than 0.05 are in bold, while p -values
 939 between 0.05 and 0.1 are italicized. Superscript letters indicate model coefficients fit to natural-log (^a) or square-root
 940 (^b) transformed data. Relationships between N_{area} and each response variable were fit using the second series of
 941 bivariate mixed-effects models, so model coefficients and results are independent of model coefficients and results
 942 reported for relationships between soil nitrogen, soil pH, and species for each response variable.

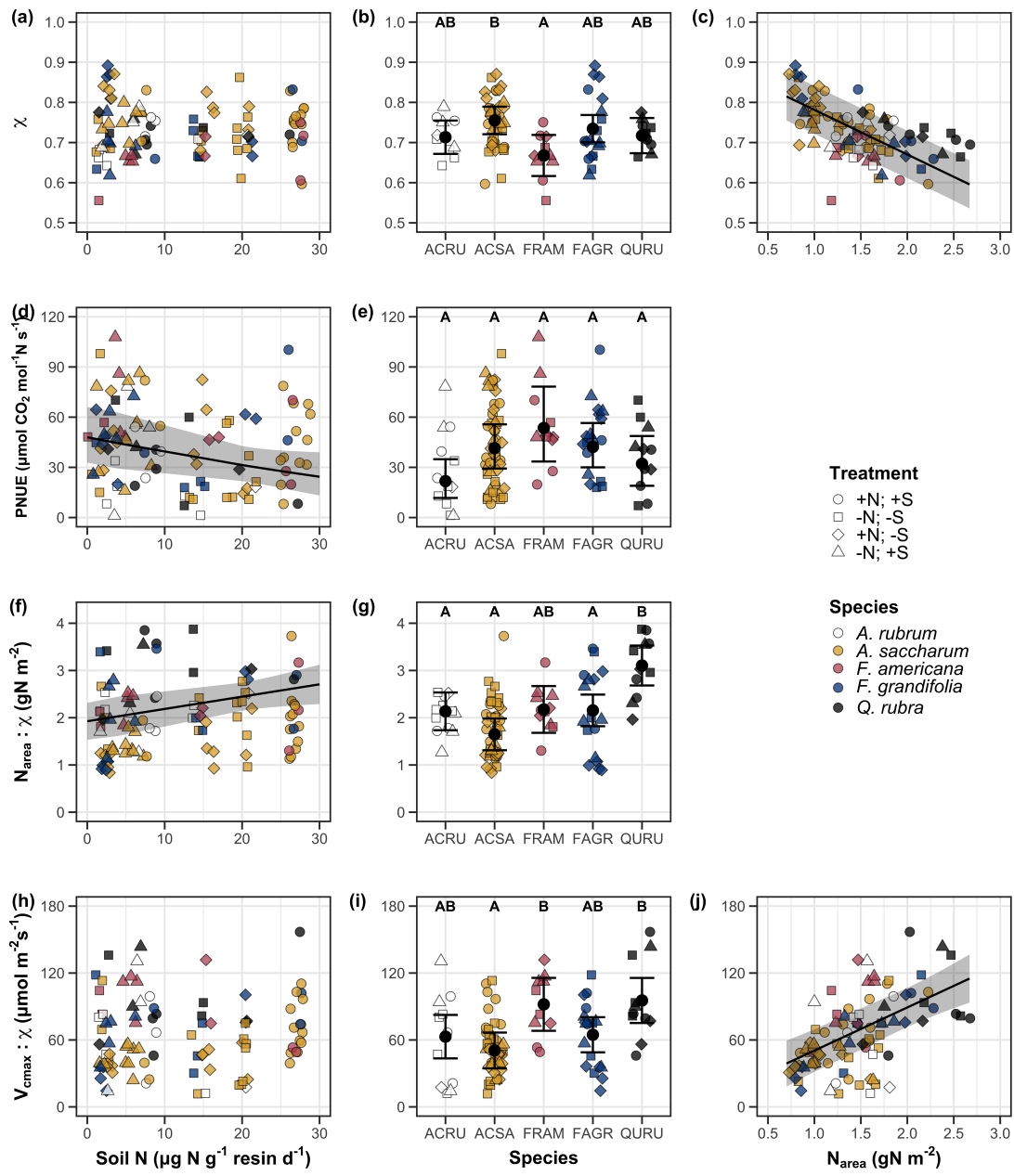


Figure 3.4. Effects of soil nitrogen availability and species on the proportion of leaf nitrogen content allocated to Rubisco (a-b), bioenergetics (c-d), photosynthesis (Rubisco + bioenergetics; e-f), and structure (g-h). Soil nitrogen availability is represented on the x-axis in the left column of panels and species are represented on the x-axis in the right column of panels. Species abbreviations and position along the x-axis in the middle column of panels, colored points, shapes, trendlines, error bars, and compact lettering are as explained in Figure 3.1.

943 3.4 Discussion

944 Photosynthetic least-cost theory provides an explanation for understanding rela-
945 tionships between soil nutrient availability, leaf nutrient allocation, and photosyn-
946 thetic capacity. The theory suggests that plants acclimate to a given environment
947 by optimizing leaf photosynthesis rates at the lowest summed cost of using nu-
948 trients and water (Prentice et al. 2014; Wang et al. 2017; Smith et al. 2019;
949 Paillassa et al. 2020). The theory predicts that an increase in soil nutrient avail-
950 ability should allow similar photosynthesis rates to be achieved with increased leaf
951 nutrient content and photosynthetic capacity (i.e., V_{cmax25} and J_{max25}) at lower
952 leaf $C_i:C_a$ (χ), resulting in an increase in water use efficiency, decrease in nutri-
953 ent use efficiency, and increase in both leaf nutrient content and photosynthetic
954 capacity per unit χ . The theory predicts similar leaf responses to increasing soil
955 pH under acidic conditions, presumably due to generally faster nutrient cycle dy-
956 namics and consequent reductions in the cost of acquiring nutrients relative to
957 water with increasing soil pH (Wang et al. 2017; Paillassa et al. 2020; Dong et al.
958 2020).

959 Supporting the theory, increasing soil nitrogen availability was associated
960 with increased leaf nitrogen content, a pattern that reduced photosynthetic nitro-
961 gen use efficiency and increased leaf N content per unit χ . Increasing soil nitrogen
962 coincided with slight, but non-significant decreases in χ and increases in V_{cmax25}
963 and J_{max25} ($p<0.2$, Table 3.2). The positive trend between soil nitrogen availabil-
964 ity and photosynthetic capacity was supported by the concurrent strong increase
965 in leaf nitrogen content with increasing soil nitrogen availability, which resulted in
966 no change in the proportion of leaf nitrogen content allocated to photosynthesis

967 across the soil nitrogen availability gradient. Additionally, leaf nitrogen content
968 exhibited a strong negative correlation with χ , indicative of strong nitrogen-water
969 use tradeoffs at the leaf level. Responses tended to vary more due to soil ni-
970 trogen availability than soil pH. Overall, these findings are consistent with the
971 nutrient-water use tradeoffs predicted from theory.

972 3.4.1 *Soil nitrogen availability modifies tradeoffs between nitrogen and water use*
973 In support of expected least-cost outcomes and past environmental gradient stud-
974 ies (Dong et al. 2017; Paillassa et al. 2020), increasing soil nitrogen availability
975 was associated with increased leaf nitrogen content. Soil nitrogen availability had
976 smaller impacts on measures of net photosynthesis and χ , which led to reductions
977 in PNUE and increases in leaf nitrogen content per unit χ , as expected from the-
978 ory. Photosynthetic least-cost theory suggests that reductions in PNUE should
979 be driven by an increase in the proportion of leaf nitrogen allocated to photosyn-
980 thetic tissue, a pattern that should allow plants to achieve optimal photosynthetic
981 rates with greater photosynthetic capacity to make better use of available light.
982 Contrasting theory predictions, I found no effect of soil nitrogen availability on
983 photosynthetic capacity. However, photosynthetic capacity did tend to increase
984 with increasing soil nitrogen availability ($p<0.20$; Table 3.2) resulting in no effect
985 of soil nitrogen availability on the relative fraction of leaf nitrogen allocated to
986 photosynthesis, Rubisco, or bioenergetics. These lines of evidence support the
987 idea that trees use additional nitrogen to support increased leaf nitrogen alloca-
988 tion toward photosynthetic tissue and enhance photosynthetic capacity (Wright
989 et al. 2003).

990 Soil nitrogen availability had a stronger effect on leaf nitrogen than photo-
991 synthetic capacity. This pattern suggests that additional plant nitrogen up-
992 take due to increased soil nitrogen availability was also being used to support
993 non-photosynthetic nitrogen pools, possibly to structural tissue or stress-induced
994 amino acid and polyamine synthesis (Minocha et al. 2000; Onoda et al. 2004;
995 Bubier et al. 2011). While I found no change in the proportion of leaf nitrogen
996 allocated to leaf structural tissue, the overall stimulation in leaf nitrogen content
997 with increasing soil nitrogen availability suggests an increase in the net amount
998 of nitrogen invested in leaf structural tissue along the N availability gradient.
999 Importantly, leaf nitrogen allocated to structure was calculated using an empiri-
1000 cal relationship between M_{area} and the amount of leaf nitrogen allocated to cell
1001 walls (Onoda et al. 2017). As the generality of relationships between M_{area} and
1002 the amount of leaf nitrogen allocated to cell walls has been called into question
1003 (Harrison et al. 2009), future work should consider explicitly measuring nitrogen
1004 allocation to cell wall tissue and stress-induced amino acid synthesis to confirm
1005 these patterns.

1006 In opposition to patterns expected from least-cost theory, increasing soil
1007 nitrogen availability had no apparent effect on χ . Interestingly, despite the null
1008 effect of soil nitrogen availability on χ , I observed a strong negative effect of in-
1009 creasing N_{area} on χ , consistent with the nitrogen-water use tradeoffs expected from
1010 theory. The null response of χ to increasing soil nitrogen availability may have
1011 been due to a lack of water limitation in the system, given that the area received
1012 approximately 20% more precipitation (1167 mm) during the 12-month period
1013 leading up to our measurement period than normally expected (972 mm). How-

1014 ever, droughts can and do occur in temperate forests of the northeastern United
1015 States (Sweet et al. 2017), so the observed increase in leaf nitrogen content with
1016 increasing soil nitrogen availability could be a strategy that allows trees to hedge
1017 bets against drier than normal growing seasons (Onoda et al. 2004; Onoda et al.
1018 2017; Hallik et al. 2009). As was suggested in Paillassa et al. (2020), and more
1019 recently by Querejeta et al. (2022), negative effects of soil nitrogen availabil-
1020 ity on χ may increase with increasing aridity. This strategy would be especially
1021 advantageous if it allows individuals growing in arid regions to maintain carbon
1022 assimilation rates with reduced water loss. Future work should attempt to quan-
1023 tify interactive roles of climate and soil nitrogen availability on nitrogen-water use
1024 tradeoffs, which could be done by leveraging coordinated and multifactor nutrient
1025 (Borer et al. 2014) and water (Knapp et al. 2017) manipulation experiments
1026 across broad climatic gradients.

1027 3.4.2 *Soil pH did not modify tradeoffs between nitrogen and water usage*

1028 While the primary purpose of this study was to examine the role of soil nitrogen
1029 availability on nitrogen-water use tradeoffs, this experimental design manipulated
1030 both soil nitrogen and pH, providing an opportunity to isolate the roles of these
1031 variables. Previous correlational studies along environmental gradients have iden-
1032 tified soil pH as a particularly important factor that can modify tradeoffs between
1033 nutrient and water use (Smith et al. 2019; Paillassa et al. 2020; Westerband et al.
1034 2023) and the proportion of leaf nitrogen allocated to photosynthesis (Luo et al.
1035 2021). Such studies implied that these patterns may be driven by reductions in
1036 the cost of acquiring nutrients relative to water with increasing pH, which may

1037 be exacerbated in acidic soils.

1038 Consistent with theory (Wright et al. 2003; Prentice et al. 2014), results
1039 indicate that increasing soil pH was negatively associated with PNUE. However,
1040 there was no effect of soil pH on leaf nitrogen content, χ , or leaf nitrogen content
1041 per unit χ , most likely because the experimental nitrogen additions increased soil
1042 nitrogen supply while both increasing (sodium nitrate) and decreasing (ammo-
1043 nium sulfate) soil pH. These results suggest that soil pH did not play a major
1044 role in modifying expected photosynthetic least-cost theory patterns, contrasting
1045 findings from Paillassa et al. (2020) and other gradient studies that note positive
1046 effects of increasing soil pH on leaf nitrogen content, Rubisco carboxylation, and
1047 χ (Viet et al. 2013; Cornwell et al. 2018; Luo et al. 2021). Instead, null responses
1048 to soil pH show that leaf photosynthetic parameters depend more on soil nitrogen
1049 availability than pH per se, and that inferences from gradient studies might be
1050 confounding covariation between nitrogen availability and soil acidity.

1051 3.4.3 *Species identity explains a large amount of variation in leaf and whole*
1052 *plant traits*

1053 Species generally explained a larger amount of variation in measured leaf traits
1054 than soil nitrogen availability or soil pH. Interspecies variation is an important
1055 factor to consider when deducing mechanisms that drive photosynthetic least-
1056 cost theory, particularly for species that form distinct mycorrhizal associations or
1057 have different photosynthetic pathways, growth forms, or leaf habit (Espelta et al.
1058 2005; Adams et al. 2016; Bialic-Murphy et al. 2021; Scott and Smith 2022). The
1059 need to consider species may also be important when comparing nutrient-water

1060 use tradeoffs in early and late successional species, or in species with different
1061 resource economic strategies (Abrams and Mostoller 1995; Ellsworth and Reich
1062 1996; Wright et al. 2004; Reich 2014; Onoda et al. 2017; Ziegler et al. 2020).

1063 A strength of the study design and sampling effort is that it controls for
1064 many species differences that should modify nitrogen-water use tradeoffs expected
1065 from theory. All tree species measured in this study shared the leaf habit of de-
1066 ciduous broadleaves, were growing in forests of similar successional stage, but
1067 differed in mycorrhizal association and consequent resource economic strategies.
1068 As stands tended to be dominated by trees that associate with arbuscular myc-
1069 orrhizae (*Fraxinus* and both *Acer* species made up roughly 70% of total above-
1070 ground biomass across stands), ecosystem biogeochemical cycle dynamics may be
1071 more closely aligned to the inorganic nutrient economy proposed in Phillips et al.
1072 (2013), which may promote stronger nitrogen-water use tradeoffs in tree species
1073 that associate with arbuscular mycorrhizae. This result was not observed here,
1074 as photosynthetic properties varied as much within as across the two mycorrhizal
1075 associations represented. Given the high variability in measured photosynthetic
1076 traits within and across species, effects of mycorrhizal association likely require
1077 more intensive sampling efforts to detect than were possible here.

1078 3.4.4 *Implications for photosynthetic least-cost theory model development*

1079 In the field, soil nutrient availability is heterogeneous across time and space (Ta-
1080 ble B4). Unaccounted within-plot heterogeneity may have contributed to the low
1081 amount of variation explained by soil nitrogen availability in statistical models,
1082 as resin bags are a coarse surrogate for soil nitrogen availability. Despite this, I

1083 still observed evidence for nutrient-water use tradeoffs, suggesting that observed
1084 responses reported here may be an underestimate toward the net effect of soil ni-
1085 trogen availability on these tradeoffs. While I urge caution in the interpretation of
1086 these results, they do provide a promising baseline for future studies investigating
1087 patterns expected from photosynthetic least-cost theory at finer spatiotemporal
1088 resolutions.

1089 The general stronger relationship between leaf nitrogen content and photo-
1090 synthetic parameters versus between leaf nitrogen content and soil nitrogen avail-
1091 ability suggests that leaf nitrogen content is more directly tied to photosynthesis
1092 than soil nitrogen availability. While this could be due to the high spatiotemporal
1093 heterogeneity of soil nitrogen availability, principles from photosynthetic least-
1094 cost theory suggest that leaf nitrogen content is the downstream product of leaf
1095 nutrient demand to build and maintain photosynthetic machinery, which is set by
1096 aboveground environmental conditions such as light availability, CO₂, tempera-
1097 ture, or vapor pressure deficit (Smith et al. 2019; Paillassa et al. 2020; Peng et al.
1098 2021; Westerband et al. 2023). The stronger relationship between leaf nitrogen
1099 and photosynthetic parameters, paired with the strong negative relationship be-
1100 tween leaf nitrogen and χ , could indicate a relatively stronger effect of climate on
1101 leaf nitrogen-photosynthesis relationships than soil resource availability. However,
1102 the short distance between plots and across sites limited our ability to test this
1103 mechanism.

1104 Variation in soil pH affected least cost responses less than variations in soil
1105 nitrogen availability, in part because experimental treatments directly increased
1106 soil nitrogen and affected soil pH in opposite directions. While soil pH has been

1107 shown to drive nitrogen-water tradeoffs in global gradient analyses (Viet et al.
1108 2013; Paillassa et al. 2020), these responses may be due to covariations between
1109 soil pH and nutrient cycling rather than a role of pH per se. The direct manipu-
1110 lations of soil pH and soil nitrogen availability in this study allowed us to partly
1111 disentangle these factors and show that variation in nitrogen availability matters
1112 more for least-cost tradeoffs than pH alone.

1113 3.4.5 *Conclusions*

1114 Increasing soil nitrogen availability generally increased leaf nitrogen content (both
1115 area- and mass-based), but did not significantly influence χ . This shift in leaf ni-
1116 trogen led to a reduction in PNUE, and an increase in leaf nitrogen per unit
1117 χ with increasing soil nitrogen availability. Despite null effects of soil nitrogen
1118 availability on χ , I observed a strong negative relationship between leaf nitrogen
1119 content and χ . These results provide empirical support for the nutrient-water use
1120 tradeoffs expected from photosynthetic least-cost theory in response to increas-
1121 ing soil nutrient availability, but suggest that all tenets of the theory may not
1122 hold in every environment. These results experimentally test previous work sug-
1123 gesting that leaf nitrogen-water economies vary across gradients of soil nutrient
1124 availability and pH, and show that variations in nutrient availability matter more
1125 for determining variation in leaf photosynthetic traits than soil pH.

1126

Chapter 4

1127 The relative cost of resource use for photosynthesis drives variance in
1128 leaf nitrogen content across a climate and soil resource availability
1129 gradient

1130 4.1 Introduction

1131 Terrestrial biosphere models, which comprise the land surface component of Earth
1132 system models, are sensitive to the formulation of photosynthetic processes (Knorr
1133 and Heimann 2001; Ziehn et al. 2011; Booth et al. 2012; Walker et al. 2021).
1134 This is because photosynthesis is the largest carbon flux between the atmosphere
1135 and terrestrial biosphere (IPCC 2021), and is constrained by ecosystem carbon
1136 and nutrient cycles (Hungate et al. 2003; LeBauer and Treseder 2008; Fay et al.
1137 2015). Many terrestrial biosphere models formulate photosynthesis by parame-
1138 terizing photosynthetic capacity within plant functional groups through empiri-
1139 cal linear relationships between area-based leaf nitrogen content (N_{area}) and the
1140 maximum carboxylation rate of Ribulose-1,5-bisphosphate carboxylase/oxygenase
1141 (V_{cmax}) (Kattge et al. 2009; Rogers 2014; Rogers et al. 2017). Models are also
1142 beginning to include connected carbon-nitrogen cycles (Wieder et al. 2015; Shi
1143 et al. 2016; Davies-Barnard et al. 2020; Braghieri et al. 2022), which allows leaf
1144 photosynthesis to be predicted directly through changes in N_{area} and indirectly
1145 through changes in soil nitrogen availability (e.g., LPJ-GUESS, CLM5.0) (Smith
1146 et al. 2014; Lawrence et al. 2019). Despite recent model developments, open
1147 questions remain regarding the generality of ecological relationships between soil
1148 nitrogen availability, leaf nitrogen content, and leaf photosynthesis across edaphic
1149 and climatic gradients.

1150 Empirical support for positive relationships between soil nitrogen availabil-
1151 ity and N_{area} is abundant (Firn et al. 2019; Liang et al. 2020), and is a result
1152 often attributed to the high nitrogen cost of building and maintaining Rubisco
1153 (Evans 1989; Evans and Seemann 1989; Onoda et al. 2004; Walker et al. 2014;
1154 Onoda et al. 2017; Dong et al. 2020). Such patterns imply that positive rela-
1155 tionships between soil nitrogen availability and N_{area} should cause an increase in
1156 leaf photosynthesis and photosynthetic capacity by increasing the maximum rate
1157 of Rubisco carboxylation through increased investments to Rubisco construction
1158 and maintenance. This integrated N_{area} -photosynthesis response to soil nitrogen
1159 availability has been observed both in manipulative experiments and across envi-
1160 ronmental gradients (Field and Mooney 1986; Evans 1989; Walker et al. 2014; Li
1161 et al. 2020), and is thought to be driven by ecosystem nitrogen limitation, which
1162 limits primary productivity globally (LeBauer and Treseder 2008; Fay et al. 2015).
1163 However, this response is not consistently observed, as recent studies note variable
1164 N_{area} -photosynthesis relationships across soil nitrogen availability gradients (Liang
1165 et al. 2020; Luo et al. 2021) and that aboveground growing conditions (e.g., light
1166 availability, temperature, vapor pressure deficit) or species identity traits (e.g.,
1167 photosynthetic pathway, nitrogen acquisition strategy) may be more important
1168 for explaining variance in N_{area} and photosynthetic capacity across environmental
1169 gradients (Adams et al. 2016; Dong et al. 2017; Smith et al. 2019; Dong et al.
1170 2020; Peng et al. 2021; Dong et al. 2022; Westerband et al. 2023).

1171 One hypothesized mechanism to explain variance in N_{area} across environ-
1172 mental gradients has been proposed via photosynthetic least-cost theory (Wright
1173 et al. 2003; Prentice et al. 2014; Paillassa et al. 2020; Harrison et al. 2021).

1174 The theory predicts that plants acclimate to environments by optimizing photo-
1175 synthetic assimilation rates at the lowest summed cost of nitrogen and water use
1176 (Wright et al. 2003; Prentice et al. 2014). In a given environment, the theory
1177 suggests that nitrogen and water use can be substituted for each other to maintain
1178 the lowest summed cost of resource use, such that optimal photosynthetic rates
1179 are achieved with less efficient use of the more abundant and less costly resource
1180 to acquire in exchange for more efficient use of the less abundant and more costly
1181 resource to acquire.

1182 Photosynthetic least-cost theory predicts that, all else equal, an increase in
1183 soil nitrogen availability should decrease the cost of acquiring and using nitrogen
1184 relative to water (a ratio referred to herein as β), resulting in optimal photosyn-
1185 thetic rates achieved with greater N_{area} at lower stomatal conductance and lower
1186 leaf $C_i:C_a$ (Wright et al. 2003; Prentice et al. 2014; Paillassa et al. 2020). Alter-
1187 natively, an increase in soil moisture should reduce costs of water acquisition and
1188 use, increasing β (Lavergne et al. 2020), stomatal conductance, and leaf $C_i:C_a$, re-
1189 sulting in optimal photosynthetic rates achieved with decreased N_{area} . The theory
1190 also predicts variability in stomatal conductance and N_{area} in response to climatic
1191 factors, suggesting that the optimal response to increased vapor pressure deficit
1192 (VPD) should be a reduction in stomatal conductance and leaf $C_i:C_a$ that is coun-
1193 terbalanced by an increase in N_{area} to support the higher photosynthetic capacity
1194 needed to maintain high assimilation at lower conductance (Grossiord et al. 2020;
1195 Dong et al. 2020; López et al. 2021; Westerband et al. 2023).

1196 Leaf nitrogen allocation responses to changing climates or soil resource
1197 availability may also depend on their mode of nutrient acquisition or photo-

1198 synthetic pathway. For example, species that form associations with symbiotic
1199 nitrogen-fixing bacteria (referred as “N-fixing species” from this point forward)
1200 should, in theory, have access to a less finite nitrogen supply, which may result in
1201 lower β values on average compared to species not capable of forming such associ-
1202 ations (referred as “non-fixing species” from this point forward). This result was
1203 previously shown in a greenhouse experiment, where a leguminous species gener-
1204 ally had lower costs of nitrogen acquisition compared to a non-leguminous species,
1205 although these differences were generally stronger under increased nitrogen limi-
1206 tation (Perkowski et al. 2021). Lower β values could be a possible explanation for
1207 why N-fixing species commonly have higher leaf nitrogen content than non-fixing
1208 species (Adams et al. 2016; Dong et al. 2017).

1209 Similarly, leaf nitrogen allocation patterns across environmental gradients
1210 may be dependent on photosynthetic pathway. Lower leaf $C_i:C_a$ values in C₄
1211 species suggests that C₄ species should have lower β values than C₃ species (Scott
1212 and Smith 2022), a pattern that could be the result of increased costs associated
1213 with water acquisition and use or reduced costs of nitrogen acquisition and use
1214 relative to C₃ species. Theory predicts that this response in C₄ species will cause
1215 C₄ species to have higher leaf nitrogen content on average compared to C₃ species,
1216 though ample evidence exists documenting general lower leaf nitrogen content in
1217 C₄ species (Schmitt and Edwards 1981; Sage and Pearcy 1987; Ghannoum et al.
1218 2011). No study to date has directly quantified β in C₄ species aside from the
1219 initial parameterization of β in an optimality model for C₄ species (Scott and
1220 Smith 2022) using a global dataset of leaf $\delta^{13}\text{C}$ values (Cornwell et al. 2018).

1221 While photosynthetic least-cost theory provides a unified framework for

1222 understanding integrated effects of climate and soil resource availability on N_{area} ,
1223 empirical tests of the theory are sparse. Previous work shows that increasing
1224 soil nitrogen availability decreases costs of acquiring nutrients (Bae et al. 2015;
1225 Perkowski et al. 2021; Lu et al. 2022), which can induce predictable nutrient-
1226 water use tradeoffs expected from the theory across broad environmental gradients
1227 (Paillassa et al. 2020; Querejeta et al. 2022; Westerband et al. 2023) and in
1228 manipulation experiments (Bialic-Murphy et al. 2021). Additionally, increasing
1229 VPD has been shown to have a positive effect on N_{area} (Dong et al. 2017; Dong
1230 et al. 2020; Firn et al. 2019; López et al. 2021). However, studies have been
1231 restricted to exploring these patterns in C₃ species and, while previous studies have
1232 shown that variance in N_{area} across environmental gradients is driven by strong
1233 negative relationships with leaf $C_i:C_a$ (Fig. 3.4) (Dong et al. 2017; Paillassa et al.
1234 2020; Westerband et al. 2023), no study has explicitly investigated effects of soil
1235 resource availability or species identity on N_{area} using β as a direct predictor of leaf
1236 $C_i:C_a$. Furthermore, as N_{area} can be broken down into structural (leaf mass per
1237 area; M_{area} ; g m⁻²) and metabolic (mass-based leaf nitrogen content; N_{mass} ; gN
1238 g⁻¹) components (Dong et al. 2017), no study has investigated which component
1239 of N_{area} drives the hypothesized response of N_{area} to leaf $C_i:C_a$. Understanding
1240 whether changes in N_{area} due to leaf $C_i:C_a$ are driven by changes in leaf morphology
1241 or stoichiometry is important, especially because N_{mass} tends to covary with M_{area}
1242 due to tradeoffs between leaf longevity and leaf productivity (Wright et al. 2004;
1243 Reich 2014; Onoda et al. 2017; Wang et al. 2023).

1244 In this study, I measured N_{area} , N_{mass} , M_{area} , leaf δ¹³C-derived estimates
1245 of leaf $C_i:C_a$, and leaf δ¹³C-derived estimates of β in 520 individuals spanning

1246 57 species scattered across 24 grassland sites in Texas, USA (Table C1). Texas
1247 contains a diverse climatic gradient, indicated by 2006-2020 mean annual precipi-
1248 tation totals ranging from 204 to 1803 mm and 2006-2020 mean annual tempera-
1249 ture ranging from 11.8° to 24.6°C. Variability in soil nitrogen availability and soil
1250 moisture was expected across sites, owing to differences in soil texture and above-
1251 ground climate that would drive differential rates of water retention and nitrogen
1252 transformations to plant-available nitrogen substrate. I leveraged the expected
1253 climatic and soil resource variability across sites to test the following hypotheses:

- 1254 1. Soil nitrogen availability will decrease β through a reduction in costs of
1255 nitrogen acquisition and use, while soil moisture will increase β through a
1256 reduction in costs of water acquisition and use. Following previous results, I
1257 expected that N-fixing species would have lower β values and that C₄ species
1258 would have lower β values.
- 1259 2. Leaf $C_i:C_a$ will be positively related to β , a pattern that will result in a
1260 negative indirect effect of increasing soil nitrogen availability on leaf $C_i:C_a$,
1261 a positive indirect effect of increasing soil moisture on leaf $C_i:C_a$, and lower
1262 leaf $C_i:C_a$ in both N-fixing species and C₄ species. I expected that leaf
1263 $C_i:C_a$ would be negatively related to VPD, as increasing atmospheric dryness
1264 should cause plants to close stomata to minimize water loss.
- 1265 3. N_{area} will be negatively related to leaf $C_i:C_a$ and β . This response will result
1266 in an indirect positive effect of increasing soil nitrogen availability, a negative
1267 effect of increasing soil moisture on N_{area} , and generally larger N_{area} values
1268 in both N-fixing species. While theory predicts that negative relationships

1269 between N_{area} and leaf $C_i:C_a$ should yield generally larger N_{area} in C₄ species,
1270 I expected that C₄ species would have lower N_{area} due to generally greater
1271 nitrogen use efficiency in C₄ species than C₃ species. Additionally, VPD
1272 was expected to increase N_{area} , a pattern that would be directly mediated
1273 through the reduction in leaf $C_i:C_a$ with increasing VPD.

1274 4.2 Methods

1275 4.2.1 *Site descriptions and sampling methodology*

1276 I collected leaf and soil samples from 24 open grassland sites across central and
1277 eastern Texas in summer 2020 and summer 2021 (Fig. 4.1). Twelve sites were
1278 visited between June and July 2020 and 14 sites (11 unique from 2020) were visited
1279 between May and June 2021 (Table 4.1). I explicitly chose sites that maximized
1280 variability in precipitation and edaphic variability between sites while minimizing
1281 temperature variability across the environmental gradient (Table 4.1). No site
1282 with personally communicated or anecdotal evidence of grazing or disturbance
1283 (e.g., mowing, feral hog activity, etc.) was used. I collected leaf material from
1284 three individuals each of the five most abundant species at random locations
1285 at each site, only selecting species that were broadly classified as graminoid or
1286 forb/herb growth habits per the USDA PLANTS database (USDA NRCS 2022).
1287 All collected leaves were fully expanded with no visible herbivory or other external
1288 damage and also free from shading by nearby shrubs or trees. Five soil samples
1289 were collected from 0-15 cm below the soil surface at each site near the leaf
1290 collection sample locations. Soil samples were later mixed together by hand to
1291 create one composite soil sample per site.

1292 4.2.2 *Leaf trait measurements*

1293 Images of each leaf were taken immediately following each site visit using a flat-
1294 bed scanner. Fresh leaf area was determined from each image using the 'LeafArea'
1295 R package (Katabuchi 2015), which automates leaf area calculations using ImageJ
1296 software (Schneider et al. 2012). Each leaf was dried at 65°C for at least 48 hours
1297 to a constant mass, weighed, and manually ground in a mortar and pestle until
1298 homogenized. Leaf mass per area (M_{area} ; g m⁻²) was calculated as the ratio of
1299 dry leaf biomass to fresh leaf area. Subsamples of dried and homogenized leaf
1300 tissue were used to measure leaf nitrogen content (N_{mass} ; gN g⁻¹) through ele-
1301 mental combustion analysis (Costech-4010, Costech Instruments, Valencia, CA).
1302 Leaf nitrogen content per unit leaf area (N_{area} ; gN m⁻²) was then calculated as
1303 the product of N_{mass} and M_{area} .

1304 Subsamples of dried and homogenized leaf tissue were sent to the University
1305 of California-Davis Stable Isotope Facility to determine leaf $\delta^{13}\text{C}$. Leaf $\delta^{13}\text{C}$ values
1306 were determined using an elemental analyzer (PDZ Europa ANCA-GSL; Sercon
1307 Ltd., Chestshire, UK) interfaced to an isotope ratio mass spectrometer (PDZ
1308 Europa 20-20 Isotope Ratio Mass Spectrometer, Sercon Ltd., Chestshire, UK).
1309 I used leaf $\delta^{13}\text{C}$ values (‰; relative to Vienna Pee Dee Belemnite international
1310 reference standard) to estimate the ratio of intercellular (C_i) to extracellular (C_a)
1311 CO₂ ratio (leaf $C_i:C_a$; unitless) following the approach of Farquhar et al. (1989)
1312 described in Cernusak et al. (2013). Specifically, I derived leaf $C_i:C_a$ as:

$$C_i : C_a = \frac{\Delta^{13}C - a}{b - a} \quad (4.1)$$

1313 where $\Delta^{13}\text{C}$ represents the relative difference between leaf $\delta^{13}\text{C}$ (\textperthousand) and air $\delta^{13}\text{C}$
1314 (\textperthousand), calculated as:

$$\Delta^{13}\text{C} = \frac{\delta^{13}\text{C}_{\text{air}} - \delta^{13}\text{C}_{\text{leaf}}}{1 + \delta^{13}\text{C}_{\text{leaf}}} \quad (4.2)$$

1315 $\delta^{13}\text{C}_{\text{air}}$, which is commonly assumed to be $-8\text{\textperthousand}$ (Keeling et al. 1979; Farquhar
1316 et al. 1989), was calculated as a function of calendar year t using an empirical
1317 equation derived in Feng (1999):

$$\delta^{13}\text{C}_{\text{air}} = -6.429 - 0.006e^{0.0217(t-1740)} \quad (4.3)$$

1318 Using this equation, $\delta^{13}\text{C}_{\text{air}}$ values were set to $-9.04\text{\textperthousand}$ and $-9.09\text{\textperthousand}$ for 2020 and
1319 2021, respectively. The parameter a represents the fractionation between ^{12}C
1320 and ^{13}C due to diffusion in air, assumed to be $4.4\text{\textperthousand}$, while b represents the
1321 fractionation caused by Rubisco carboxylation, assumed to be $27\text{\textperthousand}$ (Farquhar
1322 et al. 1989). For C_4 species, b in Eqn. 4.1 was set to $6.3\text{\textperthousand}$, and was derived from:

$$b = c + (d \cdot \phi) \quad (4.4)$$

1323 Where c was set to $-5.7\text{\textperthousand}$ and d was set to $30\text{\textperthousand}$ (Farquhar et al. 1989). ϕ , which
1324 is the bundle sheath leakiness term, was set to 0.4. All leaf $C_{\text{i}}:C_{\text{a}}$ values less than
1325 0.1 and greater than 0.95 were assumed to be incorrect and removed.

1326 I derived the unit cost of resource use (β) using leaf $C_{\text{i}}:C_{\text{a}}$ and site climate
1327 data with equations first described in Prentice et al. (2014) and simplified in
1328 Lavergne et al. (2020):

$$\beta = 1.6\eta^* D \frac{\chi - (\frac{\Gamma^*}{C_a})^2}{(1 - \chi)^2(K_m + \Gamma^*)} \quad (4.5)$$

1329 where η^* is the viscosity of water relative to 25°C, calculated using elevation and
1330 mean air temperature of the seven days leading up to each site visit following
1331 equations in Huber et al. (2009). D represents vapor pressure deficit (Pa), set
1332 to the mean vapor pressure deficit of the seven days leading up to each site visit,
1333 C_a represents atmospheric CO₂ concentration, arbitrarily set to 420 μmol mol⁻¹
1334 CO₂. K_m (Pa) is the Michaelis-Menten coefficient for Rubisco affinity to CO₂ and
1335 O₂, calculated as:

$$K_m = K_c \cdot \left(1 + \frac{O_i}{K_o}\right) \quad (4.6)$$

1336 where K_c (Pa) and K_o (Pa) are the Michaelis-Menten coefficients for Rubisco
1337 affinity to CO₂ and O₂, respectively, and O_i is the intercellular O₂ concentration.
1338 Γ^* (Pa) is the CO₂ compensation point in the absence of dark respiration. K_c , K_o ,
1339 and Γ^* were determined using equations described in Medlyn et al. (2002) and
1340 derived in Bernacchi et al. (2001), invoking an elevation correction for atmospheric
1341 pressure as explained in Stocker et al. (2020).

Table 4.1. Site locality information, sampling year, 2006-2020 mean annual precipitation (MAP; mm), mean annual temperature (MAT; °C), and water holding capacity (WHC; mm)*

Site	Latitude	Longitude	Sampling year	MAP	MAT	WHC
Edwards_2019_17	29.95	-100.36	2020	563.5	19.0	224.7
Uvalde_2020_02	29.59	-100.09	2020, 2021	648.5	19.5	224.7
Menard_2020_01	30.91	-99.59	2020	641.9	18.3	220.2
Kerr_2020_03	30.06	-99.34	2021	672.4	18.3	237.5
Bandera_2020_03	29.85	-99.30	2021	789.4	18.8	235.1
Sansaba_2020_01	31.29	-98.62	2020	733.0	18.8	234.3
Comal_2020_21	29.79	-98.43	2020	878.5	19.9	220.7
Blanco_2019_16	29.99	-98.43	2020	833.0	19.2	222.2
Bexar_2019_13	29.24	-98.43	2020	759.3	21.5	206.0
Burnet_2020_14	30.84	-98.34	2021	763.3	19.5	217.8
Comal_2020_19	30.01	-98.32	2021	845.0	19.3	220.4
Hays_2020_54	29.96	-98.17	2021	861.3	20.0	225.6
Burnet_2020_12	30.82	-98.06	2021	815.1	19.4	245.3
Williamson_2019_09	30.71	-97.86	2020	867.7	19.7	270.2
Williamson_2019_10	30.54	-97.77	2020	819.5	19.9	239.8
Bell_2021_08	31.06	-97.55	2021	937.3	19.6	232.3
Fayette_2021_12	29.86	-97.21	2021	985.7	20.4	165.6
Fayette_2019_04	30.09	-96.78	2020	1017.4	20.6	226.9
Fayette_2020_09	29.86	-96.71	2021	1002.7	20.8	187.6
Washington_2020_08	30.28	-96.41	2021	1077.4	20.4	203.9
Austin_2020_03	29.78	-96.24	2021	1108.7	20.6	253.0
Brazos_2020_16	30.93	-96.23	2021	1078.0	20.1	202.2
Brazos_2020_18	30.52	-96.21	2020, 2021	1099.4	20.4	233.5
Harris_2020_03	29.88	-95.31	2020, 2021	1492.0	21.6	265.6

1342 * Rows are arranged by longitude to visualize precipitation variability across sites

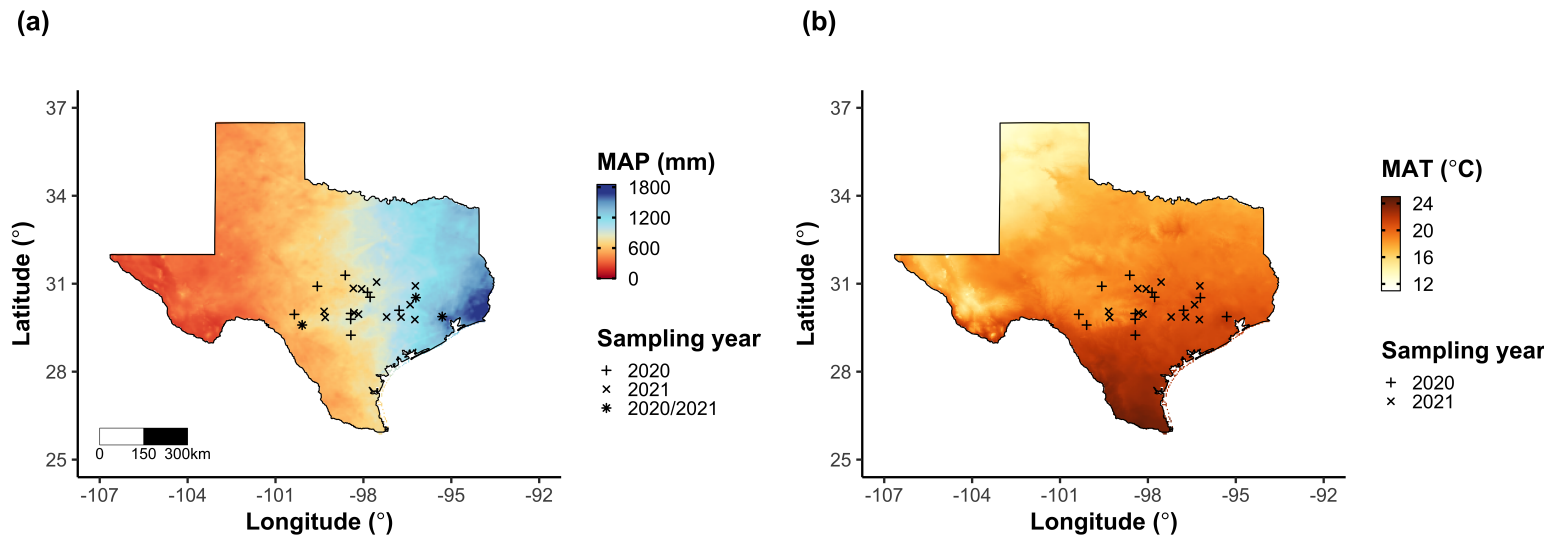


Figure 4.1. Site locations along 2006-2020 mean annual precipitation (a) and mean annual temperature (b) gradients in Texas, USA. Precipitation and temperature data were plotted at a 4-km grid resolution and are masked to include only grid cells that occur within the Texas state boundary of the United States. In both panels, addition signs refer to sites visited in 2020, multiplication signs to sites visited in 2021, and asterisks to sites visited in 2020 and 2021. The scale bar in (a) also applies to (b).

1343 4.2.3 *Site climate data*

1344 I used the Parameter-elevation Regressions on Independent Slopes Model (PRISM)
1345 (Daly et al. 2008) climate product to access gridded daily temperature and precip-
1346 itation data for the coterminous United States at a 4-km grid resolution between
1347 January 1, 2006 and July 31, 2021 (PRISM Climate Group, Oregon State Uni-
1348 versity, <https://prism.oregonstate.edu>, data created 4 Feb 2014, accessed 24 Mar
1349 2022). Daily mean air temperature, mean VPD, and total precipitation data were
1350 extracted from the grid cell that contained the latitude and longitude of each
1351 property using the ‘extract’ function in the ‘terra’ R package (Hijmans 2022).
1352 PRISM data were used in lieu of local weather station data because several rural
1353 sites did not have a local weather station present within a 20-km radius of the site.
1354 Daily site climate data were used to estimate mean annual precipitation and mean
1355 annual temperature for each site between 2006 and 2020 (Table 4.1). I calculated
1356 total precipitation and mean daily VPD for the prior 1, 2, 3, 4, 5, 6, 7, 8, 9, 10,
1357 15, 20, 25, 30, 60, and 90 days leading up to each site visit.

1358 4.2.4 *Site edaphic characteristics*

1359 Subsamples of composited soil samples were sent to the Texas A & M Soil, Water
1360 and Forage Laboratory to quantify soil nitrate concentration ($\text{NO}_3\text{-N}$; ppm). Soil
1361 $\text{NO}_3\text{-N}$ was determined by extracting composite soil samples in 1 M KCl, measur-
1362 ing absorbance values of extracts at 520 nm using the end product of a $\text{NO}_3\text{-N}$ to
1363 $\text{NO}_2\text{-N}$ cadmium reduction reaction (Kachurina et al. 2000; Keeney and Nelson
1364 1983). Soil texture data from 0-15 cm below the soil surface were accessed using
1365 the SoilGrids2.0 data product (Poggio et al. 2021) through the ‘fetchSoilGrids’

1366 function in the ‘soilDB’ R package (Beaudette et al. 2022). I used SoilGrids2.0
1367 to access soil texture data in lieu of analyses using the collected composite soil
1368 sample due to a lack of soil material from some sites after sending samples for soil
1369 NO₃-N.

1370 Soil moisture was not measured in the field, but was estimated using the
1371 ‘Simple Process-Led Algorithms for Simulating Habitats’ model (SPLASH) (Davis
1372 et al. 2017). This model, derived from the STASH model (Cramer and Prentice
1373 1988), spins up a bucket model using Priestley-Taylor equations (Priestley and
1374 Taylor 1972) to calculate daily soil moisture (W_n ; mm) as a function of the previous
1375 day’s soil moisture (W_{n-1} ; mm), daily precipitation (P_n ; mm), condensation (C_n ;
1376 mm), actual evapotranspiration (E_n^a ; mm), and runoff (RO; mm):

$$W_n = W_{n-1} + P_n + C_n - E_n^a - RO \quad (4.7)$$

1377 Models were spun up by equilibrating the previous day’s soil moisture using succes-
1378 sive model iterations with daily mean air temperature, daily precipitation total,
1379 the number of daily sunlight hours, and latitude as model inputs (Davis et al.
1380 2017). Daily sunlight hours were estimated for each day at each site using the
1381 ‘getSunlightTimes’ function in the ‘suncalc’ R package, which estimated sunrise
1382 and sunset times of each property using date and site coordinates (Thieurmel and
1383 Elmarhraoui 2019). Water holding capacity (mm), or bucket size, was estimated
1384 as a function of soil texture using pedotransfer equations explained in Saxton and
1385 Rawls (2006), as done in Stocker et al. (2020) and Bloomfield et al. (2023). A
1386 summary of these equations is included in Appendix C.1.

1387 Daily soil moisture outputs from the SPLASH model for each site were
1388 used to calculate mean daily soil moisture for the prior 1, 2, 3, 4, 5, 6, 7, 8, 9,
1389 10, 15, 20, 25, 30, 60, and 90 days leading up to each site visit. Mean daily
1390 soil moisture values were then expressed as a fraction of water holding capacity
1391 to normalize across sites with different bucket depths, as done in Stocker et al.
1392 (2018).

1393 4.2.5 *Plant functional group assignments*

1394 Plant functional group was assigned to each species and used as the primary de-
1395 scriptor of species identity. Specifically, plant functional groups were assigned
1396 based on photosynthetic pathway (C_3 , C_4) and ability to form associations with
1397 symbiotic nitrogen-fixing bacteria. The ability to form associations with symbi-
1398 otic nitrogen-fixing bacteria was assigned based on whether species were in the
1399 *Fabaceae* family, and photosynthetic pathway of each species was determined from
1400 past literature and confirmed through leaf $\delta^{13}C$ values. We chose these plant func-
1401 tional groups based on *a priori* hypotheses regarding the functional role of nitrogen
1402 fixation and photosynthetic pathway on the sensitivity of plant nitrogen uptake
1403 and leaf nitrogen allocation to soil nutrient availability and aboveground growing
1404 conditions. These plant functional group classifications resulted in three distinct
1405 plant functional groups within our dataset: C_3 legumes (n=53), C_3 non-legumes
1406 (n=350), and C_4 non-legumes (n=117).

1407 4.2.6 *Data analysis*

1408 All analyses and plotting were conducted in R version 4.1.1 (R Core Team 2021).

1409 I constructed a series of separate linear mixed-effects models to investigate en-

1410 vironmental drivers of β , leaf $C_i:C_a$, N_{area} , N_{mass} , and M_{area} , followed by a path

1411 analysis using a piecewise structural equation model to investigate direct and

1412 indirect effects of climate and soil resource availability on N_{area} .

1413 To explore environmental drivers of β , I built a linear mixed-effects model

1414 that included soil moisture, soil nitrogen availability, and plant functional group

1415 as fixed effect coefficients. Species were designated as a random intercept term.

1416 Interaction coefficients between all possible combinations of the three fixed effect

1417 coefficients were also included. β was natural log transformed to linearize data.

1418 I used an information-theoretic model selection approach to determine whether

1419 90-, 60-, 30-, 20-, 15-, 10-, 9-, 8-, 7-, 6-, 5-, 4-, 3-, 2-, or 1-day mean daily soil

1420 moisture conferred the best model fit for β . To do this, I constructed 16 separate

1421 linear mixed-effects models where log-transformed β was included as the response

1422 variable and each soil moisture time step was separately included as a single

1423 continuous fixed effect. Species were included as a random intercept term for all

1424 models. I used corrected Akaike Information Criterion (AICc) to select the soil

1425 moisture timescale that conferred the best model fit, indicated by the model with

1426 the lowest AICc score (Table C4; Fig. C1).

1427 To explore environmental drivers of leaf $C_i:C_a$, I constructed a second linear

1428 mixed effects model that included VPD, soil moisture, soil nitrogen availability,

1429 and plant functional group as fixed effect coefficients. Two-way interactions be-

1430 tween plant functional group and VPD, soil nitrogen availability, or soil moisture

1431 were also included as fixed effect coefficients, in addition to a three-way interaction
1432 between soil moisture, soil nitrogen availability, and plant functional group.
1433 Species were included as a random intercept term. I used an information-theoretic
1434 model selection approach to determine whether 90-, 60-, 30-, 20-, 15-, 10-, 9-, 8-,
1435 7-, 6-, 5-, 4-, 3-, 2-, or 1-day mean daily VPD conferred the best model fit for leaf
1436 $C_i:C_a$ using the same approach explained above for the soil moisture effect on β .
1437 The soil moisture timescale was set to the same timescale that conferred the best
1438 fit for β .

1439 To explore environmental drivers of N_{area} , N_{mass} , and M_{area} , I constructed
1440 a linear mixed effects model for each trait, including leaf $C_i:C_a$, soil nitrogen
1441 availability, soil moisture, and plant functional group as fixed effect coefficients
1442 for each model. Two-way interactions between plant functional group and β , leaf
1443 $C_i:C_a$, soil nitrogen availability, or soil moisture were included as additional fixed
1444 effect coefficients, in addition to a three-way interaction between soil nitrogen
1445 availability, soil moisture, and plant functional group. Species were included as a
1446 random intercept term, with the soil moisture timescale set to the same timescale
1447 that conferred the best fit for β .

1448 In all linear mixed-effects models explained above, including those to select
1449 relevant timescales, I used the 'lmer' function in the 'lme4' R package (Bates et al.
1450 2015) to fit each model and the 'Anova' function in the 'car' R package (Fox and
1451 Weisberg 2019) to calculate Type II Wald's χ^2 and determine the significance
1452 level ($\alpha=0.05$) of each fixed effect coefficient. I used the 'emmeans' R package
1453 (Lenth 2019) to conduct post-hoc comparisons using Tukey's tests, where degrees
1454 of freedom were approximated using the Kenward-Roger approach (Kenward and

1455 Roger 1997). Trendlines and error ribbons for all plots were drawn using a series
1456 of ‘emmeans’ outputs across the range in plotted x-axis values.

1457 Finally, I conducted a path analysis using a piecewise structural equation
1458 model to examine direct and indirect pathways that determined variance in N_{area} .
1459 Six separate linear mixed effects models were loaded into the piecewise structural
1460 equation model. Models were constructed per *a priori* hypotheses following pat-
1461 terns expected from photosynthetic least-cost theory. The first model regressed
1462 N_{area} against N_{mass} and M_{area} . The second model regressed M_{area} against leaf
1463 $C_i:C_a$. The third model regressed N_{mass} against leaf $C_i:C_a$ and M_{area} (Dong et al.
1464 2017; Dong et al. 2020). The fourth model regressed leaf $C_i:C_a$ against β and
1465 VPD. The fifth model regressed β against soil nitrogen availability, soil moisture,
1466 ability to associate with symbiotic nitrogen-fixing bacteria, and photosynthetic
1467 pathway. The sixth model regressed soil nitrogen availability against soil mois-
1468 ture. All models included the relevant timescale selected in the individual linear
1469 mixed effect models explained above. Models included species as a random inter-
1470 cept term, were built using the ‘lme’ function in the ‘nlme’ R package (Pinheiro
1471 and Bates 2022), and subsequently loaded into the piecewise structural equation
1472 model using the ‘psem’ function in the ‘piecewiseSEM’ R package (Lefcheck 2016).

1473 4.3 Results

1474 4.3.1 *Cost to acquire nitrogen relative to water*

1475 Model selection indicated that 90-day soil moisture conferred the best model fit

1476 for β (AICc=1429.14; Table C4; Fig. C1).

1477 Increasing soil nitrogen availability generally decreased β ($p<0.001$; Table

1478 4.2; Fig. 4.2a), a pattern driven by a negative effect of increasing soil nitrogen on

1479 β in C₃ nonlegumes (Tukey: $p=0.002$) and C₃ legumes (Tukey: $p=0.031$) despite

1480 a null effect of soil nitrogen on β in C₄ nonlegumes (Tukey: $p=0.905$). There was

1481 no effect of soil moisture on β ($p=0.902$; Table 4.2; Fig. 4.2b). A functional group

1482 effect ($p<0.001$; Table 4.2) indicated that C₄ nonlegumes generally had lower β

1483 values than both C₃ legumes and C₃ non-legumes (Tukey: $p<0.001$ in both cases),

1484 while β values in C₃ legumes did not differ from C₃ nonlegumes (Tukey: $p=0.804$).

Table 4.2. Effects of soil moisture, soil nitrogen availability, and plant functional group on β^*

	df	Coefficient	χ^2	p
Intercept	-	3.39E+00	-	-
Soil moisture (SM ₉₀)	1	-2.03E-01	0.015	0.902
Soil N (N)	1	-1.49E-02	13.832	<0.001
PFT	2	-	225.049	<0.001
SM ₉₀ *N	1	-8.86E-04	1.016	0.313
SM ₉₀ *PFT	2	-	0.754	0.686
N*PFT	2	-	5.236	0.073
SM ₉₀ *N*PFT	2	-	3.633	0.163

1485 *Significance determined using Type II Wald χ^2 tests ($\alpha=0.05$). P-values<0.05
1486 are in bold. Model coefficients are expressed on the natural-log scale and are only
1487 included for continuous fixed effects. Key: df=degrees of freedom; χ^2 =Wald Type
1488 II chi-square test statistic

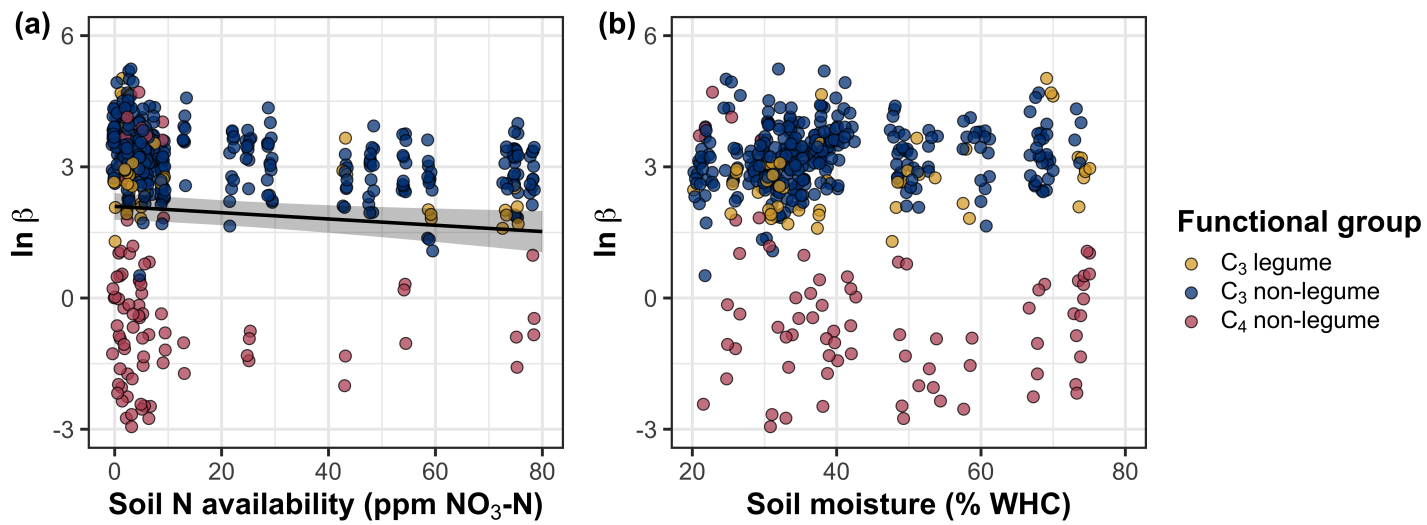


Figure 4.2. Effects of soil nitrogen availability (a) and soil moisture (b) on the cost of acquiring and using nitrogen (β ; unitless). Soil nitrogen availability is represented on the x-axis in (a), soil moisture is represented on the x-axis in (b) as a percent of site water holding capacity, and natural-log transformed β is represented on the y-axis for both panels. Yellow points represent C_3 legumes, blue points represent C_3 nonlegumes, and red points represent C_4 nonlegumes. Throughout, points are jittered for visibility. A black solid trendline is drawn to denote bivariate relationships where the slope is different from zero ($p<0.05$), with error ribbons representing the upper and lower 95% confidence intervals.

1489 4.3.2 *Leaf C_i:C_a*

1490 Model selection indicated that 4-day daily VPD was the timescale that conferred

1491 the best model fit for leaf $C_i:C_a$ (AICc=-793.49; Table C4; Fig. C1).

1492 Model results revealed that increasing VPD generally decreased leaf $C_i:C_a$

1493 ($p<0.001$; Table 4.3; Fig. 4.3a). There was no effect of soil moisture ($p=0.843$;

1494 Table 4.3; Fig. 4.3b) or soil nitrogen availability ($p=0.544$; Table 4.3; Fig. 4.3c) on

1495 leaf $C_i:C_a$. A strong plant functional group effect ($p<0.001$; Table 4.3) indicated

1496 that C₄ nonlegumes had lower leaf $C_i:C_a$ than C₃ legumes and C₃ nonlegumes

1497 (Tukey: $p<0.001$ in both cases), with no difference between C₃ legumes and C₃

1498 nonlegumes (Tukey: $p=0.865$).

Table 4.3. Effects of soil moisture, soil nitrogen availability, and plant functional group on leaf $C_i:C_a$ *

	df	Coefficient	χ^2	p
Intercept	-	1.32E+00	-	-
Vapor pressure deficit (VPD_4)	1	-4.53E-01	11.211	<0.001
Soil moisture (SM_{90})	1	-1.71E-01	0.039	0.843
Soil N (N)	1	-3.33E-03	0.369	0.544
PFT	2	-	227.005	<0.001
SM_{90}^*N	1	7.34E-03	2.361	0.124
VPD_4^*PFT	2	-	0.927	0.629
SM_{90}^*PFT	2	-	0.817	0.664
N^*PFT	2	-	4.085	0.130
$SM_{90}^*N^*PFT$	2	-	3.677	0.159

1499 *Significance determined using Type II Wald χ^2 tests ($\alpha=0.05$). P-values less
1500 than 0.05 are in bold and p-values where $0.05 < p < 0.1$ are italicized. Leaf $C_i:C_a$
1501 was not transformed prior to model fitting, so model coefficients are reported
1502 on the response scale. Model coefficients are only included for continuous fixed
1503 effects.

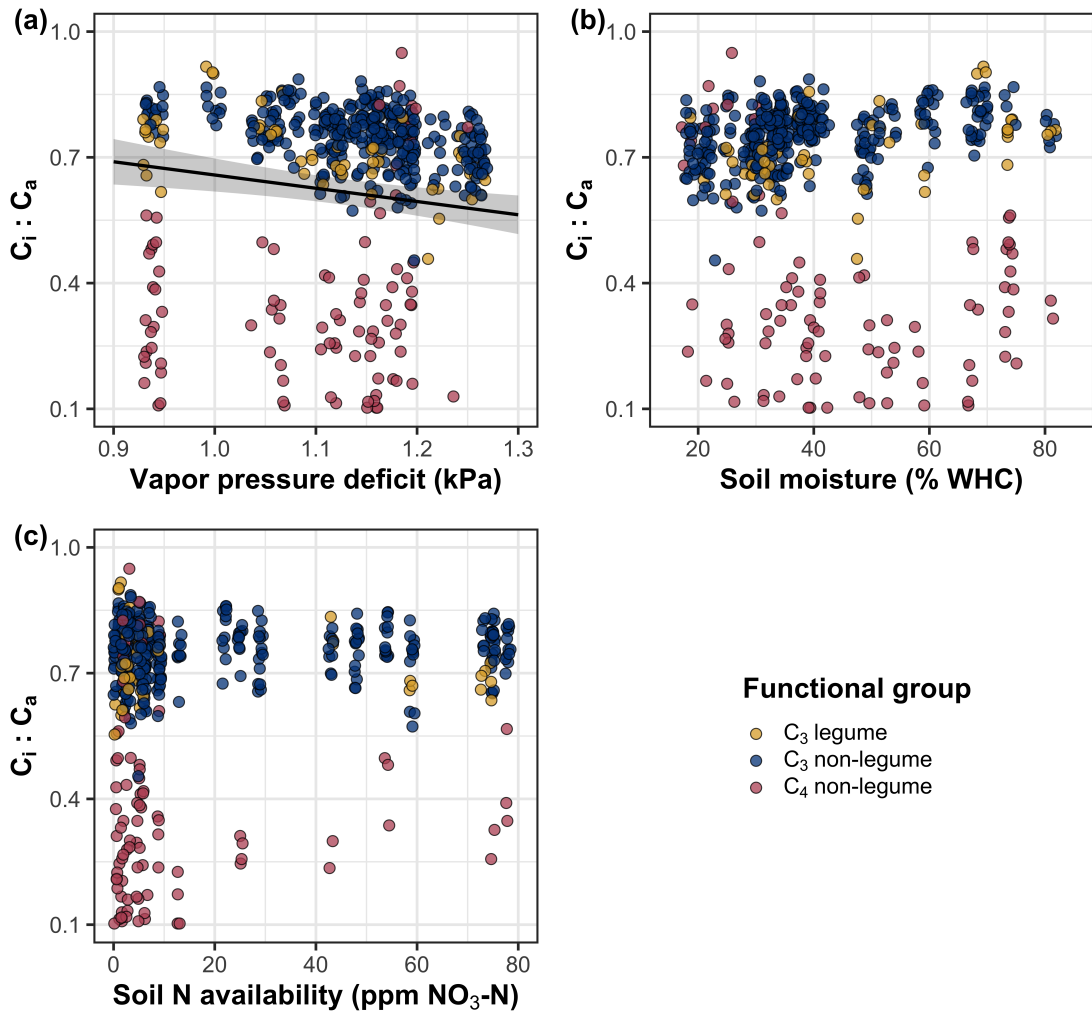


Figure 4.3. Effects of 4-day mean vapor pressure deficit (a), 90-day soil moisture (per water holding capacity; b), and soil nitrogen availability (c) on leaf $C_i:C_a$. Shading and trendlines are as explained in Figure 4.3. Points are jittered for visibility. Variably colored trendlines are only included if there is an interaction between the x-axis and plant functional group, where solid trendlines indicate slopes that are different from zero ($p < 0.05$) and dashed trendlines indicate slopes that are not different from zero ($p > 0.05$). Error ribbons represent the upper and lower 95% confidence intervals of each fitted trendline.

1504 4.3.3 *Leaf nitrogen content*

1505 An interaction between leaf $C_i:C_a$ and plant functional group ($p<0.001$; Table
1506 4.4) revealed that the negative effect of increasing leaf $C_i:C_a$ on N_{area} ($p<0.001$;
1507 Table 4.4) was driven by a negative effect of increasing leaf $C_i:C_a$ on N_{area} in
1508 C₃ nonlegumes (Tukey: $p<0.001$) and C₃ legumes (Tukey: $p=0.002$), with no
1509 observable effect in C₄ nonlegumes (Tukey: $p=0.795$; Fig. 4.4a). An interaction
1510 between soil nitrogen availability and plant functional group ($p=0.041$; Table 4.4)
1511 indicated that the positive effect of increasing soil nitrogen ($p=0.007$; Table 4.4)
1512 was only apparent in C₃ legumes (Tukey: $p<0.001$; Table 4.4; Fig. 4.4d), with no
1513 observable effect in C₃ nonlegumes (Tukey: $p=0.449$) or C₄ nonlegumes (Tukey:
1514 $p=0.680$). Increasing soil moisture increased N_{area} ($p=0.010$, Table 4.4). A plant
1515 functional group effect ($p<0.001$; Table 4.4) indicated that C₄ nonlegumes had
1516 lower N_{area} compared to C₃ legumes (Tukey: $p<0.001$) and C₃ nonlegumes (Tukey:
1517 $p<0.001$), while C₃ legumes had lower N_{area} compared to C₃ nonlegumes (Tukey:
1518 $p=0.030$).

1519 A marginal interaction between soil nitrogen availability and soil moisture
1520 ($p=0.097$; Table 4.4) indicated that the positive effect of increasing soil nitrogen
1521 on N_{mass} ($p<0.001$; Table 4.4; Fig. 4.4e) was only apparent when soil moisture was
1522 less than 50% of the maximum water holding capacity (Tukey: $p<0.05$ in all cases).
1523 There was no effect of leaf $C_i:C_a$ on N_{mass} ($p=0.447$; Table 4.4; Fig. 4.4b), but a
1524 positive effect of increasing soil moisture on N_{mass} . A plant functional group effect
1525 ($p<0.001$; Table 4.4) indicated that C₄ nonlegumes had lower N_{mass} compared to
1526 C₃ legumes (Tukey: $p=0.003$) and C₃ nonlegumes (Tukey: $p=0.011$), while N_{mass}
1527 did not differ between C₃ legumes and C₃ nonlegumes (Tukey: $p=0.231$).

1528 Variance in M_{area} was driven by a three-way interaction between soil nitro-
1529 gen availability, soil moisture, and plant functional group ($p=0.018$; Table 4.4).
1530 This interaction indicated that increasing soil moisture increased the positive effect
1531 of increasing soil nitrogen availability on M_{area} in C₃ legumes (Tukey: $p=0.030$)
1532 but did not modify the negative effect of increasing soil nitrogen on M_{area} in C₄
1533 nonlegumes (Tukey: $p=0.511$) or C₃ nonlegumes (Tukey: $p>0.999$). There was
1534 otherwise no effect of soil moisture on M_{area} ($p = 0.696$; Table 4.4). An inter-
1535 action between leaf $C_i:C_a$ and plant functional group ($p<0.001$; Table 4.4; Fig.
1536 4.4c) indicated that negative effect of increasing leaf $C_i:C_a$ on M_{area} ($p<0.001$;
1537 Table 4.4) was driven by a negative effect of increasing leaf $C_i:C_a$ on M_{area} in C₃
1538 legumes and C₃ nonlegumes (Tukey: $p<0.001$ in both cases), with no effect in C₄
1539 nonlegumes (Tukey: $p=0.343$; Fig. 4.4c).

Table 4.4. Effects of soil moisture, soil nitrogen availability, plant functional group, and leaf $C_i:C_a$ on leaf nitrogen content per unit leaf area (N_{area} ; g N m⁻²), leaf nitrogen content per unit leaf biomass (N_{mass} ; g g⁻¹), and leaf biomass per unit leaf area (M_{area} ; g m⁻²)

		N_{area}			N_{mass}			M_{area}		
	df	Coefficient	χ^2	p	Coefficient	χ^2	p	Coefficient	χ^2	p
(Intercept)	-	2.41E+00	-	-	6.28E-02	-	-	6.90E+00	-	-
$C_i:C_a$	1	-2.32E+00	7.386	0.007	8.04E-01	0.578	0.447	-3.13E+00	15.913	<0.001
Soil N (N)	1	1.26E-02	6.070	0.014	1.12E-02	90.940	<0.001	-2.66E-02	43.529	<0.001
Soil moisture (SM ₉₀)	1	5.60E-01	6.717	0.010	7.81E-01	11.205	<0.001	-2.53E-01	0.153	0.696
PFT	1	-	52.277	<0.001	-	17.184	<0.001	-	7.289	0.026
SM ₉₀ *N	1	5.44E-02	0.444	0.505	-1.91E-02	2.749	0.097	8.16E-02	1.690	0.194
$C_i:C_a$ *PFT	1	-	25.631	<0.001	-	4.864	0.078	-	34.683	<0.001
N*PFT	1	-	6.389	0.041	-	1.219	0.544	-	19.949	<0.001
SM ₉₀ *PFT	1	-	3.548	0.170	-	0.911	0.634	-	3.293	0.193
SM ₉₀ *N*PFT	1	-	3.520	0.172	-	0.092	0.955	-	7.987	0.018

96

1540 *Significance determined using Type II Wald χ^2 tests ($\alpha=0.05$). P-values less than 0.05 are in bold and p-values
 1541 where $0.05 < p < 0.1$ are italicized. Coefficients are reported on the natural-log scale for all traits and are only included
 1542 for continuous fixed effects.

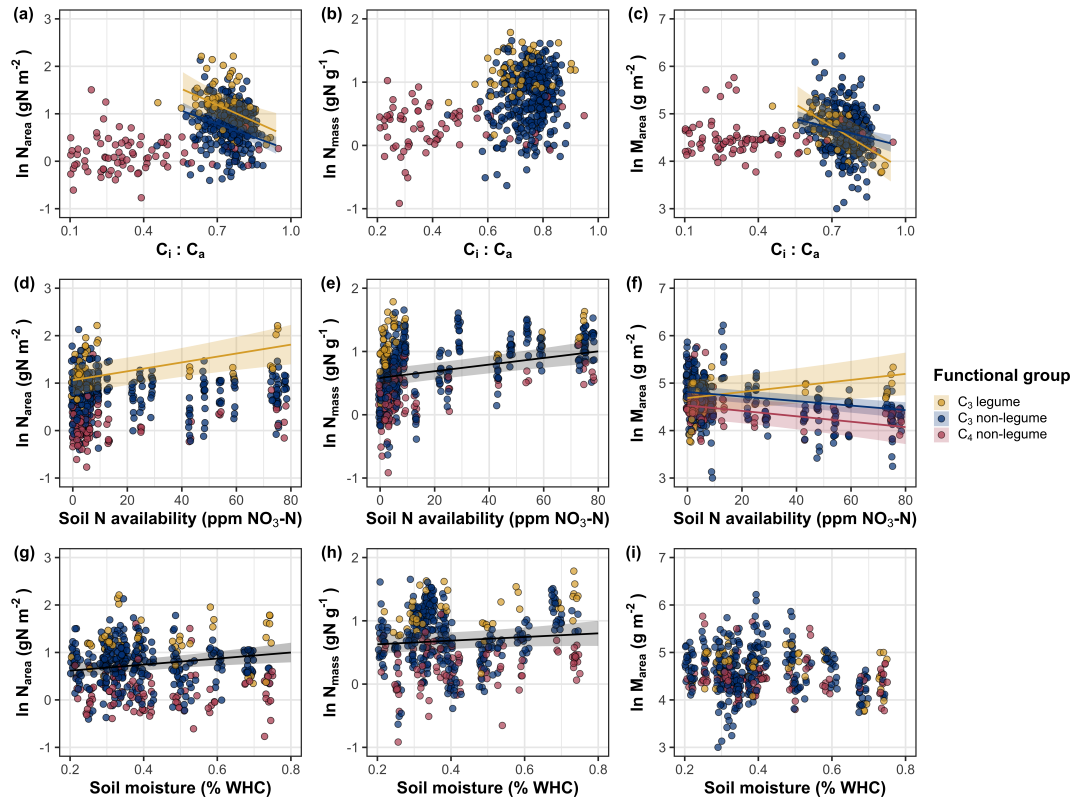


Figure 4.4. Effects of leaf $C_i:C_a$ (a-c), soil nitrogen availability (d-f), and soil moisture (g-i) on leaf nitrogen content per unit leaf area (a, d, g), leaf nitrogen content per unit leaf biomass (b, e, h), and leaf mass per area (c, f, i). Yellow points and trendlines indicate C_3 legumes, blue points and trendlines indicate C_3 nonlegumes, and red points and trendlines indicate C_4 nonlegumes. Points are jittered for visibility. Variably colored trendlines are only included if there is an interaction between plant functional group and the x-axis. Black solid trendlines denote bivariate slopes that are different from zero ($p < 0.05$) where there is no apparent interaction between plant functional group and the x-axis.

1543 4.3.4 *Structural equation model*

1544 The piecewise structural equation model explained 89%, 56%, 77%, 82%, and
1545 37% of variance in N_{area} , N_{mass} , M_{area} , leaf $C_i:C_a$, and β , respectively (Table 4.5; Fig. 4.5). Variance in N_{area} was driven by a positive effect of increasing N_{mass} and M_{area} ($p < 0.001$ in both cases; Table 4.5; Fig. 4.5). Model results indicated that an indirect negative effect of $C_i:C_a$ on N_{area} was driven by a strong reduction in M_{area} with increasing leaf $C_i:C_a$ ($p < 0.001$; Table 4.5) paired with no effect of increasing $C_i:C_a$ on N_{mass} ($p = 0.111$; Table 4.5). However, there was a strong negative effect of increasing M_{area} on N_{mass} ($p < 0.001$; Table 4.5; Fig. 4.5). Leaf $C_i:C_a$ increased with increasing β ($p < 0.001$; Table 4.5) and decreased with increasing VPD ($p < 0.001$; Table 4.5; Fig. 4.5). Variance in β was driven by a negative effect of increasing soil nitrogen availability ($p < 0.001$; Table 4.5) and was generally higher in C₃ species ($p < 0.001$; Table 4.5; Fig. 4.5). However, β did not change with soil moisture ($p = 0.904$; Table 4.5) or with ability to acquire nitrogen via symbiotic nitrogen fixation ($p = 0.495$; Table 4.5). Finally, soil nitrogen availability was positively associated with increasing soil moisture ($p = 0.002$; Table 4.5; Fig. 4.5).

Table 4.5. Structural equation model results investigating direct effects of climatic and soil resource availability on leaf nitrogen content*

Predictor	Coefficient	<i>p</i>
N_{area} ($R^2_c=0.89$)		
M_{area}	0.758	<0.001
N_{mass}	0.781	<0.001
N_{mass} ($R^2_c=0.56$)		
Leaf $C_i:C_a$	0.092	0.111
M_{area}	-0.311	<0.001
M_{area} ($R^2_c=0.77$)		
Leaf $C_i:C_a$	-0.237	<0.001
Leaf $C_i:C_a$ ($R^2_c=0.82$)		
β	0.309	<0.001
VPD_4	-0.110	<0.001
β ($R^2_c=0.37$)		
Soil N	-0.213	<0.001
SM_{90}	-0.006	0.904
Photo. pathway	0.446	<0.001
N-fixing ability	-0.056	0.495
Soil N ($R^2_c=0.35$)		
SM_{90}	-0.154	0.002

1559 *Reported coefficients are standardized across the structural equation model.
1560 *P*-values less than 0.05 are noted in bold. Positive coefficients for photosynthetic pathway indicate generally larger values in C₃ species, while positive coefficients for N-fixing ability indicate generally larger values in N-fixing species.
1561 Key: N_{area} =leaf nitrogen content per unit leaf area (gN m⁻¹), M_{area} =leaf mass per unit leaf dry biomass (g m⁻²), N_{mass} =leaf nitrogen content per unit leaf dry biomass (g g⁻¹), β =cost of acquiring nitrogen relative to water (unitless),
1562 VPD_4 =4-day mean vapor pressure deficit (kPa), SM_{90} =90-day mean soil moisture (mm), R^2_c =conditional R² value
1563
1564
1565
1566
1567

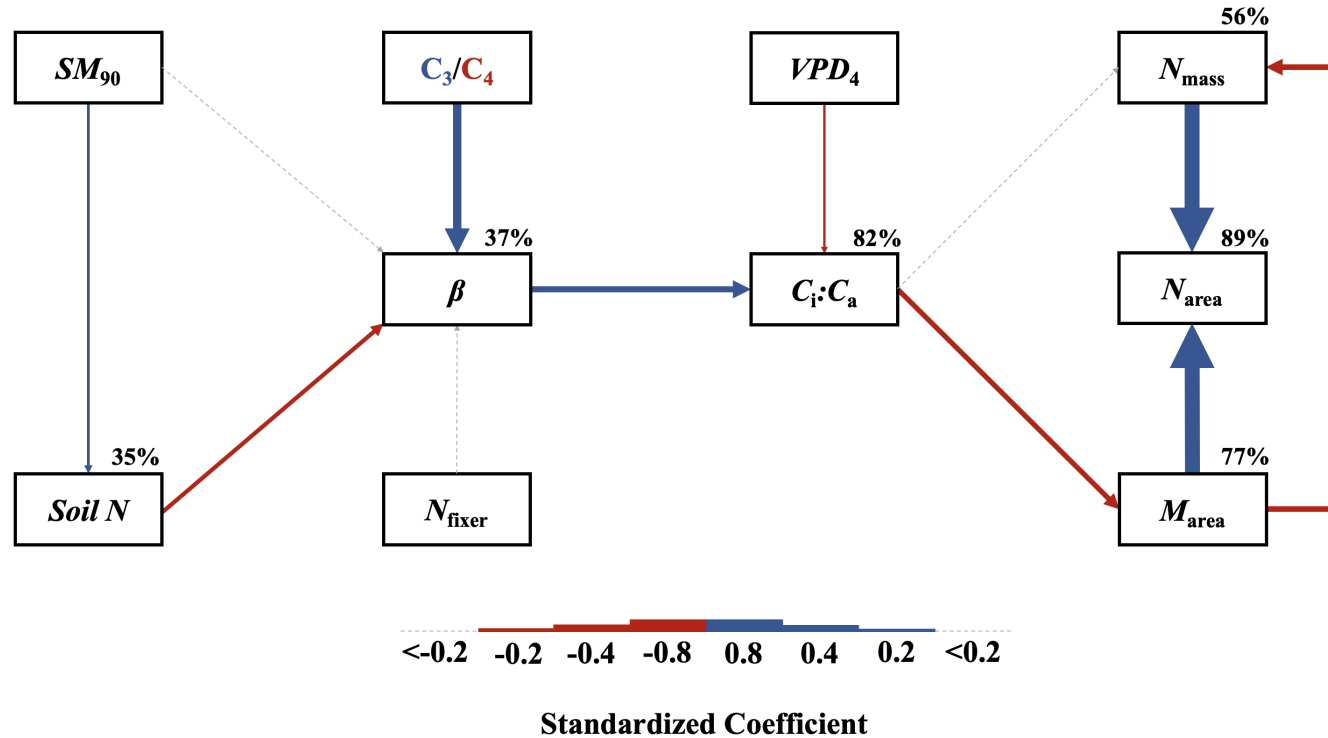


Figure 4.5. Structural equation model results exploring drivers of N_{area} . Boxes indicate measured edaphic factors, climatic factors, and leaf traits. Solid arrows indicate bivariate relationships where $p<0.05$, while dashed arrows indicate relationships where $p>0.05$. Positive model coefficients are indicated through blue arrows, negative model coefficients are indicated through red arrows, and insignificant coefficients ($p>0.05$) are indicated through gray dashed arrows. Arrow thickness scales with the standardized model coefficient of each bivariate relationship. A positive coefficient for photosynthetic pathway indicates larger values in C_3 species, while a positive coefficient for N_{fixer} indicates larger values in N-fixing species. Standardized model coefficients and associated p -values are reported in Table 4.5, with conditional R^2 values for each response variable reported on the top right of each box.

1568 4.4 Discussion

1569 In this study, I quantified direct and indirect effects of soil resource availability,
1570 climate, leaf $C_i:C_a$, and β on N_{area} and components of N_{area} (N_{mass} and M_{area}) in
1571 520 individuals spanning across a soil resource availability and climate gradient
1572 in Texas, USA. I found consistent support for patterns expected from photosyn-
1573 thetic least-cost theory, a result driven by a strong direct negative relationship
1574 between the relative costs to acquire nitrogen versus water (β) on N_{area} as me-
1575 diated through changes in the leaf $C_i:C_a$ ratio. In further support of patterns
1576 expected from theory, increasing soil nitrogen availability had a strong negative
1577 effect on β , resulting in an indirect stimulation in N_{area} . Increasing VPD also
1578 indirectly increased N_{area} through a direct negative effect of increasing VPD on
1579 leaf $C_i:C_a$. Interestingly, a strong positive association between soil moisture and
1580 N_{area} was driven by positive covariance between soil moisture and soil nitrogen
1581 availability and was not associated with a direct effect of soil moisture on β .
1582 Overall, results provide strong and consistent support for patterns expected from
1583 photosynthetic least-cost theory, showing that both soil resource availability and
1584 climate drive variance in N_{area} through changes in leaf $C_i:C_a$.

1585 4.4.1 *Negative effects of leaf $C_i:C_a$ on N_{area} are driven by reductions in M_{area} ,*
1586 *not N_{mass}*

1587 A strong negative effect of increasing leaf $C_i:C_a$ on N_{area} was detected in both
1588 the linear mixed effect and piecewise structural equation models. The negative
1589 response of N_{area} to increasing leaf $C_i:C_a$ is consistent with previous environmental
1590 gradient (Dong et al. 2017; Querejeta et al. 2022) and manipulation experiments

1591 (Perkowski et al. n.d.), showing strong support for the nitrogen-water use tradeoffs
1592 expected from photosynthetic least cost theory (Wright et al. 2003; Prentice et al.
1593 2014). Negative effects of increasing leaf $C_i:C_a$ on N_{area} were driven by a strong
1594 negative effect of increasing $C_i:C_a$ on M_{area} , with no apparent effect of leaf $C_i:C_a$
1595 on N_{mass} , suggesting that changes in N_{area} were driven by changes in leaf structure
1596 and not leaf chemistry. Interestingly, increasing M_{area} was negatively associated
1597 with N_{mass} , indicating that an increase in N_{mass} was associated with larger, thinner
1598 leaves (i.e. lower M_{area}). These results are consistent with patterns reported
1599 from previous studies indicating that variance in N_{area} is driven by changes in
1600 M_{area} across environmental gradients, and that part of this response is due to
1601 negative covariance between M_{area} and N_{mass} associated with tradeoffs between
1602 leaf longevity and leaf productivity (Wright et al. 2004; Dong et al. 2017; Dong
1603 et al. 2022; Querejeta et al. 2022; Wang et al. 2023).

1604 The negative relationship between leaf $C_i:C_a$ and M_{area} could be also re-
1605 sponse that allows leaves to maximize productivity in shorter-lived leaves. Trade-
1606 offs between leaf longevity and leaf productivity are commonly observed and are
1607 included in a continuum of coordinated leaf traits that position individuals along
1608 a fast- or slow-growing leaf economics spectrum (Wright et al. 2003; Onoda et al.
1609 2004; Onoda et al. 2017; Reich 2014; Wang et al. 2023). Negative relationships
1610 between $C_i:C_a$ and M_{area} indicate that increased stomatal conductance and re-
1611 duced water use efficiency were associated with thinner, larger leaves (i.e., lower
1612 M_{area}). These patterns, combined with the negative relationship between M_{area}
1613 and N_{mass} mentioned above, likely allowed individuals to maximize light intercep-
1614 tion and productivity by exploiting high light environments, though this may come

1615 at the expense of increased water loss and decreased water-use efficiency. This
1616 strategy may be especially advantageous for fast-growing species in open canopy
1617 systems. In this study, C₃ legumes and C₃ nonlegumes dominated the dataset
1618 (78% of total sampling effort), of which 22% (17% of total sampling effort) were
1619 classified as annual species with short growing seasons. We observed no effect of
1620 leaf C_{i:C_a} on N_{area} or M_{area} in C₄ nonlegumes, which made up 22% of the sampling
1621 effort and were generally classified as warm season graminoid species with slower
1622 growth rates and longer growing seasons. These patterns indicate that stronger
1623 tradeoffs between nitrogen and water use may be more apparent in fast-growing
1624 species with high demand for building and maintaining productive leaf tissues.

1625 4.4.2 *Soil nitrogen availability increases N_{area} through changes in the cost to
1626 acquire nitrogen*

1627 The null effect of soil nitrogen availability on N_{area} was driven by positive and neg-
1628 ative respective effects of increasing soil nitrogen availability on N_{mass} and M_{area}
1629 that were equal in magnitude. The null response of N_{area} to soil nitrogen avail-
1630 ability occurred alongside a negative effect of increasing soil nitrogen availability
1631 on β , which, paired with the negative relationship between leaf C_{i:C_a} and N_{area},
1632 suggests a general positive effect of increasing soil nitrogen availability on N_{area},
1633 but only when mediated through changes in β . This result is consistent with our
1634 hypotheses and patterns expected from photosynthetic least-cost theory. These
1635 results suggest that positive direct effects of increasing soil nitrogen availability
1636 on N_{area} are not ubiquitous across environmental gradients. Instead, as predicted
1637 by our hypotheses and patterns expected from theory, positive responses of N_{area}

1638 to increasing soil nitrogen availability are a deterministic acclimation response to
1639 shifts in climate-related demand to build and maintain photosynthetic enzymes,
1640 which allows plants to optimize photosynthetic processes and resource use to a
1641 given environment (Paillassa et al. 2020; Peng et al. 2021; Dong et al. 2022;
1642 Westerband et al. 2023).

1643 4.4.3 *Soil moisture increases N_{area} by facilitating increases in soil nitrogen
1644 availability*

1645 Increasing soil moisture generally had no effect on N_{area} , a response that was as-
1646 sociated with a null effect of soil moisture on β . These results contrast patterns
1647 expected from theory, where increasing soil moisture is expected to indirectly de-
1648 crease N_{area} through an increase in β due to a reduction in costs associated with
1649 water acquisition and use (Wright et al. 2003; Prentice et al. 2014; Lavergne
1650 et al. 2020). Interestingly, structural equation model results revealed a strong
1651 positive association between soil moisture and soil nitrogen availability, indicat-
1652 ing an indirect positive effect of increasing soil moisture on N_{area} mediated by the
1653 negative effect of increasing soil nitrogen availability on β . In Texan grasslands,
1654 productivity and nutrient uptake are often co-limited by precipitation and nutrient
1655 availability (Yahdjian et al. 2011; Wang et al. 2017). Thus, increases in soil mois-
1656 ture may have facilitated more favorable and productive environments for soil
1657 microbial communities, thereby stimulating the accumulation of plant-available
1658 nitrogen substrate through increased ammonification or nitrification rates (Reich-
1659 man et al. 1966; Stark and Firestone 1995; Paul et al. 2003). Alternatively, soil
1660 moisture may have facilitated greater nitrogen mobility through soil solution. As
1661 discussed above, the positive indirect response of N_{area} to increasing soil nitrogen
1662 availability as mediated through reductions in β follow patterns expected from

1663 theory.

1664 4.4.4 *Indirect effects of climate on N_{area} are mediated through changes in leaf*
1665 $C_i:C_a$ *and β*

1666 In support of our hypothesis and patterns expected from theory, increasing VPD
1667 indirectly increased N_{area} , mediated through the negative effect of increasing VPD
1668 on leaf $C_i:C_a$. These responses are consistent with previous work noting strong
1669 reductions in stomatal conductance with increasing VPD (Oren et al. 1999; Novick
1670 et al. 2016; Sulman et al. 2016; Grossiord et al. 2020; López et al. 2021), a
1671 response that allows plants to minimize water loss as a result of high atmospheric
1672 water demand. Results also support findings from previous experiments across
1673 environmental gradients, where increasing VPD generally increases N_{area} at lower
1674 stomatal conductance across environmental gradients (Dong et al. 2017; Dong
1675 et al. 2022; Paillassa et al. 2020; Westerband et al. 2023).

1676 4.4.5 *Species identity traits modify effects of the environment on β , leaf $C_i:C_a$,*
1677 *and N_{area}*

1678 N-fixing species generally had higher N_{area} values on average compared to non-
1679 fixing species, a pattern driven by a stronger stimulation in N_{mass} in N-fixing
1680 species coupled with no change in M_{area} between species with different N-fixation
1681 ability. We found no evidence to suggest that N-fixing species had different β or
1682 leaf $C_i:C_a$ values compared to non-fixing species across the environmental gradient.
1683 These results follow patterns from previous environmental gradient experiments
1684 that investigate variance in leaf nitrogen allocation in N-fixing species (Adams
1685 et al. 2016; Dong et al. 2017; Dong et al. 2020), and that increases in N_{mass}
1686 and N_{area} in N-fixing species are not necessarily correlated to increases in water

1687 use efficiency or reductions in leaf $C_i:C_a$ (Adams et al. 2016). While our results
1688 are consistent with results from previous environmental gradient experiments,
1689 they do not necessarily support our hypothesis or patterns expected from theory,
1690 which predicts that stimulations in N_{area} by N-fixing species should be driven
1691 by a reduction in β relative to non-fixing species, and that this response should
1692 decrease stomatal conductance and leaf $C_i:C_a$.

1693 C_4 species generally had lower β , leaf $C_i:C_a$, and N_{area} than C_3 species.
1694 Reduced β and leaf $C_i:C_a$ values in C_4 species follow our hypothesis, a pattern
1695 that could be the result of either reduced costs of nitrogen acquisition and use or
1696 increased costs of water acquisition and use or both (Wright et al. 2003; Prentice
1697 et al. 2014). Results also indicate that β in C_4 nonlegumes was unresponsive to
1698 changes in soil nitrogen availability despite an apparent negative effect of increas-
1699 ing soil nitrogen availability on β in C_3 legumes and C_3 nonlegumes. Combined
1700 with a general null response of β to soil moisture regardless of plant functional
1701 group, these patterns imply that reduced β values in C_4 species may be the re-
1702 sult of lower costs of nitrogen acquisition and use relative to C_3 species. While
1703 lower β values in C_4 species provides a possible explanation for why C_4 species
1704 often have lower leaf $C_i:C_a$ and greater water use efficiency, theory predicts that
1705 this response should cause C_4 species to have greater N_{area} values compared to
1706 C_3 species, though C_4 species commonly exhibit lower N_{area} and higher nitrogen
1707 use efficiency than C_3 species (Schmitt and Edwards 1981; Sage and Pearcy 1987;
1708 Ghannoum et al. 2011). We speculate that lowered costs of nitrogen acquisition
1709 and use in C_4 species could be driven by more efficient Rubisco carboxylation effi-
1710 ciency in C_4 species associated with CO₂ concentrating mechanisms that eliminate

1711 photorespiration (Ghannoum et al. 2011), which could reduce or eliminate the
1712 need to sacrifice inefficient nitrogen use for efficient water use to achieve optimal
1713 photosynthesis rates.

1714 4.4.6 *Next steps for optimality model development*

1715 Optimality models for both C₃ and C₄ species have been developed using principles
1716 from photosynthetic least-cost theory (Prentice et al. 2014; Wang et al. 2017;
1717 Smith et al. 2019; Stocker et al. 2020; Scott and Smith 2022). In both C₃ and
1718 C₄ model variants, β values are held constant using global datasets of leaf $\delta^{13}\text{C}$
1719 (Wang et al. 2017; Cornwell et al. 2018). Specifically, the C₃ optimality model
1720 initially assumed a constant β value of 240 (Wang et al. 2017), later corrected to
1721 146 (Stocker et al. 2020), while the C₄ optimality model assumes a constant β
1722 value of 166 (Scott and Smith 2022). Our results, which build on findings from
1723 Paillassa et al. (2020), demonstrate high variability in calculated β values across
1724 environmental gradients. Specifically, β values in C₃ species ranged from 1.7 to
1725 188.0 (mean: 30.2; median: 23.1; standard deviation: 25.4), while ranged from 0.1
1726 to 110.6 in C₄ species (mean: 7.2; median: 0.7; standard deviation: 18.6). Mean
1727 β values in both C₃ and C₄ species were consistently lower than values currently
1728 implemented in optimality models, though this was likely the result of increased
1729 water limitation across our sites relative to global averages. Regardless, the high
1730 degree of β variability across this environmental gradient, together with findings
1731 from Lavergne et al. (2020) and Paillassa et al. (2020), suggests that the use of
1732 constant β values may contribute to erroneous errors when conducting optimality
1733 model simulations. I therefore build on suggestions from Wang et al. (2017),
1734 recommending future photosynthetic least-cost model developments to consider

1735 the use of dynamic β values.

1736 4.4.7 *Conclusions*

1737 To summarize, variability in N_{area} across an environmental gradient in Texan
1738 grasslands was driven by indirect effects of climate and soil resource availability
1739 mediated. Results from this experiment provide strong and consistent support for
1740 patterns expected from photosynthetic least-cost theory, demonstrating that neg-
1741 ative relationships between $C_i:C_a$ and N_{area} unify expected effects of climatic and
1742 edaphic characteristics on N_{area} across environmental gradients. Results reported
1743 here also demonstrate a need to consider the dynamic nature of the relative cost
1744 of nitrogen versus water uptake (β) across environmental gradients in optimality
1745 models that leverage principles of photosynthetic least-cost theory.

1746

Chapter 5

1747 Optimal resource investment to photosynthetic capacity maximizes
1748 nutrient allocation to whole plant growth under elevated CO₂

1749 5.1 Introduction

1750 Terrestrial ecosystems are regulated by complex carbon and nitrogen cycles. As
1751 a result, terrestrial biosphere models, which are beginning to include coupled
1752 carbon and nitrogen cycles (Shi et al. 2016; Davies-Barnard et al. 2020; Braghieri
1753 et al. 2022), must accurately represent these cycles under different environmental
1754 scenarios to reliably simulate carbon and nitrogen atmosphere-biosphere fluxes
1755 (Hungate et al. 2003; Prentice et al. 2015). While the inclusion of coupled carbon
1756 and nitrogen cycles tends to reduce model uncertainty (Arora et al. 2020), large
1757 uncertainty in role of soil nitrogen availability and nitrogen acquisition strategy
1758 on leaf and whole plant acclimation responses to CO₂ remains (Smith and Dukes
1759 2013; Terrer et al. 2018; Smith and Keenan 2020). This source of uncertainty
1760 likely contributes to the widespread divergence in future carbon and nitrogen flux
1761 simulations across terrestrial biosphere models (Friedlingstein et al. 2014; Zaehle
1762 et al. 2014; Meyerholt et al. 2020).

1763 Plants grown under elevated CO₂ generally have less leaf nitrogen content
1764 than those grown under ambient CO₂, a response that often corresponds with
1765 reductions in photosynthetic capacity and stomatal conductance at the leaf-level
1766 and biomass stimulation over time at the whole plant level (Curtis 1996; Drake
1767 et al. 1997; Ainsworth et al. 2002; Makino 2003; Morgan et al. 2004; Ainsworth
1768 and Long 2005; Ainsworth and Rogers 2007; Smith and Dukes 2013; Poorter et al.
1769 2022). As net primary productivity is generally limited by nitrogen availability

1770 (Vitousek and Howarth 1991; LeBauer and Treseder 2008; Fay et al. 2015), and
1771 soil nitrogen availability is often positively correlated with leaf nitrogen content
1772 and photosynthetic capacity (Field and Mooney 1986; Evans and Seemann 1989;
1773 Evans 1989; Walker et al. 2014; Firn et al. 2019; Liang et al. 2020), some
1774 have hypothesized that leaf and whole plant acclimation responses to CO₂ are
1775 constrained by soil nitrogen availability. The progressive nitrogen limitation hy-
1776 pothesis predicts that elevated CO₂ will increase plant nitrogen demand, which
1777 will increase plant nitrogen uptake and progressively deplete soil nitrogen if soil
1778 nitrogen supply does not exceed plant nitrogen demand (Luo et al. 2004). The
1779 hypothesis predicts that this response should result in strong acute stimulations in
1780 whole plant growth and primary productivity that diminish over time as nitrogen
1781 becomes more limiting. Assuming a positive relationship between soil nitrogen
1782 availability, leaf nitrogen content, and photosynthetic capacity, this hypothesis
1783 also implies that progressive reductions in soil nitrogen availability should be the
1784 mechanism that drives the downregulation in leaf nitrogen content and photosyn-
1785 thetic capacity under elevated CO₂. This hypothesis has received some support
1786 from free air CO₂ enrichment experiments (Reich et al. 2006; Norby et al. 2010),
1787 although is not consistently observed across experiments (Finzi et al. 2006; Moore
1788 et al. 2006; Liang et al. 2016).

1789 While possible that progressive nitrogen limitation may determine leaf and
1790 whole plant acclimation responses to CO₂, growing evidence indicates that leaf ni-
1791 trogen and photosynthetic capacity are more strongly determined through above-
1792 ground growing conditions than by soil resource availability (Dong et al. 2017;
1793 Dong et al. 2020; Dong et al. 2022; Smith et al. 2019; Smith and Keenan 2020;

1794 Paillassa et al. 2020; Peng et al. 2021; Querejeta et al. 2022; Westerband et al.
1795 2023), and satellite-derived chlorophyll fluorescence data indicate that increasing
1796 atmospheric CO₂ may decrease leaf and canopy demand for nitrogen (Dong et al.
1797 2022). Together, results from these studies suggest that the downregulation in
1798 leaf nitrogen content and photosynthetic capacity due to increasing CO₂ may not
1799 be as tightly linked to progressive nitrogen limitation as previously hypothesized.

1800 A unification of optimal coordination and photosynthetic least-cost the-
1801 ories predicts that leaves acclimate to elevated CO₂ by downregulating nitrogen
1802 allocation to Ribulose-1,5-bisphosphate (RuBP) carboxylase/oxygenase (Rubisco)
1803 to optimize resource use efficiencies at the leaf level, which allows for greater re-
1804 source allocation to whole plant growth (Drake et al. 1997; Wright et al. 2003;
1805 Prentice et al. 2014; Smith et al. 2019). The theory predicts that the downregu-
1806 lation in nitrogen allocation to Rubisco results in a stronger downregulation in the
1807 maximum rate of Rubisco carboxylation (V_{cmax}) than the maximum rate of RuBP
1808 regeneration (J_{max}), which maximizes photosynthetic efficiency by allowing net
1809 photosynthesis rates to be equally co-limited by Rubisco carboxylation and RuBP
1810 regeneration (Chen et al. 1993; Maire et al. 2012). This acclimation response
1811 allows plants to make more efficient use of available light while avoiding overin-
1812 vestment in Rubisco, which has high nitrogen and energetic costs of building and
1813 maintaining (Evans 1989; Evans and Clarke 2019). Instead, additional acquired
1814 resources not needed to optimize leaf photosynthesis are allocated to the mainte-
1815 nance of structures that support whole plant growth (e.g., total leaf area, whole
1816 plant biomass, etc.) or to allocation processes not related to leaf photosynthesis
1817 or growth, such as plant defense mechanisms or leaf structural tissue. Regardless,

1818 optimized resource allocation at the leaf level should allow for greater resource
1819 allocation to whole plant growth. The theory indicates that leaf acclimation re-
1820 sponses to CO₂ should be independent of changes in soil nitrogen availability.
1821 While this leaf acclimation response maximizes nitrogen allocation to structures
1822 that support whole plant growth, the theory suggests that the positive effect of
1823 elevated CO₂ on whole plant growth may be further stimulated by soil nitrogen
1824 availability through a reduction in the cost of acquiring nitrogen (Bae et al. 2015;
1825 Perkowski et al. 2021; Lu et al. 2022).

1826 Plants acquire nitrogen by allocating photosynthetically derived carbon be-
1827 lowground in exchange for nitrogen through different nitrogen acquisition strate-
1828 gies. These nitrogen acquisition strategies can include direct uptake pathways
1829 such as mass flow or diffusion (Barber 1962), symbioses with mycorrhizal fungi or
1830 symbiotic nitrogen-fixing bacteria (Vance and Heichel 1991; Marschner and Dell
1831 1994; Smith and Read 2008; Udvardi and Poole 2013), or through the release
1832 of root exudates that prime free-living soil microbial communities (Phillips et al.
1833 2011; Wen et al. 2022). Plants cannot acquire nitrogen without first allocating
1834 carbon belowground, which implies an inherent carbon cost to the plant for acquir-
1835 ing nitrogen regardless of nitrogen acquisition strategy. Carbon costs to acquire
1836 nitrogen often vary in species with different nitrogen acquisition strategies and
1837 are dependent on external environmental factors such as atmospheric CO₂, light
1838 availability, and soil nitrogen availability (Brzostek et al. 2014; Terrer et al. 2016;
1839 Terrer et al. 2018; Allen et al. 2020; Perkowski et al. 2021; Lu et al. 2022), which
1840 suggests that acquisition strategy may be an important factor in determining ef-
1841 fects of soil nitrogen availability on leaf and whole plant acclimation responses to

1842 elevated CO₂.

1843 A recent meta-analysis using data across 20 grassland and forest CO₂ en-
1844 richment experiments suggested that species which acquire nitrogen from sym-
1845 biotic nitrogen-fixing bacteria had reduced costs of nitrogen acquisition under
1846 elevated CO₂ (Terrer et al. 2018). Findings from this meta-analysis indicated
1847 that reductions in costs of nitrogen acquisition in species that form associations
1848 with symbiotic nitrogen-fixing bacteria under elevated CO₂ may drive stronger
1849 stimulations in whole plant growth and downregulations in V_{cmax} than species that
1850 associate with arbuscular mycorrhizal fungi (Smith and Keenan 2020), which gen-
1851 erally have higher costs of nitrogen acquisition under elevated CO₂ (Terrer et al.
1852 2018). However, plant investments in symbiotic nitrogen fixation generally de-
1853 cline with increasing nitrogen availability (Dovrat et al. 2018; Perkowski et al.
1854 2021), a response that has been previously inferred to be the result of a shift in
1855 the dominant mode of nitrogen acquisition to direct uptake pathways as costs of
1856 direct uptake decrease with increasing soil nitrogen availability (Rastetter et al.
1857 2001; Perkowski et al. 2021). Thus, effects of symbiotic nitrogen fixation on plant
1858 acclimation responses to CO₂ should decline with increasing soil nitrogen avail-
1859 ability, although manipulative experiments that directly test these patterns are
1860 rare.

1861 Here, I conducted a 7-week growth chamber experiment using *Glycine max*
1862 L. (Merr.) to examine the effects of soil nitrogen fertilization and inoculation with
1863 symbiotic nitrogen-fixing bacteria on leaf and whole plant acclimation responses
1864 to elevated CO₂. Following patterns expected from theory, I hypothesized that in-
1865 dividual leaves should acclimate to elevated CO₂ by more strongly downregulating

1866 V_{cmax} relative to J_{max} , allowing leaf photosynthesis to approach optimal coordi-
1867 nation. I expected this response to correspond with a stronger downregulation in
1868 leaf nitrogen content than V_{cmax} and J_{max} , which would increase the fraction of
1869 leaf nitrogen content allocated to photosynthesis and photosynthetic nitrogen use
1870 efficiency. At the whole-plant level, I hypothesized that plants would acclimate
1871 to elevated CO₂ by stimulating whole plant growth and productivity, a response
1872 that would be driven by a strong positive response of total leaf area and above-
1873 ground biomass to elevated CO₂. I predicted that leaf acclimation responses to
1874 elevated CO₂ would be independent of soil nitrogen fertilization and inoculation
1875 with symbiotic nitrogen-fixing bacteria; however, I expected that increasing soil
1876 nitrogen fertilization would increase the positive effect of elevated CO₂ on mea-
1877 sures of whole plant growth due to a stronger reduction in the cost of acquiring
1878 nitrogen under elevated CO₂ with increasing fertilization. I also expected stronger
1879 stimulations in whole plant growth due to inoculation, but that this effect would
1880 only be apparent under low fertilization due to a reduction in root nodulation
1881 with increasing fertilization.

1882 5.2 Methods

1883 5.2.1 *Seed treatments and experimental design*

1884 *Glycine max* L. (Merr) seeds were planted in 144 6-liter surface sterilized pots (NS-
1885 600, Nursery Supplies, Orange, CA, USA) containing a steam-sterilized 70:30 v:v
1886 mix of Sphagnum peat moss (Premier Horticulture, Quakertown, PA, USA) to
1887 sand (Pavestone, subsidiary of Quikrete Companies, Atlanta, GA, USA). Before
1888 planting, all *G. max* seeds were surface sterilized in 2% sodium hypochlorite for 3

1889 minutes, followed by three separate 3-minute washes with ultrapure water (MilliQ
1890 7000; MilliporeSigma, Burlington, MA USA). A subset of surface sterilized seeds
1891 were inoculated with *Bradyrhizobium japonicum* (Verdesian N-DureTM Soybean,
1892 Cary, NC, USA) in a slurry following manufacturer recommendations (3.12 g
1893 inoculant and 241 g deionized water per 1 kg seed).

1894 Seventy-two pots were randomly planted with surface-sterilized seeds inoc-
1895 ulated with *B. japonicum*, while the remaining 72 pots were planted with surface-
1896 sterilized uninoculated seeds. Thirty-six pots within each inoculation treatment
1897 were randomly placed in one of two atmospheric CO₂ treatments (ambient and
1898 1000 $\mu\text{mol mol}^{-1}$ CO₂). Pots within each unique inoculation-by-CO₂ treatment
1899 combination randomly received one of nine soil nitrogen fertilization treatments
1900 equivalent to 0, 35, 70, 105, 140, 210, 280, 350, or 630 ppm N. Nitrogen fertil-
1901 ization treatments were created using a modified Hoagland solution (Hoagland
1902 and Arnon 1950) designed to keep concentrations of other macronutrients and
1903 micronutrients equivalent across treatments (Table D1). Pots received the same
1904 fertilization treatment throughout the entire duration experiment, which were ap-
1905 plied twice per week in 150 mL doses as topical agents to the soil surface through-
1906 out the duration of the experiment. This experimental design yielded a fully
1907 factorial experiment with four replicates per unique fertilization-by-inoculation-
1908 by-CO₂ combination.

1909 5.2.2 *Growth chamber conditions*

1910 Upon experiment initiation, pots were randomly placed in one of six Percival
1911 LED-41L2 growth chambers (Percival Scientific Inc., Perry, IA, USA) over two

1912 experimental iterations due to chamber space limitation. Two iterations were
1913 conducted such that one iteration included all elevated CO₂ pots and the second
1914 iteration included all ambient CO₂ pots. Average (\pm SD) CO₂ concentrations
1915 across chambers throughout the experiment were $439 \pm 5 \mu\text{mol mol}^{-1}$ for the am-
1916 bient CO₂ treatment and $989 \pm 4 \mu\text{mol mol}^{-1}$ for the elevated CO₂ treatment.

1917 Daytime growing conditions were simulated using a 16-hour photoperiod,
1918 with incoming light radiation set to chamber maximum (mean \pm SD: 1240 ± 32
1919 $\mu\text{mol m}^{-2} \text{s}^{-1}$ across chambers), air temperature set to 25°C, and relative humid-
1920 ity set to 50%. The remaining 8 hours simulated nighttime growing conditions,
1921 with incoming light radiation set to 0 $\mu\text{mol m}^{-2} \text{s}^{-1}$, chamber temperature set
1922 to 17°C, and relative humidity set to 50%. Transitions between daytime and
1923 nighttime growing conditions were simulated by ramping incoming light radiation
1924 in 45-minute increments and temperature in 90-minute increments over a 3-hour
1925 period (Table D2).

1926 Including the two, 3-hour ramping periods, pots grew under average (\pm SD)
1927 daytime light intensity of $1049 \pm 27 \mu\text{mol m}^{-2} \text{s}^{-1}$. In the elevated CO₂ iteration,
1928 pots grew under $24.0 \pm 0.2^\circ\text{C}$ during the day, $16.4 \pm 0.8^\circ\text{C}$ during the night, and
1929 51.6 $\pm 0.4\%$ relative humidity. In the ambient CO₂ iteration, pots grew under
1930 $23.9 \pm 0.2^\circ\text{C}$ during the day, $16.0 \pm 1.4^\circ\text{C}$ during the night, and $50.3 \pm 0.2\%$
1931 relative humidity. We accounted for climatic differences across the six chambers
1932 by shuffling the same group of pots daily throughout the growth chambers. This
1933 process was done by iteratively moving the group of pots on the top rack of a
1934 chamber to the bottom rack of the same chamber, while simultaneously moving
1935 the group of pots on the bottom rack of a chamber to the top rack of the adjacent

1936 chamber. I moved pots within and across chambers every day throughout the
1937 course of each experiment iteration.

1938 5.2.3 *Leaf gas exchange measurements*

1939 Gas exchange measurements were collected for all individuals on the seventh week
1940 of development. All gas exchange measurements were collected on the center leaf
1941 of the most recent fully expanded trifoliate leaf set. Specifically, I measured net
1942 photosynthesis (A_{net} ; $\mu\text{mol m}^{-2} \text{s}^{-1}$), stomatal conductance (g_{sw} ; $\text{mol m}^{-2} \text{s}^{-1}$),
1943 and intercellular CO_2 (C_i ; $\mu\text{mol mol}^{-1}$) concentrations across a range of atmo-
1944 spheric CO_2 concentrations (i.e., an A_{net}/C_i curve) using the Dynamic Assimila-
1945 tion Technique™. The Dynamic Assimilation Technique™ has been shown to
1946 correspond well with traditional steady-state CO_2 response curves in *G. max*
1947 (Saathoff and Welles 2021). A_{net}/C_i curves were generated along a reference
1948 CO_2 ramp down from $420 \mu\text{mol mol}^{-1} \text{CO}_2$ to $20 \mu\text{mol mol}^{-1} \text{CO}_2$, followed by
1949 a ramp up from $420 \mu\text{mol mol}^{-1} \text{CO}_2$ to $1620 \mu\text{mol mol}^{-1} \text{CO}_2$ after a 90-second
1950 wait period at $420 \mu\text{mol mol}^{-1} \text{CO}_2$. The ramp rate for each curve was set to 200
1951 $\mu\text{mol mol}^{-1} \text{min}^{-1}$, logging every five seconds, which generated 96 data points per
1952 response curve. All A_{net}/C_i curves were generated after A_{net} and g_{sw} stabilized
1953 in a LI-6800 cuvette set to a 500 mol s^{-1} , 10,000 rpm mixing fan speed, 1.5 kPa
1954 vapor pressure deficit, 25°C leaf temperature, $2000 \mu\text{mol m}^{-2} \text{s}^{-1}$ incoming light
1955 radiation, and initial reference CO_2 set to $420 \mu\text{mol mol}^{-1}$.

1956 With the same focal leaf used to generate A_{net}/C_i curves, I measured dark
1957 respiration (R_{d25} ; $\mu\text{mol m}^{-2} \text{s}^{-1}$) following at least a 30-minute period of darkness.
1958 Measurements were collected on a 5-second log interval for 60 seconds after stabi-

1959 lizing in a LI-6800 cuvette set to a 500 mol s^{-1} , 10,000 rpm mixing fan speed, 1.5
1960 kPa vapor pressure deficit, 25°C leaf temperature, and $420 \mu\text{mol mol}^{-1}$ reference
1961 CO₂ concentration (for both CO₂ concentrations), with incoming light radiation
1962 set to $0 \mu\text{mol m}^{-2} \text{ s}^{-1}$. A single dark respiration value was determined for each
1963 focal leaf by calculating the mean dark respiration value (i.e. the absolute value
1964 of A_{net} during the logging period) across the logging interval.

1965 5.2.4 *Leaf trait measurements*

1966 The focal leaf used to generate A_{net}/C_i curves and dark respiration was harvested
1967 immediately following gas exchange measurements. Images of each focal leaf were
1968 curated using a flat-bed scanner to determine wet leaf area using the 'LeafArea' R
1969 package (Katabuchi 2015), which automates leaf area calculations using ImageJ
1970 software (Schneider et al. 2012). Each leaf was dried at 65°C for at least 48
1971 hours, and subsequently weighed and ground until homogenized. Leaf mass per
1972 area (M_{area} ; g m⁻²) was calculated as the ratio of dry leaf biomass to fresh leaf
1973 area. Using subsamples of ground and homogenized leaf tissue, I measured leaf
1974 nitrogen content (N_{mass} ; gN g⁻¹) through elemental combustion analysis (Costech-
1975 4010, Costech, Inc., Valencia, CA, USA). Leaf nitrogen content per unit leaf area
1976 (N_{area} ; gN m⁻²) was calculated by multiplying N_{mass} and M_{area} .

1977 I extracted chlorophyll content from a second leaf in the same trifoliolate
1978 leaf set as the focal leaf used to generate A_{net}/C_i curves. Prior to chlorophyll
1979 extraction, I used a cork borer to punch between 3 and 5 0.6 cm² disks from the
1980 leaf. Separate images of each punched leaf and set of leaf disks were curated using
1981 a flat-bed scanner to determine wet leaf area, again quantified using the 'LeafArea'

1982 R package (Katabuchi 2015). The punched leaf was dried and weighed after at
1983 least 65°C in the drying oven to determine M_{area} of the chlorophyll leaf.

1984 Leaf disks were shuttled into a test tube containing 10mL dimethyl sul-
1985 foxide, vortexed, and incubated at 65degreeC for 120 minutes (Barnes et al.
1986 1992). Incubated test tubes were vortexed again before loaded in 150 μL trip-
1987 licate aliquots to a 96-well plate. Dimethyl sulfoxide was also loaded in a 150
1988 μL triplicate aliquot as a blank. Absorbance measurements at 649.1 nm ($A_{649.1}$)
1989 and 665.1 nm ($A_{665.1}$) were read in each well using a plate reader (Biotek Synergy
1990 H1; Biotek Instruments, Winooski, VT USA) (Wellburn 1994), with triplicates
1991 subsequently averaged and corrected by the mean of the blank absorbance value.
1992 Blank-corrected absorbance values were used to estimate Chl_a ($\mu\text{g mL}^{-1}$) and
1993 Chl_b ($\mu\text{g mL}^{-1}$) following equations from Wellburn (1994):

$$Chl_a = 12.47A_{665.1} - 3.62A_{649.1} \quad (5.1)$$

1994 and

$$Chl_b = 25.06A_{665.1} - 6.50A_{649.1} \quad (5.2)$$

1995 Chl_a and Chl_b were converted to mmol mL^{-1} using the molar mass of chlorophyll a
1996 (893.51 g mol^{-1}) and the molar mass of chlorophyll b (907.47 g mol^{-1}), then added
1997 together to calculate total chlorophyll content in the dimethyl sulfoxide extractant
1998 (mmol mL^{-1}). Total chlorophyll content was multiplied by the volume of the
1999 dimethyl sulfoxide extractant (10 mL) and converted to area-based chlorophyll
2000 content by dividing by the total area of the leaf disks (Chl_{area} ; mmol m^{-2}). Mass-
2001 based chlorophyll content (Chl_{mass} ; mmol g^{-1}) was calculated by dividing Chl_{area}

2002 by the leaf mass per area of the punched leaf.

2003 5.2.5 *A/C_i curve fitting and parameter estimation*

2004 I fit A_{net}/C_i curves of each individual using the ‘fitaci’ function in the ‘plantecophys’ R package (Duursma 2015). This function estimates the maximum rate of Rubisco carboxylation (V_{cmax} ; $\mu\text{mol m}^{-2} \text{s}^{-1}$) and maximum rate of electron transport for RuBP regeneration (J_{max} ; $\mu\text{mol m}^{-2} \text{s}^{-1}$) based on the Farquhar biochemical model of C₃ photosynthesis (Farquhar et al. 1980). Triose phosphate utilization (TPU) limitation was included in all curve fits, and all curve fits included measured dark respiration values. As A_{net}/C_i curves were generated using a common leaf temperature, curves were fit using Michaelis-Menten coefficients for Rubisco affinity to CO₂ (K_c ; $\mu\text{mol mol}^{-1}$) and O₂ (K_o ; $\mu\text{mol mol}^{-1}$), and the CO₂ compensation point (Γ^* ; $\mu\text{mol mol}^{-1}$) reported in Bernacchi et al. (2001). Specifically, K_c was set to 404.9 $\mu\text{mol mol}^{-1}$, K_o was set to 278.4 $\mu\text{mol mol}^{-1}$, and Γ^* was set to 42.75 $\mu\text{mol mol}^{-1}$. The use of a common leaf temperature across curves and dark respiration measurements also eliminated the need to manually standardize rate estimates. For clarity, I reference V_{cmax} , J_{max} , and R_d estimates throughout the rest of the paper as $V_{\text{cmax}25}$, $J_{\text{max}25}$, and R_{d25} .

2019 5.2.6 Stomatal limitation

2020 I quantified the extent by which stomatal conductance limited photosynthesis (l; unitless) following equations originally described in Farquhar and Sharkey (1982). **2022** Stomatal limitation was calculated as:

$$l = 1 - \frac{A_{net}}{A_{mod}} \quad (5.3)$$

2023 where A_{mod} represents the photosynthetic rate where $C_i=C_a$. A_{mod} was calculated

2024 as:

$$A_{mod} = V_{cmax25} - \frac{420 - \Gamma^*}{420 + K_m} - R_{d25} \quad (5.4)$$

2025 K_m is the Michaelis-Menten coefficient for Rubisco-limited photosynthesis, calcu-

2026 lated as:

$$K_m = K_c \cdot \left(1 + \frac{O_i}{K_o}\right) \quad (5.5)$$

2027 where O_i refers to leaf intercellular O_2 concentrations, set to $210 \mu\text{mol mol}^{-1}$.

2028 5.2.7 *Proportion of leaf nitrogen allocated to photosynthesis and structure*

2029 I used equations from Niinemets and Tenhunen (1997) to estimate the proportion

2030 of leaf nitrogen content allocated to Rubisco bioenergetics, and light harvesting

2031 proteins. The proportion of leaf N allocated to Rubisco ($\rho_{rubisco}$; gN gN^{-1}) was

2032 calculated as a function of V_{cmax25} and N_{area} :

$$\rho_{rubisco} = \frac{V_{cmax25} N_r}{V_{cr} N_{area}} \quad (5.6)$$

2033 where N_r is the amount of nitrogen in Rubisco, set to $0.16 \text{ gN (gN in Rubisco)}^{-1}$

2034 and V_{cr} is the maximum rate of RuBP carboxylation per unit Rubisco protein,

2035 set to $20.5 \mu\text{mol CO}_2 (\text{g Rubisco})^{-1}$. The proportion of leaf nitrogen allocated to

2036 bioenergetics (ρ_{bioe} ; gN gN^{-1}) was similarly calculated as a function of J_{max25} and

2037 N_{area} :

$$\rho_{\text{bioe}} = \frac{J_{\text{max}25} N_b}{J_{\text{mc}} N_{\text{area}}} \quad (5.7)$$

2038 where N_b is the amount of nitrogen in cytochrome f, set to 0.12407 gN (μmol cytochrome f) $^{-1}$ assuming a constant 1: 1: 1.2 cytochrome f: ferredoxin NADP reductase: coupling factor molar ratio (Evans and Seemann 1989; Niinemets and Tenhunen 1997), and J_{mc} is the capacity of electron transport per cytochrome f, set to 156 μmol electron (μmol cytochrome f) $^{-1}\text{s}^{-1}$.

2043 The proportion of leaf nitrogen allocated to light harvesting proteins (ρ_{light} ; **2044** gN gN $^{-1}$) was calculated as a function of Chl_{mass} and N_{mass} :

$$\rho_{\text{light}} = \frac{Chl_{\text{mass}}}{N_{\text{mass}} c_b} \quad (5.8)$$

2045 where c_b is the stoichiometry of the light-harvesting chlorophyll complexes of **2046** photosystem II, set to 2.75 mmol chlorophyll (gN in chlorophyll) $^{-1}$. We used the **2047** N_{mass} value of the focal leaf used to generate A_{net}/C_i curves instead of the leaf **2048** used to extract chlorophyll content, as the two leaves are from the same trifoliolate **2049** leaf set and are highly correlated with each other (Figure D1).

2050 The proportion of leaf nitrogen content allocated to photosynthetic tissue **2051** (ρ_{photo} ; gN gN $^{-1}$) was estimated as the sum of ρ_{rubisco} , ρ_{bioe} , and ρ_{light} . Finally, **2052** the proportion of leaf N content allocated to structural tissue ($\rho_{\text{structure}}$; gN gN $^{-1}$) **2053** was estimated as:

$$\rho_{\text{structure}} = \frac{N_{\text{cw}}}{N_{\text{area}}} \quad (5.9)$$

2054 where N_{cw} is the leaf nitrogen content allocated to cell walls (gN m $^{-2}$), calculated

2055 as a function of M_{area} using an empirical equation from Onoda et al. (2017):

$$N_{cw} = 0.000355 * M_{area}^{1.39} \quad (5.10)$$

2056 5.2.8 *Whole plant traits*

2057 Seven weeks after experiment initiation and immediately following gas exchange
2058 measurements, I harvested all experimental individuals and separated biomass of
2059 each experimental individual into major organ types (leaves, stems, roots, and
2060 nodules when present). Fresh leaf area of all harvested leaves was measured using
2061 an LI-3100C (Li-COR Biosciences, Lincoln, Nebraska, USA). Total fresh leaf area
2062 (cm^2) was calculated as the sum of all leaf areas, including the focal leaf used to
2063 collect gas exchange data and the focal leaf used to extract chlorophyll content.
2064 All harvested material was dried in an oven set to 65°C for at least 48 hours,
2065 weighed, and ground to homogeneity. Leaves and nodules were manually ground
2066 either with a mortar and pestle, while stems and roots were ground using a Wiley
2067 mill (E3300 Mini Mill; Eberbach Corp., MI, USA). Total dry biomass (g) was
2068 calculated as the sum of dry leaf (including focal leaf for both the A_{net}/C_i curve
2069 and leaf used to extract chlorophyll content), stem, root, and root nodule biomass.
2070 I quantified carbon and nitrogen content of each respective organ type through
2071 elemental combustion (Costech-4010, Costech, Inc., Valencia, CA, USA) using
2072 subsamples of ground and homogenized organ tissue.
2073 Following the approach explained in the first experimental chapter, I calcu-
2074 lated structural carbon costs to acquire nitrogen as the ratio of total belowground
2075 carbon biomass to whole plant nitrogen biomass (N_{cost} ; gC gN^{-1}). Belowground

2076 carbon biomass (C_{bg} ; gC) was calculated as the sum of root carbon biomass
2077 and root nodule carbon biomass. Root carbon biomass and root nodule carbon
2078 biomass was calculated as the product of the organ biomass and the respective
2079 organ carbon content. Whole plant nitrogen biomass (N_{wp} ; gN) was similarly
2080 calculated as the sum of total leaf, stem, root, and root nodule nitrogen biomass,
2081 including the focal leaf used for A_{net}/C_i curve and chlorophyll extractions. Leaf,
2082 stem, root, and root nodule nitrogen biomass was calculated as the product of
2083 the organ biomass and the respective organ nitrogen content. This calculation
2084 only quantifies plant structural carbon costs to acquire nitrogen and does not
2085 include any additional costs of nitrogen acquisition associated with respiration,
2086 root exudation, or root turnover. An explicit explanation of the limitations for
2087 interpreting this calculation can be found in Perkowski et al. (2021) and Terrer
2088 et al. (2018).

2089 Finally, plant investments in nitrogen fixation were calculated as the ra-
2090 tio of root nodule biomass to root biomass, where increasing values indicate an
2091 increase in plant investments to nitrogen fixation (Dovrat et al. 2018; Dovrat
2092 et al. 2020; Perkowski et al. 2021). I also calculated the percent of leaf nitrogen
2093 acquired from the atmosphere ($\%N_{dfa}$) using leaf $\delta^{15}\text{N}$ and the following equation
2094 from Andrews et al. (2011):

$$\%N_{dfa} = \frac{\delta^{15}\text{N}_{reference} - \delta^{15}\text{N}_{sample}}{\delta^{15}\text{N}_{reference} - B} \quad (5.11)$$

2095 where $\delta^{15}\text{N}_{reference}$ refers to a reference plant that exclusively acquires nitrogen via
2096 direct uptake, $\delta^{15}\text{N}_{sample}$ refers to an individual's leaf $\delta^{15}\text{N}$, and B refers to indi-

2097 individuals that are entirely reliant on nitrogen fixation. Within each unique nitrogen
2098 fertilization treatment-by-CO₂ treatment combination, I calculated the mean leaf
2099 δ¹⁵N for individuals growing in the non-inoculated treatment for δ¹⁵N_{reference}. Any
2100 individuals with visual confirmation of root nodule formation or nodule initiation
2101 were omitted from the calculation of δ¹⁵N_{reference}. Following recommendations
2102 from Andrews et al. (2011) I calculated B within each CO₂ treatment using
2103 the mean leaf δ¹⁵N of inoculated individuals that received 0 ppm N. I did not
2104 calculate B within each unique soil nitrogen-by-CO₂ treatment combination, as
2105 previous studies suggest decreased reliance on nitrogen fixation with increasing
2106 soil nitrogen availability (Perkowski et al. 2021). This approach for estimating
2107 nitrogen fixation standardizes values such that approaching 1 indicates increasing
2108 reliance on nitrogen fixation.

2109 5.2.9 *Statistical analyses*

2110 Any uninoculated pots that had substantial root nodule formation (nodule biomass:
2111 root biomass values greater than 0.05 g g⁻¹) were removed from analyses. This was
2112 because they were assumed to have been colonized by symbiotic nitrogen-fixing
2113 bacteria from outside sources. This decision resulted in the removal of sixteen
2114 pots from our analysis: two pots in the elevated CO₂ treatment that received 35
2115 ppm N, three pots in the elevated CO₂ treatment that received 70 ppm N, one pot
2116 in the elevated CO₂ treatment that received 210 ppm N, two pots in the elevated
2117 CO₂ treatment that received 280 ppm N, two pots in the ambient CO₂ treatment
2118 that received 0 ppm N, three pots in the ambient CO₂ treatment that received
2119 70 ppm N, two pots in the ambient CO₂ treatment that received 105 ppm N, and

2120 one pot in the ambient CO₂ treatment that received 280 ppm N.

2121 I built a series of linear mixed effects models to investigate the impacts of
2122 CO₂ concentration, soil nitrogen fertilization, and inoculation with *B. japonicum*
2123 on *G. max* gas exchange, tradeoffs between nitrogen and water use, whole plant
2124 growth, and investment in nitrogen fixation. All models included CO₂ treatment
2125 as a categorical fixed effect, inoculation treatment as a categorical fixed effect,
2126 soil nitrogen fertilization as a continuous fixed effect, with interaction terms be-
2127 tween all three fixed effects. All models also accounted for climatic difference
2128 between chambers across experiment iterations by including a random intercept
2129 term that nested starting chamber rack by CO₂ treatment. Models with this
2130 independent variable structure were created for each of the following dependent
2131 variables: N_{area} , M_{area} , N_{mass} , Chl_{area} , V_{cmax25} , J_{max25} , $J_{\text{max25}}:V_{\text{cmax25}}$, R_{d25} , g_{sw} ,
2132 stomatal limitation, ρ_{rubisco} , ρ_{bioe} , ρ_{light} , ρ_{photo} , $\rho_{\text{structure}}$, N_{cost} , C_{bg} , N_{wp} , total
2133 biomass, total leaf area, nodule biomass, and the ratio of nodule biomass to root
2134 biomass.

2135 I used Shapiro-Wilk tests of normality to determine whether linear mixed
2136 effects models satisfied residual normality assumptions. If residual normality as-
2137 sumptions were not met (Shapiro-Wilk: $p < 0.05$), then models were fit using
2138 dependent variables that were natural log transformed. All residual normality
2139 assumptions that did not originally satisfy residual normality assumptions were
2140 met with either a natural log or square root data transformation (Shapiro-Wilk:
2141 $p > 0.05$ in all cases). Specifically, models for N_{area} , N_{mass} , Chl_{area} , V_{cmax25} ,
2142 J_{max25} , $J_{\text{max25}}:V_{\text{cmax25}}$, g_{sw} , stomatal limitation, ρ_{rubisco} , ρ_{bioe} , ρ_{light} , ρ_{photo} , and to-
2143 tal leaf area satisfied residual normality assumptions without data transformation.

2144 Models for M_{area} , $\rho_{\text{structure}}$, N_{cost} , C_{bg} , N_{wp} , and total biomass satisfied residual
2145 normality assumptions with a natural log data transformation, while models for
2146 nodule biomass and nodule biomass: root biomass satisfied residual normality
2147 assumptions with a square root data transformation.

2148 In all statistical models, I used the 'lmer' function in the 'lme4' R package
2149 (Bates et al. 2015) to fit each model and the 'Anova' function in the 'car' R
2150 package (Fox and Weisberg 2019) to calculate Type II Wald's χ^2 and determine
2151 the significance ($\alpha = 0.05$) of each fixed effect coefficient. I used the 'emmeans'
2152 R package (Lenth 2019) to conduct post-hoc comparisons using Tukey's tests,
2153 where degrees of freedom were approximated using the Kenward-Roger approach
2154 (Kenward and Roger 1997). All analyses and plots were conducted in R version
2155 4.2.0 (R Core Team 2021).

2156 5.3 Results

2157 5.3.1 Leaf nitrogen and chlorophyll content

2158 Elevated CO₂ reduced N_{area} , N_{mass} , and Chl_{area} by 29%, 50%, and 31%,
2159 respectively, and stimulated M_{area} by 44% ($p < 0.001$ in all cases; Table 5.1). An
2160 interaction between fertilization and CO₂ (CO₂-by-fertilization interaction: $p_{N_{\text{area}}}$
2161 = 0.017, $p_{N_{\text{mass}}} < 0.001$, $p_{M_{\text{area}}} = 0.006$, $p_{Chl_{\text{area}}} = 0.083$; Table 5.1) indicated
2162 that the general positive effect of increasing fertilization on N_{area} , N_{mass} , and
2163 Chl_{area} ($p < 0.001$ in all cases; Table 5.1) was generally stronger under ambient
2164 CO₂ (Tukey _{N_{area}} : $p = 0.026$; Tukey _{N_{mass}} : $p < 0.001$; Tukey _{M_{area}} : $p = 0.009$;
2165 Tukey _{Chl_{area}} : $p = 0.065$; Table 5.1; Figs. 5.1a-d). This pattern resulted in a
2166 stronger reduction in N_{area} , N_{mass} , and Chl_{area} as well as a stronger stimulation

2167 in M_{area} under elevated CO₂ with increasing fertilization. An additional interac-
2168 tion between inoculation and CO₂ on N_{area} (CO₂-by-inoculation interaction: $p =$
2169 0.030; Table 5.1) indicated that the general positive effect of inoculation on N_{area}
2170 ($p < 0.001$; Table 5.1) was stronger under elevated CO₂ (45% increase; Tukey: p
2171 < 0.001) than under ambient CO₂ (18% increase; Tukey: $p < 0.001$), a result that
2172 increased the reduction in N_{area} in inoculated pots under elevated CO₂. Inocula-
2173 tion treatment did not modify the downregulation in N_{mass} (CO₂-by-inoculation
2174 interaction: $p = 0.148$; Table 5.1) and Chl_{area} ($p = 0.147$; Table 5.1) or the stimu-
2175 lation in M_{area} ($p = 0.866$; Table 5.1) under elevated CO₂. However, interactions
2176 between fertilization and inoculation on N_{area} (fertilization-by-inoculation inter-
2177 action: $p < 0.001$; Table 5.1; Fig. 5.1a), N_{mass} ($p = 0.001$; Table 5.1; Fig. 5.1b),
2178 M_{area} ($p = 0.025$; Table 5.1; Fig. 5.1c), and Chl_{area} ($p < 0.001$; Table 5.1; Fig.
2179 5.1d) indicated that the general positive effect of increasing fertilization on each
2180 trait was stronger in uninoculated pots (Tukey _{N_{area}} : $p < 0.001$; Tukey _{N_{mass}} : $p =$
2181 0.001; Tukey _{M_{area}} : $p = 0.031$; Tukey _{Chl_{area}} : $p < 0.001$).

Table 5.1. Effects of soil nitrogen fertilization, inoculation, and CO₂ treatments on N_{area} , N_{mass} , M_{area} , and Chl_{area}

	N_{area}			N_{mass}			M_{area}^a			
	df	Coefficient	χ^2	p	Coefficient	χ^2	p	Coefficient	χ^2	p
(Intercept)	-	1.10E+00	-	-	3.05E-02	-	-	3.64E+00	-	-
CO ₂	1	-5.67E-01	155.908	<0.001	-1.80E-02	272.362	<0.001	3.04E-01	151.319	<0.001
Inoculation (I)	1	6.21E-01	86.029	<0.001	7.54E-03	15.576	<0.001	1.81E-01	19.158	<0.001
Fertilization (N)	1	3.06E-03	316.408	<0.001	5.78E-05	106.659	<0.001	3.10E-04	21.440	<0.001
CO ₂ *I	1	2.63E-01	4.729	0.030	3.96E-03	2.025	0.155	-3.37E-02	0.029	0.866
CO ₂ *N	1	-3.68E-04	5.723	0.017	-2.85E-05	22.542	<0.001	2.80E-04	7.619	0.006
I*N	1	-1.36E-03	43.381	<0.001	-2.00E-05	11.137	0.001	-3.36E-04	5.022	0.025
CO ₂ *I*N	1	-3.23E-04	0.489	0.484	-2.59E-06	0.041	0.839	1.15E-04	0.208	0.649

	Chl_{area}			
	df	Coefficient	χ^2	p
(Intercept)	-	2.13E-02	-	-
CO ₂	1	-1.33E-02	69.233	<0.001
Inoculation (I)	1	1.24E-01	136.341	<0.001
Fertilization (N)	1	3.35E-04	163.111	<0.001
CO ₂ *I	1	-3.18E-02	2.102	0.147
CO ₂ *N	1	-8.79E-05	2.999	<i>0.083</i>
I*N	1	-2.65E-04	75.769	<0.001
CO ₂ *I*N	1	7.68E-05	2.144	0.147

129

2182 *Significance determined using Type II Wald χ^2 tests ($\alpha = 0.05$). P -values < 0.05 are in bold, while p -values between
 2183 0.05 and 0.1 are italicized. A superscript “a” is included after trait labels to indicate if models were fit with natural
 2184 log transformed response variables. Key: df = degrees of freedom, N_{area} = leaf nitrogen content per unit leaf area,
 2185 N_{mass} = leaf nitrogen content, M_{area} = leaf mass per unit leaf area.

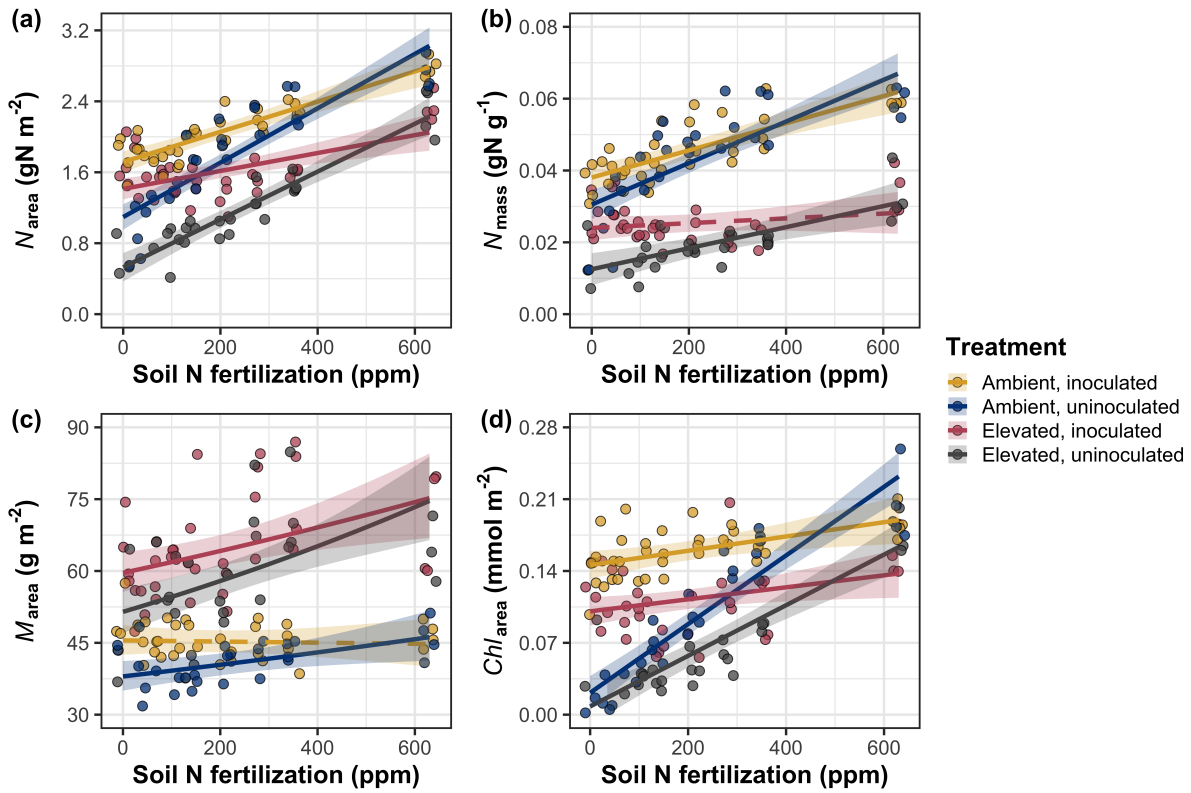


Figure 5.1. Effects of CO_2 , fertilization, and inoculation on leaf nitrogen per unit leaf area (a), leaf nitrogen content (b), leaf mass per unit leaf area (c), and chlorophyll content per unit leaf area (d). Soil nitrogen fertilization is represented on the x-axis in all panels. Yellow points and trendlines indicate inoculated individuals grown under ambient CO_2 , blue points and trendlines indicate uninoculated individuals grown under ambient CO_2 , red points and trendlines indicate inoculated individuals grown under elevated CO_2 , and grey points indicate uninoculated individuals grown under elevated CO_2 . Solid trendlines indicate regression slopes that are different from zero ($p < 0.05$), while dashed trendlines indicate slopes that are not distinguishable from zero ($p > 0.05$).

2186 5.3.2 *Leaf biochemistry and stomatal conductance*

2187 Elevated CO₂ resulted in plants with 16% lower V_{cmax25} ($p < 0.001$; Table
2188 5.2) and 10% lower J_{max25} ($p = 0.014$; Table 5.2) as compared to those grown under
2189 ambient CO₂. However, CO₂ concentration did not influence R_{d25} ($p = 0.613$;
2190 Table 5.2). A relatively stronger downregulation in V_{cmax25} than J_{max25} resulted
2191 in an 8% stimulation in $J_{max25}:V_{cmax25}$ under elevated CO₂ ($p < 0.001$; Table 5.2;
2192 Fig. 2E). The downregulatory effect of CO₂ on V_{cmax25} and J_{max25} was not modified
2193 across the fertilization gradient (CO₂-by-fertilization interaction: $p = 0.185$, $p =$
2194 0.389 for V_{cmax25} and J_{max25} , respectively; Table 5.2; Fig. 5.2a-b) or between
2195 inoculation treatments (CO₂-by-inoculation interaction: $p = 0.799$ and $p = 0.714$
2196 for V_{cmax25} and J_{max25} , respectively; Table 5.2). However, a strong interaction
2197 between fertilization and inoculation (fertilization-by-inoculation interaction: $p \leq$
2198 0.001 in all cases; Table 5.2) indicated that the general positive effect of increasing
2199 fertilization on V_{cmax25} ($p < 0.001$; Table 5.2), J_{max25} ($p < 0.001$; Table 5.2), and
2200 R_{d25} ($p = 0.015$; Table 2) was only observed in uninoculated pots (Tukey: p
2201 ≤ 0.001 in all cases), as there was no apparent effect of fertilization on V_{cmax25}
2202 (Tukey: $p = 0.456$), J_{max25} (Tukey: $p = 0.180$), or R_{d25} (Tukey: $p = 0.443$) in
2203 inoculated pots (Figs. 5.2a-d). A relatively stronger positive effect of increasing
2204 fertilization on V_{cmax25} than J_{max25} resulted in a general reduction in $J_{max25}:V_{cmax25}$
2205 with increasing fertilization ($p < 0.001$), though this pattern was only seen in
2206 uninoculated pots (Tukey: $p = 0.003$) and not inoculated plants (Tukey: $p >$
2207 0.05).

2208 Elevated CO₂ reduced stomatal conductance by 20% ($p < 0.001$; Table
2209 5.2; Fig. 5.2e) compared to ambient CO₂, but this downregulation did not influ-

ence stomatal limitation of photosynthesis ($p = 0.355$; Table 5.2; Fig. 5.2f). As with V_{cmax25} and J_{max25} , the downregulation of stomatal conductance due to elevated CO₂ was not modified across the fertilization gradient (CO₂-by-fertilization interaction: $p = 0.141$; Table 5.2) or between inoculation treatments (CO₂-by-inoculation interaction: $p = 0.179$; Table 5.2). Fertilization also did not modify the general null effect of CO₂ on stomatal limitation (CO₂-by-fertilization interaction: $p = 0.554$; Table 5.2), although an interaction between CO₂ and inoculation (CO₂-by-inoculation interaction: $p = 0.043$; Table 5.2) indicated that inoculation increased stomatal limitation under ambient CO₂ (Tukey: $p = 0.021$), but not under elevated CO₂ (Tukey: $p > 0.999$). An interaction between inoculation and fertilization on stomatal conductance (fertilization-by-inoculation interaction: $p < 0.001$; Table 5.2) indicated that increasing fertilization increased stomatal conductance in uninoculated pots (Tukey: $p = 0.003$) but decreased stomatal conductance in inoculated pots (Tukey: $p = 0.021$). The similar in magnitude, but opposite direction, trend in the effect of increasing fertilization on stomatal conductance between inoculation treatments likely drove a null general response of stomatal conductance to increasing fertilization ($p = 0.642$; Table 5.2).

Table 5.2. Effects of soil nitrogen fertilization, inoculation, and CO₂ on leaf biochemistry

	<i>V_{cmax25}</i>			<i>J_{max25}</i>			<i>R_{d25}</i>			
	df	Coefficient	χ^2	p	Coefficient	χ^2	p	Coefficient	χ^2	p
(Intercept)	-	4.36E+01	-	-	8.30E+01	-	-	1.69E+00	-	-
CO ₂	1	-7.05E+00	18.039	<0.001	-9.11E+00	6.042	0.014	4.53E-01	0.256	0.613
Inoculation (I)	1	5.87E+01	98.579	<0.001	9.62E+01	85.064	<0.001	1.04E+00	3.094	0.079
Fertilization (N)	1	1.32E-01	37.053	<0.001	2.09E-01	25.356	<0.001	2.86E-03	5.965	0.015
CO ₂ *I	1	-4.65E+00	0.065	0.799	7.84E-01	0.667	0.414	-5.71E-01	2.563	0.109
CO ₂ *N	1	-3.58E-02	1.758	0.185	-4.33E-02	0.742	0.389	-1.55E-03	2.675	0.102
I*N	1	-1.35E-01	60.394	<0.001	-2.30E-01	57.410	<0.001	-2.84E-03	12.083	0.001
CO ₂ *I*N	1	2.73E-02	0.748	0.387	3.46E-02	0.377	0.539	7.21E-04	0.244	0.622

	<i>J_{max25}:V_{cmax25}</i>			<i>g_{sw}</i>			Stomatal limitation			
	df	Coefficient	χ^2	p	Coefficient	χ^2	p	Coefficient	χ^2	p
(Intercept)	-	1.92E+00	-	-	1.95E-01	-	-	2.12E-01	-	-
CO ₂	1	5.71E-02	92.010	<0.001	-6.23E-02	9.718	0.002	3.91E-02	0.856	0.355
Inoculation (I)	1	-1.79E-01	27.768	<0.001	1.30E-01	22.351	<0.001	7.87E-02	4.582	0.032
Fertilization (N)	1	-4.61E-04	28.147	<0.001	2.50E-04	0.066	0.797	2.60E-04	32.218	<0.001
CO ₂ *I	1	8.94E-02	2.916	0.088	6.69E-02	1.810	0.179	-7.84E-02	4.093	0.043
CO ₂ *N	1	2.35E-04	3.210	0.073	-8.50E-05	2.165	0.141	-1.24E-04	0.350	0.554
I*N	1	3.27E-04	9.607	0.002	-3.09E-04	14.696	<0.001	-1.67E-04	2.547	0.110
CO ₂ *I*N	1	-1.66E-04	1.102	0.294	-8.89E-05	0.234	0.629	1.67E-04	2.231	0.135

133

2227 *Significance determined using Type II Wald χ^2 tests ($\alpha = 0.05$). *P*-values < 0.05 are in bold, while *p*-values between
 2228 0.05 and 0.1 are italicized. Key: *V_{cmax25}* = maximum rate of Rubisco carboxylation at 25°C; *J_{max25}* = maximum rate
 2229 of electron transport for RuBP regeneration at 25°C, *R_{d25}* = dark respiration at 25°C; *J_{max25}:V_{cmax25}* = the ratio of
 2230 *J_{max25}* to *V_{cmax25}*; *g_{sw}* = stomatal conductance.

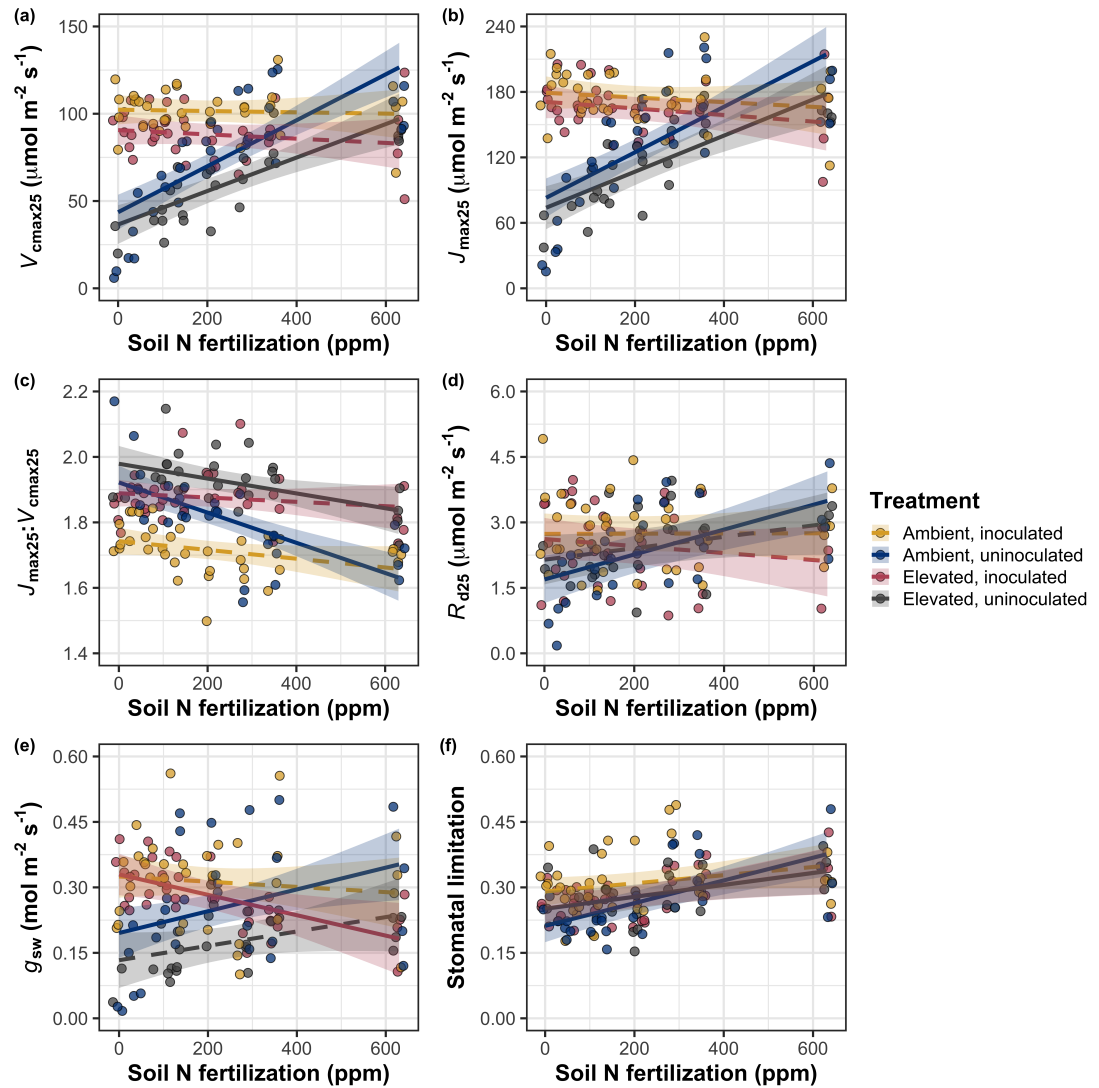


Figure 5.2. Effects of CO₂, fertilization, and inoculation on maximum rate of Rubisco carboxylation (a), the maximum rate of RuBP regeneration (b), and the ratio of the maximum rate of RuBP regeneration to the maximum rate of Rubisco carboxylation leaf mass per unit leaf area (c), dark respiration (d), stomatal conductance (e), and stomatal limitation (f). Soil nitrogen fertilization is represented on the x-axis in all panels. Colored points and trendlines are as explained in Figure 1.

2231 5.3.3 *Leaf nitrogen allocation*

2232 A relatively stronger downregulation in N_{area} than $V_{\text{cmax}25}$ or $J_{\text{max}25}$ resulted
2233 in an 20% and 29% respective stimulation in ρ_{rubisco} and ρ_{bioe} under elevated CO₂
2234 ($p < 0.001$ in both cases; Table 5.3). There was no apparent CO₂ effect on ρ_{light}
2235 ($p = 0.700$; Table 5.3), but the strong stimulation in ρ_{rubisco} and ρ_{bioe} resulted
2236 in a 21% stimulation of ρ_{photo} under elevated CO₂ ($p < 0.001$; Table 5.3; Fig.
2237 5.3a). The stimulation of ρ_{rubisco} , ρ_{bioe} , and ρ_{photo} due to elevated CO₂ was not
2238 modified across the fertilization gradient (CO₂-by-fertilization interaction: p_{rubisco}
2239 = 0.269, $p_{\text{bioe}} = 0.298$, $p_{\text{photo}} = 0.281$; Table 5.3). A marginal interaction between
2240 inoculation and CO₂ on ρ_{rubisco} and ρ_{photo} (CO₂-by-inoculation interaction: p_{rubisco}
2241 = 0.057, $p_{\text{photo}} = 0.057$; Table 5.3) indicated that the general positive effect of
2242 inoculation on ρ_{rubisco} and ρ_{photo} ($p < 0.001$ in both cases; Table 5.3) was only
2243 apparent under ambient CO₂ (Tukey: $p < 0.001$ in both cases), with no apparent
2244 effect of inoculation under elevated CO₂ (Tukey_{rubisco}: $p = 0.200$; Tukey_{photo}: p
2245 = 0.147). Inoculation did not modify the stimulation of ρ_{bioe} under elevated CO₂
2246 (CO₂-by-inoculation interaction: $p = 0.122$; Table 5.3) or the null effect of CO₂ on
2247 ρ_{bioe} (CO₂-by-inoculation interaction: $p = 0.298$; Table 5.3). Strong interactions
2248 between fertilization and inoculation on ρ_{rubisco} , ρ_{bioe} , and ρ_{photo} (fertilization-
2249 by-inoculation interaction: $p < 0.001$ in all cases; Table 5.3) indicated that the
2250 general negative effect of increasing fertilization ($p < 0.001$ in all cases; Table
2251 5.3) was only observed in inoculated pots (Tukey: $p < 0.001$ in all cases), with
2252 no apparent effect of fertilization on ρ_{rubisco} (Tukey: $p = 0.612$), ρ_{bioe} (Tukey:
2253 $p = 0.544$), or ρ_{photo} (Tukey: $p = 0.521$; Fig 5.3a) in uninoculated pots. An
2254 additional interaction between fertilization and inoculation on ρ_{light} (fertilization-

2255 by-inoculation interaction: $p < 0.001$; Table 5.3) indicated a negative effect of
2256 increasing fertilization on ρ_{light} in inoculated pots (Tukey: $p = 0.041$), but a
2257 positive effect of increasing fertilization in uninoculated pots (Tukey: $p < 0.001$).

2258 The stimulation in M_{area} resulted in an 133% stimulation of $\rho_{\text{structure}}$ under
2259 elevated CO₂ ($p < 0.001$; Table 5.3; Fig 5.3b). An interaction between fertiliza-
2260 tion and CO₂ (CO₂-by-fertilization interaction: $p = 0.039$; Table 5.3) indicated
2261 that the general negative effect of increasing fertilization ($p < 0.001$; Table 5.3) on
2262 $\rho_{\text{structure}}$ was marginally stronger under ambient CO₂ (Tukey: $p = 0.055$), resulting
2263 in a stronger stimulation in $\rho_{\text{structure}}$ under elevated CO₂ with increasing fertiliza-
2264 tion. A marginal interaction between inoculation and CO₂ (CO₂-by-inoculation
2265 interaction: $p = 0.057$; Table 5.3) indicated that the general positive effect of
2266 inoculation on $\rho_{\text{structure}}$ ($p < 0.001$; Table 5.3) was only observed under elevated
2267 CO₂ (Tukey: $p < 0.001$), with no apparent inoculation effect observed under am-
2268 bient CO₂ (Tukey: $p = 0.513$). Finally, an interaction between fertilization and
2269 inoculation (fertilization-by-inoculation interaction: $p < 0.001$; Table 5.3) indi-
2270 cated that, while increasing fertilization generally increased $\rho_{\text{structure}}$ ($p < 0.001$;
2271 Table 5.3), this response was generally stronger in uninoculated pots (Tukey: p
2272 = 0.001; Fig. 5.3b).

Table 5.3. Effects of soil N availability, soil pH, species, and N_{area} on leaf nitrogen allocation

		ρ_{rubisco}			ρ_{bioe}			ρ_{light}		
	df	Coefficient	χ^2	p	Coefficient	χ^2	p	Coefficient	χ^2	p
(Intercept)	-	2.70E-01	-	-	5.26E-02	-	-	8.48E-03	-	-
CO_2	1	1.42E-01	23.510	<0.001	3.00E-02	53.899	<0.001	2.03E-03	0.149	0.700
Inoculation (I)	1	1.83E-01	23.475	<0.001	2.80E-02	13.860	<0.001	2.04E-02	147.234	<0.001
Fertilization (N)	1	1.35E-04	16.609	<0.001	1.22E-05	26.827	<0.001	3.22E-05	19.378	<0.001
CO_2*I	1	-1.07E-01	3.629	0.057	-1.67E-02	2.390	0.122	-5.33E-03	0.684	0.408
CO_2*N	1	-2.16E-04	1.223	0.269	-3.59E-05	1.085	0.298	-7.01E-06	0.351	0.553
$I*N$	1	-4.26E-04	20.045	<0.001	-6.87E-05	15.458	<0.001	-4.37E-05	64.042	<0.001
CO_2*I*N	1	2.50E-04	3.327	0.068	4.08E-05	2.651	0.103	1.74E-05	3.735	0.053

		ρ_{photo}			$\rho_{\text{structure}}^a$					
	df	Coefficient	χ^2	p	Coefficient	χ^2	p			
(Intercept)	-	3.32E-01	-	-	-2.93E+00	-	-			
CO_2	1	1.81E-01	27.651	<0.001	8.77E-01	229.571	<0.001			
Inoculation (I)	1	2.31E-01	26.238	<0.001	-2.55E-01	13.872	<0.001			
Fertilization (N)	1	1.76E-04	15.899	<0.001	-1.51E-03	38.128	<0.001			
CO_2*I	1	-1.36E-01	3.671	0.055	-2.99E-01	3.622	0.057			
CO_2*N	1	-2.72E-04	1.163	0.281	3.14E-04	4.266	0.039			
$I*N$	1	-5.37E-04	21.355	<0.001	7.00E-04	11.025	0.001			
CO_2*I*N	1	3.29E-04	4.009	0.045	4.52E-04	0.669	0.413			

137

2273 *Significance determined using Type II Wald χ^2 tests ($\alpha = 0.05$). P-values < 0.05 are in bold, while p-values
 2274 between 0.05 and 0.1 are italicized. A superscript “a” is included after trait labels to indicate if models were fit with
 2275 natural log transformed response variables. Key: df=degrees of freedom, ρ_{rubisco} = proportion of leaf N allocated
 2276 to photosynthesis, ρ_{bioe} = proportion of leaf N allocated to bioenergetics, ρ_{light} = proportion of leaf N allocated to
 2277 light harvesting proteins, ρ_{photo} = proportion of leaf N allocated to photosynthesis, $\rho_{\text{structure}}$ = proportion of leaf N
 2278 allocated to cell wall structural tissue

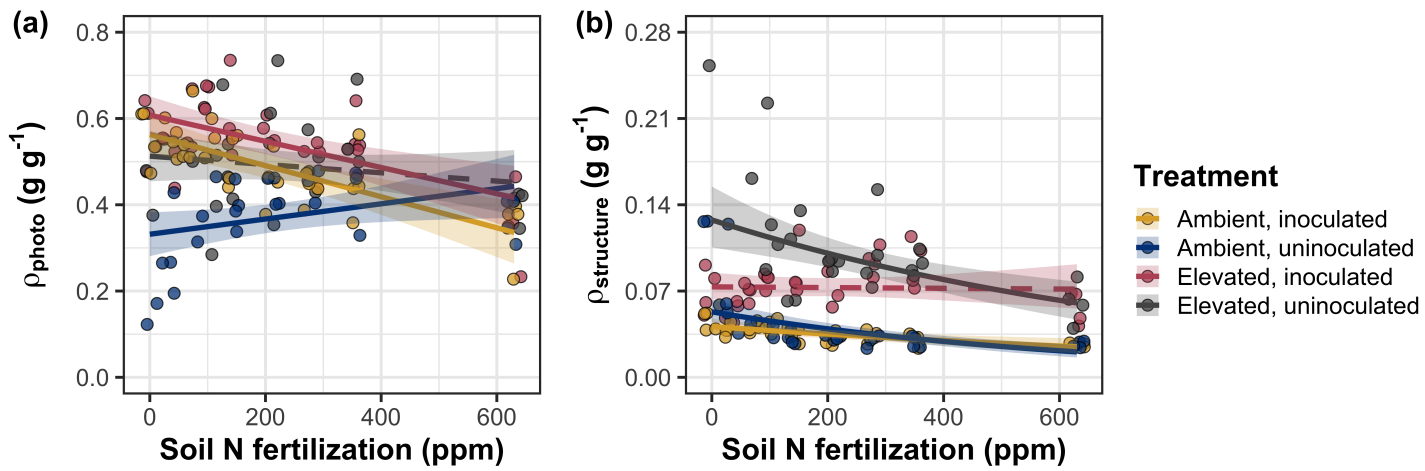


Figure 5.3. Effects of CO_2 , fertilization, and inoculation on the relative fraction of leaf nitrogen allocated to photosynthesis (a) and the fraction of leaf nitrogen allocated to structure (b). Soil nitrogen fertilization is represented on the x-axis in both panels. Colored points and trendlines are as explained in Figure 1.

2279 5.3.4 *Whole plant traits*

2280 Total leaf area was 51% greater and total biomass was 102% greater under
2281 elevated CO₂ ($p < 0.001$ in both cases; Table 5.4), a pattern that was enhanced
2282 by fertilization (CO₂-by-fertilization interaction: $p < 0.001$ in both cases; Table
2283 5.4; Figs. 5.4a-b) but was not modified across inoculation treatments (CO₂-by-
2284 inoculation interaction: $p_{total_leaf_area} = 0.151$, $p_{total_biomass} = 0.472$; Table 5.4).
2285 Specifically, the general positive effect of increasing fertilization on total leaf area
2286 and whole plant biomass ($p < 0.001$ in both cases; Table 5.4) was stronger under
2287 elevated CO₂ (Tukey: $p < 0.001$ in both cases). The general positive effect of
2288 increasing fertilization on total leaf area was modified by inoculation treatment
2289 (fertilization-by-inoculation interaction: $p < 0.001$ in both cases; Table 5.4), in-
2290 dicating a stronger positive effect of increasing fertilization in uninoculated pots
2291 (Tukey: $p_{total_leaf_area} = 0.002$, $p_{total_biomass} = 0.001$, Fig. 5.4a).

2292 A 62% stimulation in N_{cost} under elevated CO₂ was modified through a
2293 strong three-way interaction between CO₂, fertilization, and inoculation (CO₂-
2294 by-inoculation-by-fertilization interaction: $p < 0.001$; Table 5.4; Fig. 5.4). This
2295 interaction revealed a general negative effect of increasing fertilization on N_{cost}
2296 ($p < 0.001$; Table 5.4) that was observed in all treatment combinations (Tukey:
2297 $p < 0.001$ in all cases) except for inoculated pots grown under elevated CO₂
2298 (Tukey: $p = 0.779$; Fig. 5.4c). This response also resulted in generally stronger
2299 negative effects of increasing fertilization on N_{cost} in uninoculated pots grown
2300 under elevated CO₂ than uninoculated pots grown under ambient CO₂ (Tukey:
2301 $p = 0.001$) and inoculated pots grown under either ambient CO₂ (Tukey: $p <$
2302 0.001) or elevated CO₂ (Tukey: $p < 0.001$), while uninoculated pots grown under

2303 ambient CO₂ had generally stronger negative effects of increasing fertilization on
2304 N_{cost} than inoculated pots grown under elevated CO₂ (Tukey: $p = 0.002$), but
2305 not inoculated pots grown under ambient CO₂ (Tukey: $p = 0.216$; Fig. 5.4).
2306 The general reduction in N_{cost} with increasing fertilization and in uninoculated
2307 pots were driven by a stronger positive effect of increasing fertilization on N_{wp}
2308 (denominator of N_{cost}) than C_{bg} (numerator of N_{cost}), while the general stimulation
2309 in N_{cost} under elevated CO₂ was driven by a stronger positive effect of elevated
2310 CO₂ on C_{bg} than N_{wp} (Table 5.4).

Table 5.4. Effects of soil N availability, soil pH, species, and N_{area} on total leaf area, whole plant biomass, and carbon costs to acquire nitrogen

	Total leaf area			Total biomass			N_{cost}			
	df	Coefficient	χ^2	p	Coefficient	χ^2	p	Coefficient	χ^2	p
(Intercept)	-	8.78E+01	-	-	9.96E-01	-	-	8.67E+00	-	-
CO_2	1	3.36E+01	69.291	<0.001	5.07E-01	131.477	<0.001	8.75E+00	88.189	<0.001
Inoculation (I)	1	1.88E+02	35.715	<0.001	7.96E-01	34.264	<0.001	-1.68E+00	136.343	<0.001
Fertilization (N)	1	9.35E-01	274.199	<0.001	3.14E-03	269.046	<0.001	-8.50E-03	80.501	<0.001
$\text{CO}_2 * \text{I}$	1	6.44E+01	2.064	0.151	-7.69E-02	0.518	0.472	-8.38E+00	85.237	<0.001
$\text{CO}_2 * \text{N}$	1	5.05E-01	18.655	<0.001	1.61E-03	16.877	<0.001	-9.17E-03	1.050	0.306
$\text{I} * \text{N}$	1	-3.84E-01	10.804	0.001	-1.45E-03	15.779	<0.001	4.20E-03	46.489	<0.001
$\text{CO}_2 * \text{I} * \text{N}$	1	-2.97E-03	<0.001	0.990	-1.14E-04	0.023	0.880	1.32E-02	18.125	<0.001

	C_{bg}			N_{wp}			
	df	Coefficient	χ^2	p	Coefficient	χ^2	p
(Intercept)	-	-1.70E+00	-	-	1.24E-01	-	-
CO_2	1	9.21E-01	84.134	<0.001	-3.41E-03	23.890	<0.001
Inoculation (I)	1	1.18E+00	41.030	<0.001	1.68E-01	134.460	<0.001
N fertilization (N)	1	3.38E-03	152.248	<0.001	6.69E-04	529.021	<0.001
$\text{CO}_2 * \text{I}$	1	-6.18E-01	8.965	0.003	3.68E-02	1.190	0.275
$\text{CO}_2 * \text{N}$	1	-3.66E-05	1.188	0.276	1.58E-04	5.915	0.015
$\text{I} * \text{N}$	1	-2.22E-03	22.648	<0.001	-3.20E-04	55.562	<0.001
$\text{CO}_2 * \text{I} * \text{N}$	1	8.09E-04	1.109	0.292	-7.54E-05	0.620	0.431

141

2311 *Significance determined using Type II Wald χ^2 tests ($\alpha = 0.05$). P-values < 0.05 are in bold, while p-values between
 2312 0.05 and 0.1 are italicized. Key: df = degrees of freedom; N_{cost} = structural carbon cost to acquire nitrogen; C_{bg} =
 2313 belowground carbon biomass; N_{wp} = whole plant nitrogen biomass

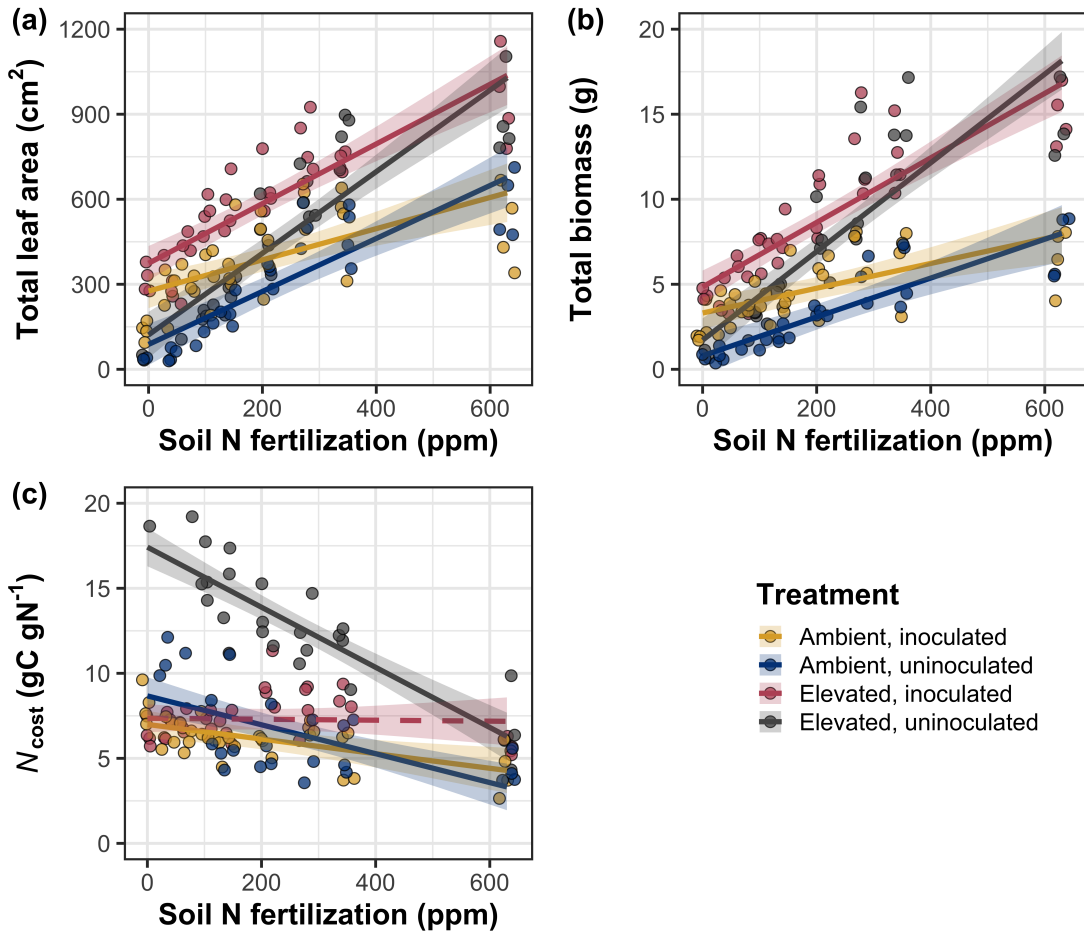


Figure 5.4. Effects of CO_2 , fertilization, and inoculation on total leaf area (a), total biomass (b), and structural carbon costs to acquire nitrogen (c). Soil nitrogen fertilization is represented continuously on the x-axis in all panels. Colored points and trendlines are as explained in Figure 1.

2314 5.3.5 *Nitrogen fixation*

2315 Nodule biomass was stimulated by 30% under elevated CO₂ ($p < 0.001$;
2316 Table 5.5), a pattern that was modified across the fertilization gradient (CO₂-
2317 by-fertilization interaction: $p = 0.479$; Table 5.5), but not between inoculation
2318 treatments (CO₂-by-inoculation interaction: $p = 0.404$; Table 5.5). Specifically,
2319 the general negative effect of increasing fertilization on nodule biomass ($p < 0.001$;
2320 Table 5.5) was stronger under elevated CO₂ than ambient CO₂ (Tukey: $p <$
2321 0.001; Fig. 5.5a), which reduced the stimulation in nodule biomass under elevated
2322 CO₂ with increasing fertilization. A strong interaction between fertilization and
2323 inoculation (fertilization-by-inoculation interaction: $p < 0.001$; Table 5.5) was
2324 driven by a stronger negative effect of increasing fertilization in inoculated pots
2325 (Tukey: $p < 0.001$; Fig. 5.5a).

2326 There was no effect of CO₂ on nodule: root biomass ($p = 0.767$; Table
2327 5.5), although an interaction between CO₂ and inoculation (CO₂-by-inoculation
2328 interaction: $p < 0.001$; Table 5.5) indicated that the general positive effect of in-
2329 oculation on nodule: root biomass ($p < 0.001$; Table 5.5) was stronger under am-
2330 bient CO₂ (3129% increase; Tukey: $p < 0.001$) than elevated CO₂ (379% increase;
2331 Tukey: $p < 0.001$; Fig. 5.5b). The null effect of CO₂ on nodule: root biomass
2332 was consistently observed across the fertilization gradient ($p = 0.183$; Table 5.5;
2333 Fig. 5.5b). An interaction between fertilization and inoculation (fertilization-by-
2334 inoculation interaction: $p < 0.001$; Table 5.5) indicated that the general negative
2335 effect of increasing fertilization on nodule: root biomass ($p < 0.001$; Table 5.5)
2336 was stronger in inoculated pots (Tukey: $p < 0.001$; Fig. 5.5b).

2337 There was no effect of CO₂ on %N_{dfa} ($p = 0.472$; Table 5.5), a pattern

2338 that was not modified by inoculation (CO_2 -by-inoculation interaction: $p = 0.156$;
2339 Table 5.5) or fertilization (CO_2 -by-fertilization interaction: $p = 0.099$; Table 5.5).
2340 An interaction between fertilization and inoculation (fertilization-by-inoculation
2341 interaction: $p < 0.001$; Table 5.5) indicated that the general negative effect of
2342 increasing fertilization on $\%N_{dfa}$ ($p < 0.001$; Table 5.5) was only observed in
2343 inoculated pots (Tukey: $p < 0.001$), with no apparent effect of fertilization on
2344 $\%N_{dfa}$ in uninoculated pots (Tukey: $p = 0.651$; Table 5.5; Fig. 5.5c).

Table 5.5. Effects of soil N availability, soil pH, species, and N_{area} on root nodule biomass and plant investments in symbiotic nitrogen fixation

	Root nodule biomass ^b			Root nodule: root biomass ^b			% N_{dfa}^b			
	df	Coefficient	χ^2	p	Coefficient	χ^2	p	Coefficient	χ^2	p
(Intercept)	-	9.41E-03	-	-	1.33E-02	-	-	7.48E-01	-	-
CO ₂	1	1.20E-01	19.258	<0.001	9.94E-02	0.087	0.768	-1.00E-01	0.518	0.472
Inoculation (I)	1	5.74E-01	755.020	<0.001	5.40E-01	903.691	<0.001	9.01E+00	955.570	<0.001
Fertilization (N)	1	7.71E-06	84.376	<0.001	-5.99E-06	258.099	<0.001	3.64E-04	292.938	<0.001
CO ₂ *I	1	-4.68E-02	0.950	0.330	-1.38E-01	20.614	<0.001	-1.44E-01	2.010	0.156
CO ₂ *N	1	-1.59E-04	2.106	0.147	-1.73E-04	1.773	0.183	-6.21E-05	2.716	0.099
I*N	1	-5.82E-04	44.622	<0.001	-7.45E-04	133.918	<0.001	-1.58E-02	231.290	<0.001
CO ₂ *I*N	1	7.26E-05	0.196	0.658	1.76E-04	2.359	0.125	2.77E-03	2.119	0.145

2345 *Significance determined using Type II Wald χ^2 tests ($\alpha = 0.05$). P-values < 0.05 are in bold, while p-values between
2346 0.05 and 0.1 are italicized. Superscript letters indicate model coefficients fit to square-root (^b) transformed data.
2347 Key: df = degrees of freedom % N_{dfa} = percent nitrogen fixed from the atmosphere.

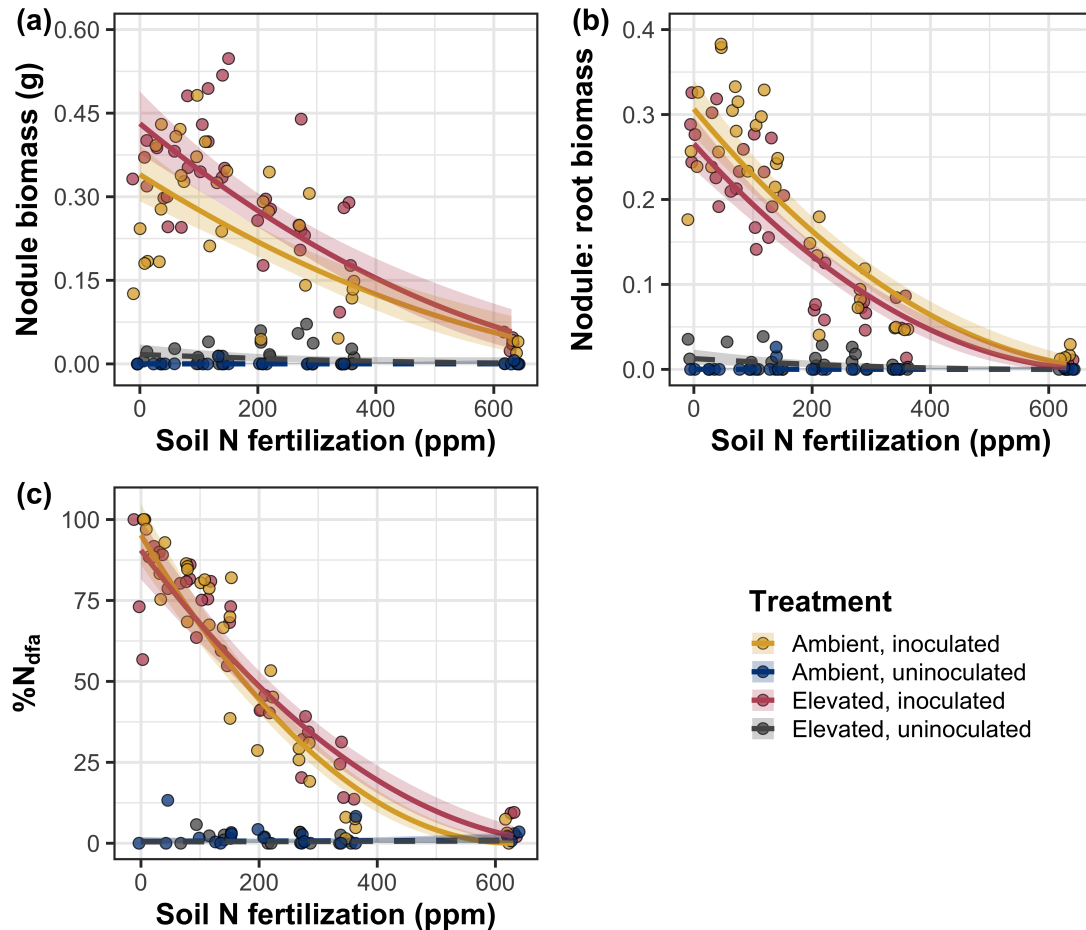


Figure 5.5. Effects of CO_2 , fertilization, and inoculation on nodule biomass (a), nodule: root biomass (b), and percent nitrogen fixed from the atmosphere (c). Soil nitrogen fertilization is represented on the x-axis. Yellow points and trendlines indicate inoculated individuals grown under ambient CO_2 , blue points and trendlines indicate uninoculated individuals grown under ambient CO_2 , red points and trendlines indicate inoculated individuals grown under elevated CO_2 , and grey points indicate uninoculated individuals grown under elevated CO_2 . Solid trendlines indicate slopes that are different from zero ($p < 0.05$), while dashed trendlines indicate slopes that are not different from zero ($p > 0.05$). Curvilinear trendlines occur as a result of back-transforming models where response variables received either a natural log or square root transformation prior to fitting.

2348 5.4 Discussion

2349 In this study, I determined leaf and whole plant acclimation responses of
2350 7-week *G. max* seedlings grown under two CO₂ concentrations, two inoculation
2351 treatments, and nine soil nitrogen fertilization treatments in a full-factorial growth
2352 chamber experiment. In support of my hypotheses and patterns expected from
2353 theory, elevated CO₂ reduced N_{area} , V_{cmax25} , and J_{max25} . The relatively stronger
2354 downregulation in V_{cmax25} than J_{max25} under elevated CO₂ resulted in a stimulation
2355 in $J_{\text{max25}}:V_{\text{cmax25}}$ under elevated CO₂. The downregulation of V_{cmax25} and J_{max25}
2356 under elevated CO₂ was similar across fertilization and inoculation treatments,
2357 indicating that the CO₂ responses were not due to nitrogen limitation. Interest-
2358 ingly, results indicate that elevated CO₂ increased the fraction of leaf nitrogen
2359 allocated to photosynthesis and structure, leading to a stimulation in nitrogen
2360 use efficiency under elevated CO₂ despite the apparent downregulation in N_{area} ,
2361 V_{cmax25} , and J_{max25} . The downregulation in leaf photosynthetic processes under
2362 elevated CO₂ also corresponded with a strong stimulation in total leaf area and to-
2363 tal biomass. Strong stimulations in whole plant growth due to elevated CO₂ were
2364 generally enhanced with increasing fertilization and were negatively related to
2365 structural carbon costs to acquire nitrogen. Inoculation generally did not modify
2366 whole plant responses to elevated CO₂ across the fertilization gradient, likely due
2367 to a strong reduction in root nodulation with increasing fertilization. However,
2368 strong positive effects of inoculation on whole plant growth were observed under
2369 low fertilization, consistent with our hypothesis. Overall, observed leaf and whole
2370 plant acclimation responses to CO₂ support hypotheses and patterns expected
2371 from photosynthetic least-cost theory, showing that leaf acclimation responses to

2372 CO₂ were decoupled from soil nitrogen availability and ability to acquire nitro-
2373 gen via symbiotic nitrogen fixation. Instead, leaf and whole plant acclimation
2374 responses to CO₂ were driven by optimal resource investment to photosynthetic
2375 capacity, where optimal resource investment at the leaf level maximized nitrogen
2376 allocation to structures that support whole plant growth.

2377 5.4.1 *Soil nitrogen fertilization has divergent effects on leaf and whole plant*
2378 *acclimation responses to CO₂*

2379 Elevated CO₂ reduced N_{area} , V_{cmax25} , J_{max25} , and stomatal conductance by
2380 29%, 16%, 10%, and 20%, respectively (Table 5.2). The larger downregulation in
2381 V_{cmax25} than J_{max25} led to an 8% stimulation in $J_{\text{max25}}:V_{\text{cmax25}}$ (Table 5.2), while
2382 the larger downregulation in N_{area} than V_{cmax25} resulted in a 21% stimulation
2383 in the fraction of leaf nitrogen allocated to photosynthesis under elevated CO₂.
2384 These acclimation responses are directionally consistent with previous studies that
2385 have investigated or reviewed leaf acclimation responses to CO₂ (Drake et al.
2386 1997; Makino et al. 1997; Ainsworth et al. 2002; Ainsworth and Long 2005;
2387 Ainsworth and Rogers 2007; Smith and Dukes 2013; Smith and Keenan 2020;
2388 Poorter et al. 2022), and follow patterns expected from photosynthetic least-cost
2389 theory (Wright et al. 2003; Prentice et al. 2014; Smith et al. 2019; Smith and
2390 Keenan 2020). Together, the stimulation in $J_{\text{max25}}:V_{\text{cmax25}}$ and the fraction of leaf
2391 nitrogen allocated to photosynthesis, and nitrogen use efficiency under elevated
2392 CO₂ provide strong support for the idea that leaves were downregulating V_{cmax25}
2393 in response to elevated CO₂ in order to optimally coordinate photosynthesis such
2394 that net photosynthesis rates approached becoming equally co-limited by Rubisco

2395 carboxylation and RuBP regeneration (Chen et al. 1993; Maire et al. 2012).

2396 Increasing fertilization and inoculation induced strong positive effects on
2397 N_{area} (Fig. 1a), $V_{\text{cmax}25}$ (Fig. 5.2a), $J_{\text{max}25}$ (Fig. 5.2b). The general positive
2398 response of N_{area} to increasing fertilization and in inoculated pots was enhanced
2399 under ambient CO_2 , which, paired with the general downregulation in N_{area} un-
2400 der elevated CO_2 , resulted in a stronger downregulation of N_{area} under elevated
2401 CO_2 with increasing fertilization and in inoculated pots (Fig. 5.1a). These pat-
2402 terns suggest that N_{area} responses to CO_2 were at least partially dependent on
2403 soil nitrogen fertilization and nitrogen acquisition strategy. However, the general
2404 stimulation in the fraction of leaf nitrogen allocated to Rubisco, bioenergetics,
2405 or photosynthesis under elevated CO_2 was not modified across the fertilization
2406 gradient and was only marginally enhanced in inoculated pots. These patterns
2407 suggest that the increased downregulation of N_{area} under elevated CO_2 with in-
2408 creasing fertilization was not associated with a change in relative investment to
2409 photosynthetic tissue. Instead, a stronger downregulation in the fraction of leaf
2410 nitrogen allocated to structure under ambient CO_2 resulted in a stronger stim-
2411 ulation in $\rho_{\text{structure}}$ under elevated CO_2 with increasing fertilization (Fig. 5.3b),
2412 indicating that fertilization shifted relative investment in leaf structural tissue un-
2413 der elevated CO_2 . These results, combined with a stimulation in PNUE (Fig. SX)
2414 and iWUE (Fig. SX) under elevated CO_2 that was independent of fertilization
2415 or inoculation treatment, provide additional support for the hypothesis that leaf
2416 acclimation photosynthetic responses to CO_2 were independent of fertilization;
2417 though fertilization may contribute to changes in leaf morphology under elevated
2418 CO_2 through shifts in M_{area} (Onoda et al. 2017; Wang et al. 2017; Dong et al.

2419 2022).

2420 The downregulation in N_{area} , V_{cmax25} , and J_{max25} under elevated CO₂ cor-
2421 responded with a respective 62% and 100% stimulation in total leaf area (Fig.
2422 5.4a) and total biomass (Fig. 5.4b). The stimulation in total leaf area and total
2423 biomass under elevated CO₂ also corresponded with generally higher structural
2424 carbon costs to acquire nitrogen (Fig. 5.4c), a pattern driven by a stimulation
2425 in belowground carbon biomass and reduction in whole plant nitrogen biomass.
2426 Alone, this result suggests that elevated CO₂ reduces plant nitrogen uptake effi-
2427 ciency, which does not explain why plants grown under elevated CO₂ generally had
2428 higher biomass and total leaf area. However, a strong negative effect of increasing
2429 fertilization on structural carbon costs to acquire nitrogen, which were generally
2430 similar between CO₂ concentrations, was driven by a stronger increase in whole
2431 plant nitrogen biomass than belowground carbon biomass. Thus, increases in the
2432 positive response of whole plant growth and total leaf area under elevated CO₂
2433 with increasing fertilization were likely driven by an increase in nitrogen uptake
2434 efficiency, allowing plants to satisfy any increase in whole plant nitrogen demand
2435 associated with increased CO₂.

2436 Interestingly, these results indicate that the general stimulation in total
2437 leaf area and whole plant growth under elevated CO₂ was not modified by inoc-
2438 ulation despite an apparent general negative effect of inoculation on N_{cost} . This
2439 response could have been due to strong negative effect of increasing fertilization on
2440 nodulation (Fig. 5.5), which may have caused the strong increase in the positive
2441 effect of elevated CO₂ on whole plant growth with increasing fertilization to mask
2442 any increase in the positive effect of elevated CO₂ on whole plant growth due to

2443 inoculation. Reductions in nodulation with increasing fertilization are commonly
2444 observed patterns that have been inferred to be a response that allows species
2445 optimize nitrogen uptake efficiency as costs to acquire nitrogen via direct uptake
2446 become more similar (Fig. 5.4c) (Gibson and Harper 1985; Rastetter et al. 2001).
2447 In this study, pairwise comparisons indicated strong positive effects of inocula-
2448 tion on total leaf area and total biomass (158% increase in total leaf area, 119%
2449 increase in total biomass) under elevated CO₂ at 0 ppm N, but no observable
2450 inoculation effect on total leaf area or total biomass under elevated CO₂ at 350
2451 ppm N or 630 ppm N. While these responses did not generally differ from those
2452 observed under ambient CO₂, they do confirm the hypothesis that positive effects
2453 of inoculation on whole plant growth responses to elevated CO₂ would decrease
2454 with increasing fertilization.

2455 Combined, results reported here suggest that soil nitrogen availability has
2456 a divergent role in modifying leaf and whole plant acclimation responses to CO₂.
2457 Leaf acclimation responses were generally decoupled from fertilization, while whole
2458 plant acclimation responses relied heavily on an increase in nitrogen uptake ef-
2459 ficiency and consequent reduction in costs of acquiring nitrogen associated with
2460 increasing fertilization. However, whole plant responses to CO₂ indicated that
2461 fertilization may play a more important role in determining whole plant acclima-
2462 tion responses to CO₂ than nitrogen acquisition strategy, although these patterns
2463 were likely driven by reductions in nodulation with increasing fertilization. These
2464 results suggest that plants acclimate to CO₂ in nitrogen-limited systems by mini-
2465 mizing the number of optimally coordinated leaves, and that the downregulation
2466 in leaf nitrogen content under elevated CO₂ is not a direct response to changes in

2467 soil nitrogen availability as previously implied.

2468 5.4.2 *Implications for future model development*

2469 Many terrestrial biosphere models predict photosynthetic capacity through
2470 plant functional group-specific linear regressions between N_{area} and V_{cmax} (Rogers
2471 2014; Rogers et al. 2017), which assumes that leaf nitrogen-photosynthesis rela-
2472 tionships are constant across growing environments. Our results build on previ-
2473 ous work suggesting that leaf nitrogen-photosynthesis relationships dynamically
2474 change across growing environments (Luo et al. 2021; Dong et al. 2022). Specif-
2475 ically, results from this experiment indicate that CO_2 concentration increased
2476 the fraction of leaf nitrogen content allocated to photosynthesis, while a general
2477 negative effect of increasing fertilization on the fraction of leaf nitrogen content
2478 allocated to photosynthesis was dependent on inoculation treatment. Similar in-
2479 creases in N_{area} , $V_{\text{cmax}25}$, and $J_{\text{max}25}$ with increasing fertilization resulted in no
2480 change in the fraction of leaf nitrogen allocated to photosynthesis in uninoculated
2481 pots, while larger increases in N_{area} than $V_{\text{cmax}25}$ and $J_{\text{max}25}$ with increasing fertil-
2482 ization decreased the fraction of leaf nitrogen allocated to photosynthesis in inoc-
2483 ulated pots (Fig. 5.3a). As inoculated pots were able to access less finite supply of
2484 nitrogen across the fertilization gradient, these patterns suggest that constant leaf
2485 nitrogen-photosynthesis relationships may only apply in environments where ni-
2486 trogen is limiting and will likely change with increasing CO_2 concentrations. Thus,
2487 terrestrial biosphere models that parameterize photosynthetic capacity through
2488 linear relationships between N_{area} and V_{cmax} (Rogers 2014; Rogers et al. 2017)
2489 may be overestimating photosynthetic capacity in systems where nitrogen is not

2490 as limiting and may contribute to erroneous model simulations under future CO₂
2491 concentrations.

2492 These results also demonstrate that optimal resource investment to photo-
2493 synthetic capacity defines leaf acclimation responses to elevated CO₂, and that
2494 these responses were independent of fertilization or inoculation treatment. Cur-
2495 rent approaches for simulating photosynthetic responses to CO₂ generally invoke
2496 patterns expected from progressive nitrogen limitation, where the downregulation
2497 in N_{area} , and therefore photosynthetic capacity, due to elevated CO₂ are com-
2498 monly a function of progressive reductions in soil nitrogen availability. Results
2499 reported here contradict this formulation, suggesting that the leaf acclimation re-
2500 sponse is driven by optimal resource investment to photosynthetic capacity and
2501 is independent of soil resource supply. Optimality models that leverage prin-
2502 ciples from optimal coordination and photosynthetic least-cost theories (Wang
2503 et al. 2017; Stocker et al. 2020; Scott and Smith 2022) are capable of capturing
2504 such acclimation responses to CO₂ (Smith and Keenan 2020), suggesting that the
2505 implementation of these models may improve the simulation of photosynthetic
2506 processes in terrestrial biosphere models under increasing CO₂ concentrations.

2507 5.4.3 *Study limitations and future directions*

2508 There are two study limitations that must be addressed to contextualize
2509 patterns observed in this study. First, restricting the volume of belowground
2510 substrate via a potted experiment does not adequately replicate belowground en-
2511 vironments of natural systems, and therefore may modify effects of soil resource
2512 availability and inoculation on plant nitrogen uptake, particularly if pot size limits

2513 whole plant growth (Poorter et al. 2012). I attempted to minimize the extent of
2514 pot size limitation experienced in the first experimental chapters while account-
2515 ing for the expected stimulation in whole plant growth under elevated CO₂ by
2516 using 6-liter pots. Despite attempts to minimize growth limitation imposed by
2517 pot volume, fertilization and CO₂ treatments increased the biomass: pot volume
2518 ratio such that all treatment combinations to exceed 1 g L⁻¹ biomass: pot volume
2519 under high fertilization. The 1 g L⁻¹ biomass: pot volume recommendation from
2520 Poorter et al. (2012) was designated to avoid growth limitation imposed by pot
2521 volume. However, if pot size limitation indeed limited whole plant growth, then
2522 structural carbon costs to acquire nitrogen, belowground carbon biomass, whole
2523 plant nitrogen biomass, and whole plant biomass should each exhibit strong sat-
2524 uration points with increasing fertilization, which was not observed here. Addi-
2525 tionally, a second set of photosynthetic measurements from one week prior to the
2526 harvest (6 weeks post-germination) revealed ... As pot limitation is expected
2527 to decrease net photosynthesis, and focal leaves were of similar ages between the
2528 sixth and seventh week, one might expect growth limitation induced by constricted
2529 pot volume to result in a dampened effect of inoculation and fertilization on net
2530 photosynthesis, V_{cmax} , and J_{max25} . Analyses from the sixth week of development
2531 revealed ... Additionally, analyses revealed a stronger/weaker downregulation in
2532 V_{cmax25} and J_{max25} on week 7, though disentangling the causality of this response
2533 (i.e. whether due to pot size limitation or simply a stronger acclimation response)
2534 would be difficult.

2535 Second, this study evaluated leaf and whole plant responses to CO₂ in 7-
2536 week seedlings. Given the long-term scale of the progressive nitrogen limitation

2537 hypothesis, patterns observed here should be validated in longer-term nitrogen
2538 manipulation experiments. Previous work in free air CO₂ enrichment experiments
2539 show some support for patterns expected from the progressive nitrogen limitation
2540 hypothesis (Reich et al. 2006; Norby et al. 2010), although results are not consis-
2541 tent across experimental sites (Finzi et al. 2006; Moore et al. 2006; Liang et al.
2542 2016). We found some support for patterns expected by the progressive nitrogen
2543 limitation hypothesis, namely an increase in plant nitrogen uptake under elevated
2544 CO₂ (Luo et al. 2004), though leaf acclimation responses to CO₂ were strongly
2545 indicative of optimal resource investment to photosynthetic capacity as expected
2546 from photosynthetic least-cost theory (Prentice et al. 2014; Smith et al. 2019;
2547 Smith and Keenan 2020).

2548 5.4.4 *Conclusions*

2549 This study provides strong evidence suggesting that leaf acclimation re-
2550 sponds to elevated CO₂ did not vary with soil nitrogen fertilization or ability
2551 to acquire nitrogen through symbiotic nitrogen fixation. However, whole plant
2552 acclimation responses to CO₂ were dependent on fertilization, where increasing
2553 fertilization increased the positive effect of whole plant growth under elevated
2554 CO₂. Results also indicate that fertilization played a relatively more important
2555 role in modifying whole plant responses to CO₂, perhaps due to a reduction in
2556 nodulation across the fertilization gradient. These patterns strongly support the
2557 hypothesis that leaf and whole plant acclimation responses are driven by opti-
2558 mal resource investment to photosynthetic capacity, and that leaf acclimation
2559 responses to CO₂ were not modified by changes in soil nitrogen availability. Ad-

2560 ditionally, strong interactions between fertilization and inoculation on leaf and
2561 whole plant traits indicated positive effects of fertilization on leaf and whole plant
2562 traits in uninoculated pots, but null effects of fertilization on leaf and whole plant
2563 traits in inoculated pots. These results build on previous work suggesting that
2564 constant leaf nitrogen-photosynthesis relationships are dynamic and change across
2565 growing environments, calling the use of constant relationships by terrestrial bio-
2566 sphere models into question.

2567

Chapter 6

2568

Conclusions

2569 The experiments included in this dissertation were designed to test mechanisms
2570 that drive patterns expected from photosynthetic least-cost theory across various
2571 edaphic and climatic gradients. Specifically, I evaluate the context dependency
2572 of carbon costs to acquire nitrogen across soil nitrogen availability and how vari-
2573 ance in carbon costs to acquire nitrogen scales to influence leaf and whole plant
2574 acclimation responses to changing environments.

2575 In the first experimental chapter, I quantified carbon costs to acquire ni-
2576 trogen in a species capable of forming associations with symbiotic nitrogen-fixing
2577 bacteria (*Glycine max*) and a species not capable of forming such associations
2578 (*Gossypium hirsutum*) grown under four soil nitrogen fertilization treatments and
2579 four light availability treatments in a full factorial greenhouse experiment. I found
2580 that increasing light availability increased carbon costs to acquire nitrogen in both
2581 species due to a larger increase in belowground carbon biomass than whole plant
2582 nitrogen biomass. These patterns were observed in both species. I also found
2583 that increasing fertilization decreased carbon costs to acquire nitrogen due to a
2584 larger increase in whole plant nitrogen biomass than belowground carbon biomass.
2585 While these patterns were observed in both species, carbon costs to acquire nitro-
2586 gen in *G. max* were less responsive to increasing fertilization than *G. hirsutum*,
2587 providing some support for my second hypothesis. Root nodulation data indicated
2588 that *G. max* shifted relative carbon allocation from nitrogen fixation to direct up-
2589 take with increasing fertilization, which may explain the reduced responsiveness

2590 of *G. max* carbon costs to acquire nitrogen across the fertilization gradient.

2591 Despite evidence that reductions in the response of *G. max* carbon costs
2592 to acquire nitrogen to increasing fertilization may have been driven by shifts away
2593 from nitrogen fixation with increasing fertilization, I urge caution in assigning
2594 causality to the differential response of carbon costs to acquire nitrogen between
2595 species. This is because *G. max* and *G. hirsutum* are not phylogenetically related
2596 and have different life histories. Specifically, *G. max* is a herbaceous annual species,
2597 while *G. hirsutum* is a woody perennial species. Differences in life history between
2598 the two species limit my ability to assess whether reductions in the negative effect
2599 of increasing fertilization on carbon costs to acquire nitrogen in *G. max* were
2600 driven by shifts to direct uptake with increasing fertilization. However, these
2601 patterns were later confirmed in the fourth experimental chapter, where I quantify
2602 similar weaker negative effects of increasing fertilization on carbon costs to acquire
2603 nitrogen in *G. max* that were inoculated with symbiotic nitrogen-fixing bacteria
2604 compared to *G. max* that were left uninoculated across a similar soil nitrogen
2605 fertilization gradient.

2606 In the second experimental chapter, I assessed whether changes in soil
2607 nitrogen availability or soil pH drove changes in nitrogen-water use tradeoffs pre-
2608 dicted by photosynthetic least-cost theory. I measured leaf traits of mature upper
2609 canopy deciduous trees growing in a nine-year nitrogen-by-sulfur field manipula-
2610 tion experiment, where experimental sulfur additions were added with intent to
2611 acidify plots. Following patterns expected from the theory, increasing soil nitrogen
2612 availability was associated with increased leaf nitrogen content, but not net pho-
2613 tosynthesis, resulting in an increase in photosynthetic nitrogen use efficiency. In

2614 further support of theory, increasing soil nitrogen availability exhibited slight, but
2615 nonsignificant, decreases in leaf $C_i:C_a$ and increases in measures of photosynthetic
2616 capacity. Perhaps the strongest evidence for the theory was a strong negative
2617 relationship between leaf nitrogen content and leaf $C_i:C_a$, of which increased with
2618 increasing soil nitrogen availability through a stronger increase in leaf nitrogen
2619 content than leaf $C_i:C_a$.

2620 I found no effect of soil pH on nitrogen-water use tradeoffs aside from a
2621 marginal reduction in net photosynthesis rates that marginally reduced photosyn-
2622 thetic nitrogen use efficiency with increasing soil pH. Directionally, reductions in
2623 photosynthetic nitrogen use efficiency with increasing soil pH were as expected per
2624 theory; however, this response was driven by no change in leaf nitrogen content
2625 and a reduction in net photosynthesis. Theory predicts that these tradeoffs should
2626 be driven by no change in net photosynthesis and an increase in leaf nitrogen con-
2627 tent. Regardless, the general null leaf response to changing soil pH may have
2628 been due to experimental treatments directly increased soil nitrogen availability
2629 and affected soil pH in opposite patterns, suggesting that soil nitrogen availability
2630 may be more important in dictating nitrogen-water use tradeoffs than soil pH per
2631 se.

2632 In the third experimental chapter, I quantified variance in leaf nitrogen
2633 content across a precipitation and soil resource availability gradient in Texan
2634 grasslands. Specifically, I measured area-based leaf nitrogen content, components
2635 of area-based leaf nitrogen content (leaf mass per unit leaf area, leaf nitrogen per
2636 unit dry biomass), leaf $C_i:C_a$, and the unit cost of acquiring nitrogen relative to
2637 water in 520 individuals comprising 57 species. I found that variance in area-

2638 based leaf nitrogen content was positively associated with increasing soil nitrogen
2639 availability, soil moisture, vapor pressure deficit, and was negatively related to
2640 increasing leaf $C_i:C_a$. Following patterns expected from theory, a path analysis
2641 revealed that the positive soil nitrogen-leaf nitrogen relationship was driven by a
2642 positive relationship between soil nitrogen availability and the unit cost of acquir-
2643 ing and using nitrogen relative to water, a positive relationship between the unit
2644 cost of acquiring and using nitrogen relative to water, and negative relationship
2645 between leaf $C_i:C_a$ and leaf mass per unit leaf area. Interestingly, there was no
2646 effect of $C_i:C_a$ on leaf nitrogen content per unit dry biomass, indicating that vari-
2647 ance in area-based leaf nitrogen content across the environmental gradient was
2648 driven by a change in leaf morphology and not leaf chemistry.

2649 In the fourth experimental chapter, I quantified leaf and whole plant accli-
2650 mation responses in *G. max* grown under two atmospheric CO₂ levels, with and
2651 without inoculation with *Bradyrhizobium japonicum*, and across nine nitrogen fer-
2652 tilization treatments in a full factorial growth chamber experiment. I found strong
2653 evidence that leaf nitrogen content, V_{cmax} , and J_{max} were each downregulated un-
2654 der elevated CO₂. A stronger downregulation in V_{cmax} than J_{max} and stronger
2655 downregulation in leaf nitrogen content than V_{cmax} or J_{max} provided strong sup-
2656 port suggesting that leaves were acclimating to elevated CO₂ by optimizing leaf
2657 photosynthetic resource use efficiency to achieve optimal coordination. In striking
2658 support of my hypotheses, I find strong evidence suggesting that leaf acclimation
2659 responses to elevated CO₂ were decoupled from soil nitrogen fertilization and in-
2660 oculation treatment, despite apparent strong increases in leaf nitrogen content,
2661 V_{cmax} , and J_{max} with increasing fertilization and in inoculated pots. These find-

2662 ings contrast the current formulation of photosynthetic processes in terrestrial
2663 biosphere models, where many models simulate downregulations in leaf nitrogen
2664 content under elevated CO₂ schemes as a function of progressive nitrogen limita-
2665 tion.

2666 There are currently two iterations of optimality models that employ the
2667 use of patterns expected from photosynthetic least-cost theory, one for C₃ species
2668 (Wang et al. 2017; Smith et al. 2019; Stocker et al. 2020) and one more recently
2669 developed for C₄ species (Scott and Smith 2022). In both model variants, costs to
2670 acquire and use nitrogen relative to water are held constant using a global dataset
2671 of δ¹³C (Cornwell et al. 2018). The C₃ optimality model initially assumed a
2672 constant cost to acquire and use nitrogen relative to water value of 240 (Wang et al.
2673 2017), later corrected to 146 (Stocker et al. 2020), while the C₄ optimality model
2674 assumes a constant value of 166 (Scott and Smith 2022). Throughout experiments,
2675 I show strong evidence suggesting that costs to acquire and use nitrogen are
2676 dynamic and vary predictably across environmental gradients, and that changes
2677 in these costs yield predictable changes in leaf nitrogen-water use tradeoffs and
2678 acclimation responses to changing environments. Thus, optimality models that
2679 hold unit costs of resource use constant may contribute to erroneous errors in
2680 model simulations. Future iterations of optimality models that leverage patterns
2681 expected from photosynthetic least-cost theory should consider development of
2682 explicit schemes for dynamically calculating costs to acquire and use nitrogen
2683 relative to water, or be coupled with previously established plant nitrogen uptake
2684 models (e.g., FUN) (Fisher et al. 2010; Brzostek et al. 2014; Allen et al. 2020).

2685 First principles of photosynthetic least-cost theory suggest that plants can

2686 optimize photosynthesis rates by sacrificing inefficient use of a relatively more
2687 abundant (and less costly to acquire) resource for more efficient use of a relatively
2688 less abundant (and more costly to acquire) resource. I show strong support for
2689 these patterns across experiments, where increasing soil nitrogen fertilization gen-
2690 erally decreased the cost of acquiring nitrogen relative to water, a pattern that
2691 scaled to influence leaf nitrogen-water use tradeoffs. These findings provide im-
2692 portant empirical validation of photosynthetic least-cost theory needed to further
2693 develop optimality models and eventually implement in terrestrial biosphere model
2694 products. Many current terrestrial biosphere model products do not include ro-
2695 bust frameworks for simulating acclimation responses to changing environmental
2696 conditions, and empirical findings shown here provide some support that optimal-
2697 ity models that leverage photosynthetic least-cost theory predictions may improve
2698 the ability of terrestrial biosphere models to accurately simulate photosynthetic
2699 processes. Future work should leverage data collected from these experiments,
2700 particularly the environmental gradient experiment across Texan grasslands, to
2701 conduct model-data comparisons to evaluate optimality model performance.

2702 Many terrestrial biosphere models predict photosynthetic capacity through
2703 plant functional group-specific linear regressions between area-based leaf nitrogen
2704 content and V_{cmax} (Rogers 2014; Rogers et al. 2017), which assumes that leaf
2705 nitrogen-photosynthesis relationships are constant across growing environments.
2706 I found constant leaf nitrogen-photosynthesis relationships with increasing soil ni-
2707 trogen availability in the nitrogen-by-sulfur field manipulation experiment. How-
2708 ever, results from the CO₂-by-nitrogen-by-inoculation manipulation experiment
2709 indicated that leaf nitrogen-photosynthesis responses to soil nitrogen availability

2710 were dependent on whether nitrogen was limiting. Specifically, similar increases in
2711 area-based leaf nitrogen content, $V_{\text{cmax}25}$, and $J_{\text{max}25}$ with increasing fertilization
2712 resulted in no change in the fraction of leaf nitrogen allocated to photosynthesis in
2713 uninoculated pots, while larger increases in area-based leaf nitrogen content than
2714 $V_{\text{cmax}25}$ and $J_{\text{max}25}$ with increasing fertilization decreased the fraction of leaf nitro-
2715 gen allocated to photosynthesis in inoculated pots. As inoculated pots were able
2716 to access less finite supply of nitrogen across the fertilization gradient, these pat-
2717 terns suggest that constant leaf nitrogen-photosynthesis relationships may only
2718 apply in environments where nitrogen is limiting. Further investigation is cer-
2719 tainly warranted regarding the effect of soil nitrogen availability in modifying leaf
2720 nitrogen-photosynthesis relationships, but findings from these experiments suggest
2721 that representing photosynthetic processes through positive relationships between
2722 soil nitrogen availability, leaf nitrogen, and photosynthetic capacity are likely con-
2723 tributing to erroneous errors in model simulations and may be an explanation for
2724 the high degree of divergence between carbon and nutrient flux simulations across
2725 terrestrial biosphere model products (Friedlingstein et al. 2014; Davies-Barnard
2726 et al. 2020).

2727 The experiments included in this dissertation have provided a strong foun-
2728 dation for me to continue growing as a plant physiological ecologist. I envision
2729 five primary avenues for future research that build on the work presented here,
2730 which are briefly summarized below:

2731 1. Manipulative and environmental gradient experiments included in this dis-
2732 sertation were designed to provide empirical data needed to test photosyn-
2733 thetic least-cost theory assumptions. While these results show promising

- 2734 patterns for patterns expected from photosynthetic least-cost theory, they
2735 do not necessarily address whether these patterns follow those simulated by
2736 optimality models that leverage photosynthetic least-cost principles. Thus,
2737 a clear future direction of this research could be to conduct model-data
2738 comparisons using data collected here (or similar experiments) to compare
2739 against optimality model simulations.
- 2740 2. Experiments included in this dissertation explicitly quantify effects of sym-
2741 biotic nitrogen fixation on carbon costs to acquire nitrogen, nitrogen-water
2742 use tradeoffs, and leaf nitrogen-photosynthesis relationships. However, car-
2743 bon costs to acquire nitrogen also vary in species that associate with dif-
2744 ferent mycorrhizal types (Brzostek et al. 2014; Terrer et al. 2018), and
2745 dominant mycorrhizal type in an ecosystem may dictate net biogeochemical
2746 cycle dynamics (Phillips et al. 2013). Thus, future work should consider
2747 conducting similar experiments while manipulating mycorrhizal association
2748 to comprehensively understand how microbial symbioses modify leaf and
2749 whole plant acclimation responses to changing environments. This avenue
2750 of research would be particularly useful in forested ecosystems, as previous
2751 work suggests that dominant mycorrhizal type in hardwood forests dictate
2752 net biogeochemical cycle dynamics
- 2753 3. Recent work indicates a high degree of variance in symbiotic nitrogen fixa-
2754 tion rates across terrestrial biosphere models (Davies-Barnard et al. 2020;
2755 Meyerholt et al. 2016), perhaps due to nitrogen fixation rates that are im-
2756 plemented across terrestrial biosphere models as a function of temperature
2757 (Houlton et al. 2008). While energetic costs of nitrogen fixation are cer-

2758 tainly temperature dependent, I show that structural costs of nitrogen fix-
2759 ation are driven by shifts in soil resource availability. The light-by-nitrogen
2760 greenhouse experiment was recently published in *Journal of Experimental*
2761 *Botany*, and a reviewer encouraged future work to include a model-data
2762 comparison comparing carbon costs to acquire nitrogen measured in the
2763 experiment to carbon costs to acquire nitrogen simulated by the FUN bio-
2764 geochemical model (Fisher et al. 2010; Brzostek et al. 2014; Allen et al.
2765 2020). Conveniently, FUN calculates carbon costs to acquire nitrogen follow-
2766 ing the same calculation used in the first and fourth experimental chapter,
2767 and doing this would be a useful next step toward understanding why ni-
2768 trogen fixation simulations in terrestrial biosphere models might deviate to
2769 such a large degree between products.

2770 4. Carbon costs to acquire nitrogen relative to water were quantified at the
2771 leaf level as a function of $\delta^{13}\text{C}$ and vapor pressure deficit, while structural
2772 carbon costs to acquire nitrogen were quantified at the whole plant level
2773 as the ratio of belowground carbon allocation per unit whole plant nitro-
2774 gen biomass. As increasing soil nitrogen availability decreases both leaf and
2775 whole plant estimates of costs to acquire and use nitrogen, one might expect
2776 leaf and whole plant carbon cost to acquire nitrogen estimates to covary. Fu-
2777 ture work should consider investigating if leaf and whole plant estimates of
2778 carbon costs to acquire nitrogen covary and evaluate whether environmental
2779 conditions (or species acquisition strategy) modifies any of this possible co-
2780 variance. Strong covariance between leaf and whole plant costs of nitrogen
2781 acquisition could be a possible avenue to implement frameworks for allowing

2782 costs of nitrogen acquisition to vary in optimality models, as the FUN model
2783 calculates carbon costs of nitrogen acquisition at the whole plant level.

2784 5. While experiments included in this dissertation target effects of soil nitrogen
2785 availability on carbon costs to acquire nitrogen and associated leaf nitrogen-
2786 water use tradeoffs, photosynthetic least-cost theory predicts that costs of
2787 nutrient use, not just nitrogen, relative to water are substitutable. Recent
2788 iterations of the FUN biogeochemical cycle includes the carbon and nitro-
2789 gen cost of acquiring and using phosphorus, which similarly varies in species
2790 with different nutrient acquisition strategies (Allen et al. 2020). The im-
2791 plementation of this model in a terrestrial biosphere model (E3SM) was
2792 recently shown to improve model performance of ecosystem nutrient lim-
2793 itation (Braghiere et al. 2022). As phosphorus commonly co-limits leaf
2794 photosynthesis and primary productivity, extending experiments reported
2795 here to investigate carbon and nitrogen costs of phosphorus use may be a
2796 useful next step in understanding extensions and limitations of photosyn-
2797 thetic least-cost theory.

2798 I conclude this dissertation with a brief word of thanks to all who have
2799 shaped me into the plant physiological ecologist that I am today. Specifically,
2800 I am thankful for the incredible mentorship of my advisor and committee chair,
2801 Dr. Nick Smith, who provided invaluable insight for each of these experimental
2802 chapters, and for my committee members for their helpful advise and support
2803 throughout these experiments. I am excited to continue growing as a plant phys-
2804 iological ecologist, look forward to continuing to understand nutrient acquisition
2805 and allocation responses to global change, and am excited to help mentor future

2806 generations of young researchers.

2807

References

- 2808** Abrams, M. D. and S. A. Mostoller (1995). Gas exchange, leaf structure and
2809 nitrogen in contrasting successional tree species growing in open and under-
2810 story sites during a drought. *Tree Physiology* 15(6), 361–370.
- 2811** Adams, M. A., T. L. Turnbull, J. I. Sprent, and N. Buchmann (2016). Legumes
2812 are different: Leaf nitrogen, photosynthesis, and water use efficiency. *Pro-
2813 ceedings of the National Academy of Sciences of the United States of Amer-
2814 ica* 113(15), 4098–4103.
- 2815** Ainsworth, E. A., P. A. Davey, C. J. Bernacchi, O. C. Dermody, E. A. Heaton,
2816 D. J. Moore, P. B. Morgan, S. L. Naidu, H. S. Y. Ra, X. G. Zhu, P. S. Curtis,
2817 and S. P. Long (2002). A meta-analysis of elevated [CO₂] effects on soybean
2818 (*Glycine max*) physiology, growth and yield. *Global Change Biology* 8(8),
2819 695–709.
- 2820** Ainsworth, E. A. and S. P. Long (2005). What have we learned from 15 years of
2821 free-air CO₂ enrichment (FACE)? A meta-analytic review of the responses
2822 of photosynthesis, canopy properties and plant production to rising CO₂.
2823 *New Phytologist* 165(2), 351–372.
- 2824** Ainsworth, E. A. and A. Rogers (2007). The response of photosynthesis and
2825 stomatal conductance to rising [CO₂]: mechanisms and environmental in-
2826 teractions. *Plant, Cell and Environment* 30(3), 258–270.
- 2827** Allen, K., J. B. Fisher, R. P. Phillips, J. S. Powers, and E. R. Brzostek (2020).
2828 Modeling the carbon cost of plant nitrogen and phosphorus uptake across
2829 temperate and tropical forests. *Frontiers in Forests and Global Change* 3,

- 2830 1–12.
- 2831 Allison, S. D., C. I. Czimczik, and K. K. Treseder (2008). Microbial activity
2832 and soil respiration under nitrogen addition in Alaskan boreal forest. *Global
2833 Change Biology* 14(5), 1156–1168.
- 2834 Andersen, M. K., H. Hauggaard-Nielsen, P. Ambus, and E. S. Jensen (2005).
2835 Biomass production, symbiotic nitrogen fixation and inorganic N use in dual
2836 and tri-component annual intercrops. *Plant and Soil* 266(1-2), 273–287.
- 2837 Andrews, M., E. K. James, J. I. Sprent, R. M. Boddey, E. Gross, and F. B. dos
2838 Reis (2011). Nitrogen fixation in legumes and actinorhizal plants in natural
2839 ecosystems: Values obtained using ^{15}N natural abundance. *Plant Ecology
2840 and Diversity* 4(2-3), 117–130.
- 2841 Arndal, M. F., A. Tolver, K. S. Larsen, C. Beier, and I. K. Schmidt (2018). Fine
2842 root growth and vertical distribution in response to elevated CO₂, warming
2843 and drought in a mixed heathland–grassland. *Ecosystems* 21(1), 15–30.
- 2844 Arnone, J. A. (1997). Indices of plant N availability in an alpine grassland under
2845 elevated atmospheric CO₂. *Plant and Soil* 190(1), 61–66.
- 2846 Arora, V. K., A. Katavouta, R. G. Williams, C. D. Jones, V. Brovkin,
2847 P. Friedlingstein, J. Schwinger, L. Bopp, O. Boucher, P. Cadule, M. A.
2848 Chamberlain, J. R. Christian, C. Delire, R. A. Fisher, T. Hajima, T. Ilyina,
2849 E. Joetzjer, M. Kawamiya, C. D. Koven, J. P. Krasting, R. M. Law, D. M.
2850 Lawrence, A. Lenton, K. Lindsay, J. Pongratz, T. Raddatz, R. Séférian,
2851 K. Tachiiri, J. F. Tjiputra, A. Wiltshire, T. Wu, and T. Ziehn (2020).
2852 Carbon-concentration and carbon-climate feedbacks in CMIP6 models and
2853 their comparison to CMIP5 models. *Biogeosciences* 17(16), 4173–4222.

- 2854 Bae, K., T. J. Fahey, R. D. Yanai, and M. Fisk (2015). Soil nitrogen availabil-
2855 ity affects belowground carbon allocation and soil respiration in northern
2856 hardwood forests of New Hampshire. *Ecosystems* 18(7), 1179–1191.
- 2857 Barber, S. A. (1962). A diffusion and mass-flow concept of soil nutrient avail-
2858 ability. *Soil Science* 93(1), 39–49.
- 2859 Barnes, J. D., L. Balaguer, E. Manrique, S. Elvira, and A. W. Davison (1992).
2860 A reappraisal of the use of DMSO for the extraction and determination
2861 of chlorophylls a and b in lichens and higher plants. *Environmental and*
2862 *Experimental Botany* 32(2), 85–100.
- 2863 Bates, D., M. Mächler, B. Bolker, and S. Walker (2015). Fitting linear mixed-
2864 effects models using lme4. *Journal of Statistical Software* 67(1), 1–48.
- 2865 Beaudette, D., J. Skovlin, S. Roeker, and A. Brown (2022). soilDB: Soil
2866 Database Interface.
- 2867 Bengtson, P., J. Barker, and S. J. Grayston (2012). Evidence of a strong cou-
2868 pling between root exudation, C and N availability, and stimulated SOM
2869 decomposition caused by rhizosphere priming effects. *Ecology and Evolu-*
2870 *tion* 2(8), 1843–1852.
- 2871 Bernacchi, C. J., E. L. Singsaas, C. Pimentel, A. R. Portis, and S. P. Long
2872 (2001). Improved temperature response functions for models of Rubisco-
2873 limited photosynthesis. *Plant, Cell and Environment* 24(2), 253–259.
- 2874 Bialic-Murphy, L., N. G. Smith, P. Voothuluru, R. M. McElderry, M. D.
2875 Roche, S. T. Cassidy, S. N. Kivlin, and S. Kalisz (2021). Invasion-induced
2876 root–fungal disruptions alter plant water and nitrogen economies. *Ecology*

- 2877** *Letters* 24(6), 1145–1156.
- 2878** Bloom, A. J., F. S. Chapin, and H. A. Mooney (1985). Resource limitation
2879 in plants - an economic analogy. *Annual Review of Ecology and Systemat-*
2880 *ics* 16(1), 363–392.
- 2881** Bloomfield, K. J., B. D. Stocker, T. F. Keenan, and I. C. Prentice (2023).
2882 Environmental controls on the light use efficiency of terrestrial gross primary
2883 production. *Global Change Biology* 29(4), 0–2.
- 2884** Bonan, G. B., M. D. Hartman, W. J. Parton, and W. R. Wieder (2013). Eval-
2885 uating litter decomposition in earth system models with long-term litter
2886 bag experiments: an example using the Community Land Model version 4
2887 (CLM4). *Global Change Biology* 19(3), 957–974.
- 2888** Bonan, G. B., P. J. Lawrence, K. W. Oleson, S. Levis, M. Jung, M. Reich-
2889 stein, D. M. Lawrence, and S. C. Swenson (2011). Improving canopy pro-
2890 cesses in the Community Land Model version 4 (CLM4) using global flux
2891 fields empirically inferred from FLUXNET data. *Journal of Geophysical Re-*
2892 *search* 116(G2), G02014.
- 2893** Booth, B. B. B., C. D. Jones, M. Collins, I. J. Totterdell, P. M. Cox, S. Sitch,
2894 C. Huntingford, R. A. Betts, G. R. Harris, and J. Lloyd (2012). High sen-
2895 sitivity of future global warming to land carbon cycle processes. *Environ-*
2896 *mental Research Letters* 7(2), 024002.
- 2897** Borer, E. T., W. S. Harpole, P. B. Adler, E. M. Lind, J. L. Orrock, E. W.
2898 Seabloom, and M. D. Smith (2014). Finding generality in ecology: A model
2899 for globally distributed experiments. *Methods in Ecology and Evolution* 5(1),
2900 65–73.

- 2901** Braghieri, R. K., J. B. Fisher, K. Allen, E. Brzostek, M. Shi, X. Yang, D. M.
- 2902** Ricciuto, R. A. Fisher, Q. Zhu, and R. P. Phillips (2022). Modeling global
- 2903** carbon costs of plant nitrogen and phosphorus acquisition. *Journal of Ad-*
- 2904** *vances in Modeling Earth Systems* 14(8), 1–23.
- 2905** Brix, H. (1971). Effects of nitrogen fertilization on photosynthesis and respi-
- 2906** ration in Douglas-fir. *Forest Science* 17(4), 407–414.
- 2907** Brzostek, E. R., J. B. Fisher, and R. P. Phillips (2014). Modeling the carbon
- 2908** cost of plant nitrogen acquisition: Mycorrhizal trade-offs and multipath
- 2909** resistance uptake improve predictions of retranslocation. *Journal of Geo-*
- 2910** *physical Research: Biogeosciences* 119, 1684–1697.
- 2911** Bubier, J. L., R. Smith, S. Juutinen, T. R. Moore, R. Minocha, S. Long, and
- 2912** S. Minocha (2011). Effects of nutrient addition on leaf chemistry, morphol-
- 2913** ogy, and photosynthetic capacity of three bog shrubs. *Oecologia* 167(2),
- 2914** 355–368.
- 2915** Cernusak, L. A., N. Ubierna, K. Winter, J. A. M. Holtum, J. D. Marshall, and
- 2916** G. D. Farquhar (2013). Environmental and physiological determinants of
- 2917** carbon isotope discrimination in terrestrial plants. *New Phytologist* 200(4),
- 2918** 950–965.
- 2919** Chen, J.-L., J. F. Reynolds, P. C. Harley, and J. D. Tenhunen (1993). Coor-
- 2920** dination theory of leaf nitrogen distribution in a canopy. *Oecologia* 93(1),
- 2921** 63–69.
- 2922** Clark, D. B., L. M. Mercado, S. Sitch, C. D. Jones, N. Gedney, M. J. Best,
- 2923** M. Pryor, G. G. Rooney, R. L. H. Essery, E. Blyth, O. Boucher, R. J.
- 2924** Harding, C. Huntingford, and P. M. Cox (2011). The Joint UK Land Envi-

- 2925 ronment Simulator (JULES), model description. Part 2: Carbon fluxes and
2926 vegetation dynamics. *Geoscientific Model Development* 4(3), 701–722.
- 2927 Cornwell, W. K., J. H. C. Cornelissen, K. Amatangelo, E. Dorrepaal, V. T.
2928 Eviner, O. Godoy, S. E. Hobbie, B. Hoorens, H. Kurokawa, N. Pérez-
2929 Harguindeguy, H. M. Quested, L. S. Santiago, D. A. Wardle, I. J. Wright,
2930 R. Aerts, S. D. Allison, P. van Bodegom, V. Brovkin, A. Chatain, T. V.
2931 Callaghan, S. Díaz, E. Garnier, D. E. Gurvich, E. Kazakou, J. A. Klein,
2932 J. Read, P. B. Reich, N. A. Soudzilovskaia, M. V. Vaieretti, and M. Westoby
2933 (2008). Plant species traits are the predominant control on litter decompo-
2934 sition rates within biomes worldwide. *Ecology Letters* 11(10), 1065–1071.
- 2935 Cornwell, W. K., I. J. Wright, J. Turner, V. Maire, M. M. Barbour, L. A.
2936 Cernusak, T. E. Dawson, D. S. Ellsworth, G. D. Farquhar, H. Griffiths,
2937 C. Keitel, A. Knohl, P. B. Reich, D. G. Williams, R. Bhaskar, J. H. C. Cor-
2938 nelissen, A. Richards, S. Schmidt, F. Valladares, C. Körner, E.-D. Schulze,
2939 N. Buchmann, and L. S. Santiago (2018). Climate and soils together regulate
2940 photosynthetic carbon isotope discrimination within C₃ plants worldwide.
2941 *Global Ecology and Biogeography* 27(9), 1056–1067.
- 2942 Cramer, W. and I. C. Prentice (1988). Simulation of regional soil moisture
2943 deficits on a European scale. *Norsk Geografisk Tidsskrift - Norwegian Jour-*
2944 *nal of Geography* 42(2-3), 149–151.
- 2945 Curtis, P. S. (1996). A meta-analysis of leaf gas exchange and nitrogen in trees
2946 grown under elevated carbon dioxide. *Plant, Cell and Environment* 19(2),
2947 127–137.
- 2948 Daly, C., M. Halbleib, J. I. Smith, W. P. Gibson, M. K. Doggett, G. H. Taylor,

- 2949** J. Curtis, and P. P. Pasteris (2008). Physiographically sensitive mapping
2950 of climatological temperature and precipitation across the conterminous
2951 United States. *International Journal of Climatology* 28(15), 2031–2064.
- 2952** Davies-Barnard, T., J. Meyerholt, S. Zaehle, P. Friedlingstein, V. Brovkin,
2953 Y. Fan, R. A. Fisher, C. D. Jones, H. Lee, D. Peano, B. Smith, D. Wårlind,
2954 and A. J. Wiltshire (2020). Nitrogen cycling in CMIP6 land surface models:
2955 progress and limitations. *Biogeosciences* 17(20), 5129–5148.
- 2956** Davis, T. W., I. C. Prentice, B. D. Stocker, R. T. Thomas, R. J. Whitley,
2957 H. Wang, B. J. Evans, A. V. Gallego-Sala, M. T. Sykes, and W. Cramer
2958 (2017). Simple process-led algorithms for simulating habitats (SPLASH
2959 v.1.0): robust indices of radiation, evapotranspiration and plant-available
2960 moisture. *Geoscientific Model Development* 10, 689–708.
- 2961** Delaire, M., E. Frak, M. Sigogne, B. Adam, F. Beaujard, and X. Le Roux
2962 (2005). Sudden increase in atmospheric CO₂ concentration reveals strong
2963 coupling between shoot carbon uptake and root nutrient uptake in young
2964 walnut trees. *Tree Physiology* 25(2), 229–235.
- 2965** Doane, T. A. and W. R. Horwáth (2003). Spectrophotometric determination of
2966 nitrate with a single reagent. *Analytical Letters* 36(12), 2713–2722.
- 2967** Dong, N., I. C. Prentice, B. J. Evans, S. Caddy-Retalic, A. J. Lowe, and I. J.
2968 Wright (2017). Leaf nitrogen from first principles: field evidence for adaptive
2969 variation with climate. *Biogeosciences* 14(2), 481–495.
- 2970** Dong, N., I. C. Prentice, I. J. Wright, B. J. Evans, H. F. Togashi, S. Caddy-
2971 Retalic, F. A. McInerney, B. Sparrow, E. Leitch, and A. J. Lowe (2020).
2972 Components of leaf-trait variation along environmental gradients. *New Phy-*

- 2973** *tologist* 228(1), 82–94.
- 2974** Dong, N., I. C. Prentice, I. J. Wright, H. Wang, O. K. Atkin, K. J. Bloomfield,
- 2975** T. F. Domingues, S. M. Gleason, V. Maire, Y. Onoda, H. Poorter, and N. G.
- 2976** Smith (2022). Leaf nitrogen from the perspective of optimal plant function.
- 2977** *Journal of Ecology* 110(11), 2585–2602.
- 2978** Dong, N., I. J. Wright, J. M. Chen, X. Luo, H. Wang, T. F. Keenan, N. G.
- 2979** Smith, and I. C. Prentice (2022). Rising CO₂ and warming reduce global
- 2980** canopy demand for nitrogen. *New Phytologist* 235(5), 1692–1700.
- 2981** Dovrat, G., H. Bakhshian, T. Masci, and E. Sheffer (2020). The nitrogen eco-
- 2982** nomic spectrum of legume stoichiometry and fixation strategy. *New Phytol-*
- 2983** *ogist* 227(2), 365–375.
- 2984** Dovrat, G., T. Masci, H. Bakhshian, E. Mayzlish Gati, S. Golan, and E. Shef-
- 2985** fer (2018). Drought-adapted plants dramatically downregulate dinitrogen
- 2986** fixation: Evidences from Mediterranean legume shrubs. *Journal of Ecol-*
- 2987** *ogy* 106(4), 1534–1544.
- 2988** Drake, B. G., M. A. Gonzàlez-Meler, and S. P. Long (1997). More efficient
- 2989** plants: a consequence of rising atmospheric CO₂? *Annual Review of Plant*
- 2990** *Biology* 48, 609–639.
- 2991** Duursma, R. A. (2015). Plantecophys - An R package for analyzing and mod-
- 2992** elling leaf gas exchange data. *PLOS ONE* 10(11), e0143346.
- 2993** Eastman, B. A., M. B. Adams, E. R. Brzostek, M. B. Burnham, J. E. Carrara,
- 2994** C. Kelly, B. E. McNeil, C. A. Walter, and W. T. Peterjohn (2021). Altered
- 2995** plant carbon partitioning enhanced forest ecosystem carbon storage after 25

- 2996** years of nitrogen additions. *New Phytologist* 230(4), 1435–1448.
- 2997** Ellsworth, D. S. and P. B. Reich (1996). Photosynthesis and leaf nitrogen in five
- 2998** Amazonian tree species during early secondary succession. *Ecology* 77(2),
- 2999** 581–594.
- 3000** Espelta, J. M., P. Cortés, M. Mangirón, and J. Retana (2005). Differences
- 3001** in biomass partitioning, leaf nitrogen content, and water use efficiency δ^{13}
- 3002** result in similar performance of seedlings of two Mediterranean oaks with
- 3003** contrasting leaf habit. *Ecoscience* 12(4), 447–454.
- 3004** Evans, J. R. (1989). Photosynthesis and nitrogen relationships in leaves of C₃
- 3005** plants. *Oecologia* 78(1), 9–19.
- 3006** Evans, J. R. and V. C. Clarke (2019). The nitrogen cost of photosynthesis.
- 3007** *Journal of Experimental Botany* 70(1), 7–15.
- 3008** Evans, J. R. and H. Poorter (2001). Photosynthetic acclimation of plants to
- 3009** growth irradiance: the relative importance of specific leaf area and nitrogen
- 3010** partitioning in maximizing carbon gain. *Plant, Cell and Environment* 24(8),
- 3011** 755–767.
- 3012** Evans, J. R. and J. R. Seemann (1989). The allocation of protein nitrogen in
- 3013** the photosynthetic apparatus: costs, consequences, and control. *Photosyn-*
- 3014** *thesis* 8, 183–205.
- 3015** Exbrayat, J.-F., A. A. Bloom, P. Falloon, A. Ito, T. L. Smallman, and
- 3016** M. Williams (2018). Reliability ensemble averaging of 21st century projec-
- 3017** tions of terrestrial net primary productivity reduces global and regional
- 3018** uncertainties. *Earth System Dynamics* 9(1), 153–165.

- 3019** Farquhar, G. D., J. R. Ehleringer, and K. T. Hubick (1989). Carbon isotope
3020 discrimination and photosynthesis. *Annual Review of Plant Physiology and*
3021 *Plant Molecular Biology* 40(1), 503–537.
- 3022** Farquhar, G. D. and T. D. Sharkey (1982). Stomatal conductance and photo-
3023 synthesis. *Annual Review of Plant Physiology* 33(1), 317–345.
- 3024** Farquhar, G. D., S. von Caemmerer, and J. A. Berry (1980). A biochemical
3025 model of photosynthetic CO₂ assimilation in leaves of C₃ species.
3026 *Planta* 149(1), 78–90.
- 3027** Fay, P. A., S. M. Prober, W. S. Harpole, J. M. H. Knops, J. D. Bakker, E. T.
3028 Borer, E. M. Lind, A. S. MacDougall, E. W. Seabloom, P. D. Wragg, P. B.
3029 Adler, D. M. Blumenthal, Y. M. Buckley, C. Chu, E. E. Cleland, S. L.
3030 Collins, K. F. Davies, G. Du, X. Feng, J. Firn, D. S. Gruner, N. Hagenah,
3031 Y. Hautier, R. W. Heckman, V. L. Jin, K. P. Kirkman, J. A. Klein, L. M.
3032 Ladwig, Q. Li, R. L. McCulley, B. A. Melbourne, C. E. Mitchell, J. L. Moore,
3033 J. W. Morgan, A. C. Risch, M. Schütz, C. J. Stevens, D. A. Wedin, and
3034 L. H. Yang (2015). Grassland productivity limited by multiple nutrients.
3035 *Nature Plants* 1(7), 15080.
- 3036** Feng, X. (1999). Trends in intrinsic water-use efficiency of natural trees for the
3037 past 100-200 years: A response to atmospheric CO₂ concentration. *Geochim-
3038 ica et Cosmochimica Acta* 63(13-14), 1891–1903.
- 3039** Field, C. B. and H. A. Mooney (1986). The photosynthesis-nitrogen relationship
3040 in wild plants. In T. J. Givnish (Ed.), *On the Economy of Plant Form and*
3041 *Function*, pp. 25–55. Cambridge: Cambridge University Press.
- 3042** Finzi, A. C., D. J. P. Moore, E. H. DeLucia, J. Lichter, K. S. Hofmockel, R. B.

- 3043 Jackson, H. S. Kim, R. Matamala, H. R. McCarthy, R. Oren, J. S. Pippen,
3044 and W. H. Schlesinger (2006). Progressive nitrogen limitation of ecosystem
3045 processes under elevated CO₂ in a warm-temperate forest. *Ecology* 87(1),
3046 15–25.
- 3047 Firn, J., J. M. McGree, E. Harvey, H. Flores Moreno, M. Schutz, Y. M. Buckley,
3048 E. T. Borer, E. W. Seabloom, K. J. La Pierre, A. M. MacDougall, S. M.
3049 Prober, C. J. Stevens, L. L. Sullivan, E. Porter, E. Ladouceur, C. Allen,
3050 K. H. Moromizato, J. W. Morgan, W. S. Harpole, Y. Hautier, N. Eisen-
3051 hauer, J. P. Wright, P. B. Adler, C. A. Arnillas, J. D. Bakker, L. Biederman,
3052 A. A. D. Broadbent, C. S. Brown, M. N. Bugalho, M. C. Caldeira, E. E. Cle-
3053 land, A. Ebeling, P. A. Fay, N. Hagenah, A. R. Kleinhesselink, R. Mitchell,
3054 J. L. Moore, C. Nogueira, P. L. Peri, C. Roscher, M. D. Smith, P. D. Wragg,
3055 and A. C. Risch (2019). Leaf nutrients, not specific leaf area, are consistent
3056 indicators of elevated nutrient inputs. *Nature Ecology and Evolution* 3(3),
3057 400–406.
- 3058 Fisher, J. B., S. Sitch, Y. Malhi, R. A. Fisher, C. Huntingford, and S.-Y. Tan
3059 (2010). Carbon cost of plant nitrogen acquisition: A mechanistic, globally
3060 applicable model of plant nitrogen uptake, retranslocation, and fixation.
3061 *Global Biogeochemical Cycles* 24(1), 1–17.
- 3062 Fox, J. and S. Weisberg (2019). *An R companion to applied regression* (Third
3063 edit ed.). Thousand Oaks, California: Sage.
- 3064 Franklin, O., R. E. McMurtrie, C. M. Iversen, K. Y. Crous, A. C. Finzi, D. Tis-
3065 sue, D. S. Ellsworth, R. Oren, and R. J. Norby (2009). Forest fine-root
3066 production and nitrogen use under elevated CO₂: contrasting responses

- 3067** in evergreen and deciduous trees explained by a common principle. *Global
3068 Change Biology* 15(1), 132–144.
- 3069** Friedlingstein, P., M. Meinshausen, V. K. Arora, C. D. Jones, A. Anav, S. K.
3070 Liddicoat, and R. Knutti (2014). Uncertainties in CMIP5 climate projections
3071 due to carbon cycle feedbacks. *Journal of Climate* 27(2), 511–526.
- 3072** Friel, C. A. and M. L. Friesen (2019). Legumes modulate allocation to rhizobial
3073 nitrogen fixation in response to factorial light and nitrogen manipulation.
3074 *Frontiers in Plant Science* 10, 1316.
- 3075** Fujikake, H., A. Yamazaki, N. Ohtake, K. Sueoshi, S. Matsuhashi, T. Ito,
3076 C. Mizuniwa, T. Kume, S. Hoshimoto, N.-S. Ishioka, S. Watanabe, A. Osa,
3077 T. Sekine, H. Uchida, A. Tsuji, and T. Ohyama (2003). Quick and reversible
3078 inhibition of soybean root nodule growth by nitrate involves a decrease in
3079 sucrose supply to nodules. *Journal of Experimental Botany* 54(386), 1379–
3080 1388.
- 3081** Ghannoum, O., J. R. Evans, and S. von Caemmerer (2011). Nitrogen and water
3082 use efficiency of C₄ plants. In A. S. Raghavendra and R. F. Sage (Eds.), *C₄
3083 Photosynthesis and Related CO₂ Concentrating Mechanisms*, Chapter 8, pp.
3084 129–146. Springer.
- 3085** Ghimire, B., W. J. Riley, C. D. Koven, J. Kattge, A. Rogers, P. B. Reich, and
3086 I. J. Wright (2017). A global trait-based approach to estimate leaf nitrogen
3087 functional allocation from observations:. *Ecological Applications* 27(5),
3088 1421–1434.
- 3089** Giardina, C. P., M. D. Coleman, J. E. Hancock, J. S. King, E. A. Lilleskov,
3090 W. M. Loya, K. S. Pregitzer, M. G. Ryan, and C. C. Trettin (2005). The

- 3091** response of belowground carbon allocation in forests to global change. In
3092 D. Binkley and O. Manyailo (Eds.), *Tree Species Effects on Soils: Implica-*
3093 *tions for Global Change* (Volume 55 ed.), Chapter Chapter 7, pp. 119–154.
3094 Berlin/Heidelberg: Springer-Verlag.
- 3095** Gibson, A. H. and J. E. Harper (1985). Nitrate effect on nodulation of soybean
3096 by *Bradyrhizobium japonicum*. *Crop Science* 25(3), 497–501.
- 3097** Gill, A. L. and A. C. Finzi (2016). Belowground carbon flux links biogeochemical
3098 cycles and resource-use efficiency at the global scale. *Ecology Letters* 19(12),
3099 1419–1428.
- 3100** Goll, D. S., V. Brovkin, B. R. Parida, C. H. Reick, J. Kattge, P. B. Reich, P. M.
3101 van Bodegom, and Ü. Niinemets (2012). Nutrient limitation reduces land
3102 carbon uptake in simulations with a model of combined carbon, nitrogen
3103 and phosphorus cycling. *Biogeosciences Discussions* 9(3), 3173–3232.
- 3104** Gregory, L. M., A. M. McClain, D. M. Kramer, J. D. Pardo, K. E. Smith, O. L.
3105 Tessmer, B. J. Walker, L. G. Ziccardi, and T. D. Sharkey (2021, oct). The
3106 triose phosphate utilization limitation of photosynthetic rate: Out of global
3107 models but important for leaf models. *Plant, Cell and Environment* 44(10),
3108 3223–3226.
- 3109** Grossiord, C., T. N. Buckley, L. A. Cernusak, K. A. Novick, B. Poulter, R. T. W.
3110 Siegwolf, J. S. Sperry, and N. G. McDowell (2020). Plant responses to rising
3111 vapor pressure deficit. *New Phytologist* 226(6), 1550–1566.
- 3112** Gulmon, S. L. and C. C. Chu (1981). The effects of light and nitrogen on pho-
3113 tosynthesis, leaf characteristics, and dry matter allocation in the chaparral
3114 shrub, *Diplacus aurantiacus*. *Oecologia* 49(2), 207–212.

- 3115 Gutschick, V. P. (1981). Evolved strategies in nitrogen acquisition by plants.
- 3116 *The American Naturalist* 118(5), 607–637.
- 3117 Hallik, L., Ü. Niinemets, and I. J. Wright (2009). Are species shade and drought
- 3118 tolerance reflected in leaf-level structural and functional differentiation in
- 3119 Northern Hemisphere temperate woody flora? *New Phytologist* 184(1), 257–
- 3120 274.
- 3121 Harrison, M. T., E. J. Edwards, G. D. Farquhar, A. B. Nicotra, and J. R.
- 3122 Evans (2009). Nitrogen in cell walls of sclerophyllous leaves accounts for
- 3123 little of the variation in photosynthetic nitrogen-use efficiency. *Plant, Cell*
- 3124 and *Environment* 32(3), 259–270.
- 3125 Harrison, S. P., W. Cramer, O. Franklin, I. C. Prentice, H. Wang,
- 3126 Å. Bränström, H. de Boer, U. Dieckmann, J. Joshi, T. F. Keenan,
- 3127 A. Lavergne, S. Manzoni, G. Mengoli, C. Morfopoulos, J. Peñuelas,
- 3128 S. Pietsch, K. T. Rebel, Y. Ryu, N. G. Smith, B. D. Stocker, and I. J.
- 3129 Wright (2021). Eco-evolutionary optimality as a means to improve vegeta-
- 3130 tion and land-surface models. *New Phytologist* 231(6), 2125–2141.
- 3131 Henneron, L., P. Kardol, D. A. Wardle, C. Cros, and S. Fontaine (2020). Rhizo-
- 3132 sphere control of soil nitrogen cycling: a key component of plant economic
- 3133 strategies. *New Phytologist* 228(4), 1269–1282.
- 3134 Hijmans, R. J. (2022). terra: Spatial Data Analysis.
- 3135 Hikosaka, K. and A. Shigeno (2009). The role of Rubisco and cell walls in the
- 3136 interspecific variation in photosynthetic capacity. *Oecologia* 160(3), 443–
- 3137 451.

- 3138** Hoagland, D. R. and D. I. Arnon (1950). The water culture method for growing
3139 plants without soil. *California Agricultural Experiment Station: 347* 347(2),
3140 1–32.
- 3141** Hobbie, E. A. (2006). Carbon allocation to ectomycorrhizal fungi correlates
3142 with belowground allocation in culture studies. *Ecology* 87(3), 563–569.
- 3143** Hobbie, E. A. and J. E. Hobbie (2008). Natural abundance of ^{15}N in nitrogen-
3144 limited forests and tundra can estimate nitrogen cycling through mycorrhizal
3145 fungi: a review. *Ecosystems* 11(5), 815–830.
- 3146** Hoek, T. A., K. Axelrod, T. Biancalani, E. A. Yurtsev, J. Liu, and J. Gore
3147 (2016). Resource availability modulates the cooperative and competitive na-
3148 ture of a microbial cross-feeding mutualism. *PLOS Biology* 14(8), e1002540.
- 3149** Höglberg, M. N., M. J. I. Briones, S. G. Keel, D. B. Metcalfe, C. Campbell, A. J.
3150 Midwood, B. Thornton, V. Hurry, S. Linder, T. Näsholm, and P. Höglberg
3151 (2010). Quantification of effects of season and nitrogen supply on tree below-
3152 ground carbon transfer to ectomycorrhizal fungi and other soil organisms in
3153 a boreal pine forest. *New Phytologist* 187(2), 485–493.
- 3154** Höglberg, P., M. N. Höglberg, S. G. Göttlicher, N. R. Betson, S. G. Keel, D. B.
3155 Metcalfe, C. Campbell, A. Schindlbacher, V. Hurry, T. Lundmark, S. Linder,
3156 and T. Näsholm (2008). High temporal resolution tracing of photosynthate
3157 carbon from the tree canopy to forest soil microorganisms. *New Phytolo-*
3158 *gist* 177(1), 220–228.
- 3159** Houlton, B. Z., Y.-P. Wang, P. M. Vitousek, and C. B. Field (2008). A uni-
3160 fying framework for dinitrogen fixation in the terrestrial biosphere. *Na-*
3161 *ture* 454(7202), 327–330.

- 3162** Huber, M. L., R. A. Perkins, A. Laesecke, D. G. Friend, J. V. Sengers, M. J.
3163 Assael, I. N. Metaxa, E. Vogel, R. Mareš, and K. Miyagawa (2009). New
3164 international formulation for the viscosity of H₂O. *Journal of Physical and*
3165 *Chemical Reference Data* 38(2), 101–125.
- 3166** Hungate, B. A., J. S. Dukes, M. R. Shaw, Y. Luo, and C. B. Field (2003).
3167 Nitrogen and climate change. *Science* 302(5650), 1512–1513.
- 3168** IPCC (2021). *Climate Change 2021: The Physical Science Basis. Contribution*
3169 *of Working Group I to the Sixth Assessment Report of the Intergovernmental*
3170 *Panel on Climate Change*, Volume In Press. Cambridge, United Kingdom
3171 and New York, NY, USA: Cambridge University Press.
- 3172** Johnson, N. C., J. H. Graham, and F. A. Smith (1997). Functioning of mycor-
3173 rhizal associations along the mutualism-parasitism continuum. *New Phytol-*
3174 *ogist* 135(4), 575–585.
- 3175** Kachurina, O. M., H. Zhang, W. R. Raun, and E. G. Krenzer (2000). Simul-
3176 taneous determination of soil aluminum, ammonium- and nitrate- nitrogen
3177 using 1 M potassium chloride. *Communications in Soil Science and Plant*
3178 *Analysis* 31(7-8), 893–903.
- 3179** Kaiser, C., M. R. Kilburn, P. L. Clode, L. Fuchsleger, M. Koranda, J. B. Cliff,
3180 Z. M. Solaiman, and D. V. Murphy (2015). Exploring the transfer of recent
3181 plant photosynthates to soil microbes: mycorrhizal pathway vs direct root
3182 exudation. *New Phytologist* 205(4), 1537–1551.
- 3183** Katabuchi, M. (2015). LeafArea: An R package for rapid digital analysis of leaf
3184 area. *Ecological Research* 30(6), 1073–1077.

- 3185 Kattge, J. and W. Knorr (2007). Temperature acclimation in a biochemical
3186 model of photosynthesis: a reanalysis of data from 36 species. *Plant, Cell*
3187 and *Environment* 30(9), 1176–1190.
- 3188 Kattge, J., W. Knorr, T. Raddatz, and C. Wirth (2009). Quantifying photosyn-
3189 thetic capacity and its relationship to leaf nitrogen content for global-scale
3190 terrestrial biosphere models. *Global Change Biology* 15(4), 976–991.
- 3191 Kayler, Z., A. Gessler, and N. Buchmann (2010). What is the speed of link
3192 between aboveground and belowground processes? *New Phytologist* 187(4),
3193 885–888.
- 3194 Kayler, Z., C. Keitel, K. Jansen, and A. Gessler (2017). Experimental evidence
3195 of two mechanisms coupling leaf-level C assimilation to rhizosphere CO₂
3196 release. *Environmental and Experimental Botany* 135, 21–26.
- 3197 Keeling, C. D., W. G. Mook, and P. P. Tans (1979, jan). Recent trends in the
3198 ¹³C:¹²C ratio of atmospheric carbon dioxide. *Nature* 277(5692), 121–123.
- 3199 Keeney, D. R. and D. W. Nelson (1983). Nitrogen—Inorganic Forms. In A. L.
3200 Page (Ed.), *Methods of Soil Analysis* (2nd ed.), Chapter 33, pp. 643–698.
3201 Madison, WI, USA: ASA and SSSA.
- 3202 Kenward, M. G. and J. H. Roger (1997). Small sample inference for fixed effects
3203 from restricted maximum likelihood. *Biometrics* 53(3), 983.
- 3204 Knapp, A. K., M. L. Avolio, C. Beier, C. J. W. Carroll, S. L. Collins, J. S.
3205 Dukes, L. H. Fraser, R. J. Griffin-Nolan, D. L. Hoover, A. Jentsch, M. E.
3206 Loik, R. P. Phillips, A. K. Post, O. E. Sala, I. J. Slette, L. Yahdjian, and
3207 M. D. Smith (2017). Pushing precipitation to the extremes in distributed

- 3208 experiments: recommendations for simulating wet and dry years. *Global*
3209 *Change Biology* 23(5), 1774–1782.
- 3210 Knorr, W. (2000). Annual and interannual CO₂ exchanges of the
3211 terrestrial biosphere: process-based simulations and uncertainties. *Global*
3212 *Ecology and Biogeography* 9(3), 225–252.
- 3213 Knorr, W. and M. Heimann (2001). Uncertainties in global terrestrial biosphere
3214 modeling: 1. A comprehensive sensitivity analysis with a new photosynthesis
3215 and energy balance scheme. *Global Biogeochemical Cycles* 15(1), 207–225.
- 3216 Kulmatiski, A., P. B. Adler, J. M. Stark, and A. T. Tredennick (2017). Water
3217 and nitrogen uptake are better associated with resource availability than
3218 root biomass. *Ecosphere* 8(3), e01738.
- 3219 Lavergne, A., D. Sandoval, V. J. Hare, H. Graven, and I. C. Prentice (2020).
3220 Impacts of soil water stress on the acclimated stomatal limitation of pho-
3221 tosynthesis: Insights from stable carbon isotope data. *Global Change Biol-*
3222 *ogy* 26(12), 7158–7172.
- 3223 Lawrence, D. M., R. A. Fisher, C. D. Koven, K. W. Oleson, S. C. Swen-
3224 son, G. B. Bonan, N. Collier, B. Ghimire, L. Kampenhout, D. Kennedy,
3225 E. Kluzek, P. J. Lawrence, F. Li, H. Li, D. L. Lombardozzi, W. J. Riley,
3226 W. J. Sacks, M. Shi, M. Vertenstein, W. R. Wieder, C. Xu, A. A. Ali,
3227 A. M. Badger, G. Bisht, M. Broeke, M. A. Brunke, S. P. Burns, J. Buzan,
3228 M. Clark, A. Craig, K. M. Dahlin, B. Drewniak, J. B. Fisher, M. Flanner,
3229 A. M. Fox, P. Gentine, F. M. Hoffman, G. Keppel-Aleks, R. Knox, S. Ku-
3230 mar, J. Lenaerts, L. R. Leung, W. H. Lipscomb, Y. Lu, A. Pandey, J. D.
3231 Pelletier, J. Perket, J. T. Randerson, D. M. Ricciuto, B. M. Sanderson,

- 3232** A. Slater, Z. M. Subin, J. Tang, R. Q. Thomas, M. Val Martin, and X. Zeng
3233 (2019). The Community Land Model Version 5: description of new features,
3234 benchmarking, and impact of forcing uncertainty. *Journal of Advances in*
3235 *Modeling Earth Systems* 11(12), 4245–4287.
- 3236** LeBauer, D. S. and K. K. Treseder (2008). Nitrogen limitation of net primary
3237 productivity. *Ecology* 89(2), 371–379.
- 3238** Lefcheck, J. S. (2016). piecewiseSEM: Piecewise structural equation modelling
3239 in r for ecology, evolution, and systematics. *Methods in Ecology and Evolu-*
3240 *tion* 7(5), 573–579.
- 3241** Lenth, R. (2019). emmeans: estimated marginal means, aka least-squares
3242 means.
- 3243** Li, W., H. Zhang, G. Huang, R. Liu, H. Wu, C. Zhao, and N. G. McDowell
3244 (2020). Effects of nitrogen enrichment on tree carbon allocation: A global
3245 synthesis. *Global Ecology and Biogeography* 29(3), 573–589.
- 3246** Liang, J., X. Qi, L. Souza, and Y. Luo (2016). Processes regulating progressive
3247 nitrogen limitation under elevated carbon dioxide: a meta-analysis. *Biogeosciences*
3248 13(9), 2689–2699.
- 3249** Liang, X., T. Zhang, X. Lu, D. S. Ellsworth, H. BassiriRad, C. You, D. Wang,
3250 P. He, Q. Deng, H. Liu, J. Mo, and Q. Ye (2020). Global response patterns of
3251 plant photosynthesis to nitrogen addition: A meta-analysis. *Global Change*
3252 *Biology* 26(6), 3585–3600.
- 3253** López, J., D. A. Way, and W. Sadok (2021). Systemic effects of rising atmo-
3254 spheric vapor pressure deficit on plant physiology and productivity. *Global*

- 3255** *Change Biology* 27(9), 1704–1720.
- 3256** Lu, J., J. Yang, C. Keitel, L. Yin, P. Wang, W. Cheng, and F. A. Dijkstra
- 3257** (2022). Belowground carbon efficiency for nitrogen and phosphorus acqui-
- 3258** sition varies between *Lolium perenne* and *Trifolium repens* and depends on
- 3259** phosphorus fertilization. *Frontiers in Plant Science* 13, 1–9.
- 3260** Luo, X., T. F. Keenan, J. M. Chen, H. Croft, I. C. Prentice, N. G. Smith,
- 3261** A. P. Walker, H. Wang, R. Wang, C. Xu, and Y. Zhang (2021). Global
- 3262** variation in the fraction of leaf nitrogen allocated to photosynthesis. *Nature*
- 3263** *Communications* 12(1), 4866.
- 3264** Luo, Y., W. S. Currie, J. S. Dukes, A. C. Finzi, U. A. Hartwig, B. A. Hungate,
- 3265** R. E. McMurtrie, R. Oren, W. J. Parton, D. E. Pataki, R. M. Shaw, D. R.
- 3266** Zak, and C. B. Field (2004). Progressive nitrogen limitation of ecosystem
- 3267** responses to rising atmospheric carbon dioxide. *BioScience* 54(8), 731–739.
- 3268** Maire, V., P. Martre, J. Kattge, F. Gastal, G. Esser, S. Fontaine, and J.-F.
- 3269** Soussana (2012). The coordination of leaf photosynthesis links C and N
- 3270** fluxes in C₃ plant species. *PLoS ONE* 7(6), e38345.
- 3271** Makino, A. (2003). Rubisco and nitrogen relationships in rice: leaf photosyn-
- 3272** thesis and plant growth. *Soil Science and Plant Nutrition* 49(3), 319–327.
- 3273** Makino, A., M. Harada, T. Sato, H. Nakano, and T. Mae (1997). Growth and N
- 3274** Allocation in Rice Plants under CO₂ Enrichment. *Plant Physiology* 115(1),
- 3275** 199–203.
- 3276** Markham, J. H. and C. Zekveld (2007). Nitrogen fixation makes biomass al-
- 3277** location to roots independent of soil nitrogen supply. *Canadian Journal of*

- 3278** *Botany* (9), 787–793.
- 3279** Marschner, H. and B. Dell (1994). Nutrient uptake in mycorrhizal symbiosis.
- 3280** *Plant and Soil* 159(1), 89–102.
- 3281** Matamala, R. and W. H. Schlesinger (2000). Effects of elevated atmospheric
- 3282** CO₂ on fine root production and activity in an intact temperate forest
- 3283** ecosystem. *Global Change Biology* 6(8), 967–979.
- 3284** Medlyn, B. E., E. Dreyer, D. S. Ellsworth, M. Forstreuter, P. C. Harley,
- 3285** M. U. F. Kirschbaum, X. Le Roux, P. Montpied, J. Strassmeyer, A. Wal-
- 3286** croft, K. Wang, and D. Loustau (2002). Temperature response of parameters
- 3287** of a biochemically based model of photosynthesis. II. A review of experimen-
- 3288** tal data. *Plant, Cell and Environment* 25(9), 1167–1179.
- 3289** Menge, D. N. L., S. A. Levin, and L. O. Hedin (2008). Evolutionary tradeoffs can
- 3290** select against nitrogen fixation and thereby maintain nitrogen limitation.
- 3291** *Proceedings of the National Academy of Sciences* 105(5), 1573–1578.
- 3292** Menne, M. J., I. Durre, R. S. Vose, B. E. Gleason, and T. G. Houston (2012).
- 3293** An overview of the global historical climatology network-daily database.
- 3294** *Journal of Atmospheric and Oceanic Technology* 29(7), 897–910.
- 3295** Meyerholt, J., K. Sickel, and S. Zaehle (2020). Ensemble projections elucidate
- 3296** effects of uncertainty in terrestrial nitrogen limitation on future carbon up-
- 3297** take. *Global Change Biology* 26(7), 3978–3996.
- 3298** Meyerholt, J., S. Zaehle, and M. J. Smith (2016). Variability of projected ter-
- 3299** restrial biosphere responses to elevated levels of atmospheric CO₂ due to
- 3300** uncertainty in biological nitrogen fixation. *Biogeosciences* 13(5), 1491–1518.

- 3301** Minocha, R., S. Long, A. H. Magill, J. D. Aber, and W. H. McDowell (2000).
- 3302** Foliar free polyamine and inorganic ion content in relation to soil and soil
- 3303** solution chemistry in two fertilized forest stands at the Harvard Forest,
- 3304** Massachusetts. *Plant and Soil* 222(1-2), 119–137.
- 3305** Moore, D. J., S. Aref, R. M. Ho, J. S. Pippen, J. G. Hamilton, and E. H. De
- 3306** Lucia (2006). Annual basal area increment and growth duration of *Pinus*
- 3307** *taeda* in response to eight years of free-air carbon dioxide enrichment. *Global*
- 3308** *Change Biology* 12(8), 1367–1377.
- 3309** Morgan, J. A., D. E. Pataki, C. Körner, H. Clark, S. J. Del Grosso, J. M.
- 3310** Grünzweig, A. K. Knapp, A. R. Mosier, P. C. D. Newton, P. A. Niklaus,
- 3311** J. B. Nippert, R. S. Nowak, W. J. Parton, H. W. Polley, and M. R. Shaw
- 3312** (2004). Water relations in grassland and desert ecosystems exposed to ele-
- 3313** vated atmospheric CO₂. *Oecologia* 140(1), 11–25.
- 3314** Muñoz, N., X. Qi, M. W. Li, M. Xie, Y. Gao, M. Y. Cheung, F. L. Wong, and
- 3315** H.-M. Lam (2016). Improvement in nitrogen fixation capacity could be part
- 3316** of the domestication process in soybean. *Heredity* 117(2), 84–93.
- 3317** Nadelhoffer, K. J. and J. W. Raich (1992). Fine root production estimates and
- 3318** belowground carbon allocation in forest ecosystems. *Ecology* 73(4), 1139–
- 3319** 1147.
- 3320** Niinemets, Ü. and J. D. Tenhunen (1997). A model separating leaf structural
- 3321** and physiological effects on carbon gain along light gradients for the shade-
- 3322** tolerant species *Acer saccharum*. *Plant, Cell and Environment* 20(7), 845–
- 3323** 866.
- 3324** Norby, R. J., J. Ledford, C. D. Reilly, N. E. Miller, and E. G. O'Neill

- 3325 (2004). Fine-root production dominates response of a deciduous forest to
3326 atmospheric CO₂ enrichment. *Proceedings of the National Academy of Sci-*
3327 *ences* 101(26), 9689–9693.
- 3328 Norby, R. J., J. M. Warren, C. M. Iversen, B. E. Medlyn, and R. E. Mc-
3329 Murtrie (2010). CO₂ enhancement of forest productivity constrained by
3330 limited nitrogen availability. *Proceedings of the National Academy of Sci-*
3331 *ences* 107(45), 19368–19373.
- 3332 Novick, K. A., D. L. Ficklin, P. C. Stoy, C. A. Williams, G. Bohrer, A. C.
3333 Oishi, S. A. Papuga, P. D. Blanken, A. Noormets, B. N. Sulman, R. L.
3334 Scott, L. Wang, and R. P. Phillips (2016). The increasing importance of
3335 atmospheric demand for ecosystem water and carbon fluxes. *Nature Climate
3336 Change* 6(11), 1023–1027.
- 3337 Noyce, G. L., M. L. Kirwan, R. L. Rich, and J. P. Megonigal (2019). Asyn-
3338 chronous nitrogen supply and demand produce nonlinear plant allocation re-
3339 sponds to warming and elevated CO₂. *Proceedings of the National Academy
3340 of Sciences* 116(43), 21623–21628.
- 3341 Onoda, Y., K. Hikosaka, and T. Hirose (2004). Allocation of nitrogen to
3342 cell walls decreases photosynthetic nitrogen-use efficiency. *Functional Ecol-
3343 ogy* 18(3), 419–425.
- 3344 Onoda, Y., I. J. Wright, J. R. Evans, K. Hikosaka, K. Kitajima, Ü. Niinemets,
3345 H. Poorter, T. Tosens, and M. Westoby (2017). Physiological and structural
3346 trade-offs underlying the leaf economics spectrum. *New Phytologist* 214(4),
3347 1447–1463.
- 3348 Oren, R., J. S. Sperry, G. G. Katul, D. E. Pataki, B. E. Ewers, N. Phillips,

- 3349 and K. V. R. Schäfer (1999). Survey and synthesis of intra- and interspecific
3350 variation in stomatal sensitivity to vapor pressure deficit. *Plant, Cell and*
3351 *Environment* 22(12), 1515–1526.
- 3352 Oreskes, N., K. Shrader-Frechette, and K. Belitz (1994). Verification, vali-
3353 dation, and confirmation of numerical models in the Earth sciences. *Sci-*
3354 *ence* 263(5147), 641–646.
- 3355 Paillassa, J., I. J. Wright, I. C. Prentice, S. Pepin, N. G. Smith, G. Ethier,
3356 A. C. Westerband, L. J. Lamarque, H. Wang, W. K. Cornwell, and V. Maire
3357 (2020). When and where soil is important to modify the carbon and water
3358 economy of leaves. *New Phytologist* 228(1), 121–135.
- 3359 Parvin, S., S. Uddin, S. Tausz Posch, R. Armstrong, and M. Tausz (2020). Car-
3360 bon sink strength of nodules but not other organs modulates photosynthesis
3361 of faba bean (*Vicia faba*) grown under elevated [CO₂] and different water
3362 supply. *New Phytologist* 227(1), 132–145.
- 3363 Paul, K. I., P. J. Polglase, A. M. O'Connell, J. C. Carlyle, P. J. Smethurst, and
3364 P. K. Khanna (2003). Defining the relation between soil water content and
3365 net nitrogen mineralization. *European Journal of Soil Science* 54(1), 39–48.
- 3366 Peng, Y., K. J. Bloomfield, L. A. Cernusak, T. F. Domingues, and I. C. Pren-
3367 tice (2021). Global climate and nutrient controls of photosynthetic capacity.
3368 *Communications Biology* 4(1), 462.
- 3369 Perkowski, E. A., E. F. Waring, and N. G. Smith (2021). Root mass carbon
3370 costs to acquire nitrogen are determined by nitrogen and light availabil-
3371 ity in two species with different nitrogen acquisition strategies. *Journal of*
3372 *Experimental Botany* 72(15), 5766–5776.

- 3373 Phillips, R. P., E. R. Brzostek, and M. G. Midgley (2013). The mycorrhizal-
3374 associated nutrient economy: a new framework for predicting carbon-
3375 nutrient couplings in temperate forests. *New Phytologist* 199(1), 41–51.
- 3376 Phillips, R. P., A. C. Finzi, and E. S. Bernhardt (2011). Enhanced root ex-
3377 udation induces microbial feedbacks to N cycling in a pine forest under
3378 long-term CO₂ fumigation. *Ecology Letters* 14(2), 187–194.
- 3379 Pinheiro, J. and D. Bates (2022). nlme: linear and nonlinear mixed effects
3380 models.
- 3381 Poggio, L., L. M. De Sousa, N. H. Batjes, G. B. M. Heuvelink, B. Kempen,
3382 E. Ribeiro, and D. Rossiter (2021). SoilGrids 2.0: Producing soil information
3383 for the globe with quantified spatial uncertainty. *Soil* 7(1), 217–240.
- 3384 Pons, T. L. and R. W. Pearcy (1994). Nitrogen reallocation and photosynthetic
3385 acclimation in response to partial shading in soybean plants. *Physiologia
3386 Plantarum* 92(4), 636–644.
- 3387 Poorter, H., J. Bühler, D. Van Dusschoten, J. Climent, and J. A. Postma (2012).
3388 Pot size matters: A meta-analysis of the effects of rooting volume on plant
3389 growth. *Functional Plant Biology* 39(11), 839–850.
- 3390 Poorter, H., O. Knopf, I. J. Wright, A. A. Temme, S. W. Hogewoning, A. Graf,
3391 L. A. Cernusak, and T. L. Pons (2022). A meta-analysis of responses of C₃
3392 plants to atmospheric CO₂: dose-response curves for 85 traits ranging from
3393 the molecular to the whole-plant level. *New Phytologist* 233(4), 1560–1596.
- 3394 Prentice, I. C., N. Dong, S. M. Gleason, V. Maire, and I. J. Wright (2014).
3395 Balancing the costs of carbon gain and water transport: testing a new theo-

- 3396** retical framework for plant functional ecology. *Ecology Letters* 17(1), 82–91.
- 3397** Prentice, I. C., X. Liang, B. E. Medlyn, and Y.-P. Wang (2015). Reliable, ro-
- 3398** bust and realistic: The three R’s of next-generation land-surface modelling.
- 3399** *Atmospheric Chemistry and Physics* 15, 5987–6005.
- 3400** Priestley, C. H. B. and R. J. Taylor (1972). On the Assessment of Surface
- 3401** Heat Flux and Evaporation Using Large-Scale Parameters. *Monthly Weather*
- 3402** *Review* 100(2), 81–92.
- 3403** Querejeta, J. I., I. Prieto, C. Armas, F. Casanoves, J. S. Diémé, M. Diouf,
- 3404** H. Yossi, B. Kaya, F. I. Pugnaire, and G. M. Rusch (2022). Higher leaf
- 3405** nitrogen content is linked to tighter stomatal regulation of transpiration
- 3406** and more efficient water use across dryland trees. *New Phytologist* 235(4),
- 3407** 1351–1364.
- 3408** R Core Team (2021). R: A language and environment for statistical computing.
- 3409** Raich, J. W., D. A. Clark, L. Schwendenmann, and T. E. Wood (2014). Above-
- 3410** ground tree growth varies with belowground carbon allocation in a tropical
- 3411** rainforest environment. *PLoS ONE* 9(6), e100275.
- 3412** Rastetter, E. B., P. M. Vitousek, C. B. Field, G. R. Shaver, D. Herbert, and
- 3413** G. I. Ågren (2001). Resource optimization and symbiotic nitrogen fixation.
- 3414** *Ecosystems* 4(4), 369–388.
- 3415** Reich, P. B. (2014). The world-wide ‘fast-slow’ plant economics spectrum: a
- 3416** traits manifesto. *Journal of Ecology* 102(2), 275–301.
- 3417** Reich, P. B., S. E. Hobbie, T. Lee, D. S. Ellsworth, J. B. West, D. Tilman,
- 3418** J. M. H. Knops, S. Naeem, and J. Trost (2006). Nitrogen limitation con-

- 3419 strains sustainability of ecosystem response to CO₂. *Nature* 440(7086), 922–
3420 925.
- 3421 Reichman, G. A., D. L. Grunes, and F. G. Viets (1966). Effect of soil moisture
3422 on ammonification and nitrification in two Northern Plains soils. *Soil Science
3423 Society of America Journal* 30(3), 363–366.
- 3424 Rhine, E. D., R. L. Mulvaney, E. J. Pratt, and G. K. Sims (1998). Improving
3425 the Berthelot reaction for determining ammonium in soil extracts and water.
3426 *Soil Science Society of America Journal* 62(2), 473.
- 3427 Rogers, A. (2014). The use and misuse of V_{cmax} in Earth System Models. *Photo-
3428 synthesis Research* 119(1-2), 15–29.
- 3429 Rogers, A., B. E. Medlyn, J. S. Dukes, G. B. Bonan, S. Caemmerer, M. C.
3430 Dietze, J. Kattge, A. D. B. Leakey, L. M. Mercado, Ü. Niinemets, I. C.
3431 Prentice, S. P. Serbin, S. Sitch, D. A. Way, and S. Zaehle (2017). A roadmap
3432 for improving the representation of photosynthesis in Earth system models.
3433 *New Phytologist* 213(1), 22–42.
- 3434 Saathoff, A. J. and J. Welles (2021). Gas exchange measurements in the un-
3435 steady state. *Plant Cell and Environment* 44(11), 3509–3523.
- 3436 Sage, R. F. and R. W. Pearcy (1987). The nitrogen use efficiency of C₃ and C₄
3437 plants: I. Leaf nitrogen, growth, and biomass partitioning in *Chenopodium
3438 album* (L.) and *Amaranthus retroflexus* (L.). *Plant Physiology* 84(3), 954–
3439 958.
- 3440 Saleh, A. M., M. Abdel-Mawgoud, A. R. Hassan, T. H. Habeeb, R. S. Yehia,
3441 and H. AbdElgawad (2020). Global metabolic changes induced by arbuscular

- 3442** mycorrhizal fungi in oregano plants grown under ambient and elevated levels
3443 of atmospheric CO₂. *Plant Physiology and Biochemistry* 151, 255–263.
- 3444** Saxton, K. E. and W. J. Rawls (2006). Soil water characteristic estimates by
3445 texture and organic matter for hydrologic solutions. *Soil Science Society of*
3446 *America Journal* 70(5), 1569–1578.
- 3447** Schaefer, K., C. R. Schwalm, C. Williams, M. A. Arain, A. Barr, J. M. Chen,
3448 K. J. Davis, D. Dimitrov, T. W. Hilton, D. Y. Hollinger, E. Humphreys,
3449 B. Poulter, B. M. Racza, A. D. Richardson, A. Sahoo, P. Thornton, R. Var-
3450 gas, H. Verbeeck, R. Anderson, I. Baker, T. A. Black, P. Bolstad, J. Chen,
3451 P. S. Curtis, A. R. Desai, M. C. Dietze, D. Dragoni, C. M. Gough, R. F.
3452 Grant, L. Gu, A. K. Jain, C. Kucharik, B. E. Law, S. Liu, E. Lokipitiya,
3453 H. A. Margolis, R. Matamala, J. H. McCaughey, R. Monson, J. W. Munger,
3454 W. Oechel, C. Peng, D. T. Price, D. Ricciuto, W. J. Riley, N. Roulet,
3455 H. Tian, C. Tonitto, M. Torn, E. Weng, and X. Zhou (2012). A model-
3456 data comparison of gross primary productivity: Results from the North
3457 American Carbon Program site synthesis. *Journal of Geophysical Research:*
3458 *Biogeosciences* 117(G3), G03010.
- 3459** Schmitt, M. R. and G. E. Edwards (1981). Photosynthetic capacity and nitrogen
3460 use efficiency of maize, wheat, and rice: A comparison between C₃ and C₄
3461 photosynthesis. *Journal of Experimental Botany* 32(3), 459–466.
- 3462** Schneider, C. A., W. S. Rasband, and K. W. Eliceiri (2012). NIH Image to
3463 ImageJ: 25 years of image analysis. *Nature Methods* 9(7), 671–675.
- 3464** Scott, H. G. and N. G. Smith (2022). A Model of C₄ photosynthetic acclima-
3465 tion based on least-cost optimality theory suitable for Earth system model

- 3466** incorporation. *Journal of Advances in Modeling Earth Systems* 14(3), 1–16.
- 3467** Shi, M., J. B. Fisher, E. R. Brzostek, and R. P. Phillips (2016). Carbon cost
- 3468** of plant nitrogen acquisition: Global carbon cycle impact from an improved
- 3469** plant nitrogen cycle in the Community Land Model. *Global Change Biology*
- 3470** 22(3), 1299–1314.
- 3471** Shi, M., J. B. Fisher, R. P. Phillips, and E. R. Brzostek (2019). Neglecting
- 3472** plant–microbe symbioses leads to underestimation of modeled climate im-
- 3473** pacts. *Biogeosciences* 16(2), 457–465.
- 3474** Smith, B., D. Wärllind, A. Arneth, T. Hickler, P. Leadley, J. Siltberg, and
- 3475** S. Zaehle (2014). Implications of incorporating N cycling and N limitations
- 3476** on primary production in an individual-based dynamic vegetation model.
- 3477** *Biogeosciences* 11(7), 2027–2054.
- 3478** Smith, N. G. and J. S. Dukes (2013). Plant respiration and photosynthesis in
- 3479** global-scale models: incorporating acclimation to temperature and CO₂.
- 3480** *Global Change Biology* 19(1), 45–63.
- 3481** Smith, N. G. and J. S. Dukes (2018). Drivers of leaf carbon exchange capacity
- 3482** across biomes at the continental scale. *Ecology* 99(7), 1610–1620.
- 3483** Smith, N. G. and T. F. Keenan (2020). Mechanisms underlying leaf photosyn-
- 3484** thetic acclimation to warming and elevated CO₂ as inferred from least-cost
- 3485** optimality theory. *Global Change Biology* 26(9), 5202–5216.
- 3486** Smith, N. G., T. F. Keenan, I. C. Prentice, H. Wang, I. J. Wright, Ü. Niinemets,
- 3487** K. Y. Crous, T. F. Domingues, R. Guerrieri, F. oko Ishida, J. Kattge, E. L.
- 3488** Kruger, V. Maire, A. Rogers, S. P. Serbin, L. Tarvainen, H. F. Togashi,

- 3489 P. A. Townsend, M. Wang, L. K. Weerasinghe, and S.-X. Zhou (2019).
3490 Global photosynthetic capacity is optimized to the environment. *Ecology*
3491 *Letters* 22(3), 506–517.
- 3492 Smith, N. G., D. L. Lombardozzi, A. Tawfik, G. B. Bonan, and J. S. Dukes
3493 (2017). Biophysical consequences of photosynthetic temperature acclimation
3494 for climate. *Journal of Advances in Modeling Earth Systems* 9(1), 536–547.
- 3495 Smith, N. G., S. L. Malyshev, E. Shevliakova, J. Kattge, and J. S. Dukes
3496 (2016). Foliar temperature acclimation reduces simulated carbon sensitivity
3497 to climate. *Nature Climate Change* 6(4), 407–411.
- 3498 Smith, S. E. and D. J. Read (2008). *Mycorrhizal Symbiosis*. Academic Press.
- 3499 Soil Survey Staff (2022). Web Soil Survey.
- 3500 Soudzilovskaia, N. A., J. C. Douma, A. A. Akhmetzhanova, P. M. van Bode-
3501 gom, W. K. Cornwell, E. J. Moens, K. K. Treseder, and J. H. C. Cornelissen
3502 (2015). Global patterns of plant root colonization intensity by mycorrhizal
3503 fungi explained by climate and soil chemistry. *Global Ecology and Biogeog-
3504 raphy* 24(3), 371–382.
- 3505 Stark, J. M. and M. K. Firestone (1995). Mechanisms for soil moisture ef-
3506 fects on activity of nitrifying bacteria. *Applied and Environmental Microbi-
3507 ology* 61(1), 218–221.
- 3508 Stocker, B. D., H. Wang, N. G. Smith, S. P. Harrison, T. F. Keenan, D. San-
3509 doval, T. Davis, and I. C. Prentice (2020). P-model v1.0: An optimality-
3510 based light use efficiency model for simulating ecosystem gross primary pro-
3511 duction. *Geoscientific Model Development* 13(3), 1545–1581.

- 3512 Stocker, B. D., J. Zscheischler, T. F. Keenan, I. C. Prentice, J. Peñuelas, and
3513 S. I. Seneviratne (2018). Quantifying soil moisture impacts on light use
3514 efficiency across biomes. *New Phytologist* 218(4), 1430–1449.
- 3515 Sulman, B. N., D. T. Roman, K. Yi, L. Wang, R. P. Phillips, and K. A.
3516 Novick (2016). High atmospheric demand for water can limit forest car-
3517 bon uptake and transpiration as severely as dry soil. *Geophysical Research*
3518 *Letters* 43(18), 9686–9695.
- 3519 Sulman, B. N., E. Shevliakova, E. R. Brzostek, S. N. Kivlin, S. L. Malyshev,
3520 D. N. L. Menge, and X. Zhang (2019). Diverse mycorrhizal associations
3521 enhance terrestrial C storage in a global model. *Global Biogeochemical Cy-*
3522 *cles* 33(4), 501–523.
- 3523 Sweet, S. K., D. W. Wolfe, A. DeGaetano, and R. Benner (2017). Anatomy
3524 of the 2016 drought in the Northeastern United States: Implications for
3525 agriculture and water resources in humid climates. *Agricultural and Forest*
3526 *Meteorology* 247, 571–581.
- 3527 Taylor, B. N. and D. N. L. Menge (2018). Light regulates tropical symbiotic
3528 nitrogen fixation more strongly than soil nitrogen. *Nature Plants* 4(9), 655–
3529 661.
- 3530 Terrer, C., S. Vicca, B. A. Hungate, R. P. Phillips, and I. C. Prentice (2016).
3531 Mycorrhizal association as a primary control of the CO₂ fertilization effect.
3532 *Science* 353(6294), 72–74.
- 3533 Terrer, C., S. Vicca, B. D. Stocker, B. A. Hungate, R. P. Phillips, P. B. Reich,
3534 A. C. Finzi, and I. C. Prentice (2018). Ecosystem responses to elevated CO₂
3535 governed by plant–soil interactions and the cost of nitrogen acquisition. *New*

- 3536** *Phytologist* 217(2), 507–522.
- 3537** Thieurmel, B. and A. Elmarhraoui (2019). suncalc: Compute sun position,
- 3538** sunlight phases, moon position, and lunar phase.
- 3539** Thomas, R. Q., E. N. J. Brookshire, and S. Gerber (2015). Nitrogen limita-
- 3540** tion on land: how can it occur in Earth system models? *Global Change*
- 3541** *Biology* 21(5), 1777–1793.
- 3542** Thomas, R. Q., S. Zaehle, P. H. Templer, and C. L. Goodale (2013). Global pat-
- 3543** terns of nitrogen limitation: confronting two global biogeochemical models
- 3544** with observations. *Global Change Biology* 19(10), 2986–2998.
- 3545** Thornton, P. E., J.-F. Lamarque, N. A. Rosenbloom, and N. M. Mahowald
- 3546** (2007). Influence of carbon-nitrogen cycle coupling on land model response
- 3547** to CO₂ fertilization and climate variability. *Global Biogeochemical Cy-*
- 3548** *cles* 21(4), GB4018.
- 3549** Tingey, D. T., D. L. Phillips, and M. G. Johnson (2000). Elevated CO₂ and
- 3550** conifer roots: effects on growth, life span and turnover. *New Phytolo-*
- 3551** *gist* 147(1), 87–103.
- 3552** Udvardi, M. and P. S. Poole (2013). Transport and metabolism in legume-
- 3553** rhizobia symbioses. *Annual Review of Plant Biology* 64, 781–805.
- 3554** USDA NRCS (2022). The PLANTS Database.
- 3555** Uselman, S. M., R. G. Qualls, and R. B. Thomas (2000). Effects of increased
- 3556** atmospheric CO₂, temperature, and soil N availability on root exudation
- 3557** of dissolved organic carbon by an N-fixing tree (*Robinia pseudoacacia* L.).
- 3558** *Plant and Soil* 222, 191–202.

- 3559 van Diepen, L. T. A., E. A. Lilleskov, K. S. Pregitzer, and R. M. Miller (2007).
- 3560 Decline of arbuscular mycorrhizal fungi in northern hardwood forests ex-
- 3561 posed to chronic nitrogen additions. *New Phytologist* 176(1), 175–183.
- 3562 Vance, C. P. and G. H. Heichel (1991). Carbon in N₂ fixation: Limitation or
- 3563 exquisite adaptation. *Annual Review of Plant Physiology and Plant Molec-*
- 3564 *ular Biology* 42(1), 373–392.
- 3565 Viet, H. D., J.-H. Kwak, K.-S. Lee, S.-S. Lim, M. Matsushima, S. X. Chang,
- 3566 K.-H. Lee, and W.-J. Choi (2013). Foliar chemistry and tree ring δ¹³C of
- 3567 *Pinus densiflora* in relation to tree growth along a soil pH gradient. *Plant*
- 3568 *and Soil* 363(1-2), 101–112.
- 3569 Vitousek, P. M., K. Cassman, C. C. Cleveland, T. Crews, C. B. Field, N. B.
- 3570 Grimm, R. W. Howarth, R. Marino, L. Martinelli, E. B. Rastetter, and
- 3571 J. I. Sprent (2002). Towards an ecological understanding of biological nitro-
- 3572 gen fixation. In *The Nitrogen Cycle at Regional to Global Scales*, pp. 1–45.
- 3573 Springer Netherlands.
- 3574 Vitousek, P. M. and R. W. Howarth (1991). Nitrogen limitation on land and in
- 3575 the sea: How can it occur? *Biogeochemistry* 13(2), 87–115.
- 3576 Vitousek, P. M., S. Porder, B. Z. Houlton, and O. A. Chadwick (2010).
- 3577 Terrestrial phosphorus limitation: mechanisms, implications, and nitro-
- 3578 gen–phosphorus interactions. *Ecological Applications* 20(1), 5–15.
- 3579 Walker, A. P., A. P. Beckerman, L. Gu, J. Kattge, L. A. Cernusak, T. F.
- 3580 Domingues, J. C. Scales, G. Wohlfahrt, S. D. Wullschleger, and F. I. Wood-
- 3581 ward (2014). The relationship of leaf photosynthetic traits - V_{cmax} and J_{max}
- 3582 - to leaf nitrogen, leaf phosphorus, and specific leaf area: a meta-analysis

- 3583 and modeling study. *Ecology and Evolution* 4(16), 3218–3235.
- 3584 Walker, A. P., A. L. Johnson, A. Rogers, J. Anderson, R. A. Bridges, R. A.
- 3585 Fisher, D. Lu, D. M. Ricciuto, S. P. Serbin, and M. Ye (2021). Multi-
- 3586 hypothesis comparison of Farquhar and Collatz photosynthesis models re-
- 3587 veals the unexpected influence of empirical assumptions at leaf and global
- 3588 scales. *Global Change Biology* 27(4), 804–822.
- 3589 Wang, H., I. C. Prentice, T. F. Keenan, T. W. Davis, I. J. Wright, W. K.
- 3590 Cornwell, B. J. Evans, and C. Peng (2017). Towards a universal model for
- 3591 carbon dioxide uptake by plants. *Nature Plants* 3(9), 734–741.
- 3592 Wang, H., I. C. Prentice, I. J. Wright, D. I. Warton, S. Qiao, X. Xu, J. Zhou,
- 3593 Kikuzawa, and N. C. Stenseth (2023). Leaf economics fundamentals ex-
- 3594 plained by optimality principles. *Science Advances* 9(3), eadd566.
- 3595 Wang, J., J. M. Knops, C. E. Brassil, and C. Mu (2017). Increased productivity
- 3596 in wet years drives a decline in ecosystem stability with nitrogen additions
- 3597 in arid grasslands. *Ecology* 98(7), 1779–1786.
- 3598 Wang, W., Y. Wang, G. Hoch, Z. Wang, and J. Gu (2018). Linkage of root mor-
- 3599 phology to anatomy with increasing nitrogen availability in six temperate
- 3600 tree species. *Plant and Soil* 425(1-2), 189–200.
- 3601 Weatherburn, M. W. (1967). Phenol-hypochlorite reaction for determination of
- 3602 ammonia. *Analytical Chemistry* 39(8), 971–974.
- 3603 Wellburn, A. R. (1994). The spectral determination of chlorophylls a and b, as
- 3604 well as total carotenoids, using various solvents with spectrophotometers of
- 3605 different resolution. *Journal of Plant Physiology* 144(3), 307–313.

- 3606** Wen, Z., P. J. White, J. Shen, and H. Lambers (2022). Linking root exuda-
3607 tion to belowground economic traits for resource acquisition. *New Phytolo-*
3608 *gist* 233(4), 1620–1635.
- 3609** Westerband, A. C., I. J. Wright, V. Maire, J. Paillassa, I. C. Prentice, O. K.
3610 Atkin, K. J. Bloomfield, L. A. Cernusak, N. Dong, S. M. Gleason, C. Guil-
3611 herme Pereira, H. Lambers, M. R. Leishman, Y. Malhi, and R. H. Nolan
3612 (2023). Coordination of photosynthetic traits across soil and climate gradi-
3613 ents. *Global Change Biology* 29(3), 1–29.
- 3614** Wieder, W. R., C. C. Cleveland, W. K. Smith, and K. Todd-Brown (2015).
3615 Future productivity and carbon storage limited by terrestrial nutrient avail-
3616 ability. *Nature Geoscience* 8(6), 441–444.
- 3617** Wieder, W. R., D. M. Lawrence, R. A. Fisher, G. B. Bonan, S. J. Cheng, C. L.
3618 Goodale, A. S. Grandy, C. D. Koven, D. L. Lombardozzi, K. W. Oleson,
3619 and R. Q. Thomas (2019). Beyond static benchmarking: using experimental
3620 manipulations to evaluate land model assumptions. *Global Biogeochemical*
3621 *Cycles* 33(10), 1289–1309.
- 3622** Wright, I. J., P. B. Reich, and M. Westoby (2003). Least-cost input mixtures
3623 of water and nitrogen for photosynthesis. *The American Naturalist* 161(1),
3624 98–111.
- 3625** Wright, I. J., P. B. Reich, M. Westoby, D. D. Ackerly, Z. Baruch, F. Bongers,
3626 J. Cavender-Bares, T. Chapin, J. H. C. Cornelissen, M. Diemer, J. Flexas,
3627 E. Garnier, P. K. Groom, J. Gulias, K. Hikosaka, B. B. Lamont, T. Lee,
3628 W. Lee, C. Lusk, J. J. Midgley, M.-L. Navas, Ü. Niinemets, J. Oleksyn,
3629 N. Osada, H. Poorter, P. Poot, L. Prior, V. I. Pyankov, C. Roumet, S. C.

- 3630** Thomas, M. G. Tjoelker, E. J. Veneklaas, and R. Villar (2004). The world-wide leaf economics spectrum. *Nature* 428(6985), 821–827.
- 3632** Xu-Ri and I. C. Prentice (2017). Modelling the demand for new nitrogen fixation by terrestrial ecosystems. *Biogeosciences* 14(7), 2003–2017.
- 3634** Yahdjian, L., L. A. Gherardi, and O. E. Sala (2011). Nitrogen limitation in arid-subhumid ecosystems: A meta-analysis of fertilization studies. *Journal of Arid Environments* 75(8), 675–680.
- 3637** Zaehle, S., B. E. Medlyn, M. G. De Kauwe, A. P. Walker, M. C. Dietze, T. Hickler, Y. Luo, Y. P. Wang, B. El-Masri, P. Thornton, A. Jain, S. Wang, D. Warlind, E. Weng, W. Parton, C. M. Iversen, A. Gallet-Budynek, H. McCarthy, A. C. Finzi, P. J. Hanson, I. C. Prentice, R. Oren, and R. J. Norby (2014). Evaluation of 11 terrestrial carbon-nitrogen cycle models against observations from two temperate Free-Air CO₂ Enrichment studies. *New Phytologist* 202(3), 803–822.
- 3644** Zaehle, S., S. Sitch, B. Smith, and F. Hatterman (2005). Effects of parameter uncertainties on the modeling of terrestrial biosphere dynamics. *Global Biogeochemical Cycles* 19(3), GB3020.
- 3647** Zhu, Q., W. J. Riley, J. Tang, N. Collier, F. M. Hoffman, X. Yang, and G. Bisht (2019). Representing nitrogen, phosphorus, and carbon interactions in the E3SM land model: development and global benchmarking. *Journal of Advances in Modeling Earth Systems* 11(7), 2238–2258.
- 3651** Ziegler, C., M. E. Dusenge, B. Nyirambangutse, E. Zibera, G. Wallin, and J. Uddling (2020). Contrasting dependencies of photosynthetic capacity on leaf nitrogen in early- and late-successional tropical montane tree species.

- 3654** *Frontiers in Plant Science* 11, 1–12.
- 3655** Ziehn, T., J. Kattge, W. Knorr, and M. Scholze (2011). Improving the pre-
3656 dictability of global CO₂ assimilation rates under climate change. *Geophys-
3657 ical Research Letters* 38(10), L10404.

3658 Appendix A: Supplemental material for "Structural carbon costs to
3659 acquire nitrogen are determined by nitrogen and light availability in
3660 two species with different nitrogen acquisition strategies"

Table A1. Summary table containing volumes of compounds used to create modified Hoagland's solutions for each soil nitrogen fertilization treatment. All volumes are expressed as milliliters per liter (mL/L)

Compound	0 ppm N	70 ppm N	210 ppm N	630 ppm N
1 M NH ₄ H ₂ PO ₄	0	0.33	1	1
2 M KNO ₃	0	0.67	2	2
2 M Ca(NO ₃) ₂	0	0.67	2	2
1 M NH ₄ NO ₃	0	0.33	1	0
8 M NH ₄ NO ₃	0	0	0	2
1 M KH ₂ PO ₄	1	0.67	0	0
1 M KCl	4	1.33	0	0
1 M CaCO ₃	4	3	0	0
2 M MgSO ₄	1	1	1	1
10% Fe-EDTA	1	1	1	1
Trace Elements	1	1	1	1

Table A2. Analysis of variance results exploring species-specific effects of light availability, nitrogen fertilization, and their interactions on the ratio of whole plant biomass to pot volume

	df	Biomass:pot volume		
		Coefficient	χ^2	p
<i>G. hirsutum</i>				
Intercept		0.740	-	-
Light (L)	1	-4.23E-03	189.581	<0.001
Nitrogen (N)	1	7.86E-04	17.927	<0.001
L*N	1	-6.61E-06	4.709	0.030
<i>G. max</i>				
Intercept		-0.233	-	-
Light (L)	1	-1.12E-02	69.500	<0.001
Nitrogen (N)	1	8.29E-04	40.297	<0.001
L*N	1	-8.51E-06	5.548	0.019

3661 *Significance determined using Wald's χ^2 tests ($P = 0.05$). P -values < 0.05 are
3662 in bold and p -values between 0.05 and 0.1 are italicized. Negative coefficients
3663 for light treatments indicate a positive effect of increasing light availability on
3664 all response variables, as light availability is treated as percent shade cover in all
3665 linear mixed-effects models.

Table A3. Slopes of the regression line describing the relationship between each dependent variable and nitrogen fertilization at each light level*

Shade cover	Slope
<i>G. hirsutum</i>	
0%	8.29E-04^a
30%	5.74E-04^a
50%	4.03E-04^a
80%	1.48E-04 ^a
<i>G. max</i>	
0%	7.86E-04
30%	5.87E-04
50%	4.55E-04
80%	<i>2.57E-05</i>

3666 *Slopes represent estimated marginal mean slopes from linear mixed-effects models described in the Methods. Slopes
3667 were calculated using the ‘emmeans’ R package (Lenth 2019). Superscripts indicate slopes fit to natural-log (^a) or
3668 square root (^b) transformed data. Slopes statistically different from zero (Tukey: $p < 0.05$) are indicated in bold.
3669 Marginally significant slopes (Tukey: $0.05 < p < 0.1$) are italicized.

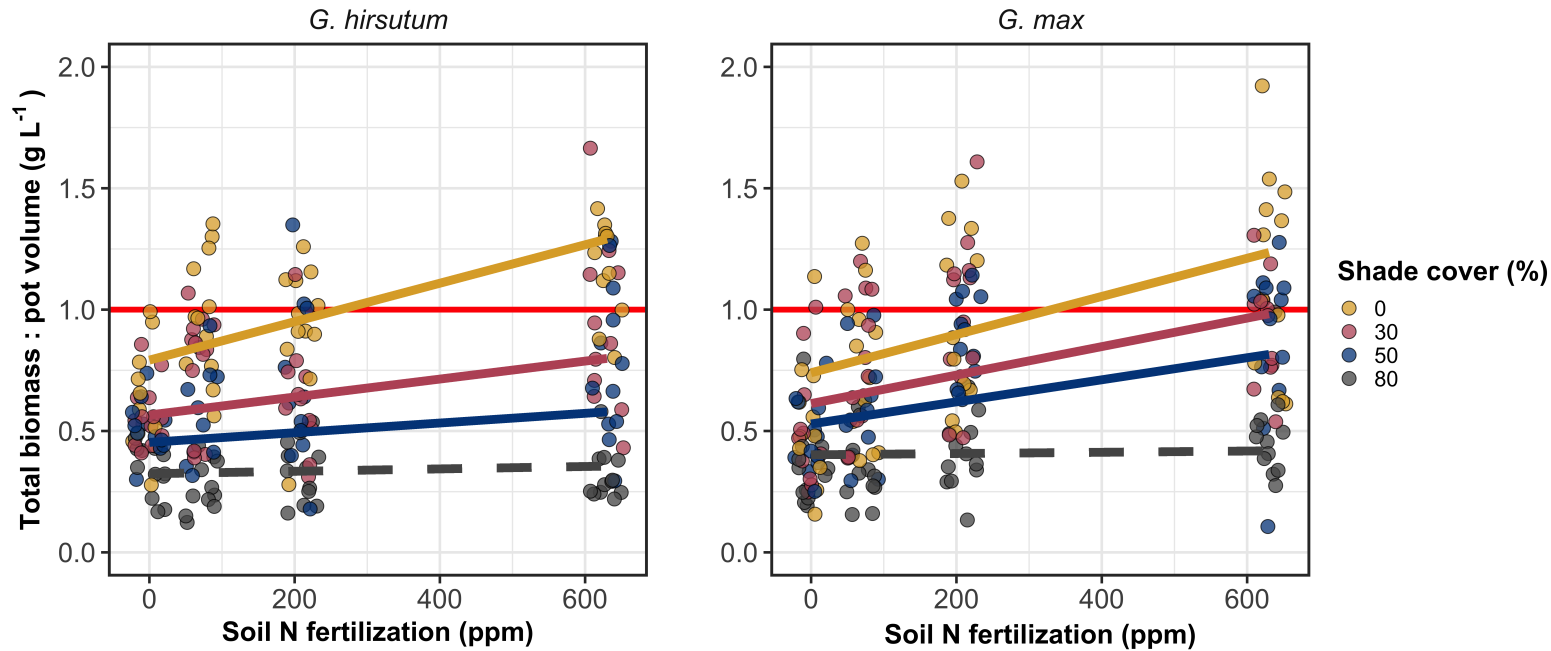


Figure A1. Effects of shade cover and nitrogen fertilization on the ratio of plant biomass to rooting volume in *G. hirsutum* (left panel) and *G. max* (right panel). The red horizontal line indicates the recommended 1 g L^{-1} threshold for BVR recommended by Poorter et al. (2012) to avoid pot size-induced growth limitation. Nitrogen fertilization treatments are represented on the x-axis. Shade cover treatments are represented through colored points and trendlines. Trendlines were created by back-transforming marginal mean slopes and intercepts from species-specific linear mixed-effects models. These values were calculated using the 'emtrends' and 'emmmeans' functions in the 'emmmeans' R package (Lenth 2019). Points are jittered for visibility. Yellow points and trendlines represent the 0% shade cover treatment, blue points and trendlines represent the 30% shade cover treatment, green points and trendlines represent the 50% shade cover treatment, and purple points and trendlines represent the 80% shade cover treatment. Solid trendlines indicate slopes that are significantly different from zero (Tukey: $p < 0.05$), while dashed trendlines indicate slopes that are not statistically different from zero.

3670 Appendix B: Supplemental material for "Soil nitrogen availability
3671 modifies leaf nitrogen economies in mature temperate deciduous
3672 forests: a direct test of photosynthetic least-cost theory"

Table B1. Sample sizes of each species, abbreviated by their USDA NRCS PLANTS database code, within each plot at each site

	ACRU	ACSA	FAGR	FRAM	QURU	N_{plot}
Bald Hill						
+N; +S	0	6	1	0	1	8
+N; -S	1	2	2	0	1	6
-N; +S	2	2	0	0	2	6
-N; -S	2	3	3	0	2	10
Carter Creek						
+N; +S	0	6	1	2	0	9
+N; -S	0	4	0	2	0	6
-N; +S	0	5	1	4	0	10
-N; -S	0	7	0	0	0	7
Mount Pleasant						
+N; +S	3	2	1	0	3	9
+N; -S	0	5	4	1	0	10
-N; +S	1	2	4	0	0	7
-N; -S	3	3	1	2	1	10
N_{spp}	12	47	18	11	10	98

3673 *Plots within each site are represented based on nitrogen and sulfur addition
3674 status. The final column on the right depicts total sample size per plot in each
3675 site (N_{plot}) and the final row on the bottom represents cumulative species sample
3676 size across all plots and all sites (N_{spp}). Key: ACRU = *A. rubrum*; ACSA = *A.*
3677 *saccharum*; FAGR = *F. grandifolia*; FRAM = *F. americana*; QURU = *Q. rubra*

Table B2. Analysis of variance results exploring the linear effect of leaf temperature on net photosynthesis rate and stomatal conductance measured at 400 $\mu\text{mol mol}^{-1}$ CO₂

		A_{net}		g_s	
	df	χ^2	p	χ^2	p
Leaf temperature	1	1.287	0.257	1.716	0.190

3678 Results detail linear mixed effects model where temperature was regressed against
3679 net photosynthesis or stomatal conductance, with site and species designated as
3680 random intercept terms. Significance was determined using Type II Wald χ^2
3681 tests ($\alpha = 0.05$). Key: A_{net} = net photosynthesis rate at 400 $\mu\text{mol mol}^{-1}$ CO₂;
3682 g_s =stomatal conductance measured at 400 $\mu\text{mol mol}^{-1}$ CO₂

Table B3. Second order log-polynomial regression coefficients that described the effect of leaf temperature on net photosynthesis and stomatal conductance measured at 400 $\mu\text{mol mol}^{-1}$ CO₂

	a	b	c
A_{net}	9.422	-0.573	0.010
g_s	-0.170	-0.186	0.003

3683 Net photosynthesis and stomatal conductance values were fit to the log-polynomial
3684 equation $\log(y) = a + bx + cx^2$, where x is leaf temperature. Key: A_{net} = net
3685 photosynthesis rate at 400 $\mu\text{mol mol}^{-1}$ CO₂; g_s = stomatal conductance measured
3686 at 400 $\mu\text{mol mol}^{-1}$ CO₂

Table B4. Mean, standard error, and 95% confidence interval ranges of soil nitrogen availability estimates across all measured plots. All units are expressed as $\mu\text{g N g}^{-1}$ resin d^{-1}

Site	Treatment	Mean	SE	Lower 95% CI	Upper 95% CI
Bald Hill	Ammonium sulfate	27.11	6.14	15.08	39.13
Bald Hill	Control	14.41	5.02	4.56	24.26
Bald Hill	Sodium nitrate	20.65	3.15	14.46	26.83
Bald Hill	Sulfur	6.33	2.19	2.04	10.62
Carter Creek	Ammonium sulfate	26.94	5.36	16.43	37.44
Carter Creek	Control	19.87	1.92	16.10	23.64
Carter Creek	Sodium nitrate	15.51	4.16	7.36	23.65
Carter Creek	Sulfur	5.50	1.40	2.75	8.25
Mount Pleasant	Ammonium sulfate	8.02	2.31	3.49	12.56
Mount Pleasant	Control	2.00	0.57	0.89	3.11
Mount Pleasant	Sodium nitrate	2.52	0.68	1.19	3.85
Mount Pleasant	Sulfur	2.42	0.39	1.66	3.17

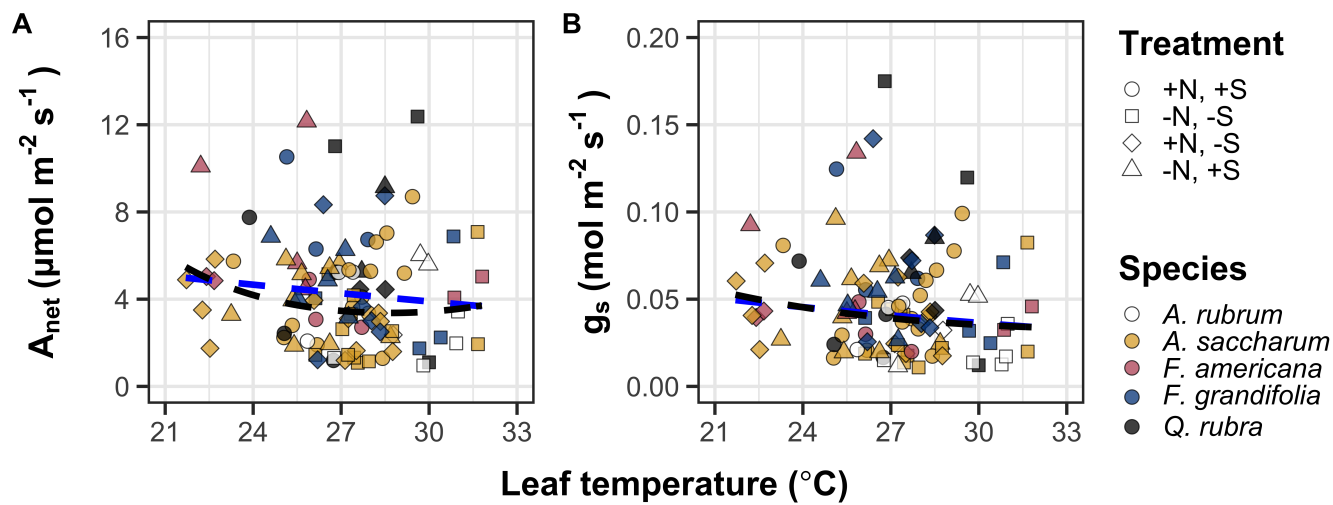


Figure B1. Effects of leaf temperature on net photosynthesis rate (panel A) and stomatal conductance (panel B) values when measured at $400 \mu\text{mol mol}^{-1} \text{CO}_2$. Leaf temperature is represented continuously on the x-axis, while species are represented as colored points. Colored points and shapes are as explained in Figure 3.1. The dashed blue trendline describes the linear relationship between leaf temperature and each response variable, while the dashed black trendline describes the same relationship with a log-polynomial regression equation.

**3687 Appendix C: Supplemental material for "The relative cost of resource
3688 use for photosynthesis drives variance in leaf nitrogen content across a
3689 climate and soil resource availability gradient"**

3690 C.1 Calculations for soil water holding capacity

3691 Water holding capacity (θ_{WHC} ; mm) was calculated as a function of the
3692 volumetric soil water storage at field capacity (W_{FC} ; m³ m⁻³), and the volumetric
3693 soil water storage at wilting point (W_{PWP} ; m³ m⁻³):

$$\theta_{WHC} = (W_{FC} - W_{PWP})(1 - f_{gravel}) * \min(z_{bedrock}, z_{max}) \quad (\text{C4.1})$$

3694 where f_{gravel} (%) is the fraction of gravel content in soil, $z_{bedrock}$ (mm) is the
3695 distance to bedrock, and z_{max} (mm) is the maximum allowable distance to bedrock,
3696 set to 2000mm. W_{FC} is calculated as:

$$\theta_{FC} = k_{fc} + (1.283 * (k_{fc})^2 - 0.374 * k_{fc} - 0.015) \quad (\text{C4.2})$$

3697 where

$$\begin{aligned} k_{fc} = & -0.251 * f_{sand} + 0.195 * f_{clay} + 0.011 * f_{OM} \\ & + 0.006 * (f_{sand} * f_{OM}) - 0.027 * (f_{clay} \\ & * f_{OM}) + 0.452 * (f_{sand} * f_{clay}) + 0.299 \end{aligned} \quad (\text{C4.3})$$

3698 W_{PWP} is calculated as:

$$W_{PWP} = k_{pwp} + (0.14 * k_{pwp} - 0.02) \quad (\text{C4.4})$$

3699 where

$$\begin{aligned} k_{pwp} = & -0.024 * f_{sand} + 0.487 * f_{clay} + 0.006 * f_{OM} \\ & + 0.005 * (f_{sand} * f_{OM}) - 0.013 * (f_{clay} \\ & * f_{OM}) + 0.068 * (f_{sand} * f_{clay}) + 0.031 \end{aligned} \quad (\text{C4.5})$$

3700 In Equations C4.4 and C4.5, f_{sand} (%) is the fraction of sand content in soil (%),
3701 f_{clay} (%) is the fraction of clay content in soil (%), and f_{OM} is the fraction of
3702 organic matter in soil (%). Organic matter in the soil was calculated in this study
3703 by converting soil organic carbon data extracted from SoilGrids 2.0 to soil organic
3704 matter using the van Bemmelen factor (1.724 conversion factor).

Table C1. List of sampled species and their plant functional group assignment

Symbol	Species	Photo. pathway	Growth duration	Growth habit	N-fixer?	Plant functional group	Number sampled
ACAN11	<i>Acaciella angustissima</i>	c3	perennial	forb	yes	c3_legume	3
AMAR2	<i>Ambrosia artemisiifolia</i>	c3	annual	forb	no	c3_nonlegume	25
AMPS	<i>Ambrosia psilostachya</i>	c3	perennial	forb	no	c3_nonlegume	32
ARAL3	<i>Argemone albiflora</i>	c3	annual	forb	no	c3_nonlegume	3
ARPU9	<i>Aristida purpurea</i>	c4	perennial	graminoid	no	c4_nonlegume	2
ASAS	<i>Asclepias asperula</i>	c3	perennial	forb	no	c3_nonlegume	3
ASLA4	<i>Asclepias latifolia</i>	c3	perennial	forb	no	c3_nonlegume	3
ASSY	<i>Asclepias syriaca</i>	c3	perennial	forb	no	c3_nonlegume	18
BASA	<i>Baccharis salicina</i>	c3	perennial	shrub	no	c3_nonlegume	3
BOIS	<i>Bothriochloa ischaemum</i>	c4	perennial	graminoid	no	c4_nonlegume	6
BOSA	<i>Bothriochloa saccharoides</i>	c4	perennial	graminoid	no	c4_nonlegume	6
CAAM2	<i>Callicarpa americana</i>	c3	perennial	shrub	no	c3_nonlegume	3
CAPL3	<i>Carex planostachys</i>	c4	perennial	graminoid	no	c4_nonlegume	3
CAREX	<i>Carex</i> spp.	c4	perennial	graminoid	no	c4_nonlegume	16
CHFE3	<i>Chamaesyce fendleri</i>	c3	perennial	forb	no	c3_nonlegume	2
CHPI8	<i>Chrysopsis pilosa</i>	c3	annual	forb	no	c3_nonlegume	3
COCO13	<i>Conoclinium coelestinum</i>	c3	perennial	forb	no	c3_nonlegume	3
COER	<i>Commelina erecta</i>	c3	perennial	forb	no	c3_nonlegume	3
CRGLL	<i>Croton glandulosus</i>	c3	annual	forb	no	c3_nonlegume	22
CYDA	<i>Cynodon dactylon</i>	c4	perennial	graminoid	no	c4_nonlegume	15
DATE3	<i>Dasyllirion texanum</i>	c3	perennial	shrub	no	c3_nonlegume	3
DIAN	<i>Dichanthium annulatum</i>	c4	perennial	graminoid	no	c4_nonlegume	8
ENPE4	<i>Engelmannia peristenia</i>	c3	perennial	forb	no	c3_nonlegume	6
EUMA8	<i>Euphorbia marginata</i>	c3	annual	forb	no	c3_nonlegume	6
GAPU	<i>Gaillardia pulchella</i>	c3	annual	forb	no	c3_nonlegume	16
GLGO	<i>Glandularia gooddingii</i>	c3	perennial	forb	no	c3_nonlegume	2
HEAN3	<i>Helianthus annuus</i>	c3	annual	forb	no	c3_nonlegume	6

Table C2. List of sampled species and their plant functional group assignment (cont.)

Symbol	Species	Photo. pathway	Growth duration	Growth habit	N-fix?	Plant functional group	Number sampled
HECA8	<i>Heterotheca canescens</i>	c3	perennial	forb	no	c3_nonlegume	2
HETE3	<i>Heliotropium tenellum</i>	c3	annual	forb	no	c3_nonlegume	3
IVAX	<i>Iva axillaris</i>	c3	perennial	forb	no	c3_nonlegume	4
LIAT	<i>Lilaeopsis attenuata</i>	c3	perennial	forb	no	c3_nonlegume	3
LIPU	<i>Liatris punctata</i>	c3	perennial	forb	no	c3_nonlegume	3
LOPE	<i>Lolium perenne</i>	c3	perennial	graminoid	no	c3_nonlegume	9
MIQU2	<i>Mimosa quadrivalvis</i>	c3	perennial	forb	yes	c3_legume	15
NALE3	<i>Nassella leucotricha</i>	c3	perennial	graminoid	no	c3_nonlegume	19
OECU2	<i>Oenothera curtiflora</i>	c3	annual	forb	no	c3_nonlegume	3
OENOT	<i>Oenothera</i> spp.	c3	annual	forb	no	c3_nonlegume	1
PAVI2	<i>Panicum virgatum</i>	c4	perennial	graminoid	no	c4_nonlegume	12
PRGL2	<i>Prosopis glandulosa</i>	c3	perennial	shrub	yes	c3_legume	33
QUHA3	<i>Quercus harvardii</i>	c3	perennial	shrub	no	c3_nonlegume	3
QUMO	<i>Quercus mohriana</i>	c3	perennial	shrub	no	c3_nonlegume	1
RACO3	<i>Ratibida columnifera</i>	c3	perennial	forb	no	c3_nonlegume	40
RHAM	<i>Rhamnus</i> spp.	c3	perennial	shrub	yes	c3_legume	1
RHSET	<i>Rhynchosia senna</i>	c3	perennial	forb	yes	c3_legume	1
RUHI2	<i>Rudbeckia hirta</i>	c3	perennial	forb	no	c3_nonlegume	3
RUNU	<i>Ruellia nudiflora</i>	c3	perennial	forb	no	c3_nonlegume	15
RUTR	<i>Rubus trivialis</i>	c3	perennial	vine	no	c3_nonlegume	3
SAFA2	<i>Salvia farinacea</i>	c3	perennial	forb	no	c3_nonlegume	7
SCHIZ4	<i>Schizachyrium</i> spp.	c4	perennial	graminoid	no	c4_nonlegume	8
SCSC	<i>Schizachyrium scoparium</i>	c4	perennial	graminoid	no	c4_nonlegume	3
SODI	<i>Solanum dimidiatum</i>	c3	perennial	forb	no	c3_nonlegume	1
SOEL	<i>Solanum elaeagnifolium</i>	c3	perennial	forb	no	c3_nonlegume	53
SOHA	<i>Sorghum halapense</i>	c4	perennial	graminoid	no	c4_nonlegume	38
STTE3	<i>Stillingia texana</i>	c3	perennial	forb	no	c3_nonlegume	3

Table C3. List of sampled species and their plant functional group assignment (cont.)

Symbol	Species	Photo. pathway	Growth duration	Growth habit	N-fixer?	Plant functional group	Number sampled
VEOC	<i>Verbesina occidentalis</i>	c3	perennial	forb	no	c3_nonlegume	3
VEST	<i>Verbena stricta</i>	c3	perennial	forb	no	c3_nonlegume	3
WEAC	<i>Wedelia acapulcensis</i>	c3	perennial	shrub	no	c3_nonlegume	6

Table C4. Model selection results for soil moisture, air temperature, and vapor pressure deficit. Soil moisture was used in a bivariate regression against β , while vapor pressure deficit was used in bivariate regressions against leaf $C_i:C_a$ *

Day	Soil moisture		VPD	
	AICc	RMSE	AICc	RMSE
1	1431.77	0.8400	-772.71	0.0853
2	1431.76	0.8400	-775.47	0.0849
3	1431.78	0.8400	-770.86	0.0854
4	1431.79	0.8401	-793.49	0.0839
5	1431.79	0.8401	-771.66	0.0853
6	1431.78	0.8401	-771.66	0.0853
7	1431.78	0.8401	-771.05	0.0854
8	1431.76	0.8401	-770.94	0.0854
9	1431.75	0.8401	-770.11	0.0854
10	1431.74	0.8401	-770.08	0.0855
15	1431.54	0.8401	-768.64	0.0856
20	1431.40	0.8401	-769.77	0.0855
30	1431.23	0.8400	-772.18	0.0853
60	1429.84	0.8391	-779.06	0.0848
90	1429.14	0.8385	-773.99	0.0852

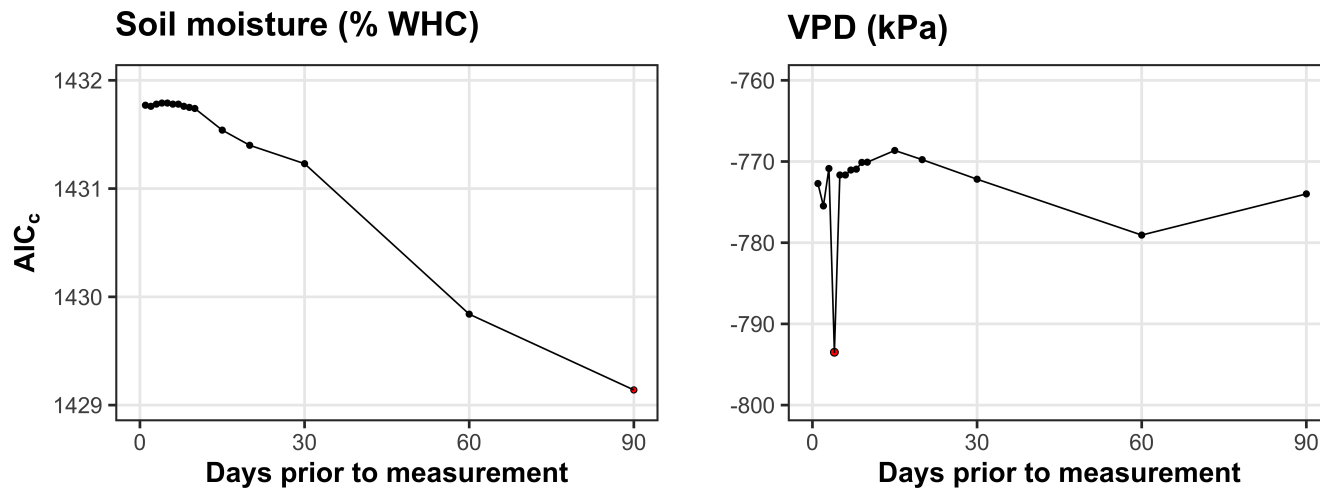


Figure C1. Model selection results exploring relevant timescales for soil moisture (left panel) and vapor pressure deficit (right panel). The x-axis indicates the number of days before each site visit and the y-axis notes the corrected Akaike Information Criterion value. The timescale with the lowest AIC_c value, and therefore most relevant timescale to include in statistical models, is noted as a red point.

**3705 Appendix D: Supplemental material for "Optimal resource investment
 3706 to photosynthetic capacity maximizes nutrient allocation to whole
 3707 plant growth under elevated CO₂"**

Table D1. Summary table containing volumes of compounds used to create modified Hoagland's solutions for each soil nitrogen fertilization treatment. All volumes are expressed as milliliters per liter (mL/L)

Compound	0 ppm N	35 ppm N	70 ppm N	105 ppm N	140 ppm N
1 M NH ₄ H ₂ PO ₄	0	0.165	0.33	0.5	0.67
2 M KNO ₃	0	0.335	0.67	1	1.33
2 M Ca(NO ₃) ₂	0	0.335	0.67	1	1.33
1 M NH ₄ NO ₃	0	0.165	0.33	0.5	0.67
8 M NH ₄ NO ₃	0	0	0	0	0
1 M KH ₂ PO ₄	1	0.85	0.67	0.5	0.33
1 M KCl	3	2.45	2	1.5	1
1 M CaCO ₃	4	3.33	2.67	2	1.33
2 M MgSO ₄	1	1	1	1	1
10% Fe-EDTA	1	1	1	1	1
Trace elements	1	1	1	1	1

Compound	210 ppm N	280 ppm N	350 ppm N	630 ppm N
1 M NH ₄ H ₂ PO ₄	1	1	1	1
2 M KNO ₃	2	2	2	2
2 M Ca(NO ₃) ₂	2	2	2	2
1 M NH ₄ NO ₃	1	3.5	0	0
8 M NH ₄ NO ₃	0	0	0.75	2
1 M KH ₂ PO ₄	0	0	0	0
1 M KCl	0	0	0	0
1 M CaCO ₃	0	0	0	0
2 M MgSO ₄	1	1	1	1
10% Fe-EDTA	1	1	1	1
Trace elements	1	1	1	1

Table D2. Summary of the daily growth chamber growing condition program

Time	Air temperature (°C)	Light (%)
09:00	21	25
09:45		50
10:30	25	75
11:15		100
22:45	21	75
23:30		50
00:15	17	25
01:00		0

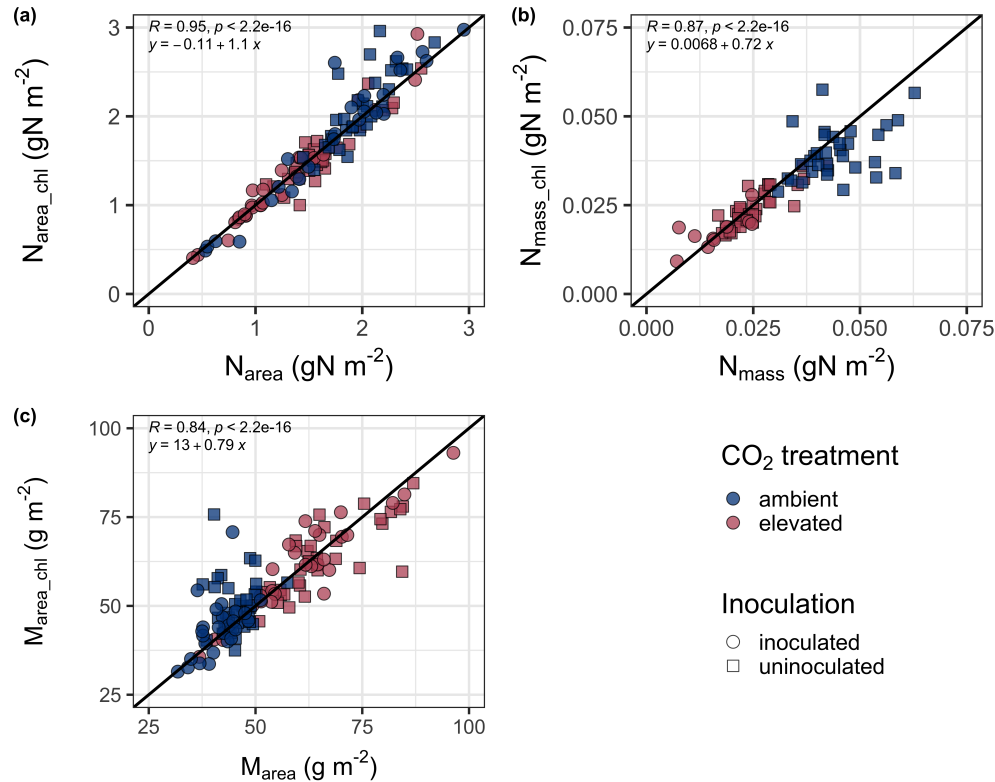


Figure D1. Relationships between area-based leaf nitrogen content (a), mass-based leaf nitrogen content (b), and leaf mass per unit leaf area (c) measured on the focal leaf used to generate A_{net}/C_i curves and leaf nitrogen content measured on the leaf used for chlorophyll extractions. Blue points refer to leaves grown under ambient CO₂ and red points refer leaves grown under elevated CO₂. Square points indicate uninoculated pots and circular points indicate inoculated pots. Pearson's correlation, associated p -values, and the line of the regression line that described each bivariate are included in the top left corner of each plot. The solid black line visualizes the trend given a 1:1 bivariate relationship.

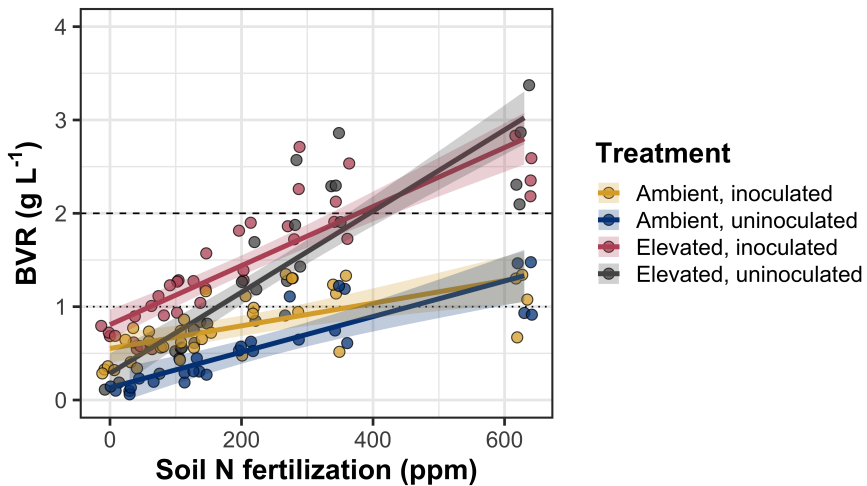


Figure D2. Effects of CO₂, fertilization, and inoculation on the ratio of whole plant biomass to pot volume. Soil nitrogen fertilization is represented on the x-axis in all panels. Yellow points and trendlines indicate inoculated individuals grown under ambient CO₂, blue points and trendlines indicate uninoculated individuals grown under ambient CO₂, red points and trendlines indicate inoculated individuals grown under elevated CO₂, and grey points indicate uninoculated individuals grown under elevated CO₂. Solid trendlines indicate regression slopes that are different from zero ($p < 0.05$), while dashed trendlines indicate slopes that are not distinguishable from zero ($p > 0.05$). The dotted horizontal line indicates the point where biomass:pot volume exceeds 1 g L⁻¹, and the dashed line indicates the point where biomass:pot volume exceeds 2 g L⁻¹.